"Elucidation of the cell-specific regulation of the novel human tumor gene *NOT*"

Dissertation

zur Erlangung des Grades

"Doktor der Naturwissenschaften"

am Fachbereich Biologie

der Johannes Gutenberg-Universität

in Mainz

Christoph Schultheiß

Geboren am 18.08.1983 in Coburg

Mainz 2016

Dekan:

1. Gutachter:

2. Gutachter:

Tag der mündlichen Prüfung:

I Table of contents

II Figures

III Tables

IV Supplementary tables

V Abbreviations

3'	3 prime end of RNA/DNA sequence
5'	5 prime end of RNA/DNA sequence
a	years
A	ampere
a. bidest	aqua bidestilata
AD	activation domain
App.	appendix
BD	binding domain
BFA	Brefeldin A
bp	base pair(s)
btn	biotinylated
c	concentration …
cDNA	complementary DNA
ChIP	chromatin immunoprecipitation
Ch.	chapter
Da	dalton (atomic mass unit)
DNA	deoxyribonucleic acid
dNTP	deoxyribonucleosidetriphosphate
ds	double-stranded
EDTA	ethylenediaminetetraacetic acid
EMSA	electromobility shift assay
et al.	*et alii* or *et aliorum*
E. coli	*Escherichia coli*
e. g.	exempli gratia
f	femto-
Fig.	Figure
g	gram
h	hour
k	kilo-
kb	kilo base pairs
kg	kilogram
l	liter
LiAc	lithium acetate
M	molar
m	murine
mM	millimolar
min.	minute(s)
mRNA	messenger ribonucleic acid
n	nano-

NBT	nitro blue tetrazolium
nm	nanometer
nt	nucleotide
ORF	open reading frame
P	phospho-
p	pico-
Pol II	DNA-dependent RNA polymerase II
PP	polypropylene
PBS	phosphate-buffered saline
PS	polystyrene
qRT-PCR	quantitative reverse transcription-PCR
RACE	rapid amplification of cDNA ends
rcf	relative centrifugal force (RCF)
RNA	ribonucleic acid
rpm	rotations per minute
RT	room temperature
Ser	serine
SDS	sodium dodecyl sulfate
sec.	second(s)
sol.	solution
SSC	saline and sodium citrate
ss	single-stranded
Tab.	table
TAE	Tris-acetate-EDTA
TBE	Tris-borate-EDTA
TBS	Tris-buffered saline
T_m	melting temperature
TNFα	Tumor necrosis factor α
Tris	tris(hydroxymethyl)aminomethane
TSS	Transcription start site
u	unit
V	volt
v/v	volume per volume
Vol.	volume(s)
WB	Western blot
w/o	without
w/v	weight per volume
Y1H	yeast one-hybrid
Y2H	yeast two-hybrid
°C	degree Celsius

1 Introduction

1.1 Identification, isolation and characterization of the *NOT* gene

1.1.1 The *lethal(2)neighbour of tid* (*l(2)not*) gene from *Drosophila*

Seminal work on the genetic, cytogenetic, and molecular identification of the *Drosophila melanogaster* (*Dm*) tumor suppressor gene *l(2)tid* (*lethal(2)tumorous imaginal discs*), a member of the DnaJ co-chaperone family (Kurzik-Dumke *et al*. 1995), yielded identification and isolation of the *l(2)not* (*lethal(2)neighbour of tid*) gene (Kurzik-Dumke *et al*. 1997). Later on, the same group isolated the *NOT* gene also from *Drosophila virilis* (*Dv*) (Kaymer *et al*. 1997) and man (Kurzik-Dumke and Kaymer 1996). Interestingly, the two evolutionary conserved genes *l(2)tid* and *l(2)not* are organized as "gene within gene" (Kurzik-Dumke *et al*. 1997). The *l(2)tid* gene resides within the 2645nt intron of *l(2)not* on its antisense strand. In addition, a further gene named *l(2)relative of tid* (*l(2)rot*) is located in the intron of *l(2)not* on the sense strand. As *l(2)rot* is complementary to *l(2)tid* and is only transcribed but not translated, it might act as an antisense regulator of *l(2)tid* (Kurzik-Dumke *et al*. 1997). This nested gene arrangement only exists in the *Schizophora* section of the *Diptera* order (which includes *Drosophilidae* and *Tephritidae*) and is not conserved in any other species. As shown in the fly, *l(2)not* encodes a 510 amino acid (aa) protein with a putative molecular weight of 56kDa, NOT56 (Kurzik-Dumke *et al*. 1997). It contains four transmembrane (TM) domains and three putative membrane-associated domains, the arginine-glycine-aspartate-threonine (RGDT) motif responsible for cell surface signaling, and a C-terminal KKLQ-motif necessary for localization within the endoplasmic reticulum (ER). The ER localization was confirmed by electron microscopy analysis (Kurzik-Dumke *et al*. 1997). In *Dm* the *l(2)not* transcript is expressed ubiquitously in all developmental stages, but the protein can only be detected in embryonal stages (Kurzik-Dumke *et al*. 1997). Genetic analysis performed using diverse *Dm* strains argue for a functional relationship between *l(2)tid* and *l(2)not* (Kurzik-Dumke 1996).

1.1.2 The human *NOT* gene

The human counterpart of the *l(2)not* gene, *NOT* (*ALG3*, *CDG1D*, *CDGS4*, *Not56*, *NOT56L*, *D16Ertd36e*), is located on chromosome 3, region 3q27.1 (NCBI Gene ID: 10195) and spans 6.9kb

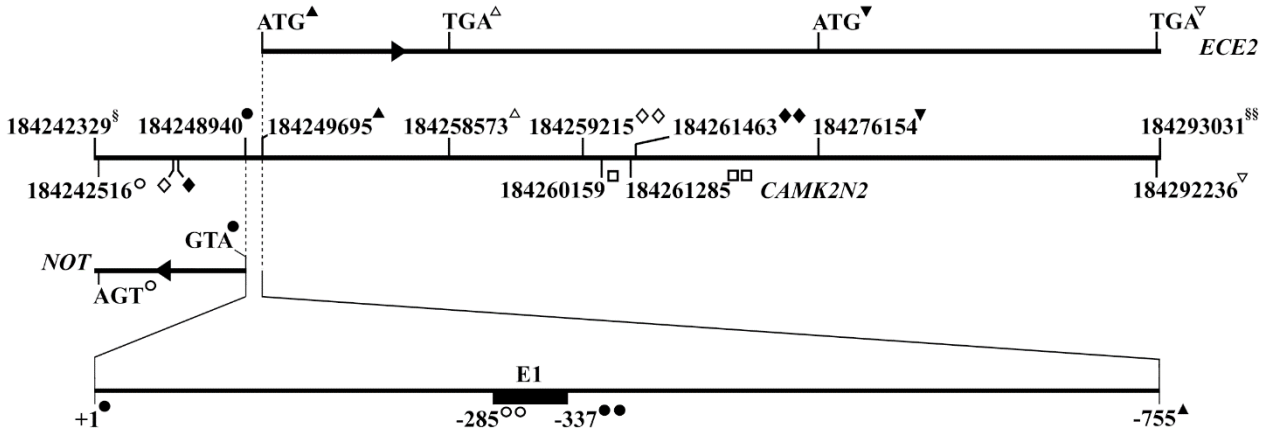

Fig. 1 Schematic representation of the *NOT* chromosomal organization. The *NOT* gene (NCBI Gene ID: 10195) is located on chromosome 3 (Reference: NC_000003.12), depicted area: 184242329nt (§) to 184293031nt (§§). The ATG of *NOT*-1, -2, and -5 (●) is located at nt 184248940 (+1). The ATG of *NOT*-4 (●●) is located 337nt upstream the *NOT*-1 ATG at nt 184249277. The first exon (E1) of *NOT*-4 ends 285nt (○○) upstream *NOT*-1 ATG. *NOT*-1 and -4 share the stop codon at nt 184242516 (○). The stop codon of *NOT*-2 is located at 184245776nt (♦), the stop codon of *NOT*-5 at nt 184245490 (◊). The ATG of *ECE2* variants 1 (NM_014693.3) and 3 (NM_032331.3) is located at nt 184249695 (▲), the ATG of variants 2 (NM_001037324.2), 4 (NM_001100120.1), and 5 (NM_001100121.1) at nt 184276154 (▼). The stop codon for variant 3 is located at nt 184258573 (Δ), the stop codon for variants 1, 2, 4, and 5 is located at nt 184292236 (∇). The *CAMK2N2* gene is located in the intron between exon3 and 4 of *ECE2* on the *NOT* strand spanning nts 184261463 (♦♦) – 184259215 (◊◊). The *CAMK2N2* start codon is located at nt 184261285 (□□), the stop codon at nt 184260159 (□).

(Fig. 1). In close proximity another gene, *ECE2* (*endothelin converting enzyme 2*, NCBI Gene ID: 9718), is located upstream on the opposite strand spanning 42.5kb (Fig. 1). *ECE2* is a type 2 integral membrane zinc-dependent metallopeptidase that is involved in processing of the endothelins, short vasoconstricting peptides, which can also work as neuropeptides (Lorenzo *et al.* 2001). In addition, structural analysis indicates methyltransferase activity through a conserved S-adenosyl-L-methionine (SAM)-dependent methyltransferase (SAM-MT) domain (Tempel *et al*. 2009). *ECE2* downregulation has been linked to Alzheimer´s disease (Weeraratna *et al*. 2007). Between exons 3 and 4 of *ECE2* the *CAMK2N2* (*calcium/calmodulin-dependent protein kinase II inhibitor 2*, NCBI Gene ID: 94032) gene is located on the same strand as *NOT*. Calmodulin-dependent kinase II is a multifunctional serine/threonine kinase, which integrates intracellular Ca^{2+} signals into diverse cellular processes like transcription, cell survival, apoptosis and cytoskeleton organization as well as synaptic plasticity and spatial memory (Swulius and Waxham 2008). In the case of *NOT* four different splice variants have been isolated (Fig. 1). The first was *NOT*-1 (Kurzik-Dumke and Kaymer 1996; GenBank: Y09022.1) corresponding to the *l(2)not* gene (Kurzik-Dumke et al. 1997). In 1999 *NOT*-2 was isolated from pooled pancreas and spleen of a 28-year-old male (Strausberg

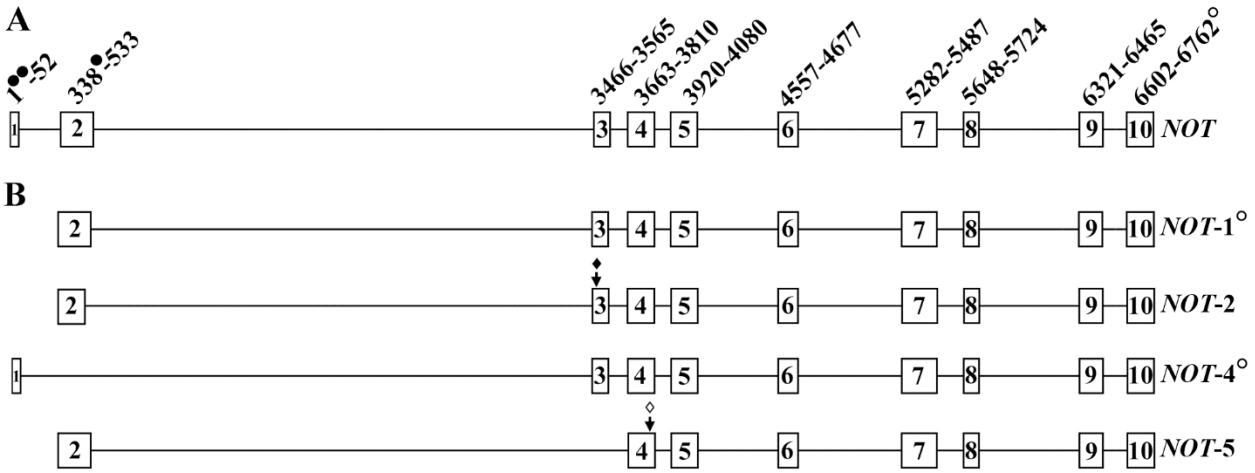

Fig. 2 Schematic representation of *NOT* splice variants. (A) Exon-intron structure and size of the ten exons of the *NOT* gene on chromosome 3, positions relative to the first ATG (●●). **(B)** Exon composition of the different *NOT* splice variants. The forms 1, 2, and 5 share the same first exon and ATG at 338nt (●). The *NOT*-4 variant lacks this exon and contains a different first exon and start codon (●●). The variants 1 and 4 contain the same TGA stop codon at 6762nt (○). The *NOT*-2 splice variant contains a shortened first exon (lacking the last 36nt) which leads to a frameshift and premature stop codon at 3502nt (♦). The *NOT*-5 variant lacks the second exon as compared to *NOT*-1. This leads to a frameshift and a premature TGA stop codon at 3790nt (◊).

1999; GenBank: BM920198.1). As compared to *NOT*-1, this variant has a shortened first exon caused by a cryptic splice site leading to a premature stop codon (Denecke *et al*. 2004; Fig. 2). The *NOT*-4 isoform, which differs from *NOT*-1 by using an alternative first exon, was isolated from human placenta in 2001 (Li *et al*.; GenBank: BX339649.2). *NOT*-4 is the only variant besides *NOT*-1 that contains a full-length open reading frame (ORF) (Fig. 2). The alternate first exon of *NOT*-4 does not cause a frameshift in the shared sequence. The *NOT*-5 transcript was isolated first from fetal brain in the context of a human cDNA sequencing project focused on splicing variants (Isogai and Yamamoto 2007; GenBank: AK299575.1). As compared to *NOT*-1, this isoform lacks exon 2 leading to a pre-mature stop codon. RNA-seq data shows that *NOT* is constantly expressed across different tissues, including adrenal, adipose, brain, breast, colon, heart, kidney, lung, lymph, ovary, prostate, skeletal muscle, testes, thyroid, and white blood cells with highest expression in liver (Asmann *et al*. 2012). High *NOT* expression was also detected in embryonic stem cells (H1-hESC) (Djebali *et al*. 2012). Hoffman *et al*. (2008) found upregulation of *NOT* in the endocrinic and exocrinic precursor cells at the early stages of pancreas development. Recent investigations of *NOT* expression in diverse human epithelial- and blood tumor-cells derived from colon, skin, lung, cervix, and breast carcinomas showed abnormal profiles for *NOT* splice forms as compared to

Tab. 1 *NOT* copy number variations in diverse cancers according to the COSMIC Database

Tissue	Samples	Amplification	Deletion	Loss of heterozygosity
Breast	900	9 (1%)		
CNS	787	11 (1.4%)		
Cervix	171	35 (20.47%)		
Endometrium	405	15 (3.7%)		
Haematopoeitic + lymphoid	277	1 (0.36%)		
Kidney	411	0	1 (0.24%)	
Large Intestine	585	0	1 (0.17%)	1 (0.2%)
Lung	986	149 (15.11%)		2 (0.2%)
Esophagus	95	11 (11.58%)		
Ovary	708	39 (5.51%)		2 (0.3%)
Skin	380	2 (0.53%)		
Stomach	339	11 (3.24%)		
Upper aerodigestive tract	440	56 (12.73%)		
Urinary tract	219	3 (1.37%)		

normal cells (Kurzik-Dumke, personal communication). This is in accordance with published data which shows significant *NOT* overexpression caused by amplification of its genomic region in esophageal squamous cell carcinoma, especially in patients with lymph node metastases (Shi *et al*. 2014). Extensive sequencing analysis of millions of different tumor samples and whole cancer genomes (Forbes *et al*. 2015; The Catalogue of Somatic Mutations in Cancer (COSMIC) database: http://cancer.sanger.ac.uk/cancergenome/projects/cosmic/) revealed that *NOT* amplification is also prevalent in cancers originating from the cervix, lung, and upper aerodigestive tract whereas loss of heterozygosity or deletions are not common (Tab. 1). In contrast, nonsense mutations are not found and missense point mutations are infrequent among diverse cancers (Tab. 2). The NOT proteins share common features with the fly´s NOT56 protein (Ch. 1.1.1). They consist of 438 aa (NOT-1) or 391 aa (NOT-4) including high amounts of the amino acids leucine (18% for NOT-1 and 17.6% for NOT-4 in man, 16.6 in *Dm*) and alanine (8.0% for NOT-1 and 7.2 for NOT-4 in man, 8.2% in *Dm*). To date, there are almost no published reports about the function(s) of the NOT proteins. A search for sequences homologous NOT revealed 34% identity with the ALG3 from yeast (Kurzik-Dumke *et al*. 1996; 1997), a protein which is associated with the N-glycosylation machinery in the ER and conserved across species (Aebi 2013).

Tab. 2 Detected missense mutations in the *NOT* gene according to the COSMIC database

Tissue / Var.	Biliary	Brain	Breast	Endome.	Intestine	Kidney	Liver	Lung	Skin	Stomach	Thyroid
***NOT*-1**	1	4	1	1	7	3	2	3	6	2	1
Samples	125	1910	1265	602	1052	1203	1270	1593	805	555	550
% mut.	0.8	0.21	0.08	0.17	0.67	0.25	0.16	0.19	0.75	0.36	0.18
***NOT*-4**	0	4	1	0	7	3	2	3	5	2	1
Samples	125	1910	1265	602	1052	1203	1270	1593	805	555	550
% mut.	0	0.21	0.08	0	0.67	0.25	0.16	0.19	0.62	0.36	0.18

1: Mutations refer to amino acid changes with respect to the *NOT*-1 reference sequence (NCBI: Y09022.1). Three mutations (S13N found in the biliary tract, A65T found in skin and F104T found in the endometrium) are specific for *NOT*-1 and its derivatives. Endome.: Endometrium.

1.1.3 The role of ALG3 in the eukaryotic N-glycosylation pathway

The most prevalent form of post-translational protein modification is the addition of a preformed uniform oligosaccharide to the side chain amide group nitrogen of an asparagine (Asn/N) called N-linked glycosylation or N-glycosylation (Weerapana and Imperiali 2006). N-glycosylation is carried out by the 13 members of *ALG* (asparagine linked glycosylation) gene family. *ALG* genes code for different glycosyltransferases, which catalyze the step-wise assembling of the branched oligosaccharide $Glc_3Man_9GlcNAc_2$ to the isoprenoid lipid dolichol-phosphate (Dol-P) starting at the cytoplasmic site of the ER and ending on its luminal site (Fig. 3) (Aebi 2013). After completion of LLO biosynthesis the oligosaccharide is transferred *en bloc* by the oligosaccharyltransferase complex (OST) onto selected target sites with the consensus N-glycosylation motif N-X-S/T (X can be any amino acid but proline) (Aebi 2013). Within the process of N-glycosylation NOT/ALG3 is assumed to represent the mannosyltransferase that catalyzes the addition the sixth mannose to the $Man_5GlcNAc_2$ oligosaccharide via an α-1,3 glycosidic bond (Aebi 2013) (Fig. 3). This assumption is based on the observation that the *NOT*/*ALG3* gene complements the defective biosynthesis of dolichol-linked oligosaccharides which leads to the accumulation of the lipid-linked glycan $Man_5GlcNAc_2$ and underglycosylated secretory proteins in the *alg3_1* mutant *Saccharomyces cerevisiae* strain (Aebi *et al*. 1996). The reverse approach, deletion of *NOT*/*ALG3* in wild-type yeast cells, which does not result in a selectable growth phenotype, yielded the same biochemical defects as observed in the *alg3_1* mutant (Aebi *et al*. 1996). However, cells containing *NOT*/*ALG3* deletions still generate correctly N-glycosylated proteins (Aebi *et al*. 1996).

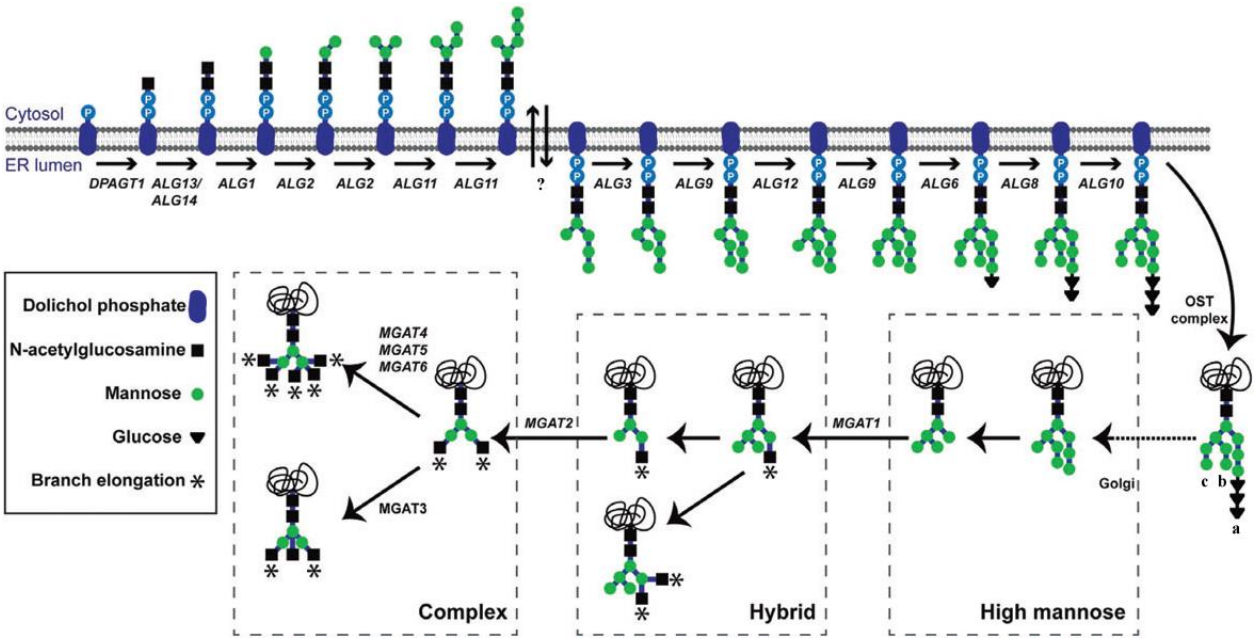

Fig. 3 Schematic representation of the N-glycosylation machinery in the ER. N-glycosylation is the covalent addition of the preformed oligosaccharide (OS) $Glc_3Man_9GlcNAc_2$ to an asparagine. The OS contains three branches called a-, b-, and c-antenna. OS-assembling is mediated by the *ALG* gene family. It starts on the cytoplasmic site of the ER membrane and ends on the luminal site with the *en bloc* transfer of the OS to the target protein by the oligosaccharyltransferase complex (OST). Depending on the function of the respective glycoprotein the glycan moieties can be further processed in the Golgi by different glycosyltransferases (MGAT1-6) to either the high mannose, hybrid or complex type. Figure modified from Varelas *et al*. (2014).

Complete N-glycosylation is also observed if the *NOT/ALG3* homologues in *Pichia pastoris* (Davidson *et al*. 2004), *Tripanosoma brucei* (Manthri *et al*. 2008), *Aspergillus* (Dai *et al*. 2013), *Arabidopsis thaliana* (Henquet *et al*. 2008; Kajiura *et al*. 2010), and man (Körner *et al*. 1999) are mutated. Interestingly, the described *NOT/ALG3* mutations in *Arabidopsis thaliana* not even exhibit the underglycosylation of glycoproteins observed in other organisms carrying *NOT/ALG3* mutations (Henquet *et al*. 2008). In fact, the only hint that NOT/ALG3 actually has glycosyl-transferase activity comes from the report published by Sharma *et al*. (2001) who showed that the introduction of a recombinant *NOT/ALG3* expression construct, whose immunoprecipitated product exhibits glycosyltransferase activity *in vitro*, restores the wild-type phenotype in the *alg3_1* mutant. In addition, Chen *et al*. (2014) reported that the rice blast fungus *Magnaporthe oryzae* fails to glycosylate the Slp1 and Bas4 effector proteins when *NOT/ALG3* is mutated. The N-glycosylation of these proteins is essential for the fungus to evade the innate immune response of infiltrated host cells. However, the direct *in vivo* evidence for NOT/ALG3 glycosyltransferase

activity is still lacking. The available data rather indicates that the activity of NOT/ALG3 is not essential for the N-glycosylation process and can be adopted, at least in part, by other enzymes of this cascade. As a consequence, ALG3/NOT possesses further cellular functions besides this enzymatic activity. One of these potential functions is suggested to depend on the topographic key-position NOT/ALG3 has within the N-glycosylation pathway. As first mannosyltransferase that acts on the luminal site of the ER (Snider and Rogers 1984), it might be involved in the yet unclear translocation of the cytoplasmic LLO or function as a central regulator of glycoprotein synthesis in general (Aebi 2013 and literature herein). The latter is supported by the observed accumulation of the intermediate glycan $Man_5GlcNAc_2$ in glucose-deprived wild-type yeast cells (Rearick *et al.* 1981). Some authors suggest the involvement of NOT/ALG3 in cell wall formation and stability. As reported by Bailey and Schulz (2013), *NOT*/*ALG3* yeast mutants display an upregulation of Cis3p (Ccw11p, Pir4p, Ccw5p, Scw8p), a protein known to be involved in maintaining the integrity and stability of the cell wall (Bailey and Schulz 2013). In addition, the elevated levels of protein secretion that were observed in *NOT*/*ALG3* mutant *A. niger* cells were linked to a less stable cell wall structure normally acting as secretion barrier (Dai *et al*. 2013). However, it is not clear if the reported effects of *NOT*/*ALG3* mutations on cell wall integrity are completely, if at all, independent of glycosylation.

1.1.4 Congenital disorders of glycosylation (CDG)

Defective glycosylation has been linked to various diseases including hereditary metabolic diseases, neurological and developmental disorders, diabetes as well as cancer (Ohtsubo and Marth 2006). Defective glycosylation caused by genetic deficiencies in single components of the glycosylation machineries have been summarized in a group of rare hereditary diseases referred to as congenital disorders of glycosylation (CDG). CDGs exhibit a broad clinical spectrum, ranging from slight mental retardation to multiorgan dysfunctions and are often associated with infantile lethality (Haeuptle and Hennet 2009). The most recent nomenclature suggests to name the CDG by using the official abbreviation of the mutated gene followed by -CDG, e. g. ALG3-CDG (Jaeken *et al.* 2008). To date from over 1000 described cases only 12 CDG patients (Tab. 3) are linked to mutations in the *NOT* gene (CDG type Id; CDG-Id; ALG3-CDG) (Lepais *et al*. 2015). The observed cases share similar symptoms like psychomotor retardation, microcephaly, facial dysmorphism, hypotonia, and visual impairment, whereas also case-specific symptoms like bone

Tab. 3 Documented cases of ALG3-CDG (CDG-Id)

Mutation		Zygosity	Gender	Age[2]	Reference
CDS[1]	Protein				
G353A	G118D	homozygous	male	1y	Stibler *et al*. (1995)
G353A	G118D	homozygous	male	5y	Körner *et al*. (1999)
C165T	-	homozygous	male	6y	Denecke *et al*. (2004)
G512A	R171Q	homozygous	female	19d[3]	Sun *et al*. (2005)
C796T	R266C	homozygous	female	4y	Schollen *et al*. (2005)
T211C	W71R	heterozygous	male	9y	Kranz *et al*. (2007)
T470A	M157K	heterozygous	female	7y	Kranz *et al*. (2007)
C116T/ G512A	P39L/ R171Q	heterozygous	male	5y	Rimella-Le-Huu *et al*. (2008)
T206C	I69T	heterozygous	male	21y	Riess *et al*. (2013)
T626C	M209T	heterozygous	female	15y	Riess *et al*. (2013)
G286A	G96R	homozygous	male	25WG[4]	Lepais *et al*. (2015)
G286A	G96R	homozygous	female	12d[5]	Lepais *et al*. (2015)

1: Positions in nt with respect to ATG of *NOT*-1 (NCBI: Y09022.1); 2: Age at documentation, y: Years; d: Days; 3: Deceased 19d after birth; 4: Symptoms detected 23 weeks after gestation (WG), termination of pregnancy was performed 25WG; 5: Patient was born 36 WG, deceased 12d after birth.

dysplasia, cataract, corneal opacities, pons hypoplasia, and epilepsy are observed (Lepais *et al*. 2015). In most cases the observed mutation is homozygous and leads to an amino acid substitution in a putative non-transmembrane part of the protein (Tab. 3). Nevertheless, the causal role of these mutations for the observed CDG phenotypes has still to be demonstrated especially with respect to the case published by Denecke *et al*. (2013) where the described phenotype is linked to a silent *NOT* mutation (Tab. 3).

1.2 Eukaryotic gene regulation on the transcript level

As it is an integrant part of this thesis, this section will give an overview of transcription in eukaryotes. The expression of each eukaryotic gene is controlled at different levels by a variety of mechanisms like transcription initiation and elongation, transcript maturation (e. g. capping, (alternative) splicing, polyadenylation, RNA editing), protein translation, and post-translational protein modification (Maston *et al.* 2006). However, transcription is considered to be the most important of these regulatory mechanisms (Maston *et al.* 2006). Transcription is the synthesis of a functional RNA from a DNA template by structurally related multiprotein complexes termed nuclear DNA-dependent RNA polymerases (Pol) to read out the genomic information encoded in

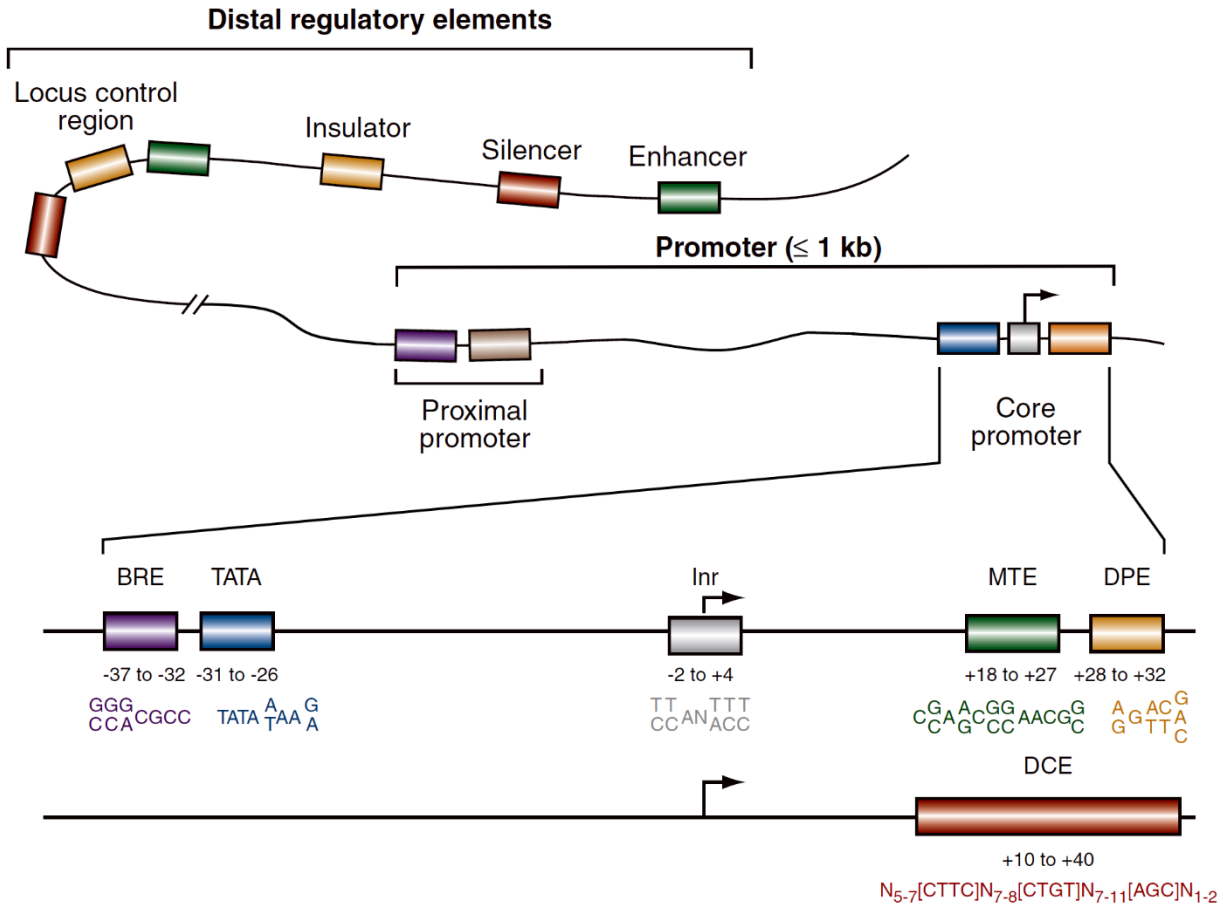

Fig. 4 Schematic representation of the regulatory region of Pol II-dependent promoters. Pol II-dependent promoters are grouped into the core promoter, the proximal promoter, and the distal promoter. This classification roughly depends on the distance of regulatory elements from the transcription start site (+1). The core promoter contains combinations of conserved binding elements like the TATA box, the Initiator element (Inr), the Downstream Promoter Element (DPE), the Downstream Core Element (DCE), TFIIB-Recognition Element (BRE), and Motif Ten Element (MTE). The DCE element is shown on a separate bar for illustration only. Presumably, the DCE element is not present in core promoters containing the MTE and/or DPE element. The indicated positions are relative to the start codon and reflect the region in which the first nt of the respective element is typically located. Regulatory elements up to 1kb upstream the core promoter are summarized as the proximal promoter. The core and the proximal promoter are often combined as "promoter". Distal regulatory elements (including locus control region (LCR), insulators, silencers, and enhancers) are all elements which regulate the respective gene of interest and are located outside the 1kb promoter. Enhancers (stimulating) and silencers (repressing) can influence target gene transcription independent of their location (upstream/downstream) or orientation (*cis*/*trans*) in an additive manner (Shlyueva *et al*. 2014). kb: Kilobase; N: Any nucleotide. (Figure adapted from Maston *et al*. 2006).

DNA. All protein coding genes (and also some noncoding RNAs (ncRNAs) and micro RNAs (miRNAs)) are transcribed by Pol II into messenger RNAs (mRNAs) (Hsin and Manley 2012). The regulatory information necessary for Pol II to initiate transcription is encoded in the DNA sequence upstream of the gene´s coding region termed promoter (Hernandez-Garcia and Finer 2013). Gene

promoters contain multiple *cis*-acting protein binding sites which provide the code that dictates when, where, and at what level specific genes are transcribed (Fuda *et al*. 2009). Promoters are typically partitioned into the core promoter, the proximal promoter, and the enhancer- and/or silencer-containing distal promoter (Maston *et al*. 2006; Fig. 4). As they are not relevant for this thesis, the locus control regions (LCR) and insulator elements found in distal promoters will not be addressed further (For review see Maston *et al*. 2006). The core promoter is defined as the genomic sequence in the immediate vicinity of the transcription start site (TSS) which is sufficient to assemble the Pol II machinery (Fuda *et al*. 2009). Because the Pol II itself is not able to recognize the TSS, core promoters contain distinct DNA-binding elements in various combinations that orchestrate the assembly of the preinitiation complexes (PICs) composed of the general transcription factors (GTFs) TFIID, TFIIA, TFIIB, TFIIF, TFIIH, and TFIIE and their coactivators to navigate the Pol II to the TSS (Narlikar and Ovcharenko 2009; Fig. 5). The most common core promoter elements are the TATA box (also named the Goldberg-Hogness box after its discoverers), the Initiator element (Inr), the Downstream Promoter Element (DPE), the Downstream Core Element (DCE), TFIIB-Recognition Element (BRE), and Motif Ten Element (MTE) (Roy and Singer 2015; Fig. 4). With the exception of the BRE, which is specifically recognized by TFIIB, all other core promoter elements described are TFIID-interaction sites (Maston *et al*. 2006). Although several of these interchangeable elements have been identified, growing evidence from genome-wide studies shows that many genes do not have any of these core promoter elements, e. g. only 5-7% of eukaryotic and less than 10% of human promoters contain a TATA box (Roy and Singer 2015). Independent of the core promoter composition, the binding of the multisubunit complex TFIID is the first step in the sequential PIC assembly (Maston *et al*. 2006; Fig. 5A). The prototypic TFIID complex consists of the TATA-box-binding protein (TBP) and a set of TBP-associated factors (TAFs) (Maston *et al*. 2006). An increasing number of cell type-specific and gene-selective homologs of TFIID components, including additional members of the TBP family such as TBP-related factors (TRFs) as well as numerous tissue-specific homologs of TAFs, allow PIC assembly in cases where core promoter elements like the TATA box are lacking (Hochheimer and Tjian 2003). Stability of the promoter bound TFIID is then reinforced by binding of TFIIA and TFIIB to TBP (Bywater *et al.* 2013). TFIIB can also contribute to TFIID stability by binding to adjacent BRE elements (Luse 2014). Another crucial function of TFIIB is the loading of the Pol II-TFIIF complex into the PIC (Luse 2014). As interactions between Pol II-TFIIB and TFIIF-TFIIB put the DNA near the active site of Pol II, TFIIB is suggested to be responsible for

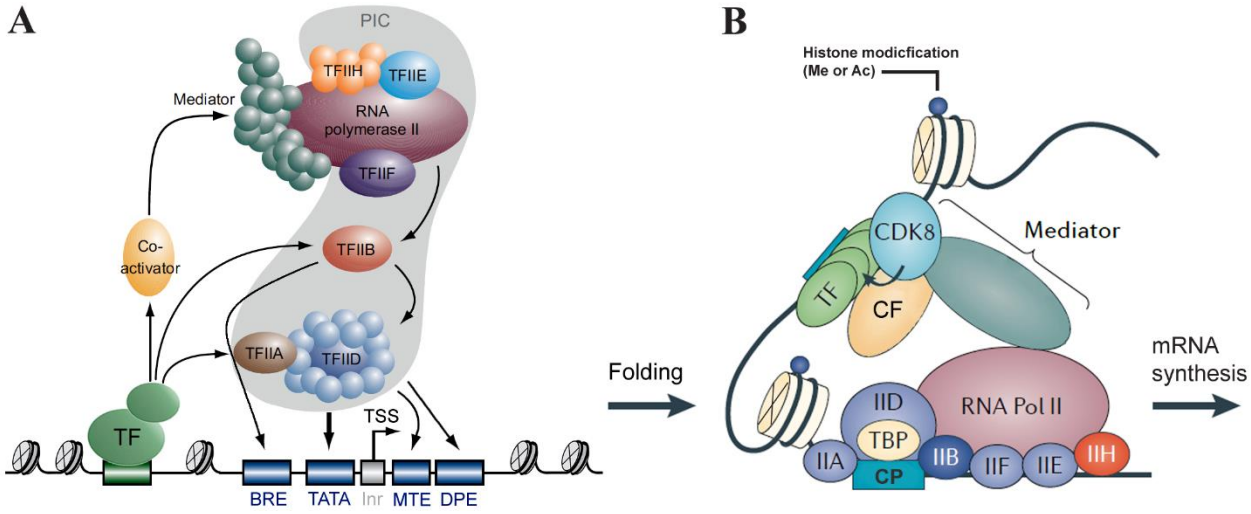

Fig. 5 Assembly of the Pol II preinitiation complex and its association with other activators to initiate transcription. (A) The preinitiation complex (PIC) is sequentially assembled by the general transcription factors (GTFs) TFIID, TFIIA, TFIIB, TFIIF, TFIIH, and TFIIE on the core promoter (For details on the BRE, TATA, Inr, MTE, and DPE elements see Fig. 4). The PIC serves as a platform to guide in cooperation with DNA-bound transcription factors (TF), their coactivators, and regulatory complexes (e. g. the mediator complex) the RNA polymerase II to the transcription start site (TSS). **(B)** For proper transcription the regulatory signals from distant bound TFs and the PIC have to be integrated. This is achieved by the multi-subunit Mediator complex via formation of a "gene-loop" that juxtaposes the proximal and distal promoter regions with the core promoter. The Mediator complex also contains regulatory subunits like the CDK8 (cyclin-dependent kinase 8) module to influence the activating or repressing action of DNA-bound TFs via phosphorylation. The regulatory elements are made accessible by reversible histone modification (Me: Methylation; Ac: Acetylation; Ch. 1.3.2). Figures adapted from Maston *et al*. (2006) in (A) and Bywater *et al.* (2013) in (B).

TSS selection (Kornberg 2007). PIC assembly is completed by recruitment of TFIIE and TFIIH. The DNA-binding factor TFIIE is primarily considered to be the loading factor for the TFIIH helicase complex but also promotes transcription and DNA melting on TFIIH-independent promoters (Luse 2014). The assembled PIC can only initiate low levels of transcription (basal transcription) (Maston *et al*. 2006). The major impact on transcriptional activity is conferred by sequence-specific DNA-binding proteins termed transcription factors (TFs) which bind alone, as dimers, or in complexes to their cognate recognition elements in the proximal promoter regions or to enhancers and silencers (Maston *et al*. 2006). These TF-binding sites are modular and degenerated 6-12bp recognition sequences, although binding specificity is usually dictated by no more than 4–6 positions within the site (Maston *et al*. 2006). Most TFs can be grouped according to their conserved DNA-binding domains like cysteine-rich zinc finger, homeobox, helix-loop-helix (HLH), or basic leucine zipper (bZIP) DNA-binding domain (Maston *et al*. 2006). In

eukaryotes the transcription of a target gene is rarely controlled by a single TF, but rather by the integration of different cooperative TF binding events (Narlikar and Ovcharenko 2009). To effectively stimulate transcription, TFs normally contain a separable activation domain to interact with the PIC and/or further coactivator molecules or regulatory complexes (Maston *et al*. 2006). The most important regulator found at almost all Pol II-dependent eukaryotic promoters is the multisubunit Mediator complex (Conaway and Conaway 2011), which cooperates with cohesin to form the "gene loop" (Fig. 5B) (Poss *et al*. 2013). This loop juxtaposes the occupied distal, proximal, and core promoter regions and allows the establishment of protein-protein interactions between the distantly bound TFs and the PIC components to relay and to integrate all regulatory signals needed for proper transcription initiation (Poss *et al*. 2013). Besides its scaffolding functions, the Mediator complex can positively and negatively influence TF signals in a gene- and context-specific manner through phosphorylation using its CDK8 (cyclin-dependent kinase 8) module (Poss *et al*. 2013). If the regulatory complex was established correctly, the transcription cycle proceeds through a series of steps, including promoter melting, Pol II clearance and escape, before a fully functional RNA polymerase II elongation complex is formed (Maston *et al*. 2006). The exact mechanism of transcription termination is still not understood in detail (Porrua and Libri 2015). The current model suggests that termination requires *cis*-acting DNA elements like an intact polyadenylation (polyA) signal and is coupled to Pol II-dependent 3´-end processing of the pre-mRNA via the cap-binding complex (CBC)-ARS2 pathway (Porrua and Libri 2015).

2 Aims of this thesis

The human *NOT* gene (Kaymer and Kurzik-Dumke 1997) is the homologue of the *l(2)not* gene which has been originally identified in *Drosophila* (Kurzik-Dumke *et al*. 1997). The elucidation of the cellular functions of the human NOT proteins is subject of current research in the Kurzik-Dumke group. The relevance of the NOT proteins in tumorous growth has been suggested by altered *NOT* expression patterns in diverse cancers and tumor cells. The identification of 17 physiological binding partners of NOT, among them essential components of the MEK-ERK, Hedgehog (Hh)/Patched (Ptc) and PI3K-AKT-mTOR signaling pathways (Hacker and Kurzik-Dumke, personal communication; B. Hacker, PhD thesis: Beitrag zur Aufklärung der zellulären Rolle des humanen *neighbour of tid* (*not*) Gens, 2016) supports this finding. The above data substantiate the necessity to elucidate the yet unknown regulatory mechanisms controlling the expression of the *NOT* gene in a cell-specific manner. In this context, the subject of this thesis is the identification of proteins binding the promoter of the human (h) and murine (m) *NOT* gene. Potential transcription factor binding sites within a putative 1.15kb promoter region of h and m *NOT* are first predicted by bioinformatics tools. Furthermore, the binding sites for the factors identified are then confirmed using *in vitro* and *in vivo* DNA-binding assays. In addition, the functional relevance of the detected protein-DNA interactions for *NOT* transcription *in vivo* is assessed by pharmacological manipulation or biological depletion of the identified transcription factors or of essential signaling components regulating their activity. The results of the experiments will provide the first insight into the cell-specific regulation of the *NOT* gene.

3 Materials and Methods

3.1 Chemicals, consumable supplies, solutions and media

3.1.1 Chemicals

Acetic acid glacial 100% ($C_2H_4O_2$)	Carl Roth GmbH & Co. KG, Karlsruhe
Acrylamid/Bisacrylamid (37.5:1)	Carl Roth GmbH & Co. KG, Karlsruhe
L-adenine hemisulfate	Sigma-Aldrich, Steinheim
L-arginine HCl	Sigma-Aldrich, Steinheim
Agar-Agar	Carl Roth GmbH & Co. KG, Karlsruhe
Agarose NEO Ultra-Quality	Carl Roth GmbH & Co. KG, Karlsruhe
AgaroseTM LE GQ (low electroendosmosis)	Thermo Scientific GmbH, Dreieich
6-Aminohexan acid	Merck KGaA, Darmstadt
3-Amino-1,2,4-triazole (3-AT)	Carl Roth GmbH & Co. KG, Karlsruhe
Ammonium peroxosulphate (APS)	Carl Roth GmbH & Co. KG, Karlsruhe
Ampicillin	Carl Roth GmbH & Co. KG, Karlsruhe
Boric acid ($H_3BO_{3)}$	Carl Roth GmbH & Co. KG, Karlsruhe
Bovine Serum Albumin (BSA)	Sigma-Aldrich, Steinheim
5-Bromo-4-chloro-3-indolyl phosphate (BCIP)	Sigma-Aldrich, Steinheim
Bromophenol blue	Carl Roth GmbH & Co. KG, Karlsruhe
Buffer solution pH 4.00 ± 0.02 (20 °C)	Carl Roth GmbH & Co. KG, Karlsruhe
Buffer solution pH 7.00 ± 0.02 (20 °C)	Carl Roth GmbH & Co. KG, Karlsruhe
Buffer solution pH 9.00 ± 0.02 (20 °C)	Carl Roth GmbH & Co. KG, Karlsruhe
1-Butanol ($C_4H_{10}O$)	Carl Roth GmbH & Co. KG, Karlsruhe
Caffeine (1,3,7-Trimethylxanthine; $C_8H_{10}N_4O_2$)	Sigma-Aldrich, Steinheim
Calcium chloride dihydrate ($CaCl_2 \cdot 2\ H_2O$)	Carl Roth GmbH & Co. KG, Karlsruhe
Chloramphenicol	Carl Roth GmbH & Co. KG, Karlsruhe
cOmplete Protease Inhibitor Cocktail Tablets	Roche Pharma AG, Grenzach-Wyhlen
Deoxynucleotidtriphosphate Mix (dNTPs)	Thermo Scientific GmbH, Dreieich
N,N-Dimethyl formamide (DMF)	Carl Roth GmbH & Co. KG, Karlsruhe
Diethanolamine ($HN(CH_2CH_2OH)_2$)	
Dimethyl sulfoxide (DMSO)	Sigma-Aldrich, Steinheim

Disodium hydrogen phosphate heptahydrate ($Na_2H_2PO_4 \cdot 7\ H_2O$)	Merck KGaA, Darmstadt
1,4-Dithiothreitol ((*2S,3S*)-1,4-bis(sulfanyl) butane-2,3-diol; $C_4H_{10}O_2S_2$)	Carl Roth GmbH & Co. KG, Karlsruhe
Ethidium bromide (EtBr)	Carl Roth GmbH & Co. KG, Karlsruhe
Ethanol absolute, ≥99.8 % (C_2H_6O)	Carl Roth GmbH & Co. KG, Karlsruhe
Ethanol denatured, ≥99.8 % (C_2H_6O)	Carl Roth GmbH & Co. KG, Karlsruhe
Ethylenediaminetetraacetic acid (EDTA)	Carl Roth GmbH & Co. KG, Karlsruhe
Formaldehyde sol. 37%	Carl Roth GmbH & Co. KG, Karlsruhe
D(+)-Glucose monohydrate ($C_6H_{12}O_6 \cdot H_2O$)	Merck KGaA, Darmstadt
Glycerol ($C_3H_8O_3$)	Carl Roth GmbH & Co. KG, Karlsruhe
Glycine ($C_2H_5O_2$)	Carl Roth GmbH & Co. KG, Karlsruhe
HEPES (4-(2-hydroxyethyl)-1-piperazine-ethanesulfonic acid; $C_8H_{18}N_2O_4S$)	Carl Roth GmbH & Co. KG, Karlsruhe
Herring testes carrier DNA (10mg/ml)	Carl Roth GmbH & Co. KG, Karlsruhe
HiPerFect Transfection Reagent	Qiagen, Hilden
L-histidine HCl monohydrate	Sigma-Aldrich, Steinheim
Hydrochloric acid 37 % (HCl)	Carl Roth GmbH & Co. KG, Karlsruhe
I-Block™ Protein-Based Blocking Reagent	Life Technologies GmbH, Darmstadt
L-isoleucine	Sigma-Aldrich, Steinheim
Kanamycin	Carl Roth GmbH & Co. KG, Karlsruhe
L-leucine	Sigma-Aldrich, Steinheim
Lithium acetate dihydrate	AppliChem GmbH, Darmstadt
Lithium chloride (LiCl)	Carl Roth GmbH & Co. KG, Karlsruhe
L-lysine	Sigma-Aldrich, Steinheim
Magnesium chloride hexahydrate ($MgCl_2 \cdot 6\ H_2O$)	Merck KGaA, Darmstadt
Manganese(II)-chloride tetrahydrate ($MnCl_2 \cdot 4\ H_2O$)	Carl Roth GmbH & Co. KG, Karlsruhe
2-Mercaptophenol (C_2H_6OS)	Sigma-Aldrich, Steinheim
Methanol (CH_4O)	Carl Roth GmbH & Co. KG, Karlsruhe
L-methionine	Sigma-Aldrich, Steinheim

MOPS (3-(N-morpholino)propane-sulfonic acid; $C_7H_{15}NO_4S$)	Carl Roth GmbH & Co. KG, Karlsruhe
Nitroblue tetrazolium chloride (NBT)	Sigma-Aldrich, Steinheim
Nitrogen (N2), liquid	Linde AG, Wiesbaden
p-Nitrophenyl phosphate (pNPP) tablets	Sigma-Aldrich, Steinheim
Nonidet P-40 (NP-40) / IGEPAL CA-630	Sigma-Aldrich, Steinheim
Parthenolide ($C_{15}H_{20}O_3$)	Sigma-Aldrich, Steinheim
Penicillin/Streptomycin	Sigma-Aldrich, Steinheim
Phenol/Chloroform/Isoamyl alcohol (25:24:1)	Carl Roth GmbH & Co. KG, Karlsruhe
L-phenylalanine	Sigma-Aldrich, Steinheim
Phenylmethylsulfonyl fluoride (PMSF)	Active Motif, La Hulpe (Belgium)
Poly(deoxyinosinic-deoxycytidylic) (dIdC)	Santa Cruz Biotechnology, Heidelberg
Polyethylene glycol wt 3.350 (PEG)	Sigma-Aldrich, Steinheim
Potassium chloride (KCl)	Carl Roth GmbH & Co. KG, Karlsruhe
2-Propanol	Carl Roth GmbH & Co. KG, Karlsruhe
Rubidium chloride (RbCl)	Carl Roth GmbH & Co. KG, Karlsruhe
SDS ultra-pure (Natriumdodecylsulfate)	Carl Roth GmbH & Co. KG, Karlsruhe
Skim Milk	Sigma-Aldrich, Steinheim
Sodium acetate ($C_2H_3NaO_2$)	Carl Roth GmbH & Co. KG, Karlsruhe
Sodium chloride (NaCl)	Carl Roth GmbH & Co. KG, Karlsruhe
Sodium dihydrogen phosphate dihydrate ($NaH_2PO_4 \cdot 2\ H_2O$)	Carl Roth GmbH & Co. KG, Karlsruhe
Sodium hydroxide (NaOH)	Carl Roth GmbH & Co. KG, Karlsruhe
TEMED (N,N,N',N'-Tetramethylethylendiamin; $C_6H_{16}N_2$)	Carl Roth GmbH & Co. KG, Karlsruhe
L-threonine	Sigma-Aldrich, Steinheim
Trichlormethane / Chloroform ($CHCl_3$)	Carl Roth GmbH & Co. KG, Karlsruhe
TRIS (2-Amino-2-hydroxymethyl-propane -1,3-diol; $C_4H_{11}NO_3$)	Carl Roth GmbH & Co. KG, Karlsruhe
Trisodium citrate dihydrate ($Na_3HC_6H_5O_7 \cdot 2\ H_2O$)	Carl Roth GmbH & Co. KG, Karlsruhe
TRIzol® Reagent	Life Technologies GmbH, Darmstadt

Trypane blue solution, 0.4%	Life Technologies GmbH, Darmstadt
Tryptone/Peptone from Casein	Carl Roth GmbH & Co. KG, Karlsruhe
L-tryptophan	Sigma-Aldrich, Steinheim
Tumor necrosis factor α (TNFα)	Sigma-Aldrich, Steinheim
Tween 20 (Polyoxyethylene (20) sorbitan monolaurate; $C_{58}H_{114}O_{26}$)	Carl Roth GmbH & Co. KG, Karlsruhe
L-tyrosine	Sigma-Aldrich, Steinheim
L-uracil	Sigma-Aldrich, Steinheim
L-valine	Sigma-Aldrich, Steinheim
X-gal (5-Bromo-4-chloro-3-indolyl β-D-galacto-pyranoside; $C_{14}H_{15}BrClNO_6$)	Sigma-Aldrich, Steinheim
Xylene cyanol	Carl Roth GmbH & Co. KG, Karlsruhe
Yeast extract	Carl Roth GmbH & Co. KG, Karlsruhe
Yeast Nitrogene Base w/o Amino Acids	Becton Dickinson GmbH, Heidelberg
Zinc chloride ($ZnCl_2$)	Carl Roth GmbH & Co. KG, Karlsruhe

3.1.2 Consumable supplies

Biodyne® Nylon Transfer Membranes	Pall GmbH, Dreieich
Cell culture dishes with vents Ø90mm, Ø140mm	Greiner Bio-One GmbH, Frickenhausen
Cell culture dishes Ø100 mm / 60 cm^2 and Ø 150 mm / 147,8 cm^2; non-pyrogenic	Greiner Bio-One GmbH, Frickenhausen
Cell culture flasks 75cm^2; non-pyrogenic	Greiner Bio-One GmbH, Frickenhausen
Cell scrubbers 20cm	Biochrom AG, Berlin
Centrifuge tubes 15ml, 50ml	Greiner Bio-One GmbH, Frickenhausen
Centrifuge tubes 50ml	Greiner Bio-One GmbH, Frickenhausen
Disposable cuvettes	VWR International GmbH, Darmstadt
Glass beads acid-washed, 425-600 microns	Sigma-Aldrich, Steinheim
Gloves, nitrile	VWR International GmbH, Darmstadt
MicroAmp® Optical Adhesive Film	Life Technologies GmbH, Darmstadt
Microplate, 96well, PS, Streptavidin-coated	Greiner Bio-One GmbH, Frickenhausen
Nunc Cryo tubes 2ml	Thermo Scientific GmbH, Dreieich

Parafilm® M	Carl Roth GmbH & Co., Karlsruhe
PCR PP-plate for ABI, 384er/96er well	Greiner Bio-One GmbH, Frickenhausen
Pipette tips (10µl, 200µl, 1000µl)	Starlab GmbH, Ahrensburg
PP disposable bags	Carl Roth GmbH & Co., Karlsruhe
PP-Safe-lock Reaction tubes (0.2ml, 1.5ml, 2ml)	Eppendorf AG, Hamburg
PP PCR tubes, thin wall 8-strip, 0.2ml	Thermo Scientific GmbH, Dreieich
Roti®-PVDF membrane	Carl Roth GmbH & Co., Karlsruhe
Serological pipettes (1-25ml)	Greiner Bio-One GmbH, Frickenhausen
Siliconized reaction tubes, 1.7ml	Active Motif, Belgium
Single-use syringes	B. Braun AG, Melsungen
Sterile syringe filter 0.2µm, 0.45µm	Schleicher & Schüll GmbH, Dassel
Whatman filter paper 3MM	VWR International GmbH, Darmstadt
X-ray film Fuji SuperRX X-Ray 30x40cm	Sigma-Aldrich, Steinheim

3.1.3 Equipment

Centrifuges:

Eppendorf 5415R	Eppendorf AG, Hamburg
Mikro Rapid/K	Hettich GmbH & Co. KG, Tuttlingen
Sigma 3K20	Sigma Laborzentrifugen GmbH, Osterode

Gel electrophoresis units:

Electrophoresis chamber Horizon 11.14	Analytik-Jena AG, Jena
SE 250 Mighty SmaII II	Hoefer, Inc., USA
SE 245 Dual Gel Caster	Hoefer, Inc., USA

Incubators:

Incubater KBW 720	Binder GmbH, Tuttlingen
Mini CO_2 incubator	CellStar, Midland (Canada)

Laminar airflows:

Laminar airflow cabinet Lamin Air HLP 2472 GS / HB 2472	Heraeus, Hanau

Laminar Flow Box antairBSK	Kendro, Langenselbold

Magnetic stirrers:

Ikamag RCT	Janke & Kunkel GmbH, Staufen
MR 2002	Heidolph Instruments GmbH, Schwabach

Microscopes:

Light optical microscope	Leitz, Wetzlar
Light optical microscope Olympus IM	Olympus, Japan

Photometer:

Bio Photometer	Eppendorf AG, Hamburg
NanoDrop 1000 V3.7	PeqLab, GmbH, Erlangen
Spectrophotometer Novaspec 4049	LKB Biochrom, England

Pipettes:

Abimed (variable)	Abimed Analysentechnik GmbH, Langenfeld
Finnpipette (variable)	Thermo Scientific GmbH, Dreieich
PIPETBOY acu 2 Integra	VWR International GmbH, Darmstadt
Research (variable)	Eppendorf AG, Hamburg

Power supply units:

Phero-Stab 200	Biotech-Fischer GmbH, Reiskirchen
E425	Biotech-Fischer GmbH, Reiskirchen
Electrophoresis Power Supply EPS 3500	Pharmacia Biotech, Schweden

Scales:

Precision scale 510-37	Kern & Sohn GmbH, Balingen
Analytic scale A120S	Sartorius AG, Göttingen

Thermocyclers / (qRT-) PCR machines:

ABI PRISM 7900HT-Fast RT-PCR System	Life Technologies GmbH, Darmstadt

Thermocycler Mastercycler gradient 5531	Eppendorf AG, Hamburg
Thermocycler	VWR International GmbH, Darmstadt

Vortexer:

VF-2	IKA Werke GmbH & Co. KG, Staufen
Reax 2000	Heidolph Instruments GmbH, Schwabach

Water baths:

2219 Multitemp II – Thermostatic Circulator	LKB Bromma, Schweden
Julabo P	Julabo Labortechnik GmbH, Seelbach
Schüttelwasserbad 3047	Köttermann AG, Laboreinrichtungen

Others:

Autoklave Systec V-150	Systec GmbH, Wettenberg
Block Heater	Stuart Scientific, Surrey, USA
Blotter, semi-dry Novoblot Electrophoretic	Pharmacia/LKB, Freiburg
ELISA plate reader	
Gel documentation system	Biostep GmbH, Jahnsdorf
Mikrowave oven Lunik 200	Aldi, Mühlheim
Nalgene 5100 Cryo 1°C Freezing Container	Thermo Fisher Scientific GmbH, Dreieich
pH meter pH526	Labotec Labortechnik Vertriebs GmbH, Wiesbaden
Rotator Reax2	Heidolph Instruments GmbH & Co. KG, Schwabach
Shaker Certomat IS	Sartorius AG, Göttingen
Shaker MaxQ	Thermo Fisher Scientific GmbH, Dreieich
Synergy Ultrapure Water Systems	Millipore GmbH, Schwalbach
UV-Crosslinker BLX-254 BIO-LINK 254 nm	Vilber Lourmat, Eberhardzell

3.1.4 Computer hardware and software

Adobe Photoshop CS2/3	Adobe Systems GmbH

Chromas 2.3	Technelysium Pty Ltd.
FastPCR Professional v.5.2.18	Primer Digital Ltd.
Geldocumentation software Phoretix Grabber	(NonLinear Dynamics)
Jellyfish software v1.5_5689	BioWire
Microsoft Office Word 2007	Microsoft Deutschland GmbH
Microsoft Office Excel 2007	Microsoft Deutschland GmbH
SDS 2.4 RT-PCR System Software	Life Technologies GmbH, Darmstadt
Scanner Canon MP630	Canon Deutschland GmbH, Krefeld

3.1.5 Buffers and solutions

All buffers and solutions were dissolved in autoclaved type I H_2O (filtered at 18.2 MΩ • cm, 25°C, "*ultra-pure water*") and stored at RT unless noted otherwise.

Tab. 4 Buffers and solutions used for DNA/RNA isolation, purification and electrophoresis

Name	Components/Storage
EB buffer	Tris/HCl (pH 8.5), 10mM
Loading Dye, 6x	Brompehnol blue, 0.03% (w/v) Xylene Cyanol FF, 0.03% (w/v) Glycerol, 60% (w/v) SDS, 1% (w/v) EDTA, pH 7.6, 1% (v/v) storage at +4°C
Solution I **(Resuspension buffer)**	Tris/HCl (pH 8), 50mM EDTA, 10mM
Solution II **(Lysis buffer)**	NaOH, 0.2M SDS, 1% (w/v)
Solution III **(Neutralization buffer)**	KAc, 3M pH 5.5 with acetic acid glacial
TAE, 50x	Tris/HCl, 40mM Acetic acid glacial, 20mM 0.5M EDTA (pH 8.0), 1mM
TE buffer (10x)	Tris/HCl (pH 8.5), 100mM EDTA, 10mM
Tricine-EDTA buffer **(Clontech)**	Tricine-KOH pH 8.5, 10mM EDTA, 1mM

Tab. 5 Buffers and solutions used for Y1H / Y2H

Name	Components/Storage
10x Drop-out solution **(omit aa(s) to be "dropped out")**	L-adenine hemisulfate, 200mg/L L-arginine HCl, 200mg/L L-histidine HCl monohydrate, 200mg/L L-isoleucine, 300mg/L L-leucine, 1000mg/L L-lysine HCl, 300mg/L L-methionine, 200mg/L L-phenylalanine, 500mg/L L-threonine, 2000mg/L L-tryptophane, 200mg/L L-tyrosine, 300mg/L L-uracil, 200mg/L L-valine, 1500mg/L storage at 4°C
LiAc buffer, 10x	Lithium acetate, 1M set pH 7.5 with HCl
PEG/LiAc solution (10ml)	PEG 3350, 40% (w/v) TE-Puffer 1x LiAc buffer, 1x
TE/LiAc solution, 1x	LiAc buffer, 2.5x TE buffer, 2.5x
X-gal stock solution	X-gal, 20mg/ml in dimethylformamide storage at -20°C, dark
Z buffer	Na_2HPO_4, 100mM NaH_2PO_4, 50mM KCl, 10mM Mg_2SO_4, 1mM set pH 7.0 with HCl and autoclave
Z buffer / X-gal **(X-gal staining solution)**	Z buffer, 100ml 2-mercaptoethanol, 0.27ml X-gal stock solution, 1.67ml

Tab. 6 Buffers and solutions used for western blot

Name	Components/Storage
Anode I buffer	Tris/HCl pH 10.4, 25mM Methanol, 20% (v/v)
Anode II buffer	Tris/HCl pH 10.4, 300mM Methanol, 20% (v/v)
BCIP stock solution	BCIP, 5% in dimethylformamide storage at -20°C, dark
Blocking buffer	I-Block, 2% (w/v) in PBS Tween-20, 0.1% (w/v)
Cathode buffer	Tris/HCl pH 9.4, 25mM Methanol, 20% (v/v) 6-Aminohexanoic Acid, 60mM
Laemmli buffer, 5x	Tires/HCl, 0.15M SDS, 5% (w/v) 2-mercaptoethanol, 3% (v/v) Glycerol, 25% (w/v) Bromophenol blue, 0.05% (w/v) set pH 6.8 with HCl storage at -20°C
Lower Tris, 4x (denaturing)[1]	Tris/HCl, 1.5M SDS, 0.4% (w/v) set pH 8.8 with HCl
NBT stock solution	NBT, 5% in dimethylformamide (70%) storage at -20°C, dark
PBS	NaCl, 137mM KCl, 2.7mM Na_2HPO_4, 10mM KH_2PO_4, 2mM set pH 7.4 with HCl
PBST	PBS + Tween20, 0.1% (v/v)
SDS running buffer	Tris/HCl, 25mM Glycine, 192mM SDS, 0.1% (w/v)
Staining Solution	NBT stock, 66µl BCIP stock, 44µl TBS, 10ml
Upper Tris, 4x (denaturing)[1]	Tris/HCl, 0.5M SDS, 0.4% (w/v) set pH 6.8 with HCl

1: For native gels the SDS was omitted (Ch. 3.4.3.4)

Tab. 7 Buffers and solutions used for colony blot

Name	Components/Storage
Blocking buffer	BSA, 0.3% (w/v) in TBS
Denaturing solution II	NaCl, 1.5M NaOH, 500mM
Neutralization solution	NaCl, 1.5M Tris/HCl, 500mM set pH 7.4 with NaOH
Denaturing solution I	SDS, 10% (w/v)
SSC, 20x	NaCl, 3M Trisodium citrate · 2 H_2O, 300mM
TBS	Tris, 100mM NaCl, 100mM MgCl2, 5mM set pH 9.5 with HCl
TBST	TBS + Tween-20, 0.1% (w/v)

Tab. 8 Buffers and solutions used for protein and chromatin isolation

Name	Components/Storage
Cell Scraping Solution	PBS, 1x PMSF, 0.5mM
Fixation Solution	Formaldehyde, 1% (v/v) in cell culture medium
Glycine Stop-Fix Solution	Glycine Buffer, 1x (Active Motif) PBS, 1x
PBS, 10x	NaCl, 1.37M KCl, 27mM Na_2HPO_4, 100mM KH_2PO_4, 18mM
TKM/NP40 lysis buffer	Tris/HCl, 50mM pH7.5 KCl, 150mM $MgCl_2$, 5mM NP-40/IGEPAL CA-630, 1% (w/v) cOmplete Protease Inhibitor Cocktail

Tab. 9 Buffers and solutions used for EMSA

Name	Components/Storage
CREB binding buffer	Tris/HCl pH 7.6, 20mM $MgCl_2$, 10mM NaCl, 120mM Glycerol, 5% (w/v) DTT, 0.4% (w/v) BSA, 10ng/ml dIdC, 50ng/µl
EGR-1 binding buffer	HEPES pH 7.5, 25mM $MgCl_2$, 12.5mM KCl, 70mM $ZnCl_2$, 10µM DTT, 1mM Glycerol, 5% (w/v) NP-40/IGEPAL CA-630, 0.1% (w/v) dIdC, 50ng/µl
EMSA Loading Dye, 3%	TBE, 1x Glycerol, 25% (w/v) Bromophenol blue, 0.05% (w/v)
Lower Tris, 4x (native)	Tris/HCl, 1.5M set pH 8.8 with HCl
MYCN binding buffer	PBS pH 7.4 BSA, 0.1% (w/v) Tween-20, 0.05% (w/v) dIdC, 50ng/µl
NFκB binding buffer	Tris/HCl, 10mM KCl, 100mM DTT pH 7.5, 1mM Glycerol, 5% (w/v) $MgCl_2$, 5mM NP-40/IGEPAL CA-630, 0.1% (w/v) dIdC, 50ng/µl
Upper Tris, 4x (native)	Tris/HCl, 0.5M set pH 6.8 with HCl
TBE, 5x	Tris/HCl, 450mM Boric acid, 450mM EDTA pH 8.3, 10mM

Tab. 10 Buffers and solutions for Southwestern blot and affinity chromatography using Dynabeads

Name	Components/Storage
B&W buffer, 2x	Tris/HCl pH 7.5, 10mM NaCl, 2M EDTA, 1mM Tween-20, 0.05% (w/v)
Coupling buffer	BSA, 0.1% (w/v) in PBS pH 7.4 Tween-20, 0.05% (w/v)
Renaturation buffer	Skim milk, 5% (w/v) in TNED
TNED	Tris/HCl pH 7.5, 10mM NaCl, 50mM EDTA, 0.1mM DTT, 1mM

3.1.6 Media and solutions for bacteria and yeast

All media were dissolved in autoclaved type I H_2O (filtered at 18.2 MΩ • cm, 25°C, "*ultra-pure water*") and stored at 4°C unless noted otherwise.

Tab. 11 Media used for cultivation of yeast cells

Name	Components/Storage
SD medium	Yeast nitrogen base w/o aa, 6.7g/L set pH 5.8 with 10M NaOH Dropout Solution (10x), 10% (v/v) Autoclave Glucose, 2% (v/v), sterile-filtered
SD agar	Yeast nitrogen base w/o aa, 6.7g/L Agar, 2g/L Dropout Solution (10x), 10% (v/v) set pH 5.8 with 10M NaOH Autoclave Glucose, 2% (v/v), sterile-filtered
YPD medium	Peptone, 20g/L Yeast extract, 10g/L set pH 6.5 with HCl Glucose, 2% (v/v), sterile-filtered
YPDA medium	YPD medium Adenine hemisulfate (0.2%), 15ml

Tab. 12 Media and solutions for generation and cultivation of competent bacterial cells

Name	Components/Storage
LB (*Luria Bertani*) medium	Tryptone/peptone, 10g/L Yeast extract, 5g/L NaCl, 10g/L set pH 7.5 with 10M NaOH storage at 4°C
LB (*Luria Bertani*) agar	Tryptone/peptone, 10g/L Yeast extract, 5g/L NaCl, 10g/L Agar, 15g/L set pH 7.5 with 10M NaOH storage at 4°C
RF1 solution	RbCl, 100mM $MnCl_2$, 50mM Potassium acetate, 30mM $CaCl_2$, 10mM Glycerol, 15% (w/v) set pH 5.8 with 0.2M acetic acid filtered with 0.22µm filter storage at -20°C
RF2 solution	RbCl, 10mM MOPS, 10mM $CaCl_2$, 75mM Glycerol, 15% (w/v) set pH 6.8 with 0.2M acetic acid filtered with 0.22µm filter storage at -20°C
SOB medium	Tryptone/Peptone, 20g/L Yeast extract, 5g/L NaCl, 10mM KCL, 2.5mM $MgCl_2$, 10mM $MgSO_4$, 10mM set pH 7.5 with 10M NaOH
SOC medium	SOB medium Glucose, 20mM

3.1.7 Media and solutions for mammalian cell culture

All media were stored at 4°C with the exception of trypsin and fetal bovine serum (FBS) which was stored at -20°C. FBS was inactivated at 55°C for 30min.

Tab. 13 Media and solutions for mammalian cell culture

Name	Purchased from
BioFreeze Medium (DMSO-free)	Biochrom AG, Berlin
DMEM-F12 (with L-glutamine)	Sigma-Aldrich, Steinheim
EMEM (w/o L-glutamine)	Biochrom AG, Berlin
Fetal bovine serum (FBS) (EU-approved from South America)	Biochrom AG, Berlin
HEPES, 1M	Sigma-Aldrich, Steinheim
Non-essential amino acids solution, 100x	Sigma-Aldrich, Steinheim
PBS (w/o Ca^{2+} and Mg^{2+})	Sigma-Aldrich, Steinheim
Penicillin-Streptomycin Mix (10000u penicillin + 10mg/ml streptomycin in 0.9% NaCl)	Sigma-Aldrich, Steinheim
RPMI (with L-glutamine)	Sigma-Aldrich, Steinheim
Sodium pyruvate, 100mM	Sigma-Aldrich, Steinheim
Ultra-pure water	Biochrom AG, Berlin

3.2 Molecular biology tools

3.2.1 Enzymes

The enzymes which were used in the experiments are grouped according to their functional characteristics and activity. All enzymes were stored at -20°C with the exception of RNase T_1, which was stored at 4°C.

Tab. 14 Applied ribonucleases

Name	Cleavage activity	Purchased from
RNase A	ssRNA at C/U	Thermo Fisher, Dreieich
RNase H	RNA (only in RNA/DNA-hybrids)	Active Motif, La Hulpe (Belgium)
RNase T_1	ssRNA at G	Roche Diagnostic, Mannheim

Tab. 15 Applied restriction endonucleases

Name	Restriction site	Purchased from
***Bam*HI** (*Bacillus amyloliquefaciens*)	G^GATCC	Thermo Fisher, Dreieich
***Eco*RI** (*Escherichia coli* RY13)	G^AATTC	Thermo Fisher, Dreieich
***Nco*I** (*Nocardia corallina*)	C^CATGG	Thermo Fisher, Dreieich
***Sal*I** (*Streptomyces albus* G)	G^TCGAC	Thermo Fisher, Dreieich
***Sma*I** (*Serratia marcescens* Sb)	CCC^GGG	Thermo Fisher, Dreieich
***Sac*I** (*Streptomyces achromogenes*)	GAGCT^C	Thermo Fisher, Dreieich
***Xho*I** (*Xanthomonas vasicola*)	C^TCGAG	Thermo Fisher, Dreieich

Tab. 16 Applied polymerases

Name	Purchased from
Advantage 2 Polymerase Mix[1]	Clontech, Heidelberg
HotStarTaq *Plus* DNA Polymerase	Qiagen, Hilden
Klenow fragment (Large fragment of DNA polymerase I)	Thermo Fisher, Dreieich
MMLV reverse transcriptase (*Mouse Moloney murine leukemia virus*)	Clontech, Heidelberg
***Taq* DNA polymerase, recombinant**	Thermo Fisher, Dreieich
SuperScript™ II Reverse Transcriptase	Life Technologies, Darmstadt

1: Contains TITANIUM™ *Taq* DNA Polymerase and an undefined proofreading polymerase.

Tab. 17 Other applied enzymes

Name	Purchased from
FastAP™ (Thermosensitive Alkaline Phosphatase)	Thermo Fisher, Dreieich
DNase I (TURBO DNA-*free*™ Kit)	Life Technologies, Darmstadt
Proteinase K	Active Motif, La Hulpe (Belgium
T4 DNA ligase	Thermo Fisher, Dreieich

3.2.2 Vectors

Positive control vectors for one-hybrid experiments to identify *NOT* promoter binding proteins and to map their DNA-interacting domains were taken from the Matchmaker™ One-Hybrid Library Construction &Screening Kit (Fig. 6).

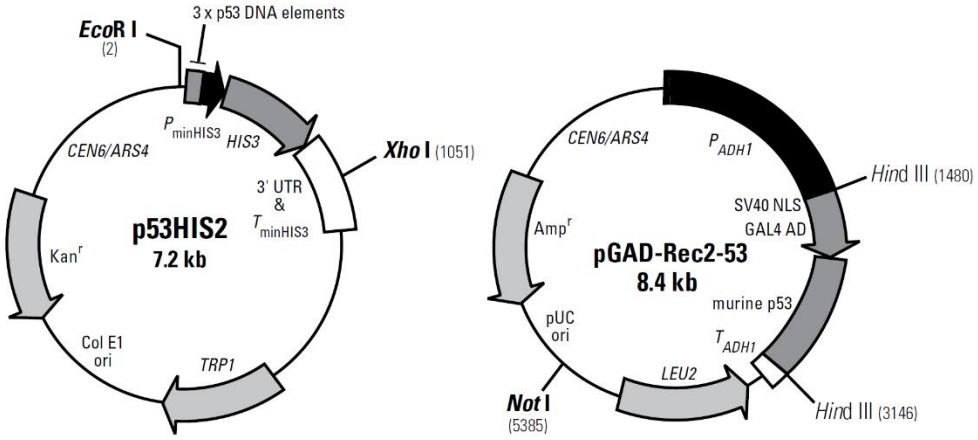

Fig. 6 Map of the control vectors p53HIS2 and pGAD-Rec2-53. The p53HIS2 vector is a derivative of pHIS2.1 (Fig. 11) and contains three tandem repeats of the consensus DNA binding sites for p53 upstream the minimal promoter of the *HIS3* reporter gene. p53HIS2 contains the *TRP1* reporter for selection in yeast and a kanamycin resistance gene (Kan^r) for selection in bacteria. The pGAD-Rec2-53 vector encodes a fusion of the GAL4 activation domain (AD) and partial p53 from mouse (aa73-391). pGAD-Rec2-53 contains the *LEU2* reporter for selection in yeast and an ampicillin resistance gene (Amp^r) for selection in bacteria. Both vectors contain an autonomous replication sequence (ARS4) and a centromeric sequence (CEN6).

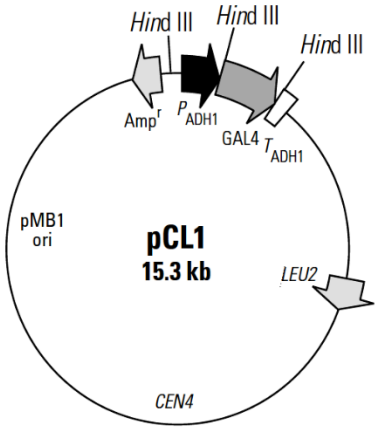

Fig. 7 Map of the vector pCL1. pCL1 is control plasmid encoding the full-length, wild-type GAL4 protein (Fields and Song 1989). GAL4 is a yeast transcription factor binding to the GAL4-responsive elements or upstream activating sequence (UAS). pCL1 is used as control in Y2H assays (Ch. 3.4.4).

NOT promoter fragments were synthesized as pBluescript II KS/SK (-) (Fig. 8) constructs.

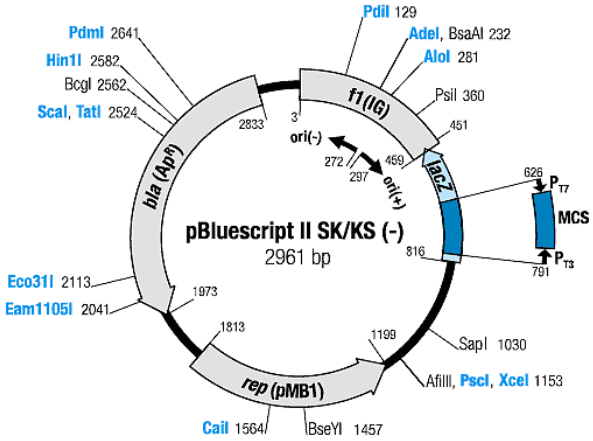

Fig. 8 Map of the phagemid vector pBluescript II SK/KS (-) (GenBank/EMBL: X52330). The 2961bp pBluescript II SK/KS (-) phagemid was used in cloning experiments. The MCS (626-701nt) is located within the *lacZ*-gene. The "(-)"-sign marks the orientation of the phage f1 intergenic region (IG; -5 to - 96nt), necessary for the direction of DNA synthesis starting at ori (-). Replication is driven by the pMB1 replicon and starts at position 1213nt. The *bla* (ApR) - gene confers resistance to ampicillin.

The full-length cDNA clone encoding EGR-1 (Ch. 3.2.7, Tab. 46) was cloned into pCMV-Sport6 (Fig. 9).

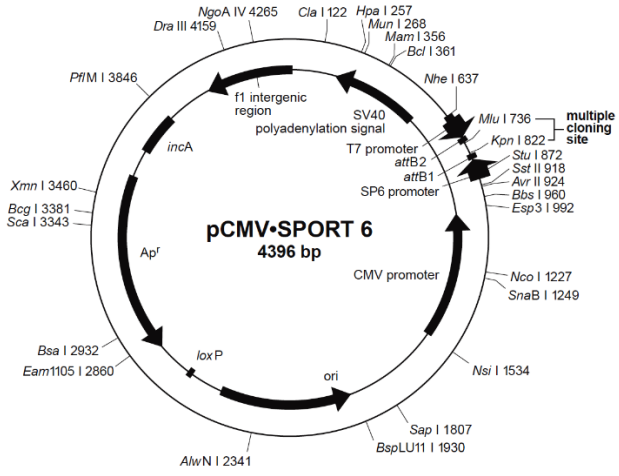

Fig. 9 Map of the phagemid vector pCMV-SPORT6. The 4396bp phagemid vector pCMV-SPORT6 allows ssDNA replication and packaging into phages and can be used as expression gateway vector. Expression is driven by the *human cytomegalovirus immediate-early gene* (CMV) promoter and stopped by the SV40 polyadenylation signal. T7 promoter and SP6 promoter are used for *in-vitro* transcription from both DNA strands. An ampicillin resistance gene (Ap^r) allows selection. The *incA* locus determines incompatibility with and exclusion of other *oriC* plasmids, assuring that only the pCMV-SPORT6 vector itself is maintained in the cell.

The full-length MYCN cDNA clone (Ch. 3.2.7, Tab. 46) was cloned into pOTB7 (Fig. 10).

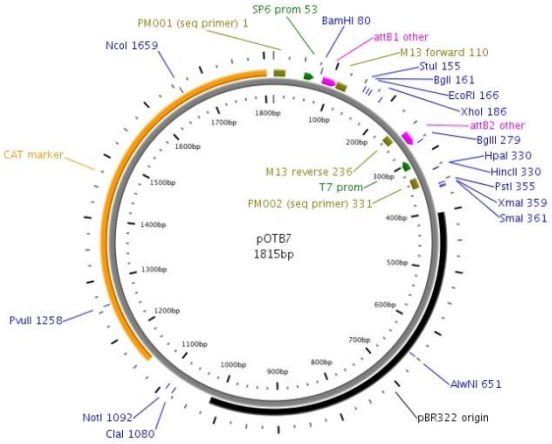

Fig. 10 Map of the gateway vector pOTB7. In the 1815bp pOTB7 vector (FlyBase ID: FBmc0002960) transcription of cloned DNA sequences is driven on the *sense*-strand by the SP6 promoter and on the *anti-sense*-strand by the T7 promoter. Replication in bacteria is driven by the pBR322 origin. The chloramphenicol acetyl transferase from *Staphylococcus aureu* (CAT protein) confers resistance to chloramphenicol.

All generated *NOT* promoter constructs (Ch. 3.3.14.1 and 3.3.14.2) were cloned into the pHIS2.1 vector (Fig. 11).

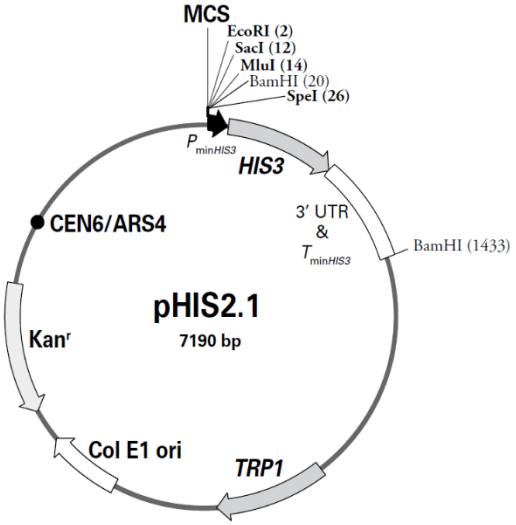

Fig. 11 Map of the reporter vector pHIS2.1 used in the yeast one-hybrid assays. The *bait* sequences were cloned into the multiple cloning site (MCS) (1-30nt) downstream the minimal promoter ($P_{minHIS3}$). The 7191bp vector contains the nutritional reporter gene *HIS3* (135-797nt). This gene encodes the imidazole-glycerol-phosphate dehydratase Hisp3 that catalyzes the transformation of D-erythro-1-(imidazol-4-yl) glycerol 3-phosphate to 3-(imidazol-4-yl)-2-oxopropyl phosphate and water, an essential step for histidine biosynthesis (Alifano *et al*. 1996). Upon *HIS3* activation auxotrophic Y187 cells can grow on media lacking histidine. *HIS3* transcription is stopped by the 3´-UTR and termination sequence ($T_{minHIS3}$; 798-1431nt). For replication and selection in yeast cells, the autonomous replication sequence (*ARS4*; 5723-6240nt) and the nutritional marker gene *TRP1* (2841-3515) necessary for tryptophane synthesis are integrated. The centromeric sequence (*CEN6*; 5723-6240) assures plasmid segregation during mitosis and meiosis (Sikorski and Hieter 1989). For replication and selection in bacteria, the vector contains the bacterial replication origin Col E1 ori (4150-4600nt) and a kanamycin resistance gene (Kan^r; 4794-5591nt).

Expression constructs for yeast experiments were cloned (Ch. 3.3.14 and Ch. 3.3.14.3 - 3.3.14.5) into the pACT2 (Fig. 12) and/or the pAS2-1 vector (Fig. 13).

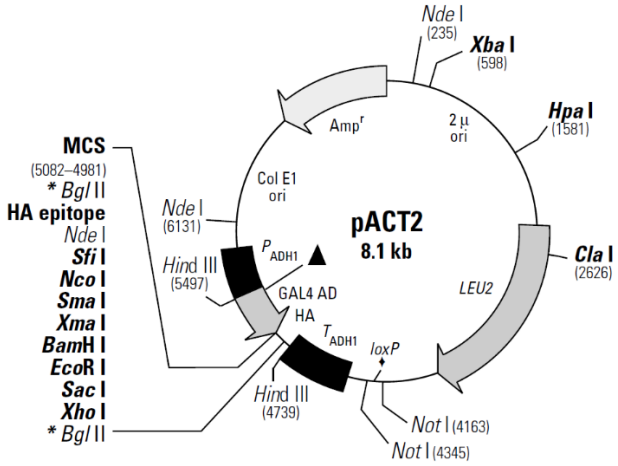

Fig. 12 Map of the pACT2 vector. The 8.1kb vector pACT2 (NCBI: U29899; Clontech PT3022-5) was used in one- and two-hybrid assays to express defined proteins. Proteins are expressed as GAL4 activation domain (AD) (5081-5419nt; the region corresponds to aa768-881 of the GAL4 transcription factor) fusions. The expressed proteins are also fused to a hemagglutinin tag (HA; 5042-5068nt). The transcription is driven by the constitutive *ADH1* promoter (P_{ADH1}; 5504-5901nt) and stopped by the *S. cerevisiae ADH1* terminator (T_{ADH1}; 4415-4742nt). For nuclear localization the *SV40 T-antigen nuclear localization sequence* (SV40 NLS; 5424-5478nt) is added to the 5´- end of the GAL4 AD domain. The 2µ origin of replication (1-2055nt) and the pBR322 plasmid replication origin Col E1 ori (6336-6979nt) allow autonomous replication in yeast and bacteria. The nutritional marker *LEU2* (2474-3568nt) is used for selection in yeast. The *bla* gene (7127-8052nt) confers ampicillin resistance (Amp^r) for selection in bacteria.

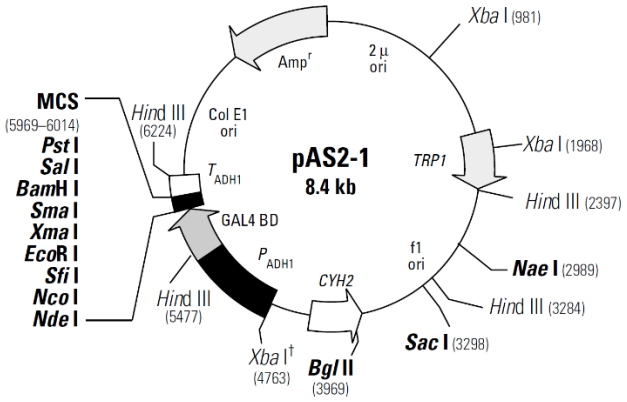

Fig. 13 Map of the pAS2-1 vector. The 8.4kb vector pAS2-1 (NCBI: U30497; Clontech PT3023-5) was used in two-hybrid assays to express defined proteins. Proteins are expressed as GAL4 BD (5502-5944nt) fusions. Transcription is driven by the constitutive *ADH1* promoter (P_{ADH1}; 5504-5901nt) and stopped by the *S. cerevisiae ADH1* terminator (T_{ADH1}; 4767-5474nt). The 2µ origin of replication (1-1348nt) allows autonomous replication in yeast and bacteria. The nutritional marker *TRP1* (1884-2256nt) is used for selection in yeast. The *bla* gene (7403-8263nt) confers ampicillin resistance (Amp^r) for selection in bacteria.

3.2.3 Molecular weight standards

Tab. 18 Molecular weight standards for DNA and protein

Name	Purchased from
GeneRuler™ 100 bp Plus DNA Ladder	Thermo Fisher, Dreieich
GeneRuler™ 1 kb DNA Ladder	Thermo Fisher, Dreieich
λ DNA / *Hind*III Marker 2	Thermo Fisher, Dreieich
λ DNA / *Eco*RI + *Hind*III Marker 3	Thermo Fisher, Dreieich
PageRuler™ Prestained Protein Ladder	Thermo Fisher, Dreieich

3.2.4 Oligonucleotides

All primers and binding sites were synthesized by Sigma-Aldrich (Steinheim). Prior to use lyophilized primers were dissolved to a final concentration of 100pmol/µl in autoclaved type I H2O (filtered at 18.2 MΩ • cm, 25°C, "ultra-pure water"). All oligonucleotides were stored at -20°C. The melting temperature (Tm) of the primers was calculated using the following equation:

$$(4 \bullet X\,[G/C]) + (2 \bullet Y\,[A/T]) = Tm$$

where X and Y are the total numbers of purines or pyrimidines in the sequence. In all primers designed the content of the nucleotides G and C was below 60%. To determine the percentage of GC nucleotides and to exclude potential secondary structures and dimerization all primers were analyzed using the computer program FastPCR Professional v.5.2.118.

3.2.4.1 Primer

Tab. 19 Primer combinations for ChIP amplifications of CREB sites in the *NOT* promoter

Name	Sequence[1]	Position[2]	Size	Sites[3]
P3F	TCTAGGAGGGCACGGAAGGA	912 – 893	227bp	16
P3R	CGCCTTCTGCATCCTGCCTT	686 – 704		
P17F	CACAAACACGTGGAACTTCCG	646 – 626	245bp	15-9
P14R	GAGCCTTCCGGATGCTGAGA	402 – 421		
P18F	GTAAGACATTGTCCCTGCTCC	207 – 187	148bp	6-3
P15R	TAGGTTCCGCTTCCCGTG	60 – 77		

1: Sequence direction 5´-3´; 2: The nt positions refer to the region upstream the *NOT*-1 start codon; 3: P-MATCH™ predicted sites (Chekmenev *et al*. 2005; Ch. 3.5.1) located in the amplified fragment. Bold nucleotides are incorporated base exchanges to reach Tm: 59°C for all combinations. P3/3 also used for NFκB ChIPs (Tab. 20).

Tab. 20 Primer combinations for ChIP amplifications of NFκB sites in the *NOT* promoter

Name	Sequence[1]	Position[2]	Size	Sites[3]
P1F	GCCTTGACTAAATACAGCCGG	1115 – 1095	184bp	22, 21
P1R	GACCGTATCCTTGTGCTAG	932 – 950		
P2F	CTAGCACAAGGATACGGTC	950 – 932	139bp	20
P2R	TACCGCGAAGTCG**C**GTACTG	812 – 831		
P3F	TCTAGGAGGGCACGGAAGGA	912 – 893	227bp	20, 19, 18, 17, 16
P3R	CGCCTTCTGCATCCTGCCTT	686 – 704		
P4F	AACCGCCG**A**GCAGCCCAGA	748 – 731	110bp	15, 14
P4R	TGTTTGTGTTGAGCAACTGC**T**G	639 – 660		
P5F	AGGCAGGATGCAGAAGGCGC	704 – 686	200bp	15, 14, 13, 12, 11, 10, 9, 8
P5R	CGTGAGTCTGACACCTTGAGTG	505 – 526		
P6F	CTGCAGTTGCTCAACACAAACA	660 – 639	190bp	13, 12, 11, 10, 9, 8
P6R	ATTGAAAATATGAGAGGACGCA	471 – 492		
P7F	TGAATCCTCCG**T**CTGTACTGC	617 – 597	97bp	8
P6R	ATTGAAAATATGAGAGGACGCA	471 – 492		
P8F	ACTCAAGGTGTCAGACTCACG	525 – 505	150bp	7
P7R	TTCGCGCC**T**CTCCTGCCTG	427 – 445		
P9F	TCTCAGCATCCGGAAGGCTC	421 – 402	194bp	7, 6, 5, 4, 3
P8R	CTGGGTACACAGGCGCTAATT	228 – 248		
P10F	CTCCTGGAGAGACAGCATGA	363 – 344	96bp	4, 3
P9R	AGCAACATTCCTGCCTACCTC	268 – 288		
P11F	AATTAGCGCCTGTGTACCCAG	248 – 228	162bp	1
P10R	CCACCAGGCTAAGCGC**T**GAT	87 – 106		

1: Sequence direction 5´-3´; 2: The nt positions refer to the region upstream the *NOT*-1 start codon; 3: P-MATCH™ predicted sites (Chekmenev *et al*. 2005; Ch. 3.5.1) located in the amplified fragment. Bold nucleotides are incorporated base exchanges to reach Tm: 59°C for all combinations. P3/3, P5/5, P11/10were also used for TBP and Pol II ChIPs (Ch. 4.2), P3/3 was also used for CREB ChIPs (Tab. 19).

Tab. 21 Primer combinations for ChIP amplifications of EGR-1 sites in the *NOT* promoter

Name	Sequence[1]	Position[2]	Size	Sites[3]
P3F	TCTAGGAGGGCACGGAAGGA	912 – 893	101bp	7
P2R	TACCGCGAAGTCG**C**GTACTG	812 – 831		
P12F	GTACTCGACTTCGC**C**GTACC	829 – 810	144bp	6
P3R	CGCCTTCTGCATCCTGCCTT	686 – 704		
P5F	AGGCAGGATGCAGAAGGCGC	704 – 686	200bp	5
P5R	CGTGAGTCTGACACCTTGAGTG	505 – 526		
P13F	TGCGTCCTCTCATATTTTCAAT	492 – 471	196bp	4
P11R	CCGCTGAAGCCAGCATTCTC	297 – 316		
P14F	GAGAATGCTGGCTTCAGCGG	316 – 297	176bp	3
P12R	GTAATTT**C**TCTGCATTTGTCTCC	141 – 163		
P15F	ATC**A**GCGCTTAGCCTGGTGG	106 – 87	109bp	2,1
P13R	CATCTTAACGGTGCGCCGCT	+3 – 17		

1: Sequence direction 5´-3´; 2: The nt positions refer to the region upstream the *NOT*-1 start codon; 3: P-MATCH™ predicted sites (Chekmenev *et al*. 2005; Ch. 3.5.1) located in the amplified fragment. Bold nucleotides are incorporated base exchanges to reach Tm: 59°C for all combinations.

Tab. 22 Primer combination for ChIP amplifications of MYCN sites in the *NOT* promoter

Name	Sequence[1]	Position[2]	Size	Sites[3]
P16F	GAGGTAGGCAGGAATGTTGCT	288 – 268	202bp	3
P10R	CCACCAGGCTAAGCGC**T**GAT	87 – 106		

1: Sequence direction 5´-3´; 2: The nt positions refer to the region upstream the *NOT*-1 start codon; 3: P-MATCH™ predicted sites (Chekmenev *et al*. 2005; Ch. 3.5.1) located in the amplified fragment. Bold nucleotides are incorporated base exchanges to reach Tm: 59°C.

Tab. 23 Primer combinations for ChIP amplifications in the m*NOT* promoter

Name	Sequence[1]	Position[2]	Size	Sites[3]			
				NFκB	CREB	EGR	MYC
P1F	GCTTGGAGAAGAGAACAGAACT	431 - 410	168bp	3-1	---	---	3-1
P1R	GGATAAGATAGCTAGTCCTTAGA	264 - 286					
P2F	TGGAGCACCTTCG**A**GTACTTG	534 - 514	125bp	7-4	1	1	4-3
P2R	AGTTCTGTTCTCTTCTCCAAGC	410 - 431					
P3F	ATTACTGCATCCTCTCGTGTTC	622 - 601	213bp	7-4	3-1	1	7-3
P2R	AGTTCTGTTCTCTTCTCCAAGC	410 - 431					
P4F	TTGTGTGGAGCAGCTGCAGG	797 - 778	197bp	12-8	7-3	---	11-6
P3R	GAACACGAGAGGATGCAGTAAT	601 - 622					
P5F	TCCAGAGTC**A**GCCGCGTCTT	997 - 978	219bp	18-12	9-8	3-2	11-10
P4R	TTGTGTGGAGCAGCTGCAGG	778 - 797					
P6F	AAGCGGATGTGATCTGGCCA	1129 - 1110	220bp	22-17	10-8	3	14-12
P5R	GTCC**T**CTCC**A**GAGTTACCGG	910 - 929					

1: Sequence direction 5´-3´; 2: The nt positions refer to the region upstream the m*NOT*-1 start codon; 3: P-MATCH™ predicted sites (Chekmenev *et al*. 2005; Ch. 3.5.1) located in the amplified fragment. Bold nucleotides are incorporated base exchanges to reach Tm: 59°C for all combinations.

Tab. 24 Primer combination used for generation of the pACT2-*MYCN* expression construct

Name	Position [1]	Sequence[2]	Enc.[3]
NMYC-For1	25-43	TTCCATGGTTATGCCGGG**T**ATGATCTGCA	9-464
NMYC-Rev1	1397-1379	GAATTCGTCTAGCAAGTCCGAGCGT	

1: The nt positions refer to the region downstream the *MYCN* start codon (NCBI: NM_001293228.1); 2: Sequence in direction 5´-3´, the restriction sites introduced for cloning purposes are underlined: *Nco*I in the forward and *Eco*RI in reverse primer; Bold nucleotides are incorporated base exchanges to reach Tm: 52°C; 3: Encoded amino acids.

Tab. 25 Primer combination used for generation of pACT2-*EGR-1* expression constructs

Name	Position [1]	Sequence[2]	Enc.[3]
EGR1-For1	1-20	ATCCATGGTTATGGC**A**GCGGCCAAGGCCGA	1-543
EGR1-Rev1	1701-1682	GAATTCCTCCTCCTCCTGTCCTTTAA	

1: The nt positions refer to the region downstream the *EGR*-1 start codon (NCBI: NM_001964.2); 2: Sequence in direction 5´-3´, the restriction sites introduced for cloning purposes are underlined: *Nco*I in the forward and *Eco*RI in the reverse primer; Bold nucleotides are incorporated base exchanges to reach Tm: 55°C; 3: Encoded amino acids.

Tab. 26 Primer combinations used for generation of pAS2-1-*RPS3* expression constructs

Name	Position [1]	Sequence[2]	Const.[3]	Enc.[4]
RPS3-For1a	1-21	CGAATTCATGGCAGTGCAAATATCCAAG	1	1-243
RPS3-Rev1a	732-717	AGGATCCCCTGTTATGCTGT**A**GGGACT		
RPS3-For2a	43-62	CGAATTCGGCATCTTCAAAGCTGAACT	2	15-100
RPS3-Rev2a	300-283	AGGATCCGGCAATGGCACACAGACC		
RPS3-For3a	301-318	CGAATTCCAGGCAGAGTC**A**CTGCGT	3	101-243
RPS3-Rev1a	732-717	AGGATCCCCTGTTATGCTGT**A**GGGACT		
RPS3-For4a	439-459	CGAATTCGCTAAATCCATGAAGTTTGTG	4	147-243
RPS3-Rev1a	732-717	AGGATCCCCTGTTATGCTGT**A**GGGACT		
RPS3-For5a	583-602	CGAATTCACTGGTAAGATTGG**T**CCTAA	5	195-243
RPS3-Rev1a	732-717	AGGATCCCCTGTTATGCTGT**A**GGGACT		
RPS3-For3a	301-318	CGAATTCCAGGCAGAGTC**A**CTGCGT	6	101-148
RPS3-Rev3a	446-428	AGGATCCGATTTAGCCCTCTGTCCTC		

1: The nt positions refer to the region downstream the *RPS3* start codon (NCBI: NM_001005.4); 2: Sequence in direction 5´-3´, the restriction sites introduced for cloning purposes are underlined: *Eco*R1 in forward and *Bam*HI in reverse primers; Bold nucleotides are incorporated base exchanges to reach to reach Tm: 53°C for all combinations; 3: RPS3 construct; 4: Encoded amino acids.

Tab. 27 Primer combinations used for generation of pACT2-*RPS3* expression constructs

Name	Position [1]	Sequence[2]	Const.[3]	Enc.[4]
RPS3-For2b	43-62	CGAATTCGAGGCATCTTCAAAGCTGAACT	2	15-100
RPS3-Rev2b	300-283	ATCTCGAGGGCAATGGCACACAGACC		
RPS3-For3b	301-318	CGAATTCGACAGGCAGAGTC**A**CTGCGT	3	101-243
RPS3-Rev1b	732-717	TCCTCGAGCCTGTTATGCTGT**A**GGGACT		
RPS3-For4b	439-459	CGAATTCGAGCTAAATCCATGAAGTTTGTG	4	147-243
RPS3-Rev1b	732-717	TCCTCGAGCCTGTTATGCTGT**A**GGGACT		
RPS3-For5b	583-602	CGAATTCGAACTGGTAAGATTGG**T**CCTAA	5	195-243
RPS3-Rev1b	732-717	TCCTCGAGCCTGTTATGCTGT**A**GGGACT		
RPS3-For3b	301-318	CGAATTCGACAGGCAGAGTC**A**CTGCGT	6	101-148
RPS3-Rev3b	446-428	ATCTCGAGGATTTAGCCCTCTGTCCTC		

1: The nt positions refer to the region downstream the *RPS3* start codon (NCBI: NM_001005.4); 2: Sequence in direction 5´-3´, added restriction sites underlined: *Eco*R1 in forward and *Xho*I in reverse primers; Bold nucleotides are incorporated base exchanges to reach Tm: 53°C for all combinations; 3: RPS3 construct; 4: Encoded aa.

Tab. 28 *NOT* and *ECE2* primers used in RACE experiments

Reverse primer, sequence, location[1]	Specificity, size[2]
1r: 5´-GTAGACTCAGGTCCTGAGGGA [a]1350-1330	***NOT*-1:** 1350; **-2:** 1313; **-5:** 1250; **-1a:** 1111; **-1b:** 801; **-2a:** 1107; **-2b:** 764; **-5a:** 1044; **-5b:** 701; **-5c:** 540
11r: 5´-CACCCTGTGAATGACCCAGAA [a]exon 1, 192-172	***NOT*-1, -5, -1a, -1b, -5a, -5b, -5b:** 192
12r: 5´-CACAACCGCTGAAGCCAGCATT [d]exon 1, 46-25	***NOT*-4, -3a, -3c -4a, -4b:** 46
13r: 5´-AGCTGGGTAC**A**TGCCACCCT [e]exon 3/**2**, 206-197/**196**-187	***NOT*-5, -5a, -5b, -5c:** 206
14r: 5´-AGCTGGGTA**C**CTCCTCCACA [c]exon 2/**1**, 62-53/**52**-43	***NOT*-3, -3a, -3c:** 62
15r: 5´-CTCTGTGT**C**TCCGCCAGGCA [b]exon 2/**1**, 167-160/**159**-148	***NOT*-2, -2a, -2b:** 62
ECE2-P1R: 5´-CGAGGAACAGCTCGTAGCTC [f]exon2, 235-216	***ECE2* v1, v3:** 235
mNOT-9r: 5´-AATCTCTGTG**T**CTCGGTGATTG [g]exon2/1, 63-54/**53**-44	**m*NOT*-4, -4a, -4b, -4c:** 63
mECE2-P1R: 5´-CACGGAAGGAAGCGAAGTCT [h]exon1, 148-128	**m*ECE2* v1, v3:** 148

1: Positions in nt relative to the ATG of respective reference: [a]: *NOT*-1 (Y09022.1); [b]: *NOT*-2 (NR_024534.1); [c]: *NOT*-3 (KP189318); [d]: *NOT*-4 (NM_001006941.2); [e]: *NOT*-5 (NR_024533.1); [f]: *ECE2* v1 (NM_014693.3); [g]: m*NOT*-4 ATG (KP189268 [h]: m*ECE2* v1 (NM_177941.1). In those cases where the used primers encompass two exons, the first nucleotide of the second exon and its position is in bold print. Underlined nucleotides are incorporated base exchanges to reach Tm: 54°C for all combinations. Wildtype bases are (Primer, position: Base): 14r, nt48: G; r: Reverse; nt: Nucleotide; m: Murine. Primer 1r was also used in isolation and sequencing of *NOT* splice variants (Ch. 4.1 and Tab. 32); 2: Primer specificity, size of the respective variant without the 5´-UTR in nt.

Tab. 29 Primers used for generation of *NOT* promoter constructs

Name	Position[1]	Sequence[2]	Site[3]	Const.[4]
Phnot-F1	10546 – 10565	CGAATTCAGGGCCCCGGGACCAACAAT	*Eco*RI	P1-4
Phnot-R1	11697 – 11682	AATGTCGACATCTTAACG**A**TGCGCC	*Sal*I	P1
Phnot-F2	10992 – 11011	AGGCAGGATGCAGAAGGCGG	---	P2
Phnot-F3	11171 – 11191	ACTCAAGGTGTCAGACTCACG	---	P3
Phnot-F4	10581 – 10601	GCCTTGACTAAATACAGCCGG	---	P4
Phnot-R2	11698 – 11679	AGAGCTCCATCTTAACGGTGCGCCGCT	*Sac*I	P2-3
Phnot-R3	11010 – 10991	AGAGCTCCGCCTTCTGCATCCTGCCTT	*Sac*I	P4

1: Position in nt according to the BAC clone RP11-488M12 (NCBI: AC061705); 2: Sequence in direction 5´-3´, the restriction sites introduced for cloning purposes are underlined; Bold nucleotides are incorporated base exchanges to reach Tm: 59°C for all combinations, with the exception of F1/R1 to generate P1: 44°C; 4: Ph*NOT* (P): *NOT* promoter construct.

Tab. 30 Additional primers and oligos

Name[1]	Sequence[4]	Application[5]
MATCHMAKER 5´ AD LD-Insert	CTATTCGATGATGAAGATACCCCACCAAACCC	Sequencing
MATCHMAKER 3´ AD LD-Insert	GTGAACTTGCGGGGTTTTCAGTATCTACGA	Sequencing
MATCHMAKER 5´ BD LD-Insert	TCATCGGAAGAGAGTAGT	Sequencing
MATCHMAKER 3´ BD LD-Insert	CGTTTTAAAACCTAAGAGTCAC	Sequencing
SMARTer II A Oligo	AAGCAGTGGTATCAACGCAGAGTACXXXXX	RACE
USP primer	CTAATACGACTCACTATAGGGC	RACE
Oligo(dT)12-18[2]	5'd PO4 [(T)12-18]	cDNA synthesis
pHIS2.1-Seq-F1[3]	ATGTGCTGCAAGGCGATTAAGT	Sequencing

1: The primers were purchased from Clontech; 2: Primer mix purchased from Life Technologies. The mix contains primers consisting of 12-18 dT stretches; 3: The pHIS2.1-Seq-F1 primer corresponding to the 5´ AD/BD LD-Insert primers (Clontech) was synthesized by Sigma-Aldrich. This primer is located at 7091-7112nt upstream the MCS of pHIS2.1 (Ch. 3.3.2, Fig. 11); 4: X = undisclosed base in the proprietary SMARTer oligo sequence (PT4096-1, Clontech); 5: (Sequencing: Ch. 3.3.6; cDNA synthesis: Ch. 3.3.16; RACE: Ch. 3.3.18).

Tab. 31 Primer combinations used for qRT-PCR

Name	Position[1]	Sequence[2]	Size[3]	Reference
CREB1b-For1	283 - 304	AGACTTTTCTCCGGAACACAGA	430	NM_134442.3
CREB1b-Rev1	712 - 692	TGCTGGGCACTAAGATCTGCT		
CREB3-For1	260 - 281	CTGTCTCTATGGATCTAGAGAG	362	NM_006368.4
CREB3-Rev1	621 - 599	TAGAAGGGACAAATTCTGTTCCT		
EGR1-For1	180 - 199	CAACAGCAGCAGCAGCAGCA	233	NM_001964.2
EGR1-Rev1	412 - 391	AAAAGCGGCCAGTATAGGTGAT		
p65-For1	641 - 662	TACTGTGTGACAAGGTGCAGAA	261	NM_021975.3
p65-Rev1	901 - 881	TCTCCTCAATCCGGTGACGAT		
p50-For1	704 - 725	TGGTATCAGACGCCATCTATGA	320	NM_003998.3
p50-Rev1	1023 - 1002	TTCCAAGTCAGATTTCCTCCGA		
RPS3-For1	439 - 461	GCTAAATCCATGAAGTTTGTGGA	298	BC100284.1
RPS3-Rev1	736 - 717	CCTGTTATGCTGTAGGGACT		
IkBa-For1	308 - 329	TCCTCAACTTCCAGAACAACCT	334	NM_020529.2
IkBa-Rev1	641 - 621	GGCTCCTGAGCATTGACATCA		
ECE2-For1	1 - 19	ATGGCCTCTCCAGGGGCAG	477	NM_014693.3
ECE2-Rev1	477-457	ACTCAACACCTGGTCCACAGT		
Actinb-For1	550 - 569	GACCTGACTGACTACCTCAT	308	NM_001101.3
Actinb-Rev1	857 - 835	TCACACTTCA**A**GATGGAGTTGAA		
SMAD4-For1	562-583	AATCGTGCATCGACAGAGACAT	254	NM_005359.5
SMAD4-Rev1	815-795	CTACTTCCAGTCCAGGTGGTA		
mCREB3-For1	249-271	CATTCTCCATGATCACAACTACT	379	NM_013497.3
mCREB3-Rev1	627-607	CAAACGCTGCACCTTGTTCTG		
HGPRT-For1[4]	411 - 431	TGACACTGGCAAAACAATGCA	94	NM_000194.2
HGPRT-Rev1[4]	504 - 484	GGTCCTTTTCACCAGCAAGCT		

All primer efficiencies are listed in Tab. S9, except for m*CREB3* (Tab. S5); 1: The nt positions refer to the region downstream the respective start codon; 2: Sequence in direction 5´-3´, bold nucleotides are incorporated base exchanges to reach Tm: 54°C for all combinations; 3: Size of the amplificate in bp; 4: Primer also used for mouse.

Tab. 32 Primer combinations used for isolation and sequencing of *NOT* variants in man

Forward primer, sequence, location[1]	Reverse primer, sequence, location[1]	Specificity, size[2]
1f 5´-ACAAGCGGCGCACCGTTAA [a]-20 - -1	1r 5´-GTAGACTCAGGTCCTGAGGGA [a]1350-1330	***NOT*-1:** 1370; **-2:** 1333; **-5:** 1270; **-1a:** 1131; **-1b:** 821; **-2a:** 1127; **-2b:** 784; **-5a:** 1064; **-5b:** 721; **-5c:** 560
2f 5´-TTCACAGGGTGGCAT**A**CCCAG [a]exon 1/**2**, 182-196/**197**-202	1r 5´-GTAGACTCAGGTCCTGAGGGA [a]1350-1330	***NOT*-1:** 1196; **-1a:** 963; **-1b:** 620
3f 5´-TGCCTGGCGGAG**A**CACAGAG [b]exon 1/**2**, 148-159/**160**-167	1r 5´-GTAGACTCAGGTCCTGAGGGA [b]1313-1293	***NOT*-2:** 1166; **-2a:** 960; **-2b:** 617
4f 5´-ATGGCGGCTGAGCTGCGGAA [a]exon 1, 1-20	2r 5´-AGGTTGATACTGAGGAAGAGC [a]exon 4, 563-543	***NOT*-1:** 563; **-2:** 526; **-5:** 463
4f 5´-ATGGCGGCTGAGCTGCGGAA [a]exon 1, 1-20	3r 5´-GCACCAACAAC**C**TGAAAAAGCA [a]exon 9/4, 1165-1155/**605**-595	***NOT*-1b:** 616; **-2b:** 579; **-5b:** 516
5f 5´-TCTCAGCATCCGGAAGGCTC [d]-84 - -65	1r 5´-GTAGACTCAGGTCCTGAGGGA [d]1206-1186	***NOT*-3:** 1190; **-4:** 1290; **-3a:** 984; **-3b:** 1028; **-3c:** 641; **-4a:** 1084; **-4b:** 580
6f 5´-AGGGTGGCAT**G**TACCCAGCT	1r 5´-GTAGACTCAGGTCCTGAGGGA	***NOT*-5:** 1064; **-5a:** 858; **-5b:** 515; **-5c:** 354
7f 5´-ATGTTCCCAGCGCAGGCGAAG [d]exon 1, 1-21	1r 5´-GTAGACTCAGGTCCTGAGGGA [d]1206-1186	***NOT*-3:** 1106; **-4:** 1206; **-3a:** 900; **-3b:** 944; **-3c:** 557; **-4a:** 1000; **-4b:** 496
8f 5´-TGTGGAGGAG**G**TACCCAGCT [d]exon 1/**3**, 43-52/**153**-162 [c]exon 1/**2**, 43-52/**53**-62	1r 5´-GTAGACTCAGGTCCTGAGGGA [d]1206-1186 [c]1106-1086	***NOT*-3:** 1064; **-3a:** 858; **-3b:** 903; **-3c:** 515
4f 5´-ATGGCGGCTGAGCTGCGGAA [a]exon 1, 1-20	1r 5´-GTAGACTCAGGTCCTGAGGGA [a]1350-1330	***NOT*-1:** 1350; **-2:** 1313; **-5:** 1250; **-1a:** 1111; **-1b:** 801; **-2a:** 1107; **-2b:** 764; **-5a:** 1044; **-5b:** 701; **-5c:** 540

1: Positions in nt relative to the ATG of the respective variant; [a]: Positions relative to *NOT*-1 (Y09022.1); [b]: Positions relative to *NOT*-2 (NR_024534.1); [c]: Positions relative to *NOT*-3 (KP189318); [d]: Positions relative to *NOT*-4 (NM_001006941.2); [e]: Positions relative to *NOT*-5 (NR_024533.1). In those cases where the used primers encompass two exons, the first nucleotide of the second exon and its position is in bold print. Underlined nucleotides are incorporated base exchanges to reach to reach Tm: 54°C for all combinations. Wildtype bases are (Primer, position: Base): 2f, nt199: A; 4f, nt11: G; 8f, nt48: G; f: Forward; r: Reverse; nt: Nucleotide. Primer 1r was also used in RACE experiments (Ch. 3.3.18 and Ch. 4.1.3; Tab. 28); 2: Specificity of the respective primer combinations, size of the amplificate in nt.

Tab. 33 Primer combinations used for specific amplification of *NOT* variants in man

Variant	Forward primer, sequence, location[1]	Reverse primer, sequence, location[1]	Size[2]
***NOT*-1**	2f: 5´-TTCACAGGGTGGCAT**A**CCCAG exon 1/**2**, 182-196/**197**-202	4r: 5´-CCAGTTCACTGTCCAGTGGAACA exon 6, 828-806	647
***NOT*-2**	3f: 5´-TGCCTGGCGGAG**A**CACAGAG exon 1/**2**, 148-159/**160**-167	4r: 5´-CCAGTTCACTGTCCAGTGGAACA exon 6, 791-769	644
***NOT*-3**	8f: 5´-TGTGGAGGAG**G**TACCCAGCT exon 1/**2**, 43-52/**53**-62	4r: 5´-CCAGTTCACTGTCCAGTGGAACA exon 5, 584-562	542
***NOT*-4**	9f: 5´-TTGTGGGGGAG**A**CACAGAGATT exon 1/**2**, 42-52/**53**-63	4r: 5´-CCAGTTCACTGTCCAGTGGAACA exon 6, 684-662	643
***NOT*-5**	6f: 5´-AGGGTGGCAT**G**TACCCAGCT exon 1/**2**, 187-196/**197**-206	4r: 5´-CCAGTTCACTGTCCAGTGGAACA exon 5, 728-706	542
***NOT*-1a**	2f: 5´-TTCACAGGGTGGCAT**A**CCCAG exon 1/**2**, 182-196/**197**-202	5r: 5´-TTCCCCTGTC**C**TGAAGGCCA exon 6/**5**, 736-727/**726**-717	555
***NOT*-1b**	2f: 5´-TTCACAGGGTGGCAT**A**CCCAG exon 1/**2**, 182-196/**197**-202	3r: 5´-GCACCAACAAC**C**TGAAAAAGCA exon 5/**4**, 616-606/**605**-595	435
***NOT*-2a**	3f: 5´-TGCCTGGCGGAG**A**CACAGAG exon 1/**2**, 148-159/**160**-167	5r: 5´-TTCCCCTGTC**C**TGAAGGCCA exon 6/**5**, 699-690/**689**-680	552
***NOT*-2b**	3f: 5´-TGCCTGGCGGAG**A**CACAGAG exon 1/**2**, 148-159/**160**-167	3r: 5´-GCACCAACAAC**C**TGAAAAAGCA exon 5/**4**, 579-569/**568**-558	432
***NOT*-3a**	8f: 5´-TGTGGAGGAG**G**TACCCAGCT exon 1/**2**, 43-52/**53**-62	5r: 5´-TTCCCCTGTC**C**TGAAGGCCA exon 5/**4**, 492-483/**482**-473	450
***NOT*-3b**	8f: 5´-TGTGGAGGAG**G**TACCCAGCT exon 1/**2**, 43-52/**53**-62	6r: 5´-GACTGCCAGG**C**ATGCAGGTC exon 3/**2**, 210-201/**200**-191	168
***NOT*-3c**	8f: 5´-TGTGGAGGAG**G**TACCCAGCT exon 1/**2**, 43-52/**53**-62	3r: 5´-GCACCAACAAC**C**TGAAAAAGCA exon 4/**3**, 372-362/**361**-351	330
***NOT*-4a**	9f: 5´-TTGTGGGGGAG**A**CACAGAGATT exon 1/**2**, 42-52/**53**-63	5r: 5´-TTCCCCTGTC**C**TGAAGGCCA exon 6/**5**, 592-583/**582**-573	551
***NOT*-4b**	9f: 5´-TTGTGGGGGAG**A**CACAGAGATT exon 1/**2**, 42-52/**53**-63	7r: 5´-GCACCAACAAC**C**TTGCAGGTCT exon 4/**3**, 311-301/**300**-290	270
***NOT*-5a**	6f: 5´-AGGGTGGCAT**G**TACCCAGCT exon 1/**2**, 187-196/**197**-206	5r: 5´-TTCCCCTGTC**C**TGAAGGCCA exon 5/**4**, 636-627/**626**-617	450
***NOT*-5b**	6f: 5´-AGGGTGGCAT**G**TACCCAGCT exon 1/**2**, 187-196/**197**-206	3r: 5´-GCACCAACAAC**C**TGAAAAAGCA exon 4/**3**, 516-506/**505**-495	330
***NOT*-5c**	6f: 5´-AGGGTGGCAT**G**TACCCAGCT exon 1/**2**, 187-196/**197**-206	7r: 5´-GCACCAACAAC**C**TTGCAGGTCT exon 3/**2**, 355-345/**344**-334	169

1: Positions in nt relative to the respective ATG, accession numbers are listed Tab. 55. In those cases where the used primers encompass two exons, the position of the first nucleotide of the second exon is in bold print. Underlined nucleotides are incorporated base exchanges to reach Tm: 54°C for all combinations. Wildtype bases are (Primer, position: Base): 2f, nt199: A; 8f, nt48: G; 6r, nt199: G. f: Forward; r: Reverse; 2: Size of the amplificate in nt.

Tab. 34 Primer combinations used for isolation and sequencing of *NOT* variants in mice

Forward primer, sequence, location[1]	Reverse primer, sequence, location[1]	Specificity, size[2]
1f 5´-CAAAAGAGTGGTGCACTGTCAAG [a]-23 - -1	1r 5´-TGATGCTGAGCACGTCCTAGA [a]1353-1333	**m*NOT*-1:** 1376; **-2:** 1239; **-5:** 1276; **-1a:** 1115; **-1b:** 969; **-2a:** 1078; **-5a:** 1115
2f 5´-TTCACAGGGTGGCAT**A**CCCAG [a]exon 1/**2**, 182-196/**19**7-202	1r 5´-TGATGCTGAGCACGTCCTAGA [a]1353-1333	**m*NOT*-1:** 1172; **-1a:** 1011
3f 5´-CATAGCAGAC**C**TACCCAGCT [b]exon 1/**2**, 150-159/**160**-169	1r 5´-TGATGCTGAGCACGTCCTAGA [b]1216-1196	**m*NOT*-2:** 1067; **-2a:** 906
1f 5´-CAAAAGAGTGGTGCACTGTCAAG [a]-23 - -1	2r 5´-GAAGAGCAAGGCCATAGCTA [a]exon 4, 548-529	**m*NOT*-1:** 571; **-2:** 435; **-5:** 471
4f 5´-TCCAGAGTCAGCCGCGTCTT [d]-109 - -89	1r 5´-TGATGCTGAGCACGTCCTAGA [d]1210-1190	**m*NOT*-3:** 1219; **-4:** 1319; **-3a:** 1131; **-3b:** 1058; **-3c:** 997; **-4a:** 1158; **-4b:** 754; **4c:** 620
5f 5´-ATGCTCAGGGCATCGCCGCA [d]exon 1, 1-20	1r 5´-TGATGCTGAGCACGTCCTAGA [d]1210-1190	**m*NOT*-3:** 1110; **-4:** 1210; **-3a:** 1022; **-3b:** 949; **-3c:** 888; **-4a:** 1049; **-4b:** 645; **4c:** 511
6f 5´-AATCAACGAG**C**TACCCAGCT [c]exon 1/**2**, 44-53/**54**-63	1r 5´-TGATGCTGAGCACGTCCTAGA [c]1110-1090	**m*NOT*-3:** 1067; **-3a:** 979; **-3b:** 906; **-3c:** 845;
7f 5´-CAATCACCGAG**A**CACAGAGATT [d]exon 1/**2**, 43-53/**54**-64	1r 5´-TGATGCTGAGCACGTCCTAGA [d]1210-1190	**m*NOT*-4:** 1168; **-4a:** 1007; **-4b:** 603
8f 5´-AGGGTGGCAT**C**TACCCAGCT [e] exon 1/**2**, 187-196/**197**-206	1r 5´-TGATGCTGAGCACGTCCTAGA [e]1253-1233	**m*NOT*-5:** 1067; **-5a:** 906

[a]: Positions relative to m*NOT*-1 ATG (NM_145939.2); [b]: Positions relative to m*NOT*-2 ATG (KP189262); [c]: Positions relative to m*NOT*-3 (KP189264); [d]: Positions relative to m*NOT*-4 ATG (KP189268); [e]: Positions relative to m*NOT*-5 ATG (KP189272); In those cases where the used primers encompass two exons, the first nucleotide of the second exon and its position is in bold print. Underlined nucleotides are incorporated base exchanges to reach Tm: 54°C for all combinations. Wildtype bases are (Primer, position: Base): 2f, nt199: A; 4f, nt100: G; 5f, nt13: G; 6f, nt49: C; f: Forward; r: Reverse; nt: Nucleotide. 2: Specificity of the respective primer combinations, size of the amplificate in nt.

Tab. 35 Primer combinations used for specific amplification of *NOT* variants in mice

Variant	Forward primer, sequence, location[1]	Reverse primer, sequence, location[1]	Size[2]
m*NOT*-1	2f: 5´-TTCACAGGGTGGCAT**A**CCCAG exon 1/**2**, 182-196/**197**-202	2r: 5´-GAAGAGCAAGGCCATAGCTA exon 4, 548-529	367
m*NOT*-2	3f: 5´-CATAGCAGAC**C**TACCCAGCT exon 1/**2**, 150-159/**160**-169	2r: 5´-GAAGAGCAAGGCCATAGCTA exon 3, 412-393	263
m*NOT*-3	6f: 5´-AATCAACGAG**C**TACCCAGCT exon 1/**2**, 44-53/**54**-63	2r: 5´-GAAGAGCAAGGCCATAGCTA exon 3, 308-287	263
m*NOT*-4	7f: 5´-CAATCACCGAG**A**CACAGAGATT exon 1/**2**, 43-53/**54**-64	2r: 5´-GAAGAGCAAGGCCATAGCTA exon 4, 406-387	301
m*NOT*-5	8f: 5´-AGGGTGGCAT**C**TACCCAGCT exon 1/**2**, 187-196/**197**-206	2r: 5´-GAAGAGCAAGGCCATAGCTA exon 3, 308-287	263
m*NOT*-1a	2f: 5´-TTCACAGGGTGGCAT**A**CCCAG exon 1/**2**, 182-196/**197**-202	3r: 5´-GACAGCCAGG**C**TTGGAGGTC exon 4/**3**, 453-445/**444**-435	273
m*NOT*-1b	9f: 5´-GTGGCAT**A**CACAG**G**CTGTCT exon 1/**2**/**3**, 190-196/**197**-202/**203**-209	4r: 5´-ACGATGCAGGAAGATGGTTTCA exon 4, 454-433	435
m*NOT*-2a	3f: 5´-CATAGCAGAC**C**TACCCAGCT exon 1/**2**, 150-159/**160**-169	3r: 5´-GACAGCCAGG**C**TTGGAGGTC exon 3/**2**, 317-308/**307**-289	168
m*NOT*-3a	6f: 5´-AATCAACGAG**C**TACCCAGCT exon 1/**2**, 44-53/**54**-63	5r: 5´-GAGCAAGGCCATAC**C**TTGGAGG exon 3/**2**, 215-202/**201**-194	172
m*NOT*-3b	6f: 5´-AATCAACGAG**C**TACCCAGCT exon 1/**2**, 44-53/**54**-63	3r: 5´-GACAGCCAGG**C**TTGGAGGTC exon 3/**2**, 211-202/**201**-192	168
m*NOT*-3c	6f: 5´-AATCAACGAG**C**TACCCAGCT exon 1/**2**, 44-53/**54**-63	6r: 5´-CACCAGCAAC**C**TATGCCACC exon 6/**5**, 699-690/**689**-680	656
m*NOT*-4a	7f: 5´-CAATCACCGAG**A**CACAGAGATT exon 1/**2**, 43-53/**54**-64	3r: 5´-GACAGCCAGG**C**TTGGAGGTC exon 4/**3**, 311-302/**301**-292	269
m*NOT*-4b	7f: 5´-CAATCACCGAG**A**CACAGAGATT exon 1/**2**, 43-53/**54**-64	7r: 5´-GGAAACAATCT**C**TTGGAGGTCT exon 4/**5**, 312-302/**301**-291	270
m*NOT*-4c	10f: 5´-CCCAATCACC**T**TAGCCTCCT exon 1/**2**, 41-50/**51**-60	8r: 5´-ATCT**G**GTTAGGTGTGAGGGCT exon 4/**3**, 171-168/**167**-151	130
m*NOT*-5a	8f: 5´-AGGGTGGCAT**C**TACCCAGCT exon 1/**2**, 187-196/**197**-206	3r: 5´-GACAGCCAGG**C**TTGGAGGTC exon 3/**2**, 354-345/**344**-335	168

1: Positions relative to the respective ATG, accession numbers Tab. 64. Primer 2F was also used for amplification of *NOT*. In those cases where the used primers encompass two or more exons, the position of the first nucleotide of the second (and third) exon is in bold print. Underlined nucleotides are incorporated base exchanges to reach Tm: 54°C for all combinations. Wildtype bases are (Primer, position: Base): 2f, nt199: A; 3f, nt159: G; 6f, nt49: C; 6r, nt687: C. Annealing temperature for all 54°C; f: Forward; r: Reverse; 2: Size of the amplificate in nt.

3.2.4.2 Putative binding sites

All synthesized putative binding sites are biotinylated (btn) at the 5´ of the sense strand.

Tab. 36 Potential CREB binding sites within the human *NOT* promoter

Site[1]	Orientation	Sequence[2]
CREB s1	trans	(-15) 5´- cggcgcaccgttaag**atg**gcgg 3´- gccgc**gtgGCAATtcta**ccgcc
CREB s 2	cis	(-64) 5´- accta**agTGTCGaaggt**tcggg 3´- tggattcacagcttccaagccc
CREB s 3/4	cis/trans	(-96) 5´- agcct**ggtgGGACGccagg**cacggga 3´- tcggacc**accctGCGGTccgt**gccct
CREB s 5	cis	(-133) 5´- tggag**taaaTGAAGact**ggcta 3´- acctcatttacttctgaccgat
CREB s 6	trans	(-180) 5´- gcgtggagtgcatcagaggagaca 3´- cgcac**ctcacGTAGTctcc**tctgt
CREB s 7	cis	(-222) 5´- ggtat**aaacTGAGGagt**aagac 3´- ccatatttgactcctcattctg
CREB s 8	trans	(-315) 5´- agaatgctggcttcagcggttgtg 3´- tctta**cgaccGAAGTcgcc**aacac
CREB s 9	cis	(-474) 5´- caata**tgaaTGACTtttat**cagga 3´- gttatacttactgaaaatagtcct
CREB s 10/11	trans/trans	(-501) 5´- gctcatcactgcgtcctctcatatttt 3´- **cgaGTAGTgacGCAGGagagta**taaaa
CREB s 11/12	trans/cis	(-527) 5´- gcactcaaggtgtc**agacTCACGtgg** 3´- cgtga**gttccACAGTctga**gtgcacc
CREB s 13	trans	(-554) 5´- tgtactgccaagtcatttcctagg 3´- acatg**acggtTCAGTaaag**gatcc
CREB s 14	trans	(-588) 5´- ggaaaactatcgtccagaccct 3´- cctttt**gataGCAGGtc**tggga
CREB s 15	trans	(-637) 5´- gtggaacttccgtcctttacta 3´- cacct**tgaagGCAGGaa**atgat
CREB s 16	trans	(-729) 5´- ccgccggcccttcagccaatacgga 3´- ggcgg**ccggGAAGTcggtta**tgcct
CRE	cis	5´- aacctgctga**TGAAGTCA**caaaatgac 3´- ttggacgactacttcagtgttttactg

1: Potential CREB binding sites; 2: Positions upstream the *NOT*-1 ATG. Predicted sites in bold, core sequences in bold capital letters. The oligos were synthesized as single strands. The sense strands were labeled with biotin (btn) at 5´. For competition assays the unbiotinylated counterpart of each oligo was also synthesized. CRE: Reference oligo (Zhou and Chen 1999). ATG of *NOT*-1 in bold and underlined. The putative binding sites were predicted using the P-MATCH™ algorithm (Chekmenev *et al*. 2005; Ch. 3.5.1).

Tab. 37 Potential NFκB binding sites within the human *NOT* promoter

Site[1]	Specificity[2]	Orientation	Sequence[3]
NFκB s1	NFκB	cis	(-228) 5´- gggct**GGGTATAAAC**tgagg 3´- cccgacccatatttgactcc
NFκB s 2	NFκB	cis	(-270) 5´- gcttt**TCTGGACATTCGTT**ctaaa 3´- cgaaaagacctgtaagcaagattt
NFκB s 4/3	NFκB, p65 (s4)	cis/trans	(-346) 5´- tgaaca**CAGATGTTCCC***Cagcgcag* 3´- acttg**TGTCTACAAGGGTC**gcgtc
NFκB s 6/5	p50 (s5)	cis/trans	(-380) 5´- cgaac**AGGGGCTTTGC**cctcctgg 3´- gcttg**TCCCCGAAACGGGA**ggacc
NFκB s 7	NFκB	trans	(-415) 5´- catccggaaggctcgaaggg 3´- gtagg**CCTTCCGAGC**ttccc
NFκB s 8	NFκB	cis	(-549) 5´- tgcca**AGTCATTTCC**taggg 3´- acggttcagtaaaggatccc
NFκB s 10/9	NFκB	trans	(-594) 5´- cggctgggaaaactatcgtccagaccctgaat 3´- gccga**CCCTTTTGAT**ag**CAGGTCTGGG**actta
NFκB s 11	NFκB	trans	(-612) 5´- gctcttcgaagaatcctccggctg 3´- cgaga**AGCTTCTTAGGAGG**ccgac
NFκB s 13/12	p65	cis/trans	(-643) 5´- aaaca**CGTGGAACTTCCGTC**cttta 3´- tttgtg**CACCTTGAAGGCAG**gaaat
NFκB s 15/14	p65 (s15)	cis/trans	(-685) 5´- gggcgc**TGGTGTCTCC**gcccacca 3´- cccgc**GACCACAGAGGCGG**gtggt
NFκB s 17/16	NFκB	cis/trans	(-773) 5´- ctgcc**CCTGGAGAGGCCAT**gctct 3´- gacgggga**CCTCTCCGGT**acgaga
NFκB s 19/18	NFκB (s18), p65 (s19)	cis/trans	(-800) 5´- gctccGGTAAC**TCCGGAGGCGCCCT**acctg 3´- **CGAGGCCATTGAGGCCTCCGCGGG**atggac
NFκB s 18	p65	trans	(-816) 5´- cggtacccgcagttccgctccggta 3´- gccat**GGGCGTCAAGGCGAGGCCAT**
NFκB s 20	p50	trans	(-898) 5´- gaaggaggagaagtccccgaacca 3´- cttcc**TCCTCTTCAGGGGC**ttggt
NFκB s 22/21	p50/p65 (s22), p65 (s21)	cis/trans	(-978) 5´- ctggc**GGGGCCGCGCCGGGATTACCCAC**ctagc 3´- gaccgccccggcgcgg**CCCTAATGGG**tggatcg
NFκB R1	NFκB	cis	5´- GATCGCTGGGACTTTCCAGGA 3´- CTAGCGACCCTGAAAGGTCCT
NFκB R2	NFκB	cis	5´- CCACAGTTGGGATTTCCCAACCTGACCAG 3´- GGTGTCAACCCTAAAGGGTTGGACTGGTC

1: Potential NFκB binding sites; 2: Binding specificity; If an oligo contains overlapping sites on the complementary strands the *cis* site is indicated first; s4/3 overlaps with the potential EGR-1 site shown in italics (site 4, Tab. 38); 3: Positions upstream the *NOT*-1 ATG, predicted sites in bold. The oligos were synthesized as single strands. The sense strands were labeled with biotin (btn) at 5´. For competition assays the unbiotinylated counterpart of each oligo was also synthesized. NFκB R1: Reference oligo 1 (Armstrong *et al*. 1993); NFκB R2: Reference oligo 2 (Ron *et al*. 1990). The putative binding sites were predicted using the P-MATCH™ algorithm (Chekmenev *et al*. 2005; Ch. 3.5.1).

Tab. 38 Potential EGR-1 binding sites within the human *NOT* promoter

Site[1]	Orientation	Sequence[2]
EGR-1 s2	cis	(-46) 5´- cgggt**ttccGGGGGtgg**tgggc 3´- gcccaaaggcccccaccacccg
EGR-1 s3	cis	(-301) 5´- agcgg**ttgtGGGGGagg**taggc 3´- tcgccaacacccccctccatccg
EGR-1 s4[1]	cis	(-335) 5´- *gttcc**cag**cGCAGGcGAAGGaga*atgct 3´- caagggtcgcgtccgcttcctcttacga
EGR-1 s5	cis	(-690) 5´- aggcg**gggcGCTGGtgt**ctccg 3´- tccgccccgcgaccacagaggc
EGR-1 s6	cis	(-795) 5´- ggtaa**ctccGGAGGcgc**cctac 3´- ccattgaggcctccgcgggatg
EGR-1 s7	cis	(-880) 5´- gaacc**aatcGTAGGggg**cagaa 3´- cttggttagcatcccccgtctt
EGR-1 R1		5´- ggatccagcgggggcgagcgggggcg 3´- cgcccccgctcgcccccgctggatcc
EGR-1 s4[2]	5´- a***CAGATGTTCCCag*cGCAGGcGAAGGaga**atgctggcttca 3´- tgtctacaagggtcgcgtccgcttcctcttacgaccgaagt	
EGR-1 s4[3]	5´- *CCag*cGCAGGcGAAGGac**agcGCAGGcGAAGGaga**atgctggcttca 3´- ggtcgcgtccgcttcctgtcgcgtccgcttcctcttacgaccgaagt	
EGR-1 s4[4]	5´- agacagcatgaaca***CAGATGTTCC**atgctggcttcagcgg 3´- tctgtcgtacttgtgtctacaaggtacgaccgaagtcgcc	
EGR-1 s4[5]	5´- cagcatgaac**cGCAGGcGAAGGaga**atgctggcttcagcgg 3´- gtcgtacttggcgtccgcttcctcttacgaccgaagtcgcc	

1: Potential EGR-1 binding sites. S4 overlaps with the potential NFκB binding site shown in italics (site 4/3 in Tab. 37); 2: Positions upstream the *NOT*-1 ATG. Position of s4 variants: s4[2]: 341; s4[4]: 354; s4[5]: 351; s4[3] contains a tandem repeat of s4 (underlined with one site in bold), first nt is 332nt upstream *NOT*-1 ATG. Predicted sequences in bold. The oligos were synthesized as single strands. The sense strands were labeled with biotin (btn) at 5´. For competition assays the unbiotinylated counterpart of each oligo was also synthesized. EGR-1 R1: Reference oligo (De Backer *et al.* 2009). The putative binding sites were predicted using the P-MATCH™ algorithm (Chekmenev *et al.* 2005; Ch. 3.5.1).

Tab. 39 Potential MYCN binding sites within the human *NOT* promoter

Site[1]	Orientation	Sequence[2]
MYCN s1/2	trans	(-85) 5´- acgcc**aggcACGGGaag**cggaac 3´- tgcgg**tccGTGCCcttc**gccttg
MYCN s 3	cis	(-189) 5´- tccta**tggaGCGTGgag**tgcat 3´- aggatacctcgcacctcacgta
MYCN s 4/5	trans/cis	(-516) 5´- gtcag**actCACGTgggc**tcatc 3´- cagtc**tgaGTGCAcccg**agtag
MYCN s 6/7	trans/cis	(-648) 5´- aacac**aaaCACGTggaa**cttcc 3´- ttgtg**tttGTGCAcctt**gaagg
MYCN s 8/9	trans/cis	(-671) 5´- ccgcc**cacCACCTgcag**ttgct 3´- ggcgg**gtgGTGGAcgtc**aacga
MYCN s 10	trans	(-910) 5´- taggagggcacggaaggaggag 3´- atcct**cccGTGCCttcc**tcctc
MYCN R1	cis	5´- cttcagcgagc**CACGTG**gaccaactc 3´- gaagtcgctcggtgcacctggttgag

1: Potential MYCN binding sites; 2: Positions upstream the *NOT*-1 ATG. Predicted sequences in bold letters, core sequences in capital bold letters. The oligos were synthesized as single strands. The sense strands were labeled with biotin (btn) at 5´. For competition assays the unbiotinylated counterpart of each oligo was also synthesized. MYCN R1: Reference oligo (Perini *et al*. 2005). The putative binding sites were predicted using the P-MATCH™ algorithm (Chekmenev *et al*. 2005; Ch. 3.5.1).

Tab. 40 Potential NFκB binding sites within the m*NOT* promoter

Site[1]	Specificity[2]	Orientation	Sequence[3]
NFκB s1	NFκB	cis	(-362) 5´- tctga**AAGGGACATACACC**gagaa 3´- agactttccctgtatgtggctctt
NFκB s 3	NFκB	cis	(-399) 5´- tttct**GGGCAAACAC**tgata 3´- aaagacccgtttgtgactat
NFκB s 4	NFκB/p65	cis	(-461) 5´- actct**GGGCATAGGC**agagt 3´- tgagacccgtatccgtctca
NFκB s 6	NFκB/p65	cis	(-498) 5´- tactg**AAAGGAGCTTTCCC**ctcta 3´- atgactttcctcgaaaggggagat
NFκB s 11	NFκB/p65	cis	(-779) 5´- aaaca**CGTGGAACTTCCGTC**acctt 3´- tttgtgcaccttgaaggcagtggaa

1: Potential NFκB binding sites; 2: Binding specificity; 3: Positions upstream the m*NOT*-1 start codon, predicted sites in bold capital letters. The oligos were synthesized as single strands. The sense strands were labeled with biotin (btn) at 5´. For competition assays the unbiotinylated counterpart of each oligo was also synthesized. The putative binding sites were predicted using the P-MATCH™ algorithm (Chekmenev *et al*. 2005; Ch. 3.5.1).

Tab. 41 Potential CREB binding sites within the m*NOT* promoter

Site[1]	Orientation	Sequence[2]	
CREB s1	trans	(-484) 5´-	ttcccctctacgtgaacacaactact
		3´-	aagggGAGATGCACTTGTGTTgatga
CREB s2	trans	(-581) 5´-	caataagaggcgtgattaattaaa
		3´-	gttatTCTCCGCACTAATTaattt
CREB s3/4	trans/cis	(-655) 5´-	aaccggatctggtCACTAGACGTGACCAGGCTcatta
		3´-	ttggcCTAGACCAGTGATCTGCACTGGTCCGagtaat
CREB s5	trans	(-716) 5´-	aattacttggtgtcatattaacga
		3´-	ttaatGAACCACAGTATAAttgct
CREB s6	cis	(-707) 5´-	GTGTCATATTAACGAACTGcccgt
		3´-	cacagtataattgcttgacgggca
CREB s7	trans	(-773) 5´-	gtggaacttccgtcaccttctaagct
		3´-	cacctTGAAGGCAGTGGAAGAttcga
CREB s8	cis	(-958) 5´-	ctggaCTTGGCGGTACTggaag
		3´-	gacctgaaccgccatgaccttc
CREB s9	trans	(-993) 5´-	gagtcggccgcgtctttgtagcgc
		3´-	ctcagCCGGCGCAGAAACAtcgcg
CREB s10	trans	(-1074) 5´-	aggatacggtcctcaggacacagc
		3´-	tcctaTGCCAGGAGTCCTGtgtcg

1: Potential CREB binding sites; 2: Positions upstream the m*NOT*-1 start codon, predicted sites in bold capital letters. The oligos were synthesized as single strands. The sense strands were labeled with biotin (btn) at 5´. For competition assays the unbiotinylated counterpart of each oligo was also synthesized. The putative binding sites were predicted using the P-MATCH™ algorithm (Chekmenev *et al*. 2005; Ch. 3.5.1).

3.2.4.3 siRNAs

Tab. 42 Applied siRNAs

Target	siRNA	Cat. No.	Concentration
scrambled (AllStars Negative Control siRNA)		1027280	10nM
p50	Hs_NFKB1_7	SI02654932	50nM
p65	Hs_RELA_7	SI02663094	25nM
RPS3	Hs_RPS3_2	SI00707798	Mix: 12.5nM each
	Hs_RPS3_8	SI04238808	
	Hs_RPS3_7	SI04340777	
	Hs_RPS3_9	SI04189262	
EGR-1	Hs_EGR1_6	SI03069108	Mix: 12.5nM each
	Hs_EGR1_7	SI03078950	
	Hs_EGR1_4	SI00030709	
	Hs_EGR1_5	SI03052511	

3.2.5 Antibodies

Tab. 43 Primary antibodies

Name/Target	Source	Epitope	Dilution	Obtained from
Actin (20-33) A5060	rabbit polyclonal	aa20-33	1:1000	Sigma-Aldrich
BiP (GRP78) #3183	rabbit polyclonal	full-length	1:1000	Cell Signaling
Caspase-3 (H-277): sc-7148	rabbit polyclonal	aa1-277	1:200	Santa Cruz
CBP (H-300): sc-20686	rabbit polyclonal	aa671-970	1:200	Santa Cruz
CREB-1 (240): sc-58	rabbit polyclonal	α-region	1:200	Santa Cruz
p-CREB-1 (Ser 133): sc-7978	rabbit polyclonal	aa around Ser-133-P	1:200	Santa Cruz
CREB3 (D01P)	rabbit polyclonal	full-length	1µg/ml	Abnova
Cyclin D1 (DCS-6): sc-20044	mouse monoclonal	full-length	1:200	Santa Cruz
EGR-1 (15F7) #4153	rabbit monoclonal	N-terminus	1:1000	Cell Signaling
GAL4-AD (G9293)	rabbit polyclonal	aa867-881	1µg/ml	Sigma-Aldrich
GAL4-BD (G3042)	rabbit polyclonal	aa39-52	1µg/ml	Sigma-Aldrich
IKBbeta ab7547	rabbit polyclonal	C-terminus	1µg/ml	Abnova
IKKβ (62AT216): sc-130152	mouse monoclonal	full-length	1:200	Santa Cruz
KPNA4 A301-627A		aa471-521	1:1000	Bethyl
NFKBIA, clone 6A055 MAB1760	mouse monoclonal	full-length	1µg/ml	Abnova
NFκBp65 (F6): sc-8008	mouse monoclonal	aa1-286	1:200	Santa Cruz
NFκBp65 (phospho S276) ab30623	rabbit polyclonal	aa around Ser276-P	1:1000	Abcam
NFκBp65 (phospho S536) ab76302	rabbit monoclonal	aa around Ser536-P	1:1000	Abcam
NFκBp50 (4D1): sc-53744[1]	mouse monoclonal	full-length	1:200	Santa Cruz
NFκB p50 (C-19): sc-1190[2]	goat polyclonal	C-terminus	1:200	Santa Cruz
NOT 1/4	rabbit polyclonal	C-terminus	1µg/ml	Kurzik-Dumke, U.
NOT 1[b]	rabbit polyclonal	N-terminus NOT-1	1µg/ml	Kurzik-Dumke, U.
NOT 4	rabbit polyclonal	N-terminus NOT-4	1µg/ml	Kurzik-Dumke, U.
n-Myc ab24193	rabbit polyclonal	aa1-100	1µg/ml	Abcam
n-Myc (phospho S54) (ab70234)	rabbit polyclonal	aa around Ser54-P	1:1000	Abcam
p300 (H-272): sc-8981	rabbit polyclonal	aa774-1045	1:200	Santa Cruz
p53 (13-4000)	mouse monoclonal	aa32-79	1:2000	Life Technologies
RNA polymerase II (ab52202)	rabbit polyclonal	CTD repeat	1:1000	Abcam
RNA polymerase II (phospho S5) (ab5131)	rabbit polyclonal	Ser5-P CTD repeat	1:1000	Abcam
RPS3 (M03) H00006188-M03	mouse monoclonal	aa144-244	1µg/ml	Abnova
TBP (1TBP18)	mouse monoclonal	aa1-20	1:2000	Abcam
Tid	rabbit polyclonal	full-length	3µg/ml	Kurzik-Dumke, U.

1: Used for western blots (Ch. 3.4.3) and ELISAs (3.5.4); 2: Used for ChIPs (Ch. 3.5.7)

Tab. 44 Secondary antibodies

Name	Source	Conjugate[1]	Dilution	Obtained from
anti-mouse IgG (A3562)	goat polyclonal	AP	1:5000	Sigma-Aldrich
anti-rabbit IgG (A3687)	goat polyclonal	AP	1:5000	Sigma-Aldrich
anti-goat IgG (A4187)	rabbit polyclonal	AP	1:30000	Sigma-Aldrich
anti-mouse IgG (A9044)	rabbit polyclonal	HRP	1:5000	Sigma-Aldrich
anti-rabbit IgG (A6154)	goat polyclonal	HRP	1:5000	Sigma-Aldrich

1: Antibody labeled with alkaline phosphatase (AP) or horseradish peroxidase (HRP).

3.2.6 Recombinant proteins and nuclear extracts

Recombinant proteins and nuclear extracts were used as positive controls in transcription factor ELISAs (Ch. 3.4.5). In addition, recombinant proteins were used as molecular weight standard in EMSAs (Ch. 3.5.3). All recombinant proteins and nuclear extracts were stored at -80°C.

Tab. 45 Recombinant proteins and nuclear extracts

Name	Expressed in	Tag[1]	Manufacturer
EGR-1 (E5777)	Sf9	---	Sigma-Aldrich
CREB3 (H00010488-P01)	Wheat germ	GST	Abnova
p50 (31101)	*E. coli*	---	Active Motif
p65 (31102)	*E. coli*	---	Active Motif
HeLa NE[2]	---	---	Active Motif
HeLa + TNFα 20ng/ml, 30min. NE[2]	---	---	Active Motif
HeLa + TPA 62ng/ml, 10min. NE[2]	---	---	Active Motif

1: Affinity tag used for protein purification; 2: Nuclear extract (NE).

3.2.7 Purchased full-length cDNA clones and cDNA libraries

Tab. 46 Full-length cDNA clones

Gene	Clone name	Reference[1]	Host	Vector	Cloning sites
EGR-1	IRATp970D09107D	NM_001964	DH10B	pCMV-SPORT6	5´: *Sal*I; 3´: *Not*I
MYCN	IRALp962C0412Q	NM_005378	DH10B	pOTB7	5´: *Eco*RI; 3´: *Xho*I

All clones were purchased from Source BioScience (Berlin); 1: NCBI reference number.

Tab. 47 Purchased cDNA library

Name	Host	Vector	Cloning sites
Human Mammary Gland cDNA library	*E. coli* BNN132	pACT2	5´: *Eco*RI; 3´: *Xho*I

The library was purchased from Clontech (Heidelberg).

3.2.8 Bacterial cells

Tab. 48 Characteristics of the applied bacterial cell lines

Strain	Genotype[1]	Resistance	Transformation efficiency (cfu/µg)	Manufacturer
XL1-Blue (*E. coli*)	*recA1 endA1 gyrA96 thi-1 hsdR17 supE44 relA1 lac* [F´ *proAB lacI*^{q}*ZΔM15* Tn*10* (Tetr)]	tetracycline	> 1x10^{9}	Stratagene (USA)
DH10B (*E. coli*)	F- *mcr*A Δ(*mrr-hsd*RMS-*mcr*BC) φ80*lacZ*ΔM15 Δ*lac*X74 *rec*A1 *end*A1 *ara*D139 Δ (*ara, leu*)7697 *gal*U *gal*K λ- *rps*L *nup*G /pMON14272 / pMON7124	---	> 1x1^{10}	Source BioScience

1: The genes indicated are mutated alleles, the genes on the F´ episome are wild-type alleles unless indicated otherwise.

3.2.9 Yeast cell line

Tab. 49 Characteristics of the *Saccharomyces cerevisiae* strain Y187

Strain	Genotype[1]	Reporters	Markers	Manufacturer
Y187 (*Saccharomyces cerevisiae*)	*MATα, ura3-52, his3-200, ade2-101, trp1-901, leu2-3, 112, gal4Δ, gal80Δ, met–, URA3 : : GAL1*$_{UAS}$*-GAL1*$_{TATA}$*-LacZ MEL1*	*MEL1, LacZ*	*trp1, leu2*	Clontech

1: Y187 cells are auxotroph for leucine, tryptophan and histidine.

3.2.10 Mammalian cell lines

Techniques for cultivation and storage are described in Ch. 3.6.

Tab. 50 Applied murine cell lines

Name	Type	Morphology	Medium	Doubling	Reference
NIH-3T3	Embryonal fibroblast	adherent monolayer	RPMI	~20h	Jainchill *et al*. (1969)
MOCHA	Skin fibroblast	adherent monolayer	DMEM-F12	~20h	Peden *et al.* (2002)
BC3H1	Smooth muscle derived from a nitrosoethylurea induced neoplasm	adherent monolayer	DMEM-F12		Schubert *et al*. (1974)
C127I	Epithelioid mammary gland carcinoma	adherent monolayer	DMEM-F12		Lowy *et al*. (1978)

Tab. 51 Applied human cell lines

Name	Type	Age[1]	Karyotype	Morphology	Medium	Doubling	Reference
HaCaT	normal (not tumorigenic) caucasian keratinocyte	62a	male, hypo-tetraploid	adherent monolayer	DMEM/F-12	~20h	Boukamp *et al.* (1988)
HT-29	caucasian colon adeno-carcinoma epithelioid	44a	male, hypertriploid	adherent monolayer / colonies	RPMI	~40-60h	Fogh *et al.* (1975)
T98G	caucasian glioblastoma	61a	male, hyper-pentaploid	adherent monolayer	EMEM	~20h	Stein (1979)
HeLa	negroid epi-thelioid cervix carcinoma	58a	female, aneuploid	adherent monolayer	RPMI	~48h	Gey *et al.* (1952)
HEK293	embryonal kidney	---	hypotriploid	semi-adherent monolayer	DMEM/F-12	~24h	Graham *et al.* (1977)

1: Age at the time of isolation, a: Years. In the case of HEK293 the cells were isolated from an abortion of unknown origin.

3.2.11 Applied Kit systems

Tab. 52 Applied Kit systems

Name	Manufacturer
Advansta Western Bright™ Quantum™ Chemiluminescent Kit	Biozym Scientific GmbH, Oldendorf
ChIP-IT™ Express	Active Motif, Rixensart (Belgium)
CREB (Phospho-Ser^{133}) Transcription Factor Assay Kit	Biomol GmbH, Hamburg
Dynabeads® M-280 Streptavidin	Life Technologies, Darmstadt
GenElutePCR™ Clean-Up Kit	Sigma-Aldrich, Steinheim
GenElutePCR™ Gel Extraction Kit	Sigma-Aldrich, Steinheim
KAPA SYBR® FAST qPCR Kit	PeqLab GmbH, Erlangen
LightShift®Chemiluminescent EMSA Kit	Pierce, Rockford (USA)
Matchmaker™ One-Hybrid Library Construction &Screening Kit	Clontech, Heidelberg
NF-kB (human p50) Transcription Factor Assay Kit	Biomol GmbH, Hamburg
NF-kB (p65) Transcription Factor Assay Kit	Biomol GmbH, Hamburg
Nuclear Extract Kit	Active Motif, Rixensart (Belgium)
peqGOLD Plasmid Miniprep KitII	PeqLab GmbH, Erlangen
QuantiTect® SYBR® Green PCR Kit	Qiagen, Hilden
Re-ChIP-IT™	Active Motif, Rixensart (Belgium)
SMARTer™ RACE cDNA Amplification Kit	Clontech, Heidelberg
TURBO DNA-*free*™ Kit	Life Technologies, Darmstadt
Venor®GeM Mycoplasm Detection Kit	Minerva Biolabs GmbH, Berlin

3.3 DNA and RNA techniques

3.3.1 Isolation and purification of plasmid DNA from bacterial cells

Plasmid DNA isolation was performed according to the alkaline lysis method (Brinboim and Doly 1979). Bacterial cultures used for DNA isolation were raised from single colonies. Cells were grown in LB medium (Ch. 3.1.6, Tab. 12) supplemented with the respective antibiotic (ampicillin: 100µg/ml; kanamycin: 50µg/ml; chloramphenicol: 30µg/ml) for 16-20h at 37° on a shaking incubator at 180rpm.

3.3.2 Quantification of nucleic acids using spectrophotometry

To determine the concentration of the DNA- and RNA-samples, the optical density (OD) was measured at 260nm wavelength. The concentration was calculated according to the formula:

$$c\ [\mu g/ml] = OD260 \times \text{dilution factor} \times 50\ \mu g/ml\ (dsDNA)$$

The OD of a solution containing 50 µg/ml dsDNA (or 40 µg/ml ssDNA or 33 µg/ml ssRNA) is 1. To estimate the purity of the preparations the OD260/OD280 ratio was determined. Values 1.6-1.8 describe pure DNA/RNA samples. The DNA concentration was determined using the Bio Photometer (Eppendorf) and RNA concentration using the NanoDrop1000 (PeqLab).

3.3.3 Separation of nucleic acids using agarose gel electrophoresis

To separate DNA molecules according to their molecular weight, agarose gel electrophoresis was performed according to standard procedures. Depending on the size of the DNA to be separated 0.8% - 2% horizontal agarose gels in 1x TAE buffer (Ch. 3.1.5, Tab. 4) supplemented with 0.5µg ethidium bromide per 100ml were used. The samples were supplemented with 6x DNA Loading Dye (Thermo Fisher; Ch. 3.1.5, Tab. 4) to a final concentration of 1x prior to loading onto the gel. Evaluation took place under UV-light (λ = 316 nm) using the gel documentation software Phoretix Grabber v3.01 (NonLinear Dynamics).

3.3.4 Amplification of DNA using polymerase chain reaction (PCR)

The polymerase chain reaction (PCR) method (Saiki *et al.* 1985) was used to selectively and exponentially amplify nucleic acids in repeated cycles of primer annealing, amplification by a thermostable DNA polymerase, and denaturation. Depending on the experimental question different polymerases (Ch. 3.2.1, Tab. 16), reaction conditions (Tab. 53), and PCR programs were used (Tab. 54).

Tab. 53 PCR reaction set-ups

Approach / Components[1]	Cloning[2]	(Re-)ChIP[2]	RT-PCR/cDNA-Amplification[3]	RACE[4]
Forward Primer	10pmol	10pmol	10pmol	10pmol
Reverse Primer	10pmol	10pmol	10pmol	10pmol
Template	50ng-1µg	5µl	0.5µl	10µl
10mM dNTPs	1µl	1µl	1µl	1µl
25mM $MgCl_2$	4µl	2.5µl	---	---
10x Taq-buffer with $(NH_4)_2SO_4$	5µl	2.5µl	---	---
10x PCR buffer	---	---	3µl	---
10X Advantage 2 PCR Buffer	---	---	---	3µl
Polymerase	5u	1u	5u	1µl
H_2O	to 50µl	to 25µl	to 30µl	to 30µl

1: The indicated buffers were provided with the respective polymerase (Ch. 3.2.1, Tab. 16) used for amplification; 2: Amplified using recombinant *Taq* DNA Polymerase (Thermo Fisher); 3: Amplified using HotStarTaq Plus DNA Polymerase (Qiagen); 4: Amplified using the Advantage 2 Polymerase Mix (Clontech).

Tab. 54 Applied PCR programs

Approach / Components	Cloning/RACE[1]		(Re-)ChIP		cDNA amplification		Sequencing[2]	
	T [°C]	Time	T [°C]	Time	T [°C]	Time	T [°C]	Time
1. Activation	94	3min.	94	3min.	95	5min.	98	30sec.
2. Denaturation	94	30sec.	94	20sec.	94	30sec.	96	10sec.
3. Annealing	44-59	30sec.	59	30sec.	54	30sec.	50	5sec.
4. Extension	72	1min.	72	30sec.	72	3min.	60	4min.
5. Final extension	72	15min.	---	---	72	15min.	60	1sec.
6. End temp.	4	HOLD	4	HOLD	4	HOLD	4	HOLD
Repeat steps 2. - 4.	40x		40x		40x		25x	

1: For amplification of RACE cDNA the annealing was performed at 68°C, 30sec. and extension at 72°C, 3min.; 2: Sequencing is described in Ch. 3.3.6.

3.3.5 Purification of DNA fragments after enzymatic restriction and amplification

Purification of DNA fragments generated by enzymatic restriction or amplification was performed using the GenElute™ PCR Clean-Up Kit (Sigma-Aldrich) according to the manufacturer´s instructions. DNA fragments separated by gel electrophoresis (Ch. 3.3.3) were extracted from the gels using the GenElute™ Gel Extraction Kit (Sigma-Aldrich) according to the manufacturer´s instructions. The DNA was eluted with 30-40µl of the preheated (65°C) Elution Buffer provided with the kit.

3.3.6 DNA sequencing

DNA sequencing was performed according to the chain termination method first described by Frederick Sanger *et al*. (1977) and modified by Lee *et al.* (1992). The sequencing reaction was set up in 10µl as follows:

template DNA (20-100ng PCR product / 100-700ng plasmid DNA)
10pmol sequencing primer
1x BigDye buffer
2µl 3.1 BigDye terminators.

BigDye components were purchased from GENterprise Genomics, Mainz (Germany). The amplification reaction was performed using the sequencing program (Tab. 54). Sequencing was conducted by GENterprise Genomics. Sequence analysis was performed using the FinchTV (Geospiza) and Jellyfish software v1.5_5689 (Biowire).

3.3.7 Enzymatic restriction of DNA for cloning purposes

For cloning purposes DNA was restricted using diverse restriction endonucleases (Tab. 15) in the following reaction:

5-15µg plasmid DNA / 1-5µg linear DNA
1x enzyme specific reaction buffer
3u/µg DNA enzyme
to 50µl H_2O

The samples were incubated for 90min. in a water bath at 37°C (*Sma*I at 30°C). The DNA fragment(s) of interest were purified as described in Ch. 3.3.5.

3.3.8 Dephosphorylation of restricted plasmid DNA

To prevent self-ligation, restricted purified plasmid DNA was dephosphorylated using FastAP™ Thermosensitive Alkaline Phosphatase (Thermo Fisher; Ch. 3.2.1, Tab. 17) according to the manufacturer´s instructions. The reaction mix consisted of:

5µg DNA
1u Fast-AP™
1x Fast-AP™ buffer
to 50µl H_2O

The dephosphorylated vector DNA was purified as described in Ch. 3.3.5.

3.3.9 Blunting of overhangs

To generate blunt-ended DNA, digestion using the Klenow fragment (Klenow Fragment is the Large Fragment of DNA Polymerase I from *E. coli*; Ch. 3.2.1, Tab. 16) was performed. This enzyme exhibits 5´-3´ polymerase activity and 3´-5´exonuclease activity but lacks 5´-3´exo-nuclease activity. Thus it can be used to either fill in 5´ overhangs or to remove 3´overhangs. The reaction mix was set up according to the manufacturer´s instructions.

3.3.10 Ligation of restricted DNA fragments for cloning purposes

Ligation of linear DNA fragments was performed using bacteriophage derived T4 DNA ligase (Ch. 3.2.1, Tab. 17). For ligation 50-100ng restricted and dephosphorylated vector DNA was used. The amount of the insert DNA was calculated using the following formula:

$$\frac{([ng]\ \text{vector}) \times ([bp]\ \text{insert})}{[bp]\ \text{vector}} \times \text{molar ratio insert/vector} = [ng]\ \text{insert}$$

The reaction mix consisted of:

50-100ng vector DNA
x ng insert DNA (ratio insert/vector 1:5)
1u T4 Ligase (5u for blunt-end ligation)
1x T4 DNA Ligase buffer
to 20µl H_2O

For ligation of blunted DNA ends, 2µl of 50% PEG4000 (polyethylene glycol) was added to the reaction mix in order to increase the ligation rate (Pheiffer and Zimmerman 1983). The reaction was carried out for 1h at 22°C in a water bath. The enzyme was inactivated by heat-shock at 65°C for 10min. Ligated DNA was identified by separation on agarose gels (Ch. 3.3.3). The correctness of the cloning was controlled by restriction (Ch. 3.3.7) and sequencing (Ch. 3.3.6).

3.3.11 Preparation of competent XL1-Blue bacterial cells

Competent XL1-Blue *E. coli* cells (Ch. 3.2.8, Tab. 48) were generated using the rubidium chloride technique as described by Hanahan (1983). Cells were shock-frozen in liquid nitrogen as 100µl aliquots and stored at -80°C.

3.3.12 Transformation of competent XL1-Blue bacterial cells

For propagation purposes, plasmid DNA was transformed to competent XL-1 Blue *E. coli* cells (Ch. 3.2.8, Tab. 48) according to the heat-shock method (Cohen *et al*. 1972). Competent cells (Ch. 3.3.11) were thawed on ice and mixed with 10-100ng plasmid DNA or the complete reaction samples from ligations (Ch. 3.3.10). After 30min. incubation on ice, the cells were heat-shocked at 42°C for 1 min and then immediately cooled down on ice. Prior to incubation (37°C, 45min, 180rpm) 500µl SOC medium was added to the sample. After incubation the cells were pelleted by centrifugation at 12000rpm for 15s and resuspended in 100µl sterile 0.9% NaCl. Cells were plated on LB agar (Ch. 3.1.6, Tab. 12) supplemented with 100µg/ml ampicillin or 50µg/ml kanamycin.

3.3.13 Generation of bacterial and yeast glycerol stocks

For long-time storage of bacterial and yeast cells glycerol stocks were generated. Bacterial cells

were grown as described in Ch. 3.3.1. In the case of yeast single colonies of untransformed Y187 cells (Ch. 3.2.9, Tab. 49) were cultured in YPDA (Ch. 3.1.6, Tab. 11), whereas transformed cells (Ch. 3.4.4.1) were cultured in SD medium (Ch. 3.1.6, Tab. 11) lacking the respective amino acids used as growth marker (Ch. 3.4.4 and Ch. 3.5.2). Incubation of yeast cells was performed for 16-20h at 30°C on a shaking incubator at 230rpm. All cells to be stored were harvested at the exponential phase of growth. The cells were aliquoted á 500µl and supplemented 1:1 with sterile glycerol (50%). The bacterial cells were shock frozen in liquid nitrogen and stored at -80°C, whereas the yeast cells were stored directly at -80°C.

3.3.14 Vector constructs

The full-length expression constructs pACT2-NFκBp50, pAS2-1-NFκBp50, pACT2-NFκBp65, pAS2-1-NFκBp65, pACT2-RPS3, pACT2-p53, pACT2-CREB1, and pACT2-CREBL1 were generated in the Kurzik-Dumke laboratory by M. Szydlowski (PhD thesis: Identification of the regulatory elements and factors of the human tumor suppressor gene *tumorous imaginal discs*, 2011). The full-length pACT2-CREB3 construct and the deletion constructs pACT2-CREB3-2 (aa1-231), pACT2-CREB3-3 (aa1-154), pACT2-CREB3-4 (aa155-231), pACT2-CREB3-5 (aa155-315), and pACT2-CREB3-6 (aa93-154) were generated in the Kurzik-Dumke laboratory by B. Hacker (PhD thesis: Beitrag zur Aufklärung der zellulären Rolle des humanen *neighbour of tid* (*not*) Gens, 2016). The full-length pEGFP-N3-CREB3 construct was generated in the Kurzik-Dumke laboratory by M. Döring (Diploma thesis: Generierung von Vektoren zur kontrollierbaren transienten Expression und Abschaltung des humanen *not* Gens, 2012). All other constructs were generated as described below (Ch. 3.3.14.1-3.3.14.5).

3.3.14.1 Generation of *NOT* promoter constructs

All 19 *NOT* promoter constructs (Ph*NOT*; P; Ch. 3.3.14.1 and Ch. 3.3.14.2) were cloned into pHIS2.1 (Ch. 3.2.2, Fig. 11). The Ph*NOT*-1 construct was generated by amplification (Ch. 3.3.4) using the BAC clone RP11-488M12 (NCBI: AC061705) as template and the primers Phnot-F1 (equipped with an *Eco*RI site) and Phnot-R1 (equipped with an *Sal*I site) (Ch. 3.2.4.1, Tab. 29). It encompasses the 1150nt upstream of the *NOT*-1 start codon. The fragment was cloned via *Eco*RI at 5´ and *Sal*I at 3´. The constructs Ph*NOT*-2 to -4 were generated by amplification using specific

forward primer primers in combination with *Sac*I-equipped reverse primers (Ch. 3.2.4.1, Tab. 29) and Ph*NOT*-1 as template. The fragments were cloned via blunted 5´ and *Sac*I at the 3´ into pHIS2.1. Construct Ph*NOT*-2 encompasses the region 704nt to ATG, Ph*NOT*-3 525nt to ATG and Ph*NOT*-4 1115nt to 686nt.

3.3.14.2 Generation of *NOT* promoter constructs with deleted NFκB binding sites

Using the P-MATCH^{TM} algorithm (Chekmenev *et al*. 2005; Ch. 3.5.1) 22 potential NFκB sites (Ch. 3.2.4.2, Tab. 37), thereof 10 in *cis*, were predicted within the 1150bp *NOT* promoter region. To determine their binding capacity via yeast one-hybrid (Y1H) (Ch. 3.5.2), 5 constructs, Ph*NOT*-5 to -9 (P5-9), encompassing the following regions upstream the *NOT*-1 start codon have been generated: P5: 1115-932nt; P6: 912-686nt; P7: 704-504nt; P8: 421-228nt, P9: 248-87nt. For the synthesis of the Ph*NOT* promoter fragments the services of the ATG:biosynthetics GmbH (Merzhausen) have been used. The fragments were equipped with the restriction sites *Eco*RI at 5´ and *Bam*HI at 3´ and cloned into the pBluescript vector (Ch. 3.2.2, Fig. 8). For recloning into pHIS2.1 (Ch. 3.2.2, Fig. 11) the pBluescript constructs were digested with *Eco*RI and *Bam*HI (Ch. 3.3.7) and recloned into pHIS2.1 (Ch. 3.2.2, Fig. 11) via *Eco*RI at 5´ and blunted *Bam*HI at 3´ (Ch. 3.3.8 -3.3.10). In addition derivatives of P5-9 were generated containing defined deletions of the predicted NFκB binding sites in *cis* (Ch. 3.2.4.2, Tab. 37) termed (D for deletion): P5^{D1}: P5 without s22 (973-951nt); P6^{D1}: P6 without s19/18 (789-776nt); P6^{D2}: P6 without s17/16 (768-755nt); P7^{D1}: P7 without s15/14 (679-670nt); P7^{D2}: P7 without s13/12 (638-624nt); P7^{D3}: P7 without s8 (544-535nt); P8^{D1}: P8 without s6/5 (375-363nt); P8^{D2}: P8 without s4/3 (339-330nt); P8^{D3}: P8 without s2 (265-252nt); P9^{D1}: P9 without s1 (223-214nt). They were generated as described for P5-9. The construct characteristics are summarized together with the obtained Y1H results in Tab. 61.

3.3.14.3 Generation of the *EGR-1* expression construct

The EGR-1 construct was generated by amplification (Ch. 3.3.4) using the primers listed in Tab. 25 (Ch. 3.2.4.1). As template the full-length EGR-1 cDNA clone (IRATp970D09107D (Ch. 3.2.7; Tab. 46) was used. The forward primer was equipped with the *Nco*I site and the reverse primer with the *Eco*RI site. The construct was cloned via *Nco*I at 5´ and blunted *Eco*RI at 3´ into pACT2 (Ch. 3.2.2, Fig. 12).

3.3.14.4 Generation of the *MYCN* expression construct

The MYCN construct was generated by amplification (Ch. 3.3.4) using the primers listed in Tab. 24 (Ch. 3.2.4.1). As template the full-length MYCN cDNA clone (IRALp962C0412Q, (Ch. 3.2.7; Tab. 46) was used. The forward primer was equipped with the *Nco*I site and the reverse primer with the *Eco*RI site. The construct was cloned via *Nco*I at 5´ and blunted *Eco*RI at 3´ into pACT2 (Ch. 3.2.2, Fig. 12).

3.3.14.5 Generation of *RPS3* expression constructs

All constructs were generated by amplification (Ch. 3.3.4) using the primers listed in Tab. 26 and Tab. 27 (Ch. 3.2.4.1). As template the full-length pACT2-RPS3 construct (Ch. 3.3.14) was used. For cloning into pAS2-1 all forward primers were equipped with the *Eco*RI site and all reverse primers with the *Bam*HI site. The constructs were cloned via *Eco*RI at 5´ and *Bam*HI at 3´ into the pAS2-1 (Ch. 3.2.2, Fig. 13). For cloning into pACT2 all forward primers were equipped with the *Eco*RI site and all reverse primers with the *Xho*I site. The constructs were cloned via *Eco*RI at 5´ and *Xho*I at 3´ into the pAS2-1 (Ch. 3.2.2, Fig. 13).

3.3.15 Isolation of total RNA from mammalian cells using the TRIzol® reagent

Total RNA from mammalian cells grown to 70-80% confluency was isolated using the TRIzol® reagent (Life Technologies), a monophasic solution of phenol and guanidine isothiocyanate (Chomczynski and Sacchi 1987), according to the manufacturer´s instructions. The precipitated RNA was resuspended in 44µl RNase-free water and then purified from DNA contaminations using the TURBO DNA-*free*™ Kit (Applied Biosystems) according to the manufacturer´s instructions. The reaction mix consisted of:

44µl total RNA
1x TURBO DNase buffer
2u TURBO DNase

The final volume of this reaction was 50µl. The RNA concentration was determined spectrophotometrically using the NanoDrop (Ch. 3.3.2). RNA was stored at -80°C.

3.3.16 Synthesis of the first cDNA strand

First strand cDNA synthesis was performed using SuperScript™ II Reverse Transcriptase (Tab. 16; Ch. 3.2.1) according to the manufacturer´s instructions. The reaction mix consisted of:

2.5µg total RNA (Ch. 3.3.15)
500ng oligo$(dT)_{12\text{-}18}$ primer (Ch. 3.2.4.1, Tab. 30)
0.5mM dNTP Mix
1x First-strand buffer
200u SuperScript™ II
to 20µl H_2O

After the procedure, the reaction was diluted with 36µl RNase-free water and stored at -20°C.

3.3.17 Quantitative real-time reverse transcription polymerase chain reaction (qRT-PCR)

To detect and quantify cellular mRNA levels, quantitative real-time reverse transcription polymerase chain reaction (qRT-PCR) was used. In this technique, the amplification of cDNA via PCR is combined with the "real-time" monitoring of the increase of newly synthesized DNA in each cycle using the fluorophore SYBR green (Pfaffl 2001). When SYBR green intercalates into the minor groove of dsDNA, it emits a 1000x higher fluorescent signal at 580nm as unbound in solution (Wittwer *et al.* 1997). Because in the exponential amplification phase the amount of PCR product doubles with each cycle, the emitted fluorescent signal also doubles with each cycle. The obtained fluorescence intensities can be used to quantify the (initial) cDNA amounts over a wide concentration range (Wilhelm and Pingoud 2003). The course of the reaction is illustrated in an amplification plot showing the fluorescent reporter signal normalized to a passive reference dye (ROX) in a logarithmic scale plotted against the number of performed PCR cycles. This plot is used to determine the cycle threshold, the C_T value, which refers to the cycle number during the exponential phase of amplification at which the fluorescent reporter signal was first detected being higher than the background fluorescence. The C_T value is inversely proportional to the amount of DNA in the starting PCR sample. The higher the concentration of an amplified target was in the initial sample the faster a significant increase in fluorescence is detected during PCR resulting in a lower C_T value. The analysis of relative changes in gene expression was performed using the

comparative C_T or $2^{-\Delta C}{}_T$ method which allows to present the data as "fold change" in expression (Livak and Schmittgen 2001; Schmittgen and Livak 2008). For that purpose, all C_T values (X) were normalized to the internal control, the housekeeping gene (R) *hypoxanthine-guanine phospho-ribosyltransferase* (*HGPRT*), as follows: $\Delta C_T(X) = C_T(X) - C_T(R)$. The relative concentration of a target with respect to *HGPRT* is then calculated with $2^{-\Delta C}{}_T$. A $\Delta C_T = 0$ indicates a ratio of 1 between the target and the reference ($2^{-\Delta C}{}_T = 2^0 = 1$). The number 2 defines the doubling of the amount of the amplicon with each reaction by 100% efficiency (E) (Livak and Schmittgen 2001). It is known from laboratory practice that, as a result of sample-to-sample variations, biological and even technical replicates result in significantly different fluorescence curves and thus in different efficiencies (Pfaffl 2006). For correct ΔC_T calculation, the amplification efficiency of both the target and the reference must be approximately equal. For that purpose, the E values were optimized for each target gene investigated prior to the sample analysis using the LinRegPCR software application for calculation (Ramakers *et al*. 2003). LinReg uses data points from the exponential amplification phase and draws a regression line representing the PCR efficiency (Ruijter *et al*. 2009). The predominant advantage of this method is that the LinReg algorithm performs a correction of baseline fluorescence estimation errors per amplicon before fitting (Ruijter *et al*. 2009). This is of particular importance as no or improper baseline correction has been identified as the most important factor for variability and bias in the calculation of PCR efficiencies (Ruijter *et al*. 2009). To determine the relative gene expression of a target in different samples with respect to the respective physiological sample conditions (e. g. chemical induction/inhibition, siRNA silencing), the yielded $\Delta C_T(X)$ values are compared to a normalized calibrator (e. g. untreated cell, *scrambled* siRNA) $\Delta C_T(C)$ as follows: $\Delta\Delta C_T(X) = \Delta C_T(X) - \Delta C_T(C)$. The expression of the gene of interest relative to the internal control in the treated sample compared with the untreated control was calculated with $2^{-\Delta\Delta C}{}_T$. For RT-PCR analysis, 0.5µl first-strand cDNA (Ch. 3.3.16) were amplified using the KAPA SYBR® FAST qPCR Kit (PeqLab) according to the manufacturer´s instructions and transcript-specific primer combinations (10pmol each; Ch. 3.2.4.1, Tab. 31, 33 and 35) in a 10µl reaction. Each PCR reaction was performed as duplicate using the ABI PRISM 7900HT Fast System (Life Technologies) and the following reaction conditions: initial denaturation/activation for 1min. at 95˚C, 3sec at 95˚C, 20sec of annealing at 54°C, and 20sec of elongation at 72˚C for 40 cycles. The specificity of the amplification was determined using a dissociation curve. For this purpose, the samples were cooled to 62°C after the last amplification cycle and heated with a constant ramp rate of 2% (= 0.16°C/sec.) to 95°C. Depending on the length

and base composition the respective amplicons dissociate at distinct temperatures resulting in a steep specific decrease of fluorescence signal in the amplification blot (Wilhelm and Pingoud 2003). Data analysis was performed using the SDS 2.4 RT-PCR System Software.

3.3.18 Determination of transcription start sites using rapid amplification of cDNA ends (RACE)

The transcription start sites (TSS) of the target transcripts were determined using the rapid amplification of cDNA ends (RACE) technique with the help of the SMARTer RACE cDNA Amplification Kit (Tab. 52). The RACE technique is based on the addition of the SMARTer II A oligonucleotide (Ch. 3.2.4.1, Tab. 30) to the reverse-transcribed cDNA using the Switching Mechanism at 5´ end of RNA Transcript (SMART^{TM}) method described by Zhu *et al*. (2001). The tagged cDNA can then be amplified with a tag-specific forward primer (USP primer, Ch. 3.2.4.1, Tab. 30) in combination with a gene specific reverse primer (Ch. 3.2.4.1, Tab. 28, 32, and 34). The RACE reaction was performed according to the kit instructions using 5µg total RNA (Ch. 3.3.15). After the procedure, the sample was brought to a final volume of 50µl with Tricine-EDTA buffer (Ch. 3.1.5, Tab. 4). The amplification of RACE cDNA was performed as described in Ch. 3.3.4. The amplificates were separated on an 1.5% agarose gel (Ch. 3.3.3). The detected bands were isolated (Ch. 3.3.5) and sequenced (Ch. 3.3.6).

3.4 Standard protein working methods

3.4.1 Protein extraction from mammalian cells

3.4.1.1 Preparation of crude cell extracts from mammalian cells

Cells were grown on 24 well plates to 70-80% confluency and harvested as described in Ch. 3.6.1. The cells from two wells were pelleted by centrifugation at 2000rcf and 4°C for 5min. The pellet was resuspended in 120µl ice-cold TKM/NP-40 buffer (Ch. 3.1.5, Tab. 8) supplemented with protease inhibitors according to the manufacturer´s instructions (Roche) and incubated on ice for 30min. After incubation the cells were vortexed at maximum speed for 30sec. and the cell debris was pelleted by centrifugation at 14000rcf and 4°C for 10min. The protein containing supernatant

was shock frozen in liquid nitrogen and stored at -80°C. Protein quantification was performed according to Bradford (1976) using the BioRad™ protein assay as described in Ch. 3.4.2

3.4.1.2 Preparation of cytoplasmic and nuclear protein extracts from mammalian cells

Cytoplasmic and nuclear protein fractions were isolated from cells grown to 70-80% confluency (Ch. 3.6.1) in a two-step centrifugation approach using the Nuclear Extract Kit (Active Motif) according to the manufacturer´s instructions. Fractions were aliquoted, shock frozen in liquid nitrogen, and stored at -80°C. Protein quantification was performed according to Bradford (1976) using the BioRad™ protein assay as described in Ch. 3.4.2

3.4.2 Protein quantification using Bradford

Protein concentrations were determined using the BioRad™ protein assay according to the manufacturer´s instructions. This dye-binding assay is based on the method of Bradford (Bradford 1976). The determination of the protein concentration was performed in comparison to a bovine serum albumin (BSA) standard curve.

3.4.3 Western blot

To detect specific proteins in cell extracts, the western blot technique was applied (Burnette 1981). SDS-PAGE of the protein homogenates was performed as described in Ch. 3.4.3.1. To analyze detected complexes in EMSA experiments (Ch. 3.5.3), proteins were separated on native polyacryl-amide gels (without SDS). After separation, the proteins were transferred to a polyvinylidene fluoride (PVDF) membrane via electroblotting (Ch. 3.4.3.2). The proteins of interest were detected using specific primary antibodies (Ch. 3.2.5, Tab. 43) in combination with secondary antibodies (Ch. 3.2.5, Tab. 44) coupled to either alkaline phosphatase (AP) or horseradish peroxidase (HRP) (Ch. 3.4.3.3). As substrate for the enzymatic AP reaction 5-Bromo-4-chloro-3-indolyl phosphate (BCIP) was used in combination with Nitro Blue Tetrazolium (NBT) (Ch. 3.1.5, Tab. 6). As substrate for HRP luminol was used according to the instructions of the Advansta Western Bright™ Quantum™ Chemiluminsecent Kit (Biozym). Signals were quantified using ImageJ software (Schneider *et al*. 2012). The determined relative intensities (RI) were normalized to Actin.

3.4.3.1 Separation of proteins using sodium dodecyl sulfate polyacrylamide gel electrophoresis (SDS-PAGE)

Electrophoresis was carried out under denaturing conditions using 10% SDS-polyacrylamide (SDS-PAGE) gels or under native conditions using 5% polyacrylamide gels (without SDS). The separating gel (5-10% polyacrylamide, 1x lower tris (Ch. 3.1.5, Tab. 6), 0.05% APS, and 0.2% TEMED) and the stacking gel (5% polyacrylamide, 1x upper tris (Ch. 3.1.5, Tab. 6), 0.05% APS, and 0.2% TEMED) were casted in the 10x8cm Hoefer™ SE 250 gel electrophoresis unit. For separation, 15-40µg protein extracts (Ch. 3.4.1) were loaded. Prior to loading, the samples were dissolved in 5x Laemmli buffer (Ch. 3.1.5, Tab. 6) to a final concentration of 1x and heated for 90sec. at 70°C. As standard for evaluation of protein size 2.5µl of the PageRuler Prestained Protein Ladder (Fermentas; Ch. 3.2.3, Tab. 18) was used. Gels were run at 20mA.

3.4.3.2 Transfer of separated proteins to a PVDF membrane (electroblotting)

To transfer proteins from a polyacrylamide gel to a PVDF membrane, the semi-dry blotting technique was applied (Kyhse-Anderson 1984). The gel was put on top of a methanol activated PVDF membrane between a sandwich composed of 9 whatman filter papers wetted in three different buffers (Ch. 3.1.5, Tab. 6). The sandwich was built as follows: three papers in Anode buffer II, three papers in anode buffer I, activated PVDF membrane, gel, three papers in Cathode buffer. The blotting of proteins from a 10% PAGE gel was accomplished with an applied rated current of 1mA per cm^2 of membrane for 90min. and for blot transfer of 5% PAGE for 40min.

3.4.3.3 Immunodetection of proteins with alkaline phosphatase or chemiluminescence

After blotting, the membrane was blocked using 0.2% I-Block (Ch. 3.1.5, Tab. 6) for 1h at RT or overnight at 4°C. The primary antibody used to detect the protein of interest was diluted in I-Block (Ch. 3.2.5, Tab. 43) and incubated with the membrane for 1h at RT or overnight at 4°C. After incubation, the membrane was washed four times in PBS at RT, 10min. per wash. A 1h incubation at RT with the secondary AP- or HRP-coupled antibody diluted in I-Block (Ch. 3.2.5, Tab. 44) followed. After incubation, the membrane was washed four times in PBS at RT, 10min. per wash. For protein detection using alkaline phosphatase, the membrane was incubated with 10ml staining

solution (Ch. 3.1.5, Tab. 6) for 1min. up to 1h. For protein detection using chemiluminescence, the Advansta Western Bright™ Quantum™ Chemiluminsecent Kit (Biozym) and SuperRX X-Ray films (Fuji) were applied according to the manufacturer's instructions.

3.4.4 The yeast two-hybrid system (Y2H)

The yeast two-hybrid system (Y2H; Fields and Song 1989) was used to detect protein-protein interactions and to map the responsible binding domain. This system is based on the yeast transcription factor GAL4, composed of a DNA-binding domain (BD) and a transcriptional activation domain (AD). The BD recognizes and binds to the upstream activating sequence (UAS) located upstream the transcription start of GAL4-responsive genes, the AD interacts with components of the transcription machinery needed for initiation (Traven *et al*. 2006). In this study, the proteins or protein fragments of interest (Ch. 3.3.14 and Ch. 3.3.14.3 - Ch. 3.3.14.5) are expressed as fusions of the GAL4-AD (if cloned into pACT2; Ch. 3.2.2, Fig. 12) and/or the GAL4-BD (if cloned into pAS2-1; Ch. 3.2.2, Fig. 13) domains. If those two proteins interact, the GAL4 transcription factor is reconstituted and can bind to its UAS recognition sequence thus activating the transcription of the Y187 *lacZ* reporter gene (Ch. 3.2.9, Tab. 49). The activity of *lacZ* expressed β-galactosidase can be shown by staining with X-gal (Ch. 3.4.4.3).

3.4.4.1 Cotransformation of Y187 cells using the LiAc method

The expression vectors of interest (Ch. 3.3.14 and Ch. 3.3.14.3 - Ch. 3.3.14.5) were cotransformed into the yeast strain Y187 (Ch. 3.2.9, Tab. 49), which is auxotroph for the amino acids histidine (His), leucine (Leu), and tryptophan (Trp), according to the LiAc method (Gietz and Woods 2002). In this study 50µl competent cells were transformed with 500ng of *bait* and 500ng of *prey* as follows: From an 50ml overnight culture (Ch. 3.3.13) 7.5ml were transferred to 150ml YPD medium and incubated at 30°C, 230rpm, until a cell density of OD_{600} = 0.4 – 0.6 was reached. The culture was centrifuged for 5min. at 700 x g. The cell pellets were resuspended in 30ml sterile H_2O and centrifuged at 700 x g for 5min. Pellets were than redissolved in 1.5ml 1.1x TE/LiAc, centrifuged at 13000rpm for 30sec. and resuspended in 600µl 1.1x TE/LiAc. To the reaction 500ng Herring Testes Carrier DNA and 500µl PEG/LiAc were added for higher transformation efficiencies (Kawai *et al*. 2010). After vortexing and incubation for 30min. at 30°C, 20µl DMSO

were added to each sample. The samples were incubated at 42°C for 15min. and pelleted by centrifugation at 13000rpm, 15sec. The pellets were resuspended in 1ml YPD medium and incubated at 30°C, 230rpm, for 90min. Cells were then pelleted by centrifugation at 13000rpm, 15sec. and redissolved in 700µl 0.9% sterile NaCl solution. Because the cotransformed cells contain the nutritional marker genes necessary for the synthesis of leucine (conferred by pACT2; Ch. 3.2.2, Fig. 12) and tryptophan (conferred by pAS2-1; Ch. 3.2.2, Fig. 13), they can be selected on SD/-Leu/-Trp medium for 2-7 days at 30°C.

3.4.4.2 Monitoring of protein expression using yeast colony blot

To monitor the expression of the proteins encoded by the recombinant vectors transformed into the yeast cells (Ch. 3.4.4.1), the yeast colony blot technique was applied. Protein detection was performed using antibodies directed against the encoded proteins or the AD/BD fusion domains (Ch. 3.2.5, Tab. 43) of the vectors. Yeast colonies to be examined were transferred to a nitrocellulose membrane and incubated sequentially at RT in Denaturing solution I for 10min., in Denaturing solution II for 5min., two times in neutralization solution for 5min. and in 2x SSC for 15min (Ch. 3.1.6; Tab. 7). Membranes were washed with TBS and blocked with 5% BSA in TBS for 1h at RT (Ch. 3.1.6; Tab. 7). The primary antibodies diluted in I-Block were added for 1h, RT. After incubation, the membranes were washed twice in TBS-Tween/Triton buffer and once in TBS buffer for 10min. Then the secondary alkaline phosphatase (AP)-labeled antibodies diluted 1:5000 in I-Block (Ch. 3.2.5, Tab. 44) were added for 1h at RT. After incubation, the membranes were washed three times in TBS-Tween/Triton buffer. Finally, the blots were incubated in the staining solution as described for western blot in Ch. 3.4.3.3.

3.4.4.3 β-Galactosidase (X-gal) assay

To visualize protein-protein interactions detected with the Y2H method (Ch. 3.4.4), the β-galactosidase (β-Gal) assay was used. Monitoring of β-Gal activity was performed using the indole-coupled galactose analog X-gal (5-bromo-4-chloro-3-indolyl-β-D-galactopyranoside) as substrate. For that purpose, selected colonies were placed on a filter paper with forceps and cracked in a freeze/thaw step using liquid nitrogen. The filters were than incubated in X-gal staining solution (Ch. 3.1.5, Tab. 5) at 30°C up to 24h. In all Y2H experiments performed Y187 cells cotransformed

with the pAS2-1-p65 and the pACT2-RPS3 constructs (Ch. 3.3.14) served as positive control and cells containing the empty pACT2 (Fig. 12; Ch. 3.2.2) and pAS2-1 (Fig. 13; Ch. 3.2.2) vectors as negative control. As control for the staining reaction Y187 cells were cotransformed with the pCL1 vector encoding the full-length GAL4 transcription factor (Ch. 3.2.2, Fig. 7).

3.4.5 Determination of relative nuclear protein activity using ELISA

The relative nuclear activity of NFκB and CREB1 was determined using the specific enzyme-linked immunosorbent assay (ELISA) kits CREB (Phospho-Ser^{133}) Transcription Factor Assay Kit, NF-kB (human p50) Transcription Factor Assay Kit and NF-kB (p65) Transcription Factor Assay Kit according to the manufacturer´s instructions. The underpinning principle of this assays is the binding of nuclear proteins to their specific DNA binding site spotted as double-stranded biotin-labeled oligonucleotides on streptavidin coated 96well microplates. The bound protein is than detected using a specific antibody. The secondary antibody is coupled to horseradish peroxidase (HRP). For detection, the kits supply the chromogenic substrate 3,3',5,5" - tetramethyl-benzidine (TMB). In all cases 15µg nuclear extracts (Ch. 3.4.1.2) were used for binding. The readout was performed in an ELISA plate reader at 450nm wavelength after 40min. substrate incubation.

3.5 Techniques for identification of protein-DNA interactions

3.5.1 Computational analysis of putative promoter DNA sequences

Potential transcription factor binding sites and motifs for the general transcription machinery were predicted using the P-MATCH^{TM} algorithm (Chekmenev *et al*. 2005; web: http://www.gene-regulation.com/index2) and the JASPAR database (Mathelier *et al.* 2014; web: http://jaspar.cgb.ki.se/). The JASPAR database is a collection of positional weight matrices (PWMs) (Stormo 2000) based on a curated, non-redundant set of experimentally verified and published transcription factor binding sites for eukaryotes. This database predicts potential binding sites based on sequence similarity to the annotated sites. The P-MATCH^{TM} algorithm is based on the combination of pattern matching approaches using the TRANSFAC® database (Matys *et al*. 2003), a collection of known transcription factor binding sites and PWMs. As first step the algorithm determines the PWM of the core protein recognition sequence using all known binding

sites of a specific transcription factor deposited in the TRANSFAC® database and computes "d-scores" which are values for similarity between a DNA sequence and a transcription factor binding site. A score of 1.0 indicates exact matching of the analyzed sequences. For the final report of potential binding sites two d-scores are calculated, one for the whole site and one for the nucleotides of the core site, which are the five most conserved nucleotides within the alignment. Only the results are listed whose both d-scores exceed one of the three pre-selected cut-off values to either minimize false negative (under-prediction error) and false positive results (over-prediction error) or the sum of both. Predicted sites were analyzed in different *in vitro* (Ch. 3.5.2 - Ch. 3.5.6) and *in vivo* experiments (Ch. 3.5.7) for their binding capacities.

3.5.2 The yeast one-hybrid system (Y1H)

To identify and characterize protein-DNA interactions, the yeast one-hybrid technique (Fields *et al*. 1993; Durfee *et al*. 1993) using the Matchmaker™ One-Hybrid Library Construction & Screening Kit (Clontech; Ch. 3.2.11, Tab. 52) was applied. This technique can be used to screen cDNA libraries for DNA-binding proteins or to detect the binding of a distinct protein to a defined DNA (*bait*). The defined or potential DNA-binding protein (*prey*) is expressed as fusion to the activation domain (AD) of the yeast GAL4 transcription factor which is necessary for transcriptional activation by recruiting coactivators and the general transcription machinery (Traven *et al*. 2006). In this study, the *preys* were cloned into pACT2 (Ch.3.3.14 and Ch. 3.3.14.3 - Ch.3.3.14.5) and the *baits* into pHIS2.1 (Ch. 3.3.14.1 - Ch. 3.3.14.2). After cotransformation (Ch. 3.4.4.1) of the *bait* and *prey* constructs into Y187 cells (Ch. 3.2.9, Tab. 49), the expressed AD-fusion protein can bind to its cognate DNA target sequence and activate transcription of the *HIS3* reporter gene. The *HIS3* expression enables yeast cells which are auxotroph for histidine (such as Y187) to grow on SD selection medium lacking this amino acid (Ch. 3.1.6; Tab. 11). Selection stringency can be increased using the nutritional markers of the pACT2 (*LEU2*; Ch. 3.2.2, Fig. 12) and pHIS2.1 (*TRP1*; Ch. 3.2.2, Fig. 11) vectors. As result, Y187 cells cotransformed with *bait* and *prey* constructs grow on SD medium lacking the amino acids histidine (His), tryptophan (Trp) and leucine (SD/-His/-Trp/-Leu) in case the *bait* and *prey* vectors interact with each other. The growth medium is also supplemented with the competitive Hisp3 inhibitor 3-amino-1-2-4-triazole (3-AT). In the absence of a *prey* vector endogenous yeast transcription factors can bind the minimal promoter and drive reporter gene expression (*leaky expression*) resulting in basal Hisp3 activity.

In order to avoid false positive results, the concentration of the 3-AT necessary to inhibit this basal activity has to be established for each of the generated *bait* constructs on its own (3-AT test). This was performed by cotransformation (Ch. 3.4.4.1) of 500ng promoter construct and 500ng empty pACT2 vector into Y187 cells. The cotransformed cells were plated on SD/-His-/-Trp/-Leu supplemented with 50mM, 60mM, 70mM, 100mM or 150mM 3-AT. The concentration at which cell growth could not be observed anymore was chosen for Y1H experiments. As positive control 500ng of the p53 expression vector (Ch. 3.2.2, Fig. 6) and 500ng of the p53-promoter containing reporter vector (Ch. 3.2.2, Fig. 6) were transformed and selected under identical conditions.

3.5.3 Electrophoretic mobility shift assay (EMSA)

To investigate the binding of a protein to a specific DNA binding site, the electromobility shift assay (EMSA; also known as gel retardation or band shift assay) was applied. This technique (Fried and Crothers 1981) is based on the fact that protein-DNA complexes migrate slower in a native polyacrylamide gel compared to the respective unbound DNA. Potential DNA binding sites predicted using the P-MATCH^{TM} algorithm (Chekmenev *et al*. 2005; Ch. 3.5.1) were synthesized as single stranded deoxyoligonucleotides with a 5´-prime biotin tag on the sense strand (Ch. 3.2.4.2). The complementary oligonucleotides were heated to 95°C for 5min. and cooled down 45min. at RT for annealing. EMSAs were performed according to the LightShift® Chemiluminescent EMSA Kit (Tab. 52). For complex formation, transcription factor-specific binding buffer (Tab. 9), 7µg nuclear extract (Ch. 3.4.1.2), and 20fmol ds oligo (Tab. 36-41) were mixed in a 20µl reaction and incubated on a rotating platform for 20min. at RT. After incubation, the reactions were mixed with 3µl EMSA loading dye (Tab. 9) and loaded on a 5% native PAGE-gel (Ch. 3.4.3.4). The gels were run in 0.5x TBE buffer (Tab. 9) at 100V until the bromophenol band reached the end of the gel. The semi-dry transfer of separated protein-DNA complexes to a Biodyne® B 0.45µM nylon membrane (Pall) was performed with 1mA/cm^2 for 40min. as described in Ch. 3.4.3.2. Signals were detected using chemiluminescence and SuperRX X-Ray films (Fuji) according to the EMSA kit.

3.5.4 Identification of protein-DNA interactions using ELISA

To investigate the binding of the NFκB subunits p50 and p65 to P-MATCH^{TM}-predicted NFκB sites within the *NOT* promoter (Ch. 3.2.4.2, Tab. 37), the ELISA technique was applied. For that

purpose, the biotinylated NFκB binding sites were immobilized on a 96well streptavidin coated microplate (Greiner Bio-One) by incubating 10ng ds oligo per well in a buffer consisting of 1% BSA in 0.05% Tween20/ PBS solution, pH 7.2, at RT (200µl total volume/well). After immobilization, the plate was blocked for 2h at RT with 200µl 5% BSA in 0.05% Tween20/ PBS solution, pH 7.2, per well. For protein binding, 30ng recombinant p50 or p65 (Ch. 3.2.6, Tab. 45) were incubated in 200µl 1% BSA in 0.05% Tween20/ PBS solution, pH 7.2, per well at 4°C overnight. The binding specificity was confirmed by competition with 10x excess of cold oligo before loading on the plate. After incubation, the plate was washed three times with 200µl BSA in 0.05% Tween20/ PBS solution, pH 7.2, per well. For detection, the plate was incubated for 1h at RT with the anti-p50 or anti-p65 antibody (Ch. 3.2.5, Tab. 43) diluted 1:30 in 200µl 1% BSA in 0.05% Tween20/ PBS solution, pH 7.2, per well. After incubation, the plate was washed three times with 200µl BSA in 0.05% Tween20/PBS solution, pH 7.2, per well and loaded with anti-mouse-AP antibody (Ch. 3.2.5, Tab. 44) diluted 1:5000 in 200µl 1% BSA in 0.05% Tween20/PBS solution, pH 7.2, per well. After incubation, the plate was washed three times with 200µl BSA in 0.05% Tween20/ PBS solution, pH 7.2, per well. For development, 200µl pNPP substrate (1mg/ml pNPP (Sigma-Aldrich) in 1M diethanolamine pH9.8/0.5mM $MgCl_2$ per well) were added per well and incubated for 35min. in the dark. The readout was performed after 40min. staining with an ELISA reader using a 405nm filter.

3.5.5 Identification of NFκB, EGR-1, and MYCN binding to the *NOT* promoter using affinity chromatography

The binding of NFκB, EGR-1, and MYCN to the predicted sites in the *NOT* promoter (Ch. 3.2.4.2, Tab. 37, 38 and 39) was determined by affinity chromatography using Dynabeads M-280 (Tab. 52) according to the manufacturer´s instructions. The studies were performed using nuclear extracts (Ch. 3.4.1.2) isolated from HeLa cells. For immobilization, 60pmol ds-btn-oligo were mixed with 300µg beads prewashed in the 2x B&W buffer (Ch. 3.1.5, Tab. 10) and incubated on a rotator for 15min. at RT. After washing, the Dynabeads-oligo complexes three times with the 2x B&W buffer 20µg of the HeLa nuclear extract were added to the sample and incubated on a rotating platform for 45min. Total volume of the reaction was 30µl in the respective binding buffer (Ch. 3.1.5, Tab. 9). The specificity of the binding was determined by competition assay. For this purposes, the nuclear extracts were preincubated with 10x excess of the cold oligo for 30min. before adding the

immobilized btn-oligos. After binding, the beads were washed three times with coupling buffer (Ch. 3.1.5, Tab. 10). The captured complexes were eluted in 20µl 1% Laemmli (Ch. 3.1.5, Tab. 6) for 15min. at 50°C. The complete eluates were analyzed using western blot (Ch. 3.4.3).

3.5.6 Southwestern blot

To identify protein-DNA interactions, the Southwestern technique was applied (Siu *et al*. 2008). This technique allows hybridization of btn-labeled oligonucleotides to immobilized proteins after gel electrophoretic separation (Ch. 3.4.3). 3µg of the nuclear extracts (Ch. 3.4.1.2) were separated under denaturing conditions and blotted as described for western blot (Ch. 3.4.3). After blotting the PVDF membrane was incubated shaking at 150rpm, RT, in renaturation buffer (Ch. 3.1.5, Tab. 10) overnight. For binding, 20fmol btn-oligos (Ch. 3.2.4.2, Tab. 37 and 38) were diluted in 3ml renaturation buffer supplemented with 1µg dIdC and incubated shaking 150rpm, 15min., RT. The specificity of the binding was determined by competition assay. For this purposes, the blots were preincubated with 3000x excess of the cold oligo for 30min. before adding the btn-oligos. After binding, the membranes were washed three times with TENED buffer (Ch. 3.1.5, Tab. 10). Signals were detected using the Chemiluminescent Detection Kit (Pierce) and SuperRX X-Ray films (Fuji) according to the manufacturer´s instructions.

3.5.7 Chromatin immunoprecipitation (ChIP) and sequential ChIP (Re-ChIP)

To identify protein-DNA interactions *in vivo*, chromatin immunoprecipitation (ChIP) and sequential ChIP (Re-ChIP) were used. This technique is based on the preservation of native protein-DNA interactions in the cell by cross-linking using the fixative formaldehyde. The fixed chromatin is then enzymatically sheared into fragments of about 200-1500bp in length. The DNA-bound protein (or protein complex) of interest is immunoprecipitated using a specific antibody and protein G coated magnetic beads. After chromatin elution, the cross-links are reversed and the DNA is purified from the immunoprecipitates. The DNA fragments bound by the factors of interest can then be identified using PCR (Ch. 3.3.4). To prove that two proteins are simultaneously located on the same DNA fragment, sequential ChIP (Re-ChIP) was applied. In this approach a second ChIP with a different antibody is performed using the immunoprecipitated protein-DNA complexes from a first ChIP reaction. DNA purification and analysis is then performed as described above. ChIPs

were performed using the ChIP-IT™ Express Kit (Tab. 52) according to the manufacturer´s instructions. Cells were grown to 70-80% confluency (Ch. 3.6.1) and $4.5x10^7$ cells were fixed using 1% formaldehyde. After harvesting, the chromatin was isolated from the nuclei and sheared with 200u/ml of the supplied enzymatic shearing cocktail for 15min. at 37°C. To control the shearing efficiency, an aliquot of the sheared chromatin was purified from proteins as described in the manual. The quality of the remaining DNA fragments was checked by gel electrophoretic separation (Ch. 3.3.3). All immunoprecipitations were performed at 4°C overnight using 5µg of sheared chromatin and 3µg antibody (Ch. 3.2.5, Tab. 43) in combination with protein G-agarose coated magnetic beads to capture the immune complexes. After extensive washing and elution, the DNA was purified from the captured complexes. From these samples 5µl were subjected to amplification via PCR in 25µl total volume (Ch. 3.3.4). After PCR, the samples were mixed with 5µl 6x loading dye (Ch. 3.1.5, Tab. 4) and 20µl were separated on a 2% agarose gel (TopVision Agarose, Thermo Scientific) as described in Ch. 3.3.3. The Re-ChIPs were performed according to Re-ChIP-IT™ Kit (Tab. 52) with 7µg of sheared chromatin and 3µg antibody for both ChIP reactions. After the first immunoprecipitation, the chromatin was selectively eluted while the first antibody remained bound to the beads using a special buffer (Re-ChIP-IT Elution Buffer). This mechanism assures that the first antibody is not active in the second ChIP to produce false positive results. To control this step, a small aliquot of the eluted chromatin was incubated during the second ChIP reaction without the second antibody. The eluates were desalted followed by a second ChIP. DNA purification and amplification as in ChIP.

3.6 Mammalian cell culture techniques

Cells were incubated in a humidified incubator at 37 °C with an atmosphere containing 5% CO_2. All cell culture media were supplemented with 10% inactivated fetal calf serum (FCS) (Biochrom), 100 U/ml penicillin and 100 µg/ml streptomycin (Sigma-Aldrich). Cells were checked for Mycoplasma contaminations using the Venor®GeM Mycoplasm Detection Kit (Minerva GmbH) according to the manufacturer´s instructions. The applied human cell lines are listed in Tab. 51 (Ch. 3.2.10). The cell lines HT-29 (ACC 299) and HeLa (ACC 57) were obtained from the Leibniz Institute DSMZ-German Collection of Microorganisms and Cell Cultures (Braunschweig). The T98G cell line (CRL-1690) was obtained from the American Type Culture Collection (ATCC). The HaCaT cell line was obtained from CLS Cell Lines Service GmbH (Eppelheim). HT-29 and

HeLa cells were cultivated in RPMI1640 with L-glutamine (Sigma-Aldrich). T98G cells were grown in Minimal essential medium (MEM) with Earle´s salts (EMEM) and stable glutamine (Biochrom) supplemented with 1mM sodium pyruvate (Sigma-Aldrich) and 1% non-essential amino acids (Sigma-Aldrich). HaCaT cells were grown in Dulbecco's MEM / HAM's F-12 (DMEM-F12) L-glutamine and sodium bicarbonate (Sigma-Aldrich) supplemented with 10mM HEPES. The applied murine cell lines are listed in Tab. 50 (Ch. 3.2.10). The 3T3 cell line (ACC 299) was obtained from the Leibniz Institute DSMZ. The 3T3 (CRL-1658), MOCHA (CRL-2709), BC3H1 (CRL-1443) and C127I (CRL-1616) cell lines were obtained from the American Type Culture Collection (ATCC). 3T3 cells were grown in RPMI1640 medium. MOCHA, BC3H1 and C127I cells were grown in Dulbecco's MEM / HAM's F-12 (DMEM-F12) (Sigma-Aldrich) supplemented with 10mM HEPES (1%).

3.6.1 Seeding, propagation and counting of cells

Cells stored in liquid nitrogen (Ch. 3.6.2) were thawed in a 37°C water bath, resuspended in the respective pre-warmed culture medium (Ch. 3.6.1 and Ch. 3.2.10, Tab. 50 and 51) and pelleted by centrifugation at 600g for 5min. The pellet was resuspended in medium and the cells were plated and cultured under the conditions described in Ch. 3.6. After 24h hours the cells were washed with 1x PBS (w/o Ca^{2+} and Mg^{2+}) and supplemented with fresh medium. For splitting, cells grown to 70-80% confluency were washed with 1x PBS (w/o Ca^{2+} and Mg^{2+}) and detached from the culture dish using trypsin (Sigma-Aldrich). The cells were mixed 1:1 with medium, pelleted by centrifugation at 600g, 5min. and washed three times in the respective culture medium. An aliquot was diluted 1:10 in 0.4% trypane blue solution in order to determine the vitality and cell number using a Neubauer chamber (Also called trypan blue exclusion assay if the amount of viable to dead cells is determined; Strober 2001). Since the volume of one square in the Neubauer chamber is 0.1 mm^3, the cell number in 1 ml medium is calculated by multiplication of the average cell number from all four chamber squares with factor 10^4. The desired cell amount was then resuspended in an appropriate amount of culture or freeze medium for further propagation or storage (Ch. 3.6.2).

3.6.2 Storage of cells

Cells to be stored were harvested and quantified (Ch. 3.6.1). The desired amount of cells to be

frozen was pelleted ($1x10^6$ - $1x10^7$ per pellet) and diluted in 500µl DMSO-free BioFreeze medium (Biochrom). After cooling at -80°C overnight using the 2-propanol filled polycarbonate Mr. Frosty Freezing Container (Nalgene) the cells were put into liquid nitrogen (-192°C).

3.6.3 Serum response

To test the effect of serum in the culture medium on transcription factor activation and NOT expression, cells were grown under normal conditions to 60-70% confluency (Ch. 3.6.1) and washed with 1x PBS (w/o Ca^{2+} and Mg^{2+}). The cells were then incubated for 24h in the respective culture medium without serum (serum free, SF). After incubation, the serum-free medium was replaced by the respective culture medium supplemented with 10% FBS for 2h (serum response, SR). RNA and proteins were isolated as described in Ch. 3.3.15 and Ch. 3.4.1.1.

3.6.4 Pharmacological stimulation of cells

3.6.4.1 Caffeine

HT-29 cells were treated with different concentrations of the nonsense mediated mRNA decay pathway (NMD) inhibitor caffeine (Sigma-Aldrich) as described by Johnson *et al*. (2012). The cells were grown to 60-70% confluency (Ch. 3.6.1), washed, and supplemented with fresh medium containing 5mM, 10mM, and 20mM caffeine. After 4h incubation under normal growth conditions, the medium was replaced by fresh medium containing the respective caffeine concentrations for another 4h hours. RNA and proteins were isolated as described in Ch.3.3.15 and Ch.3.4.1.1.

3.6.4.2 Parthenolide

The sesquiterpene lactone parthenolide from the anti-inflammatory medicinal herb Feverfew (*Tanacetum parthenium*) inhibits the NFκB signaling (Kwok *et al*. 2001; Garcia-Pineres *et al*. 2001). Parthenolide was harnessed to assess the specificity of the NFκB binding to the *NOT* promoter as detected using EMSA (Ch. 3.5.3) and to measure its impact on *NOT* expression using qRT-PCR (Ch. 3.3.17). For that purpose, serum-starved cells (Ch. 3.6.3) were treated with 100µM parthenolide for 10, 30 and 60min. After incubation, RNA and proteins were isolated as described

in Ch.3.3.15 and Ch.3.4.1.1. The nuclear fractions were subjected to EMSAs as described in Ch. 3.5.3, the RNAs were analyzed using qRT-PCR (Ch. 3.3.17).

3.6.4.3 TNFα

Tumor necrosis factor α (TNFα), a member of TNF family of cytokines is one of the prototypic inducers of NFκB signaling (Hayden and Ghosh 2014). It was used to assess the impact of the activated canonical NFκB pathway on *NOT* expression (Ch. 4.6.4). For that purpose, serum-starved cells (Ch. 3.6.3) were treated with 50ng/ml TNFα for 10min., 30min., and 60min. After incubation RNA and proteins were isolated as described in Ch.3.3.15 and Ch.3.4.1.1. The cytosolic and nuclear fractions were subjected to western blot (Ch. 3.4.1.2), the RNAs were analyzed using qRT-PCR (Ch. 3.3.17).

3.6.4.4 Brefeldin A

Brefeldin A (BFA) is a macrocyclic lactone produced by *Penicillium brefeldianum* and shown to be a potent Golgi-stress inducer by inhibiting ER-Golgi protein trafficking (Nebenführ *et al*. 2002). The cells were grown to 60-70% confluency (Ch. 3.6.1), washed and supplemented with fresh medium containing 2µg/ml BFA. After incubation for 10min., 30min. and 24h RNA and proteins were isolated as described in Ch. 3.3.15 and Ch. 3.4.1.1.

3.6.5 Transient transfection of mammalian cells with siRNAs

HT-29 and HeLa cells were transiently transfected with siRNAs to silence the expression of the genes of interest. The cells were harvested in the proliferation phase (60-70% confluency) and seeded on 24 well plates with $1.4x10^5$ (HT-29) and $7x10^4$ (HeLa) cells per well (Ch. 3.6.1). After 1h hour incubation, 10-50nM siRNAs (Ch. 3.2.4.3, Tab. 42) were transfected using 3µl HiPerFect Transfection Reagent (Qiagen) according to the manufacturer´s instructions. After 48h incubation, the cells were harvested for RNA (Ch. 3.3.15) and protein isolation (Ch. 3.4.1). The samples were analyzed using qRT-PCR (Ch. 3.3.17) and western blot (Ch. 3.4.3).

4 Results

4.1 Identification and characterization of *NOT* splice variants

4.1.1 Isolation of different *NOT* transcripts from diverse cell lines

The *l(2)not* gene has been originally discovered together with the *l(2)tid* tumor suppressor gene in the Kurzik-Dumke group (Kurzik-Dumke *et al*. 1995; 1996; Kaymer *et al*. 1997). The same group also isolated the human counterpart *NOT*-1 (Kurzik-Dumke and Kaymer 1996; GenBank: Y09022.1). The *NOT* variants 2 (GenBank: BM920198.1), 4 (GenBank: BX339649.2), and 5 (GenBank: AK299575.1) isolated from diverse tissues were published later on (Fig. 2; Ch. 1.2.1). To check if these transcripts are expressed in diverse cell lines or if they are (cancer-) cell-specific, different primers were designed (Tab. 32) to detect the single forms via RT-PCR (Ch. 3.3.4). After gel electrophoretic separation the detected bands were isolated and sequenced. Amplification using a forward primer residing just upstream the start codon of *NOT*-1, -2, and -5 in combination with a reverse primer in the 3´- UTR shared by all variants yielded amplification of *NOT*-1 and -5 (Fig. 14A, Tab. 32; 1f/1r), whereas the strong signal of *NOT*-1 superimposed the only 67nt smaller *NOT*-2 variant. In addition, two yet unidentified *NOT* variants, *NOT*-1a and -1b (Fig. 14A; Tab. 55), were detected. The *NOT*-1a variant lacks exon 6 leading to a frameshift and a different TAA stop codon residing 154nt downstream the *NOT*-1 TGA (Tab. 55). The *NOT*-1b variant lacks exons 5-8 causing no frameshift but a smaller protein (Tab. 55). Using the *NOT*-1 specific forward primer and the 3´-UTR reverse primer for amplification the variants 1a and 1b could be confirmed (Fig. 14, Tab. 32; 2f/1r). Amplification using a *NOT*-2 or -5 specific forward primer (Tab. 32, 3f or 6f,) in combination with the 3´-UTR primer (Tab. 32, 1r) yielded four additional forms, *NOT*-2a, -2b, -5a, and -5b (Fig. 14A), containing the identical 3´exon combinations as *NOT*-1a and 1b. In the case of the amplification using the *NOT*-5-specific forward primer (Tab. 32, 6f) a third form, *NOT*-5c, lacking the exons 3-7 as compared to *NOT*-5 (Tab. 55) was isolated. These splicing events have no effect on translation as all of them occur downstream the respective premature stop codons of *NOT*- 2 and -5 (Tab. 55). The 5´ sequence of the variants detected using the *NOT*-1, -2, and -5-specific forward primers (Tab. 32, 2f, 3f, and 6f) was completed by amplification using a forward primer encompassing the *NOT*-1, -2, and -5 ATG (Tab. 32, 4f) in combination with a reverse primer located in the third exon (as compared to *NOT*-1; Tab. 32, 2r) which is present in all three variants.

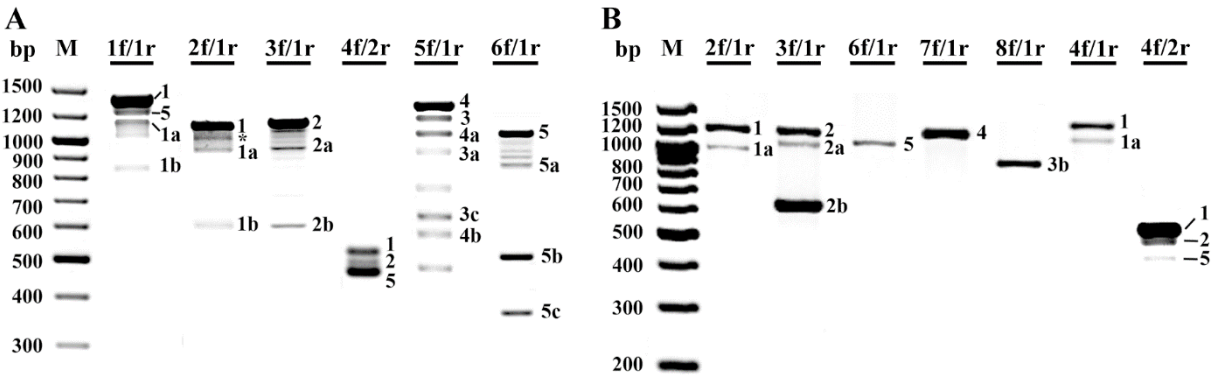

Fig. 14 Amplification and isolation of *NOT* splice variants. Gel electrophoretic separation of amplificates generated using the indicated primer combinations and cDNA from either T98G cells **(A)** or the Mammary gland cDNA library. **(B)**. Samples were separated on a 2% agarose gel. Applied primer combinations are shown in the upper lane (f: Forward, r: Reverse). Bands were extracted from the gel and sequenced. The identified variants are indicated. *: Non-specific; bp: Base pairs; M: Marker Gene Ruler 100bp ladder.

The obtained results show the expected three band pattern representing variants 1, 2, and 5 (Fig. 14A, Tab. 32; 4f/2r). Amplification using a forward primer upstream the *NOT*-4 start codon in combination with the 3´-UTR reverse yielded detection of *NOT*-4 (Fig. 14A, Tab. 32; 5f/1r). In addition, two yet unidentified *NOT* variants, *NOT*-4a and -4b (Fig. 14A; Tab. 55), were detected. The *NOT*-4a variant lacks exon 6 causing no frameshift but a smaller protein (Tab. 55). The *NOT*-4b lacks exons 4-8 leading to a frameshift and shorter protein (Tab. 55). As compared to *NOT*-4, the splicing of *NOT*-4a and -4b generates a different TAA stop codon located 154nt downstream of the *NOT*-4 TGA (Tab. 55). This stop codon is also used in the *NOT*-1a variant (Tab. 55). In addition, three other forms, *NOT*-3, -3a, and -3c, were isolated using the 5f/1r primer combination (Fig. 14A; Tab. 32). These three variants lack exon 2 as compared to *NOT*-4 leading to a frameshift and a premature TGA stop codon located 178nt downstream ATG (Tab. 55). This stop codon is also used in the *NOT*-5 variants (Tab. 55). Whereas *NOT*-3 only lacks exon 2 as compared to *NOT*-4, variant 3a lacks exon 5 and variant 3c lacks exons 4-7 as compared to *NOT*-3 (Tab. 55). To confirm the detected *NOT* variants, the amplifications were also performed using the Mammary gland cDNA library (Tab. 47). In this case *NOT*-1, -1a, -2, -2a, -2b, -4, and -5 could be isolated (Fig. 14B). Interestingly, an additional variant, *NOT*-3b, which lacks exon 3 as compared to *NOT*-3, was exclusively found in this library. All amplifications were also performed using cDNA from HaCaT, HT-29, HeLa, MDA-MB-468 cells and primary keratinocytes yielding similar signal patterns (not shown). In those cells only the variants 1-5 were sequenced. Taken together, 13 yet unidentified *NOT* variants, which can be grouped according to the composition of their first two

Tab. 55 Characterization of *NOT* splice variants

Variant	CDS/Stop[1]	Length[2]	Molecular weight[3]	Reference[4]
***NOT*-1**	TGA/1315	438	50.13	KP189312
***NOT*-2**	TAG/196	65	7.45	KP189315
***NOT*-3**	TGA/178	59	6.11	KP189318
***NOT*-4**	TGA/1171	390	44.37	KP189321
***NOT*-5**	TGA/322	107	11.87	KP189324
***NOT*-1a**	TAA/1276	425	47.28	KP189313
***NOT*-1b**	TGA/766	255	29.05	KP189314
***NOT*-2a**	TAG/196	65	7.45	KP189316
***NOT*-2b**	TAG/196	65	7.45	KP189317
***NOT*-3a**	TGA/178	59	6.11	KP189319
***NOT*-3b**	TGA/178	59	6.11	KP189298*
***NOT*-3c**	TGA/178	59	6.11	KP189320
***NOT*-4a**	TAA/1132	377	41.53	KP189322
***NOT*-4b**	TAA/628	209	22.82	KP189323
***NOT*-5a**	TGA/322	107	11.87	KP189325
***NOT*-5b**	TGA/322	107	11.87	KP189326
***NOT*-5c**	TGA/322	107	11.87	KP189327

1: Size of the coding sequence (CDS) in nt. The position indicates the T in the TGA/TAG/TAA stop codon with respect to ATG = 1; 2: Length of the translated proteins in aa; 3: Molecular weight (kDa) calculated using the Protein Identification and Analysis Tools on the ExPASy Server (Artimo *et al*. 2012): http://web.expasy.org/compute_pi/; 4: GeneBank accession numbers; All variants were sequenced from T98G cDNA with exception of *NOT*-3b (*) sequenced from Mammary gland cDNA library.

exons into transcripts derived from *NOT*-1, -2, -3, -4 or -5, were isolated from diverse cell lines. With the exception of the already published *NOT*-2 variant (Denecke *et al*. 2004) and its derivatives, which all contain a shortened first exon, the newly detected forms encompass the complete exonic sequences. The results indicate that the *NOT* transcripts are generated by alternative splicing. All obtained nucleotide sequences were deposited in the GenBank Sequence Database. The consequences of the observed splicing events for NOT protein structure is addressed elsewhere (B. Hacker, PhD thesis: Beitrag zur Aufklärung der zellulären Rolle des humanen *neighbour of tid* (*not*) Gens, 2016).

4.1.2 Identification of splicing motifs for the *NOT* transcripts

Sequence analysis of the diverse *NOT* variants suggests that they are generated by alternative

Tab. 56 Splicing motifs for the different *NOT* variants

Intron	5´splice site	Branch point	Polypyrimidine tract	3´ splice site
1[1]	(50) 5´-GAGgtaggc	(3441) 5´-accagAt	(3450) 5´-tcttgtcttcttcc	(3461) 5´-tccagAC
2a[2]	(531) 5´-CATgtgagt	(3441) 5´-accagAt	(3450) 5´-tcttgtcttcttcc	(3461) 5´-tccagAC
2b[3]	(494) 5´-GAGgtgggc	(3441) 5´-accagAt	(3450) 5´-tcttgtcttcttcc	(3461) 5´-tccagAC
3	(3563) 5´-TGTgtgagt	(3639) 5´-ctcacAt	(3645) 5´-ttttctctcatcttcc	(3658) 5´-tccagGT
4	(3808) 5´-AAGgtgagt	(3897) 5´-accttAc	(3906) 5´-tgttttcccttt	(3915) 5´-tttagGT
5	(4078) 5´-CAGgtcaac	(4535) 5´-tcctcTc	(4540) 5´-tcccctgctcacccc	(4552) 5´-cccagCC
6	(4675) 5´-CAGgtaccc	(5258) 5´-tgctgAc	(5269) 5´-caccaatcctc	(5277) 5´-ctcagGT
7	(5485) 5´-CAGgtgaga	(5604) 5´-ctcacAa	(5637) 5´-cttttctcc	(5643) 5´-tccagGA
8	(5722) 5´-ACCatatcc	(6283) 5´-cacacAc	(6291) 5´-ctcctgccctt	(6318) 5´-tacagAT
9	(6463) 5´-CAGgtacca	(6534) 5´-gcatgAg	(6584) 5´-cctgtttctcatctcc	(6597) 5´-tccagGT

All positions relative to ATG of *NOT*-4 = +1. Sequence derived from the BAC clone Homo sapiens 3 BAC RP11-488M12 (NCBI: AC061705). Splice sites were calculated using the Alternative splice site predictor (ASSP) at http://wangcomputing.com/assp/index.html. Exonic sequences in capital letters. The branch points were calculated using the Human splicing finder at http://www.umd.be/HSF3. The polypyrimidine tracts were calculated using the Intron Analysis tool from EMBL at http://www.ebi.ac.uk/asd-srv/wb.cgi?method=6. 1: Intron between exons 1 and 2 of *NOT* variants 3 and 4; 2: Intron for splicing of *NOT*-1 and derivatives; 3: Intron for splicing of *NOT*-2 and its derivatives.

splicing. The information required for splicing is contained in exonic and intronic *cis*-regulatory elements that function by recruitment of sequence-specific RNA-binding proteins, which either activate or repress the use of adjacent splice sites (Wang and Burge 2008). Motifs known as the core splicing signals are present at every exon/intron boundary (the 5´ and 3´ splice sites) and in every intron (the branch point sequence (BPS) and the polypyrimidine tract (PPT)) (Wang and Burge 2008). To identify splice sites for *NOT*, the Alternative splice site predictor (ASSP) (Wang and Marin 2006) was used. To identify BPs, the Human splicing finder (Desmet *et al*. 2009) was used. The PPTs were calculated using the Intron Analysis tool from EMBL at http:// www.ebi.ac.uk/asd-srv/wb.cgi?method=6 (offline). As shown in Tab. 56, these motifs are found in all nine *NOT* introns and at all exon/intron borders. Interestingly, in the case of the cryptic splice site within the first exon of *NOT*-1, which leads to generation of the *NOT*-2 transcript described by Denecke *et al*. (2004), the sequence of the 5´ (cryptic) splice site has a higher sequence identity to the consensus splice site than the one used for the higher expressed *NOT*-1 (Tab. 56+57).

4.1.3 Determination of *NOT* and *ECE2* transcription start sites

In eukaryotic cells RNA polymerase II mediated transcription starts from a specific promoter region upstream the translation start codon called the transcription start site (TSS). The TSSs for the *NOT* variants were determined using the RACE-technique and HaCaT cells as described in Ch.

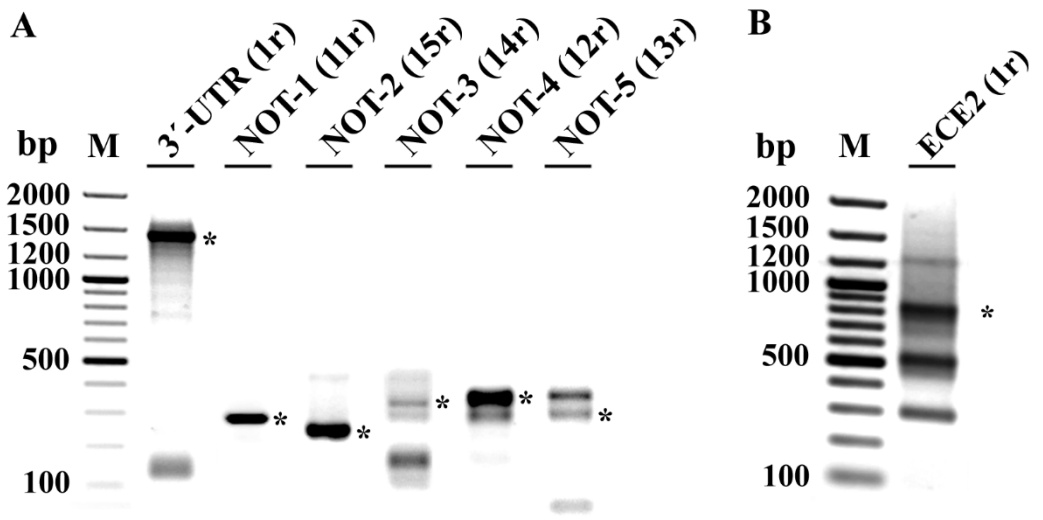

Fig. 15 Determination of *NOT* and *ECE2* transcription start sites (TSS) using RACE. Gel electrophoretic separation of DNA fragments amplified using RACE cDNA from HaCaT cells. The complete PCR samples were separated on a 1.5% agarose gel. For TSS identification all detected amplification products were extracted from the gel and sequenced. **(A)** Amplification of *NOT* variants. *NOT* bands are marked with asterisks, all other bands are unspecific amplificates. All bands were sequenced with the indicated reverse primer (Exception: Indicated band from the first lane was sequenced with primer 2r). **(B)** Amplification of *ECE2* using a primer specific for variants 1 and 3. Specific band marked with asterisk. bp: Base pairs; M: Marker Gene Ruler 100bp ladder.

3.3.18. All primers used for the amplifications are listed in Tab. 28. Amplification of RACE cDNA using the *NOT* 3´-UTR reverse primer (1r) able to recognize all *NOT* variants in combination with the RACE-tag-specific forward primer (USP primer) yields detection of one strong signal (Fig. 15A). Gel extraction and sequencing revealed that the isolated band corresponds to *NOT*-1 with the TSS located 23nt upstream ATG. In addition, smaller and significantly weaker signals were detected potentially corresponding to other *NOT* variants. Because of their slight intensities, they could not be sequenced. As shown above, the *NOT* transcripts can be classified depending on the compositions of their first two exons (Ch. 4.1.1). To determine if class-specific TSSs exist, RACE cDNA from HaCaT was amplified using group-specific reverse primers in combination with the USP primer. The obtained results confirm the TSS for *NOT*-1 and show that this TSS is also shared by *NOT*-2 and -5 (Fig. 15A). For *NOT*-3 and -4 the obtained results show that both variants share the same TSS located 285nt upstream their start codon (Fig. 15A). Because *NOT* and *ECE2* contain overlapping promoter regions, the TSS of *ECE2* was also determined. For that purpose, RACE cDNA from HaCaT cells was amplified using a reverse primer specific for the *ECE2* variants 1 and 3 in combination with the USP primer. These two *ECE2* variants were chosen, because they

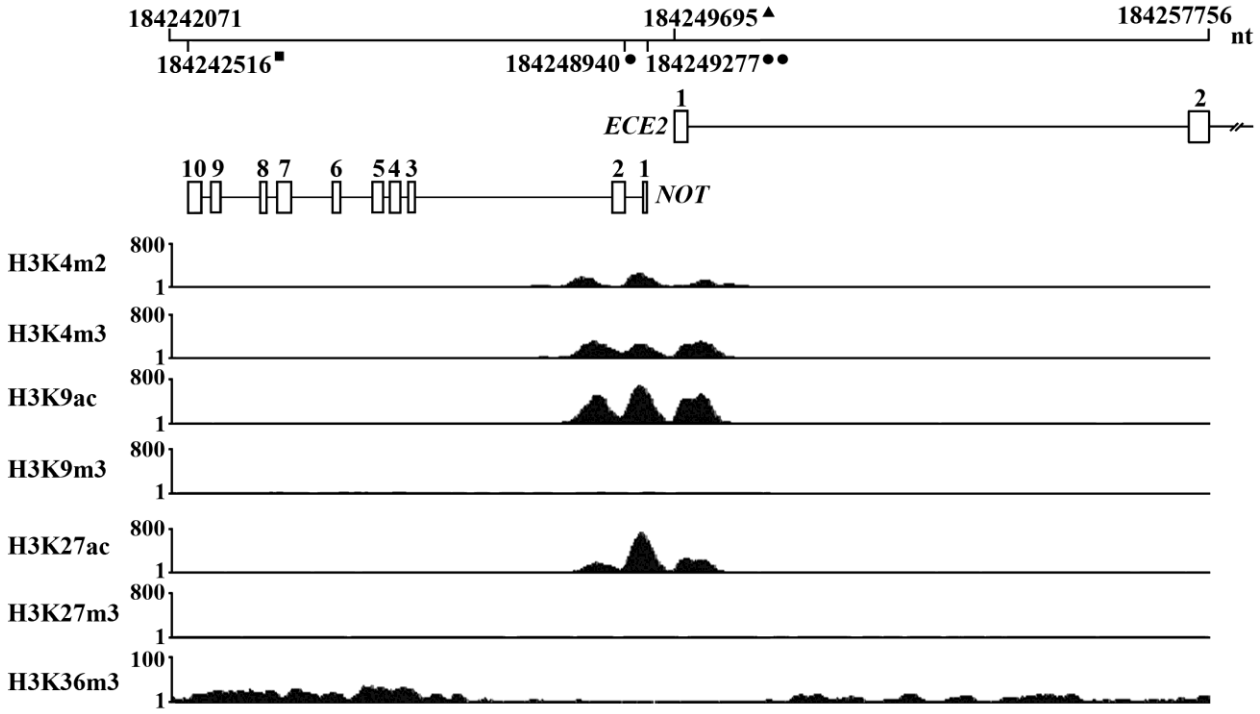

Fig. 16 Histone modifications within the *NOT* promoter region highlight the presence of three separate transcription units. Upper lane: Schematic representation of the chromosomal region encompassing the *NOT* gene and the first to exons of *ECE2* located on the opposite strand on chromosome 3 (Chromosome 3 genomic scaffold, GRCh38 Primary Assembly NT_005612.17). ChIP-seq data from HeLa cells generated in the context of the ENCODE at the Broad Institute (http://www.broadinstitute.org/science/projects/epigenomics/epigenomics-initiative) and in the Bernstein lab at the Harvard Medical School (http://bernstein.mgh.harvard.edu/) (Rosenbloom *et al*. 2013; 2015). Visualization using the UCSC genome browser (http://genome.ucsc.edu/) using the Human Dec. 2013 (GRCh38/hg38) Assembly (Kent *et al*. 2002). The H3K9m3 and H3K27m3 marks are typical for transcriptional inactive euchromatin (Sims 3rd *et al*. 2003) and served as negative control. H: Histone; K: Lysine; m: Methyl; ac: Acetyl; ●: ATG of *NOT*-1; ●●: ATG of *NOT*-4;▲: ATG of *ECE2*; ■: TGA of *NOT*-1/4.

are the only *ECE2* isoforms that contain the first exon 755nt upstream the *NOT*-1 ATG. The other three variants share a different leader exon 26.5kb upstream *NOT* -1 (Fig. 1). For simplicity, *ECE2* will refer to the *ECE2* variants 1 and 3 in the following sections. The RACE analysis revealed the TSS of *ECE2* to be located 33nt upstream its ATG (Fig. 15B). The *NOT* and *ECE2* TSSs were confirmed in HeLa and HT-29 cells. Experimental support for the three identified TSSs comes from available ChIP-seq data generated in the context of the ENCODE project to map epigenetic marks (ENCODE project consortium 2012; www.genome.gov/10005107/encode-project/). Active promoters contain the histone modifications H3K4m(methyl)2, H3K4m3, H3K9ac(acetyl) and H3K27ac, which are predominantly found around TSSs and the beginning coding region (Bernstein *et al*. 2002; Miao and Natarajan 2005; Shahbazian and Grunstein 2007). H3K36m3 marks regions

of PolII elongation, including coding and non-coding genes and regulates DNA mismatch repair/ proofreading activity (Li 2013). The visualization of these epigenetic marks across the *NOT-ECE2* genomic locus using the UCSC genome browser (Kent *et al*. 2002; https://genome.ucsc.edu/) reveals the presence of three separate transcription units, two for *NOT* and one for *ECE2* (Fig. 16). Taken together, the results show that two different TSSs for *NOT* exist and that the variants which share the same first exon also share the same TSS. The detection of two different TSSs also indicates that the different *NOT* variants are transcribed from two different promoters.

4.1.4 Identification of RNA motifs within the *NOT* UTRs

To further characterize the *NOT* transcripts, the presence of functional RNA motifs in their untranslated regions (UTRs) was investigated using the RegRNA2.0 web tool (Chang *et al*. 2013). This analysis revealed that there exist no motifs for the universal 3'-UTR and for the 5'-UTR of *NOT*-1. In the case of *NOT*-4 three elements were detected. A Musashi binding element (MBE; MacNicol *et al*. 2011) located at 104-99nt upstream the TSS (5´-ATTAGT) and two upstream ORFs (uORFs; Wethmar 2014) termed N4-uORF1 (5´-ATGAATGACTTTTATCAGGAAATC TGA; 133-107nt) and N4-uORF2 (5´-ATGACTTTTATCAGGAAATCTGAAAATTAG; 129-100nt). Both elements are known to repress translation of most mRNAs they are found in (MacNicol *et al*. 2011; Wethmar 2014). The efficiency of translation initiation also strongly depends on the nucleotide composition around the start codon, the so-called Kozak sequence (Fig. 17). For most efficient translation the position at -3 nt has to be A or G (R), the position +4nt G (Kozak 2005). Transcripts whose Kozak sequences only fit at one position with the consensus site are less efficiently translated, whereas transcripts which do not share these positions are, if at all, only weakly translated (Kozak 2005). As shown in Fig. 17, the sequence analysis revealed that *NOT*-1 shares the two important positions with the reference, whereas *NOT*-4 does not. Interestingly, the Kozak sequence of the N4-uORF1 matches better with reference than does the

Kozak	GCC**R**CC**ATGG**
***NOT*-1**	GTT**A**AG**ATGG**
***NOT*-4**	ACACAG**ATG**T
N4-uORF1	TTC**A**AT**ATG**A
N4-uORF2	ATATGA**ATG**A

Fig. 17 Kozak sequences within the *NOT* transcripts. Alignment of the sequences around the ATGs (bold and underlined) of the *NOT* transcripts 1 and 4 and the two uORFs of *NOT*-4 with the Kozak reference sequence (Kozak 2005). The key positions of the Kozak sequence are in bold. Other sequence matches are underlined. R: Purine (A/G).

normal full-ORF. Taken together, the compositions of the RNA motifs suggest, that *NOT*-1 is more efficiently translated than *NOT*-4.

4.1.5 Quantification of the expression of the *NOT* transcripts in diverse cell lines

The *NOT* gene encodes 17 splice forms generated by alternative splicing (Ch. 4.1.1). To determine the expression of the distinct *NOT* transcripts in diverse cell lines, qRT-PCR analysis was performed (Ch. 3.3.17). Splice variant-specific primers were designed (Tab. 33) and their efficiencies were determined using the LinReg evaluation software (Table S1-S4). As *NOT* and *ECE2* might be coregulated because of their overlapping promoter regions, the samples were further investigated for *ECE2* mRNA levels. The levels of the ubiquitously expressed *ACTIN* were also determined as comparison. The evaluation of the amount of the targets investigated was performed using

Tab. 57 Quantification of the relative amounts ($2^{-\Delta Ct}$) of the *NOT*, *ECE2*, and *ACTIN* transcripts in diverse cell lines

	$2^{-\Delta CT}$			
Target	**HaCaT**	**HT-29**	**T98G**	**HeLa**
NOT-1	0.10	0.12	0.19	0.12
NOT-1a	1.70×10^{-2}	2.11×10^{-2}	2.32×10^{-2}	3.85×10^{-2}
NOT-1b	0.12×10^{-2}	0.37×10^{-3}	0.18×10^{-2}	0.58×10^{-3}
NOT-2	5.83×10^{-2}	9.81×10^{-2}	8.90×10^{-2}	3.40×10^{-2}
NOT-2a	2.11×10^{-2}	2.54×10^{-2}	1.64×10^{-2}	1.52×10^{-2}
NOT-2b	0.16×10^{-2}	0.39×10^{-3}	0.15×10^{-2}	0.39×10^{-3}
NOT-3	0.08×10^{-2}	0.40×10^{-3}	0.89×10^{-3}	0.79×10^{-3}
NOT-3a	0.05×10^{-2}	0.16×10^{-3}	0.31×10^{-3}	0.70×10^{-3}
NOT-3b	0.01×10^{-2}	8.51×10^{-5}	0.11×10^{-3}	0.24×10^{-3}
NOT-3c	0.38×10^{-4}	9.46×10^{-6}	0.20×10^{-3}	0.03×10^{-3}
NOT-4	0.95×10^{-2}	1.94×10^{-2}	1.51×10^{-2}	1.15×10^{-2}
NOT-4a	0.35×10^{-2}	0.54×10^{-2}	0.50×10^{-2}	0.37×10^{-2}
NOT-4b	0.37×10^{-2}	0.51×10^{-2}	0.49×10^{-2}	0.44×10^{-2}
NOT-5	0.08×10^{-2}	0.39×10^{-3}	0.80×10^{-3}	0.12×10^{-2}
NOT-5a	0.04×10^{-2}	0.98×10^{-3}	0.50×10^{-3}	0.10×10^{-2}
NOT-5b	0.94×10^{-4}	0.32×10^{-5}	0.14×10^{-3}	0.46×10^{-5}
NOT-5c	0.35×10^{-3}	0.18×10^{-3}	0.39×10^{-3}	0.50×10^{-3}
ECE2	0.33	0.21	0.29	0.90
ACTIN	28.44	18	38.59	30.27

The ΔCt value is determined by subtracting the *HGPRT* (endogenous reference) C_T-value from the C_T value of the target investigated: $\Delta C_T = C_T$ (*NOT* target) - C_T (*HGPRT*); The relative concentration of the target (amount of target), $2^{-\Delta CT}$, is calculated for the average ΔC_T values.

the ΔC_T method. As shown in Tab. 57, the *NOT* splice forms are expressed at distinct levels in different cells. The $2^{-\Delta CT}$ values indicate that *NOT*-1 is the highest expressed variant in all four cell lines (Tab. 57). In HaCaT, HT-29, and HeLa cells *NOT*-1 mRNA levels are almost identical (0.1, 0.12, and 0.12 respectively), whereas in T98G the amount is doubled (0.19). All other *NOT* variants are expressed at significant lower levels. Furthermore, the expression data shows that in all cells investigated the basic variants 1, 2, 3, 4, and 5 are expressed at a higher level than the derivatives of these forms, in some cases this difference is three orders of magnitude (e. g. *NOT*-3 and -3c or *NOT*-5 and -5b). Despite this observation, a constant ratio of the amount of the basic variants to the amount of their derivatives could not be detected. For *ECE2* the $2^{-\Delta CT}$ values indicate higher expression levels as compared to *NOT*, whereas an inter-cell correlation between the detected *ECE2* transcript patterns with any of the *NOT* multiple variants could not be detected. In all four cell lines both, *NOT* and *ECE2*, are expressed at significantly lower levels as *ACTIN*.

4.1.6 Determination of the physiological relevance of the different *NOT* transcripts

Most of the isolated *NOT* variants contain a premature stop codon (Tab. 55). Transcripts which harbor premature stop codons are selectively removed by the nonsense-mediated mRNA decay (NMD) pathway to avoid deleterious effects for the cell (Chang *et al*. 2007). To test if *NOT* variants are targeted by this pathway, HT-29 cells were treated with different concentrations of the NMD inhibitor caffeine as described in Ch. 3.6.4.1. Transcripts which are removed under normal physiological conditions via NMD should be accumulated after blocking this pathway. Using cDNA from caffeine-treated and -untreated cells as template the specific amplification of the *NOT* variants shows the enrichment of variants 2, 3, 5, 1a, 1b, 2a, 2b, 3a, 3c, 5a, 5b, and 5c at 10mM caffeine (Fig. 18A). Variants 5, 5a, 5c, and 3a are also stabilized at lower and/or higher concentrations (Fig. 18A). The full-length variants 1 and 4 as well as *HGPRT* are not enriched. Interestingly, the *NOT*-4 derived variants 4a and 4b which potentially code for 41.53kDa and 22.82kDa proteins (Tab. 55) are not stabilized in contrast to *NOT*-1 derived variants 1a and 1b potentially coding for 47.28kDa and 29.05kDa proteins (Tab. 55). *SMAD4* was amplified as positive control for NMD inhibition (Johnson *et al*. 2012). Dassesse *et al.* (1999) reported that the transcription factors EGR-1, c-Fos, and Arc are activated by caffeine to upregulate their target genes. Because EGR-1 also regulates *NOT* (Ch. 4.4), the NOT protein expression was determined using western blot (Ch. 3.4.3), to show that the observed increase of *NOT* transcripts is not due to

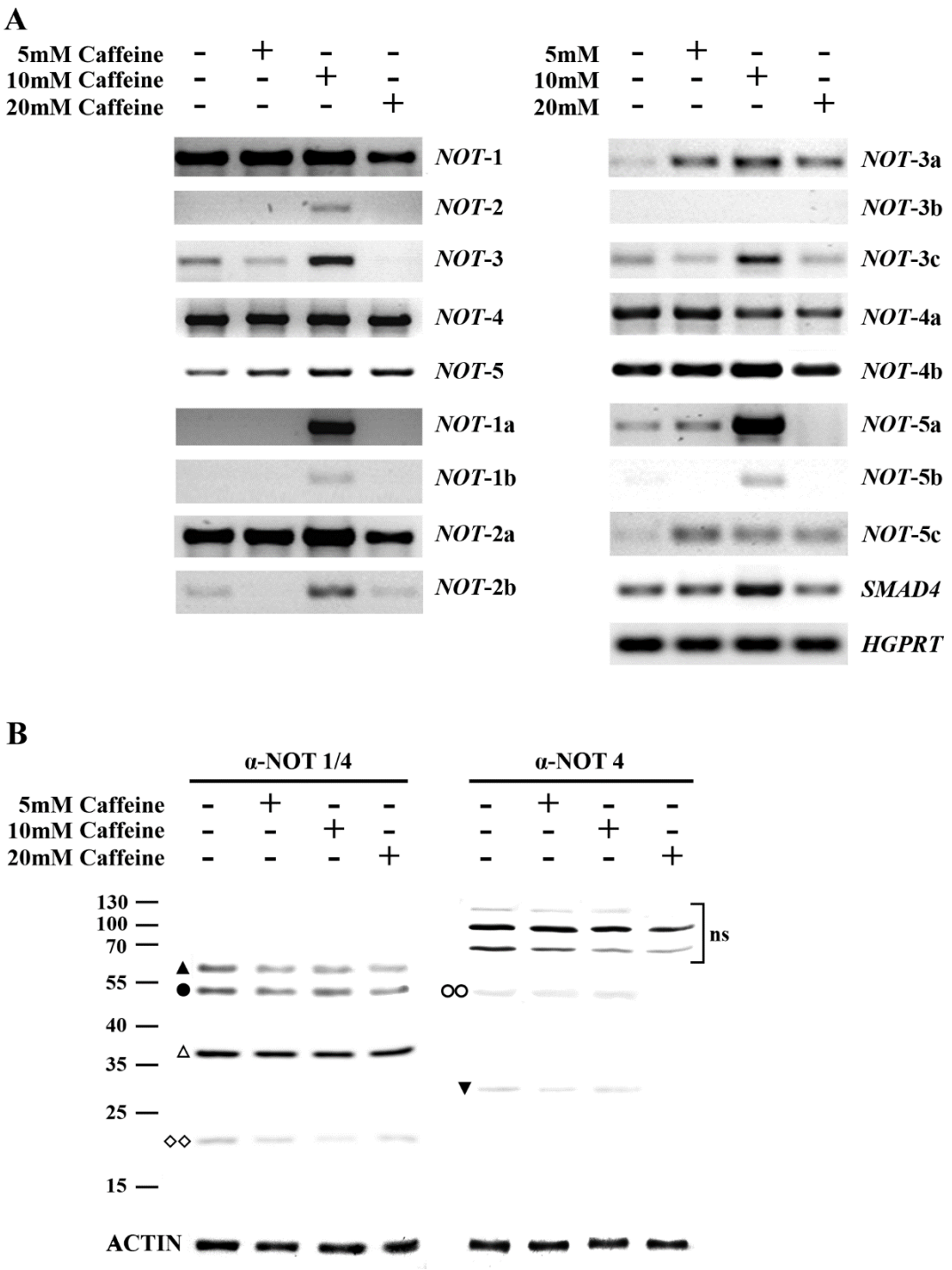

Fig. 18 Accumulation of *NOT* mRNAs in caffeine-treated HT-29 cells. (A) Gel electrophoretic separation of amplified cDNAs generated from Caffeine-treated and -untreated HT-29 cells. Amplifications were performed using variant-specific primer combinations. 20µl of the amplificates were loaded on a 2% agarose gel. **(B)** NOT expression as determined using crude homogenates from Caffeine-treated and -untreated HT-29 cells. 15µg crude homogenates were separated on a 10% PAGE gel and analyzed using the α-NOT 1/4 and α-NOT 4 antibodies. α-NOT 1/4 recognizes the full-length NOT-1 precursor (●), the potential post-translational modified full-length NOT-1 (▲), the N-terminal NOT-1 cleavage product (Δ), and the C-terminal NOT-1 cleavage product (◊◊). α-NOT 4 recognizes full-length NOT-4 (○○) and the N-terminal NOT-4 cleavage product (▼). ns: Non-specific. M: Marker.

induced gene expression. As shown in Fig. 18B, no increase of NOT-protein amount can be detected after treating HT-29 cells with caffeine.

4.2 Identification of *NOT* and *ECE2* core promoter elements

Initiation of transcription occurs at the core promoter. It is defined as the genomic sequence in the immediate vicinity of the TSS, which can contain various combinations of distinct DNA-binding elements that orchestrate the assembly of the preinitiation complex to navigate Pol II to the TSS (Fuda *et al*. 2009) (Fig. 5). To predict conserved core promoter elements, the Elements Navigation Tool (ElemeNT; Sloutskin *et al.* 2015) and the Jaspar database (Mathelier *et al*. 2014) were used (Ch. 3.5.1). As the core promoter is always defined relative to the TSS, the region 100nt up- and downstream of the determined *NOT*-1, *NOT*-4, and *ECE2* TSSs (Ch. 4.1.3) were analyzed. The obtained results show that the TSSs for *NOT*-1 and *NOT*-4 are both located at an Initiator (Inr) element (Tab. 58). In addition, a downstream promoter element (DPE) is located near the *NOT*-1 TSS and a downstream core element (DCE) is located near the *NOT*-4 TSS. No core promoter elements were detected for *ECE2*. With the exception of the B recognition element (BRE), which is specifically recognized by TFIIB, all other core promoter elements are described as TFIID-interaction sites (Maston *et al*. 2006). To confirm the functional relevance of the predicted core promoter elements *in vivo*, chromatin immunoprecipitation (ChIP) was applied (Ch. 3.5.7). The ChIPs were performed using an antibody directed against TBP (Tab. 43) and chromatin from HT-29 and HeLa cells. The transcription factor p53 was used as negative control as it does not bind to

Tab. 58 Potential core promoter elements within the *NOT* promoter

	Sequence		
CPE[1]	***NOT*-1[2]**	***NOT*-4[2]**	**Consensus[3]**
Initiator	(-24)5´- C<u>C</u>ACACA	(-284)5´- TTACTAA	YYANWYY
TATA	---	---	TATAWAAR
BRE[u]	---	---	SSRCGCC
BRE[d]	---	---	RTDKKKK
DPE	(+6)5´- GGCTGG		DSWYVY
DCE	---	(-272)5´- CTTCN$_{14}$CTGGN$_{7}$ATCN$_{2}$	N$_{5-7}$CTTCN$_{7-8}$CTGTN$_{7-11}$AGCN$_{1-2}$

1: Core promoter elements; The BRE element can be located upstream (u) or downstream (d) of the TSS (Sloutskin *et al*. 2015); 2: Sequence relative to ATG, the TSS is underlined; 3: Consensus motifs from Sloutskin *et al*. 2015; N$_x$: Any base in the next x positions; Y: C or T; W: A or T; R: A or G; S: G or C; D: A or G or T; K: G or T; V: A or C or G. The putative core promoter elements were predicted using the ElemeNT tool (Sloutskin *et al*. 2015). The lack of TATA boxes was confirmed using the Jaspar Database (Mathelier *et al*. 2014).

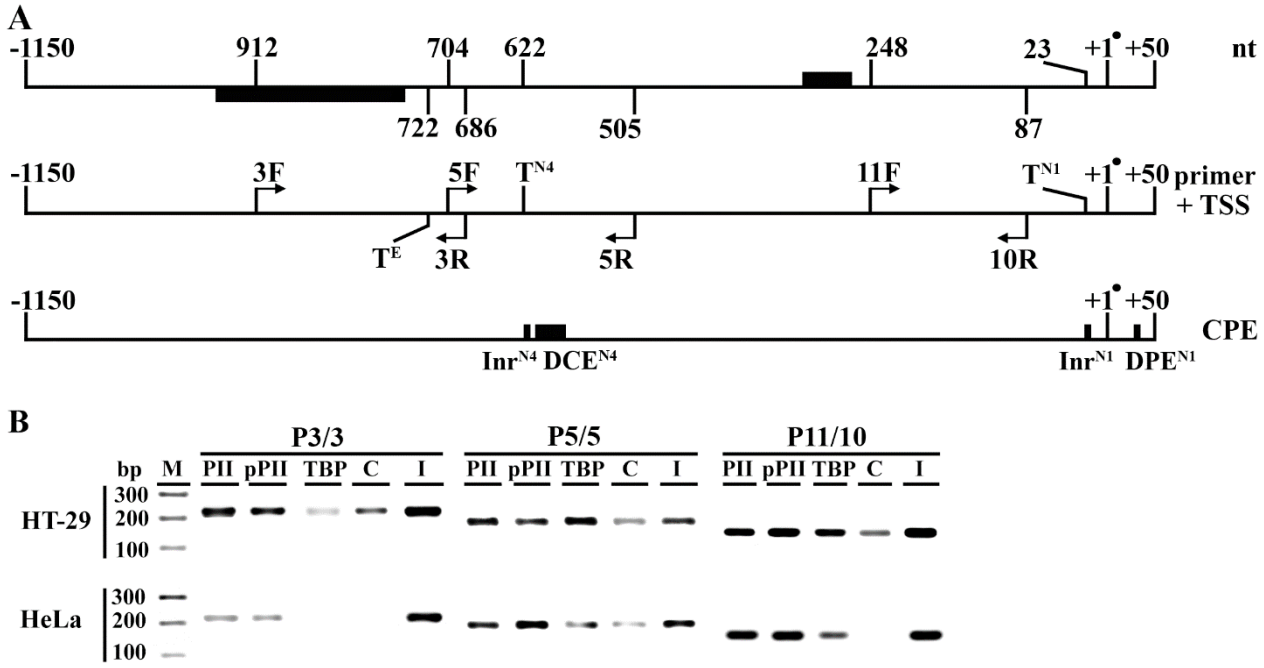

Fig. 19 Identification of Pol II and TBP binding in the *NOT* promoter *in vivo* using the ChIP technique. **(A)** Schematic representation of the 1.15kb *NOT* promoter. First bar: Positions in nt upstream the *NOT*-1 start codon; The respective first exon of *NOT*-4 and *ECE2* is indicated as thicker bar; second bar: Primers (F: Forward; R: Reverse) used for amplification and identified transcription start sites (T) for *NOT*-1 (T^{N1}), *NOT*-4 (T^{N4}) and *ECE2* (T^{E}); third bar: Core promoter elements (CPE) predicted using the ElemeNT tool (Sloutskin *et al*. 2015). **(B)** Gel electrophoretic separation (2% agarose gel) of DNA fragments amplified from ChIPs performed using antibodies directed against TBP, polymerase II (PII), polymerase II phosphorylated on Ser 5 (pPII) and p53. C: p53 ChIP, negative control; I: Input DNA; bp: Base pairs; M: Marker Gene Ruler 100bp ladder.

the *NOT* promoter (Ch. 4.4.1). Because the ChIP technique not only allows identification of proteins directly bound to DNA but of all chromatin proteins in a defined chromosomal area, the ChIP experiments were also performed using antibodies directed against Pol II and Pol II phosphorylated on Ser5 of its C-terminal repeat domain (CTD) (Tab. 43). Although unphosphorylated Pol II can be loaded to the PIC, the Pol II holoenzyme can only escape the promoter and enter the elongation phase if Ser5 in the CTD is hyper-phosphorylated (Phatnani and Greenleaf 2006). Amplifications performed using the primer combination P5/5 indicates binding of TBP to the 704-505nt fragment encompassing the TSS of *NOT*-4 in HT-29 and HeLa cells (Fig. 19B). Identical results were obtained for amplifications of the *NOT*-1 TSS-containing fragment using the primer combination P11/10 (Fig. 19B). Amplifications of the 912-704nt fragment encompassing the *ECE2* TSS using the P3/3 primer combination showed no TBP binding within this region (Fig. 19B). In addition, these amplifications also indicate that the pre-initiating Pol II (unphosphorylated) and the

initiating Pol II (Ser5 phosphorylated) are present near the TSSs of *NOT*-1, *NOT*-4, and *ECE2* (Fig. 19B). Taken together, the obtained results suggest that the transcription of *NOT* is initiated from two different promoters containing different core promoter elements in a TBP-dependent manner. In contrast, transcription from the *ECE2* promoter on the complementary strand is initiated in a TBP-independent manner.

4.3 Generation of *NOT* promoter constructs

The yeast one-hybrid technique (Y1H) was used to identify protein-DNA interactions and to map the protein domains necessary for these interactions. For this purpose, nine *NOT* promoter fragments were cloned into the pHIS2.1 reporter vector (P1-9, Fig. 20) (Ch. 3.3.14.1). To minimize false positive results due to leaky expression of the *HIS3* reporter gene, a 3-AT test was performed for every construct (Ch. 3.5.2). The pGADT7- Rec2-p53 vector carrying a DNA fragment encoding aa73-392 of the murine p53 protein was cotransformed with the p53 binding sites containing p53pHIS2 reporter vector as positive control (Thukral *et al*. 1994) (Fig. 6). As shown in Tab. 59, the required concentration of 3-AT to inhibit the basal reporter activity depends on the construct. 50mM 3-AT is sufficient for constructs 1-3, whereas in the case of construct 4 colonies still grow on medium containing 100mM of the inhibitor. Generally, with increasing amount of inhibitor the number of grown colonies decreases. At 150mM 3-AT none of the transformed *NOT* promoter

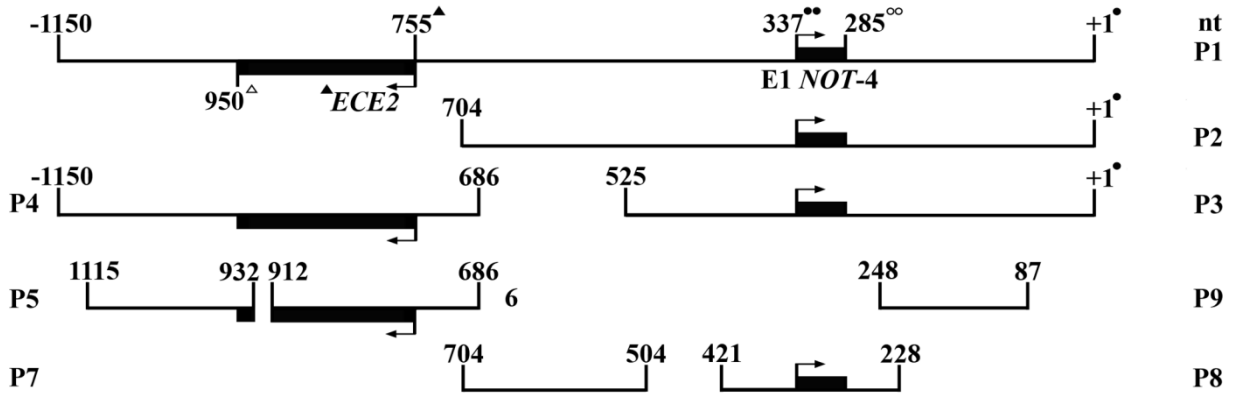

Fig. 20 Schematic representation of the nine *NOT* promoter constructs, Ph*NOT*-1 to -9 (P1-9), used for identification of DNA binding sites with the Y1H system. The constructs encompass the 1150bp promoter region. The promoter fragments were cloned into the pHIS2.1 reporter vector. Indicated positions are upstream of the *NOT*-1 start codon +1 (●). The first exon of *NOT*-4 is located from 337nt (●●) to 285nt (○○). The first exon of *ECE2* is located at located from 755nt (▲) to 950nt (Δ).

Tab. 59 Results of the 3-AT test performed for the generated *NOT* promoter constructs

	SD/-His/-Trp/-Leu + 3-AT					
Construct[1]	**0mM**	**50mM**	**60mM**	**70mM**	**100mM**	**150mM**
Ph*NOT*-1	+++	-	-	-	-	-
Ph*NOT*-2	+++	-	-	-	-	-
Ph*NOT*-3	+++	-	-	-	-	-
Ph*NOT*-4	+++	+++	+++	++	+	-
Ph*NOT*-5	+++	++	++	+	-	-
Ph*NOT*-6	+++	++	+	+	-	-
Ph*NOT*-7	+++	+	-	-	-	-
Ph*NOT*-8	+++	++	+	+	-	-
Ph*NOT*-9	+++	++	++	-	-	-
p53[2]	+++	+++	+++	+++	+++	+++

1: Cotransformation of the pACT2 vector with the indicated promoter construct (Fig. 20) into Y187 cells. Cells were plated on SD/-His/-Trp/-Leu supplemented with the indicated concentrations of 3-AT. 2: Cotransformation of pGADT7-Rec2-p53 and p53pHIS2 as positive control. +++: Strong growth; ++: Considerable growth; +: Weak growth; -: No growth.

constructs exhibits colony growth anymore. The p53 positive control grows independent of the 3-AT concentration. Thus, a 3-AT concentration of 150mM was chosen for all constructs in the further experiments.

4.4 Determination of EGR-1 binding to the *NOT* promoter

To identify *NOT* promoter DNA-binding proteins, the human mammary gland MATCHMAKER cDNA library (Tab. 47) was screened using the Y1H technique. This screen yielded isolation of the C-terminal part (aa 236-543) of the EGR-1 zinc finger transcription factor (zif268, NGFI-A, Krox-24, TIS8, ZENK; NCBI Gene ID: 1958) as potential *NOT* regulator (C. Schultheiss, diploma thesis: Identification and isolation of regulatory proteins of the novel human tumor-related gene h*NOT*, 2009). EGR-1 is a tumor suppressor well known for regulating replicative senescence via activating the p53-MDM2-p19ARF pathway and promoting apoptosis (Krones-Herzig *et al*. 2003). It also regulates other tumor suppressors like TGFβ, PTEN, and fibronectin (Baron *et al*. 2006). To confirm the binding of full-length EGR-1 to the *NOT* promoter and to map the single binding site(s), the Y1H (Ch. 4.4.1), EMSA (Ch. 4.4.3), affinity chromatography (Ch. 4.4.4), Southwestern blot (Ch. 4.4.4), and ChIP (Ch. 4.4.5) techniques were applied. In addition, the *in vivo* relevance of these interactions for the regulation of NOT protein expression was assessed (Ch. 4.4.6).

4.4.1 Identification of EGR-1 binding to the *NOT* promoter using the Y1H technique

As determined using the P-MATCH^{TM} algorithm (Chekmenev *et al*. 2005), the 1.15kb *NOT* promoter region contains seven potential EGR-1 binding sites (six in *cis*, one in *trans*) (Fig. 21A and Tab. 38). To examine which of these sites can actually be bound, the Y1H technique was used (Ch. 3.5.2). For this purpose, the full-length pACT2-EGR-1 expression construct (Fig. 21B, Ch. 3.3.14.3) was cotransformed with either of the pHIS2.1-Ph*NOT* constructs P1-9 (Fig. 20) into Y187 cells. The promoter regions represented by P5 and P9 (Fig. 20) contain no putative EGR-1

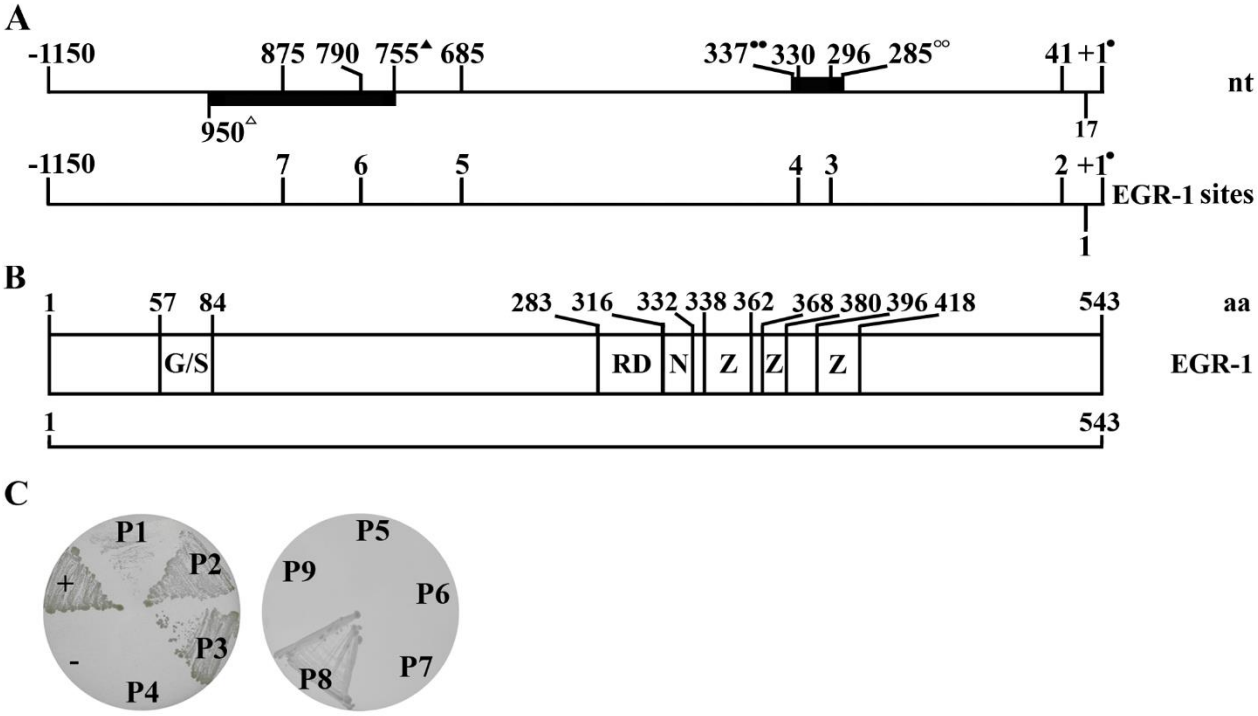

Fig. 21 Identification of EGR-1 binding to the *NOT* promoter using the Y1H technique. (A) Schematic representation of the 1.15kb *NOT* promoter region (upper bar) with potential EGR-1 binding sites (lower bar) predicted using the P-MATCH^{TM} algorithm (Chekmenev *et al*. 2005). The *cis* sites are shown on the upper side on the second bar, the *trans* sites on the lower site. Positions are upstream the *NOT*-1 start codon (+1/●). The first exon of *NOT*-4 is located from 337nt (●●) to 285nt (○○). The first exon of *ECE2* v1 and v3 is located from 755nt (▲) to 950nt (Δ). **(B)** Schematic representation of the EGR-1 protein structure (UniProtKB: P18146) with the generated pACT2 expression constructs below. EGR-1 is composed of 543aa and contains three zinc-fingers (Z) for DNA binding spanning aa338-362, 368-380, and 396-418. The aa57-84 constitute a glycine/serine rich region (G/S). A domain responsible for transcriptional repression (RD) encompasses aa283-316. A bipartite nuclear localization signal (N) is composed of basic residues aa317-332 and the third zinc-finger, aa396-418. The mapped DNA-binding domain is shown in thicker bars. **(C)** Determination of EGR-1 binding to the *NOT* promoter. Y187 cells were cotransformed with the pACT2-EGR-1 construct and the indicated pHIS2.1-Ph*NOT* promoter constructs (P1-P9, Fig. 20). Cells were grown on SD/-His/-Trp/-Leu + 150mM 3-AT. Control transformations: -: pACT2-p53; +: pGADT7-Rec2-p53 + p53pHIS2.

Tab. 60 Identification of EGR-1 binding to the *NOT* promoter using Y1H

Promoter construct[1]	Region (5´- 3´)[2]	EGR-1 binding sites (5´-3´)[3]		Y1H result[4]
		cis	trans	
P1	1150 -ATG	7 (875-864); 6 (790-673); 5 (685-673); 4 (330-313); 3 (296-285); 2 (41-30)	1 (17-28)	+
P2	704 - ATG	5, 4, 3, 2	1	+
P3	525 - ATG	4, 3, 2	1	+
P4	1150 - 686	7, 6		+
P5	1115 - 932			-
P6	912 - 686	7, 6		-
P7	704 - 504	5		-
P8	421 - 228	4, 3		+
P9	248 - 87			-

1: All promoter fragments were cloned into pHIS2.1; 2: Nt positions upstream the *NOT*-1 ATG; 3: Potential EGR-1 binding sites predicted using the P-MATCH™ algorithm (Chekmenev *et al*. 2005); 4: Y1H results for the EGR-1 full-length expression construct in pACT2 cotransformed into Y187 cells with the indicated promoter constructs. The cells were plated on SD/-His/-Trp/-Leu + 150mM 3-AT. +: Growth.

binding sites and served as negative controls. The obtained results show that constructs P1, P2, P3, and P8 (Fig. 20) can be bound by EGR-1 whereas P4, P6, and P7 (Fig. 20) cannot (Fig. 21C and Tab. 60). This indicates that EGR-1 sites 5, 6, and 7 cannot be bound. Because regulation of *NOT* by EGR-1 via sites 1 and 2 would not be compatible with the mapped minimal promoter (Kurzik-Dumke and M. Szydlowski, personnel communication), sites 3 (296-285nt) and 4 (330-313nt) emerge as potential EGR-1 target sites.

4.4.2 Expression of EGR-1 under normal growth conditions and during serum response in diverse cell lines

The Y1H experiments identified EGR-1 as potential *NOT* regulator. To further validate this finding and determine the single binding sites *in vitro* and *in vivo*, EMSAs, affinity chromatography, Southwestern blotting, and ChIPs were performed (Ch. 4.4.3 - 4.4.6). For that purpose, the HaCaT (primary immortalized keratinocytes), HT-29 (colon adenocarcinoma), HeLa (cervix carcinoma), and T98G (glioblastoma) cell lines (Tab. 51) were first checked for their applicability in these downstream experiments by determining the EGR-1 expression using western blot (Ch. 3.4.3). The expression of the NOT proteins in these cells was determined by B. Hacker (PhD thesis: Beitrag zur Aufklärung der zellulären Rolle des humanen *neighbour of tid* (*not*) Gens, 2016). The results

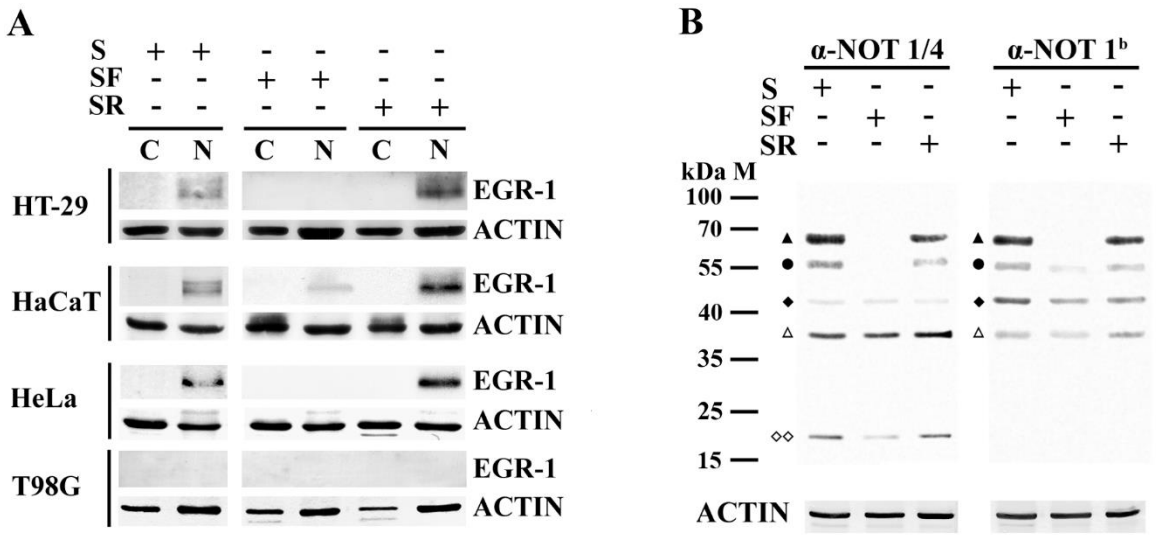

Fig. 22 Expression of EGR-1 and NOT under normal growth conditions and during serum response as determined using western blot. Crude homogenates from HT-29 cells **(in B)** or cytosolic (C) and nuclear (N) extracts (15µg each) isolated from diverse cell lines **(in A)** incubated under the indicated conditions were separated on a 10% SDS-PAGE gel. Indicated proteins were detected using specific antibodies. The α-NOT 1/4 and α-NOT 1^b antibodies recognize the full-length NOT-1 precursor (●), the potential post-translational modified full-length NOT-1 (▲), the 42kDA cleavage product (NOT42; ♦), and the N-terminal NOT-1 cleavage product (Δ). The C-terminal NOT-1 cleavage product (◊◊) is only detected by α-NOT 1/4. S: Cells grown under normal serum conditions; SF: Serum free; SR: Serum response 2h; ns: Non-specific; M: Marker.

show the nuclear localization of the EGR-1 protein in HaCaT, HT-29, and HeLa cells (Fig. 22A). In accordance with previous observations, EGR-1 protein cannot be detected in T98G cells using western blot (Liu *et al*. 2000). As a member of the immediate-early response gene family EGR-1 is not expressed in non-tumorigenic cells after serum deprivation but it can be (re-)induced by the mitogenic factors contained in serum (Lemaire *et al*. 1990). To assess, if this mechanism is operative in the applied cell lines, they were grown under serum free conditions for 24h (SF) and then incubated again with serum containing medium for 2h (serum response; SR) (Ch. 3.6.3). The immunoblots show that serum starved HT-29 and HeLa cells lack EGR-1 (Fig. 22A). Notably, serum starved HaCaT cells still contain a low amount of nuclear EGR-1, which might be a proliferative mechanism to maintain their unlimited growth potential. After SR, HaCaT, HT-29, and HeLa cells accumulate EGR-1 in their nuclei (Fig. 22A). The amount of nuclear EGR-1 is even higher as compared to cells grown under normal conditions. To check if this EGR-1 dynamic has an influence on NOT expression, whole cell extracts from HT-29 cells grown under normal, SF and SR conditions were subjected to western blot using anti-NOT antibodies (Tab. 43). The results show that the NOT-1 precursor (●) and its potential processed counterpart (▲) are not expressed

under SF conditions (Fig. 22B). The detectable amounts of the NOT-1 cleavage products (♦, Δ, and ◊◊) may be due to their stability (Hacker and Kurzik-Dumke, personal communication). Under serum response conditions with induced EGR-1 the NOT expression is restored (Fig. 22B). Similar results were obtained for HeLa cells (not shown). Serum starvation and response have no effect on NOT-4 expression in HT-29 cells (not shown).

4.4.3 Identification of EGR-1 binding sites in the *NOT* promoter using EMSA

The binding analysis performed using the Y1H technique indicates that EGR-1 binds to the *NOT* promoter region between 421-228nt upstream the *NOT*-1 start codon. This region harbors two potential EGR-1 binding sites, s3 (296-285nt) and s4 (330-312nt). To determine the binding capacity of this two sites and to verify the negative results for the others, EMSAs were performed (Ch. 3.5.3). Protein-DNA complexes were identified by incubating the nuclear extracts from HaCaT, HT-29, and HeLa cells with biotin (btn)-labeled double-stranded (ds) oligonucleotides representing the predicted binding sites (Tab. 38). For HaCaT (Fig. 23A) and HeLa (Fig. 23B) extracts, positive results have been obtained for site 4. The EGR-1 specificity of the shift was determined in a control reaction performed using an EGR-1 reference oligo (Backer *et al*. 2009) either incubated with nuclear extract (Fig. 23A-C) or recombinant EGR-1 (Fig. 23B). In addition, the obtained signals were compared to the EGR-1 signal detected using native western blot (Fig. 23A). The P-MATCH^{TM} analysis (Chekmenev *et al*. 2005; Ch. 3.5.1) revealed, that EGR-1 s4 is partially overlapped by a potential NFκB site (NFκB s4, Tab. 38). To determine if both sites can be used in a competitive manner, derivatives of the s4 oligo were synthesized either lacking the EGR-1 part (oligo name: s4^4) or the NFκB part (s4^5) (Tab. 38). As these oligos are too short for the use in gel shift assays, the s4^4 and s4^5 oligos were extended on both ends. To ensure that these added nucleotides do not influence the binding, two additional control oligos were also synthesized. One is an extended version of s4 (named s4^2) and one contains the predicted EGR-1 site as a tandem repeat (s4^3) (Tab. 38). Incubation of oligos s4^2 and s4^3 with nuclear extracts from HaCaT and HeLa cells show the previously identified EGR-1 shift (Fig. 23A+B). Because incubation with oligo s4^3 does not generate a second shift, the two tandem EGR1 sites in oligo s4^3 are too closely arranged to bind two EGR-1 molecules at once. Incubation of s4^4 with nuclear extracts from HaCaT and HeLa cells does not exhibit the EGR-1 shift, whereas incubation with s4^5 does (Fig. 23A+B). These results implicate that s4 is bound by EGR-1 and not NFκB. Interestingly, incubation of the EGR-1

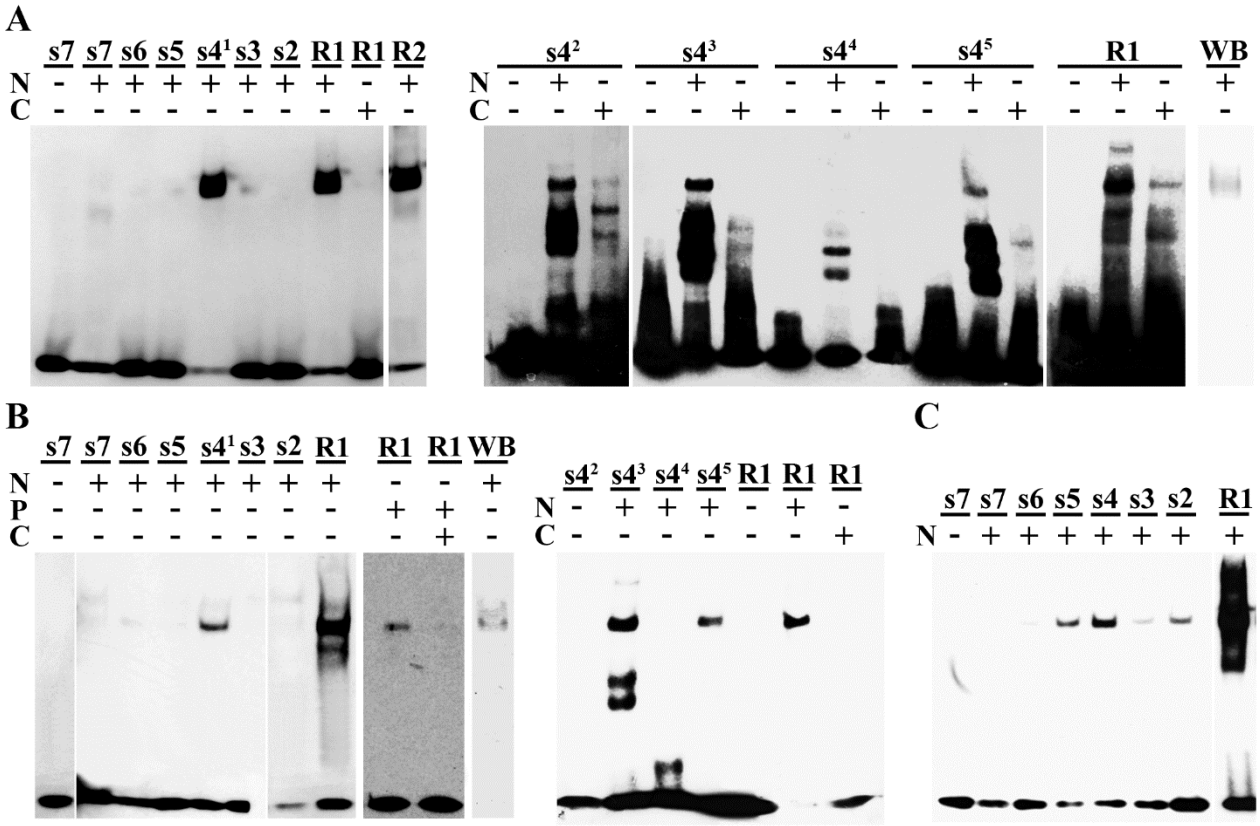

Fig. 23 Identification of EGR-1 binding sites in the *NOT* promoter using EMSA. The protein-DNA complexes were detected by incubating 7µg nuclear extracts (N) from HaCaT **(A)**, HeLa **(B)**, and HT-29 **(C)** cells with btn-labeled ds EGR-1 binding sites. Protein-DNA complexes were separated on a 5% native PAGE gel and visualized using chemiluminescence. EGR-1 specificity was determined by using published EGR-1 reference oligos as comparison: R1 (De Backer *et al*. 2009), R2 (Koyano-Nakagawa *et al*. 1994). The R1 oligo was also incubated with 1bfu recombinant EGR-1 (P) protein. In addition, a lane on the EMSA blot was loaded with 40µg nuclear extract for detection of EGR-1 protein by western blot (WB) using a specific antibody. C: Competition with 3000x excess of unlabeled ds oligos.

oligos with nuclear extracts from HT-29 cells shows weaker shifts for s5, s3, and s2 (Fig. 23C). This observation might be explained with the high sequence similarity to the reference sequence.

4.4.4 Identification of EGR-1 binding sites in the *NOT* promoter using affinity chromatography and Southwestern blot

To further validate the binding capacity of the potential EGR-1 sites, affinity chromatography using Dynabeads M-280 (Ch. 3.5.5) and the Southwestern technique (Ch. 3.5.6) were applied. For affinity chromatography, protein-DNA complexes were captured by incubating nuclear extracts from HeLa cells with the btn-labeled binding sites (Tab. 38) immobilized on streptavidin-coated

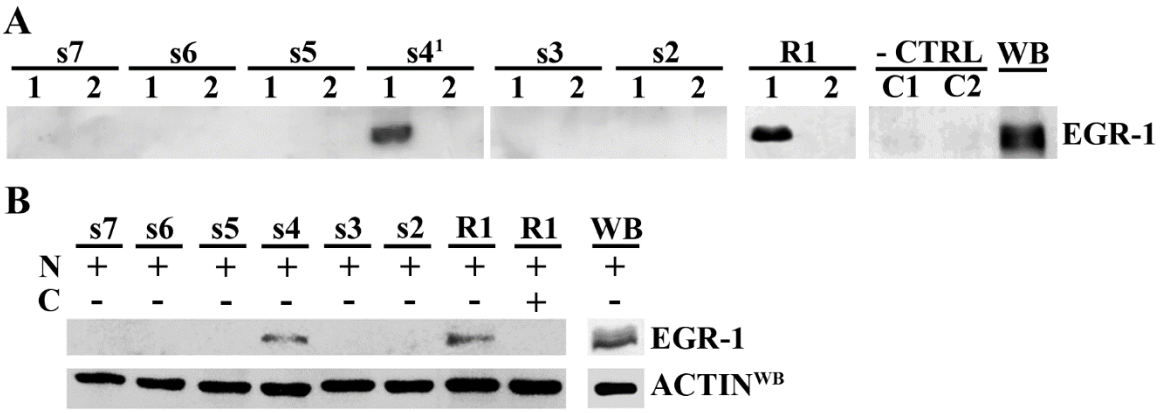

Fig. 24 Identification of EGR-1 binding sites in the *NOT* promoter using affinity chromatography (A) and Southwestern blot (B). EGR-1 binding sites were predicted using the P-MATCH^{TM} algorithm (Chekmenev *et al*. 2005). EGR-1 specificity was determined using a EGR-1 reference oligo (R1; De Backer *et al*. 2009) and a control lane loaded with 15µg of HeLa nuclear extract (WB) for comparison. **(A)** Eluates were separated on a 10% SDS-PAGE gel and analyzed using an EGR-1 antibody. 300µg beads alone (C1) or incubated with 20µg HeLa nuclear extracts (C2) served as negative control (-CTRL). 1: Binding; 2: Competition with 10x excess of cold oligo. **(B)** 3µg of HeLa nuclear extract was separated on 10% SDS-PAGE The blots were hybridized with 20fmol of a btn-labeled binding sites and read out using chemiluminescence After hybridization and detection, the membrane was stained with an Actin antibody to control loading. N: HeLa nuclear extract; C: Competition with 10x excess of cold oligo.

Dynabeads. The eluted protein complexes have been investigated by western blot. For Southwestern blotting, protein-DNA interactions were identified by hybridization the btn-labeled binding sites with membrane-blotted nuclear extracts from HeLa cells after gel electrophoretic separation. The results show in both cases that EGR-1 only binds to site 4 and the reference oligo (Fig. 24). All other sites were negative.

4.4.5 Identification of EGR-1 binding in the *NOT* promoter using ChIP / Re-ChIP

To confirm the *in vitro* binding results for EGR-1 *in vivo*, the ChIP and sequential ChIP (Re-ChIP) techniques were performed (Ch. 3.5.7). For that purpose, HT-29 and HaCaT cells grown under normal, serum-free (SF), and serum-response (SR) conditions were used to test if the observed nuclear EGR-1 protein kinetics (Fig. 22A) are reflected in *NOT* promoter occupancy. Because the transcriptional activity of EGR-1 depends on its association with the paralogue histone acetyltransferases (HATs) CREB-binding protein (CBP) and E1A-associated protein 300 (p300, EP300) (Silverman *et al*. 1998), they were also included in these experiments. The expression and nuclear localization of the two coactivators in diverse cell lines was validated using western blot (Fig. 25). The EGR-1, CBP, and p300 antibodies used for immunoprecipitation are listed in Tab.

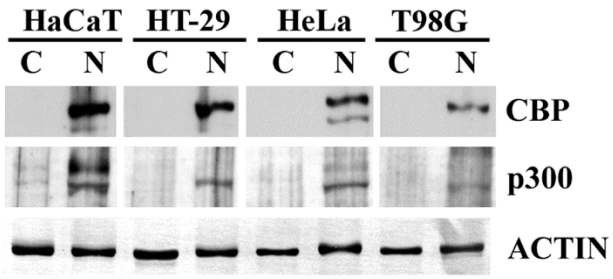

Fig. 25 Expression of the EGR-1 cofactors CBP and p300 in diverse cell lines as determined using western blot. Cytosolic (C) and nuclear (N) extracts (15µg each) were separated on a 5% SDS-PAGE gel. Indicated proteins were detected using specific antibodies.

43. Negative control ChIPs were performed with an antibody directed against the DNA-binding protein p53 which cannot bind the *NOT* promoter (Ch. 4.4.1). Amplifications performed using the primer combination P13/11 indicate binding of EGR-1 to the 492-297nt fragment encompassing site 4 in HaCaT and HeLa cells (Fig. 26B). CBP and p300 were also detected to be located within this fragment in HaCaT cells, with CBP exhibiting a much stronger signal than p300. None of the cofactors is present in HeLa cells (Fig. 26B). In HT-29 cells the same amplification produces a strong signal for EGR-1, CBP, and p300 which cannot be evaluated because of a strong p53 signal (not shown). To bypass this obstacle, the P15/13 primer combination was used for amplification yielding a positive EGR-1 signal and strong signals for CBP and p300 as compared to a weaker p53 signal (Fig. 26B). Amplification of Input DNA from HT-29, HaCaT, and HeLa cells using the primer combination P13/13 demonstrates that the applied chromatin pools contain *NOT* promoter fragments which encompass at least the s4-containing 492nt upstream ATG (Fig. 26C). These fragments can be used as template for amplifications using either P13/11 or P15/13. Because the *in vitro* DNA-binding studies show that the only positive EGR-1 site is site 4, all EGR-1 signals obtained from amplifications using any primer combinations that amplifies parts of these 492nts are considered to originate from this site. In SF HT-29 and HeLa cells the P13/11-amplification detects no EGR-1, CBP, or p300 binding, whereas SF HaCaT cells exhibit weak EGR-1 and CBP signals (Fig. 26B). The same amplification indicates EGR-1 binding in HT-29, HaCaT, and HeLa cells under SR conditions. In HaCaT and HeLa cells this signal is stronger as compared to signal detected under normal conditions. In these cells the CBP and p300 status remains unchanged after SR as compared to the SF, whereas CBP can be detected again during SR in HT-29 cells. The EGR-1 ChIP signals detected under the different serum conditions are congruent to the nuclear EGR-1 kinetics found in HaCaT, HT-29, and HeLa cells (Fig. 22).

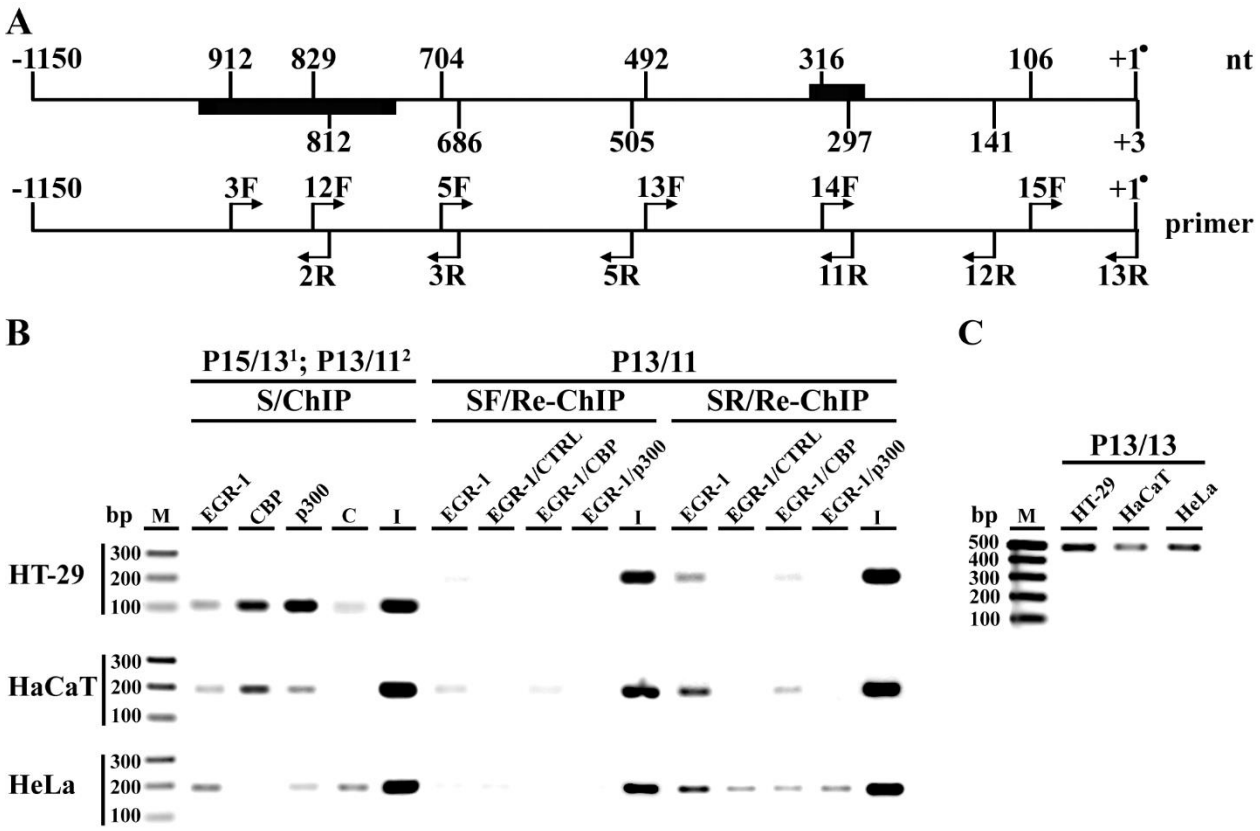

Fig. 26 Identification of EGR-1 binding to the *NOT* promoter *in vivo* using the ChIP/Re-ChIP technique. (A) Schematic representation of the 1.15kb *NOT* promoter with primers used for ChIP amplifications. Upper bar: Primer positions with indicated first exons of *ECE2* and *NOT*-4; lower bar: Primer names; F: Forward; R: Reverse. **(B)** Gel electrophoretic separation (2% agarose gel) of DNA fragments amplified from ChIPs performed using antibodies directed against EGR-1, CBP, p300, and p53. ChIPs/Re-ChIPs were performed using HT-29, HaCaT, and HeLa cells cultured under normal serum conditions (S), under serum-free (SF), and serum response conditions (SR). The first immunoprecipitation in all Re-ChIPs was performed using the EGR-1 antibody. For Re-ChIPs, an aliquot of the first ChIP reaction was used as control for non-specific binding on the beads by incubating it during the second ChIP reaction without antibody (EGR-1/CTRL). C: negative control; I: Input DNA. 1: Amplification using primer combination P15/13 in HT-29 cells; 2: Amplification using primer combination P13/11 in HaCaT and HeLa cells. **(C)** Gel electrophoretic separation of DNA fragments amplified using ChIP Input DNA from HT-29, HaCaT or HeLa cells and the primer combination P13/13. M: Marker Gene Ruler 100bp ladder.

4.4.6 Influence of RNAi-mediated knockdown of *EGR-1* on NOT expression

The data obtained from Y1H (Ch. 4.4.2), EMSA (Ch. 4.4.4), affinity chromatography (Ch. 4.4.5), Southwestern blot (Ch. 4.4.6), and ChIP/Re-ChIP (Ch. 4.4.7) experiments show that the EGR-1 protein can bind to the *NOT* promoter at site 4 (330-312nt) *in vitro* and *in vivo*. To determine the impact of endogenous EGR-1 on *NOT* mRNA and protein expression, HT-29 cells were transiently transfected with EGR-1 siRNAs (si *EGR-1*) or 10nM scrambled siRNA (si *SCR*) (Ch. 3.6.5) and analyzed using qRT-PCR (Ch. 3.3.17) and western blot (Ch. 3.4.3). As shown in Fig. 27A,

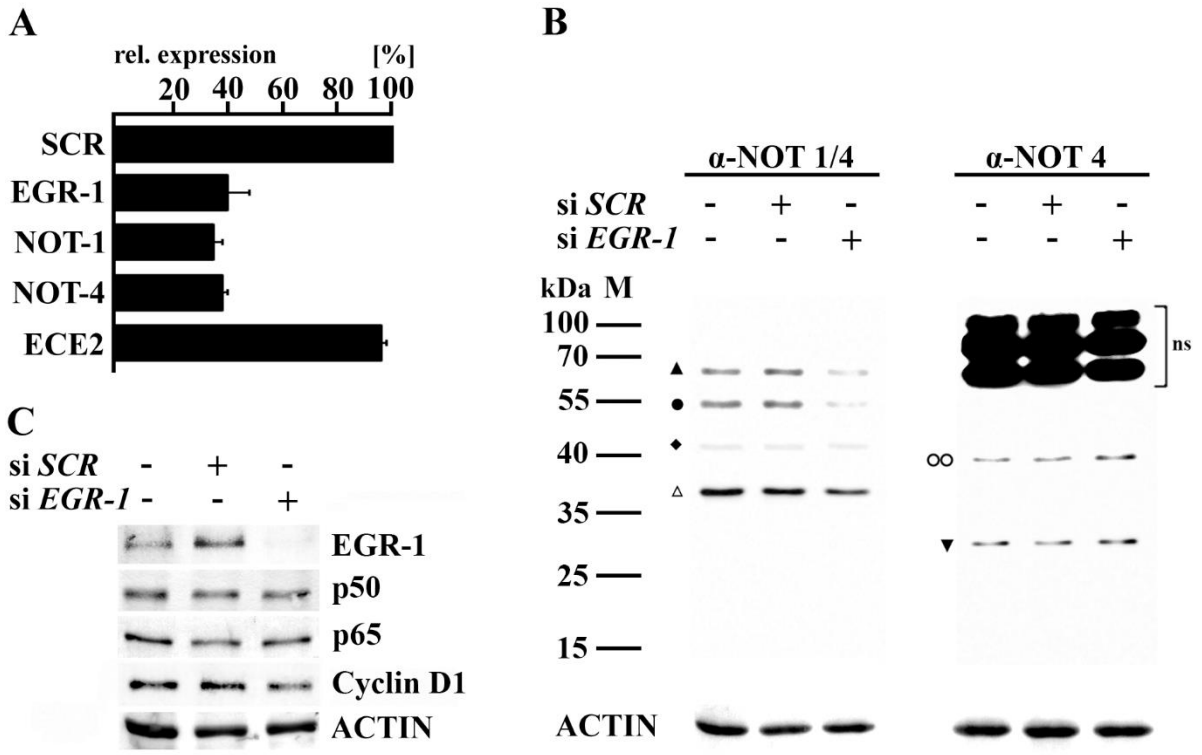

Fig. 27 Expression of *NOT* mRNA and protein after RNAi-mediated knockdown of *EGR-1* in HT-29. HT-29 cells were transiently transfected either with a 50nM mix of *EGR*-1 siRNAs (si *EGR-1*) or 10nM *scrambled* siRNA (si *SCR*) and subjected to qRT-PCR and western blot analysis. **(A)** Quantification of mRNA levels via qRT-PCR. The evaluation of the amount of the targets investigated was performed using the comparative ΔΔCt method: $\Delta\Delta C_T = \Delta C_T$ (si *EGR-1*) - ΔC_T (si *SCR*). The ΔC_T values are standardized to *HGPRT* used as endogenous control. The relative expression in % is calculated with respect to the si *SCR* sample as follows: $2^{-\Delta\Delta CT}$x 100%. **(B) + (C)** To analyze the expression of NOT (in B), EGR-1, and different EGR-1 targets (in C) 15µg crude homogenates were separated on a 10% SDS-PAGE gel and analyzed using western blot. Detection of the indicated proteins using specific antibodies. The α-NOT 1/4 antibodies recognize the full-length NOT-1 precursor (●), the potential post-translational modified full-length NOT-1 (▲), the 42kDA cleavage product (NOT42; ♦), and the N-terminal NOT-1 cleavage product (Δ). The α-NOT 4 antibody recognizes full-length NOT-4 (○○) and the N-terminal NOT-4 cleavage product (▼); ns: Non-specific. M: Marker.

transfection of HT-29 cells with *EGR-1* siRNA decreases endogenous *EGR-1* mRNA expression to 40% of the level observed in the *scrambled* control sample. The *EGR-1* knockdown is accompanied by an almost even decrease of *NOT*-1 (35.8%) and *NOT*-4 (38.4%). The *ECE2* mRNA level remains unchanged (97.3%). On the protein level, EGR-1 is almost completely depleted (Fig. 27C). Detection of NOT using the anti-NOT 1/4 antibody shows downregulation of the full-length NOT-1 precursor (●) to 19% and its putative post-translational derivate (▲) to 38% of the level observed in the *scrambled* control sample (Fig. 27B). This downregulation is accompanied by a decrease of the N-terminal cleavage product (Fig. 27B, Δ), whereas the band detected around 42kDa (♦) remains unchanged. The expression of NOT-4 is not affected (Fig.

27B). In addition, the cell cycle regulator *Cyclin D1*, an EGR-1 target gene (Xiao *et al*. 2005), was included in the analysis as control for the transcriptional activity of EGR-1 in HT-29 cells. The obtained immunoblots show a slight reduction of Cyclin D1 after EGR-1 knockdown (Fig. 27C). As reviewed by Guo *et al*. in 2011, the expression of Cyclin D1 can also be controlled by the NFκB subunits p50 and p65, which are target genes of EGR-1 (Parra *et al*. 2011). Furthermore, NFκB can regulate *NOT* (Ch. 4.6). To exclude the possibility that EGR-1 regulates *NOT* (and *Cyclin D1*) indirectly via NFκB, the expression of p50 and p65 was assessed after EGR-1 knockdown using immunoblot. As shown in Fig. 27C, *EGR-1* silencing has no effect on p50 and p65 expression. This argues for a direct regulation of *NOT* (and *Cyclin D1*) by EGR-1 in HT-29 cells.

4.5 Determination of CREB family members binding to the *NOT* promoter

Y1H and ChIP experiments performed in the Kurzik-Dumke laboratory showed binding of the cAMP response element binding protein 1 (CREB1) (NCBI Gene ID: 1385) to the 1.15kb *NOT* promoter region (Schultheiss and Kurzik-Dumke, unpublished). The bioinformatical analysis of this region using the P-MATCH^{TM} algorithm (Chekmenev *et al*. 2005) yielded identification of 16 potential CRE sites (six in *cis*, ten in *trans*) (Tab. 36; Fig. 30A). To determine the binding capacity of these sites, Y1H (Ch. 4.5.1), EMSA (Ch. 4.5.4), affinity chromatography (Ch. 4.5.5), and ChIP (Ch. 4.5.6) experiments were performed. Because CRE sites can be bound by any CREB family member, CREB3 (lZIP, Luman) (NCBI Gene ID: 10488), which was recently identified as a physiological partner of NOT (B. Hacker, PhD thesis: Beitrag zur Aufklärung der zellulären Rolle des humanen *neighbour of tid* (*not*) Gens, 2016), was also included in this analysis to check a possible regulatory loop. In addition, the binding of CREBL1 (ATF6b/CREB-RP; NCBI Gene ID: 1388) was also analyzed, because it is structural and functional related to CREB3 and might act on the same target genes (Okada *et al.* 2003). The impact of the detected interactions on *NOT* was analyzed using qRT-PCR and western blot in CREB3-overexpressing cells (Ch. 4.5.7) or after activation of CREB3 using Brefeldin A (Ch. 4.5.8).

4.5.1 Identification of CREB1, CREB3, and CREBL1 binding to the *NOT* promoter using the Y1H technique

To check the binding capacity of CREB3 and CREBL1 as well as to refine the CREB1-binding

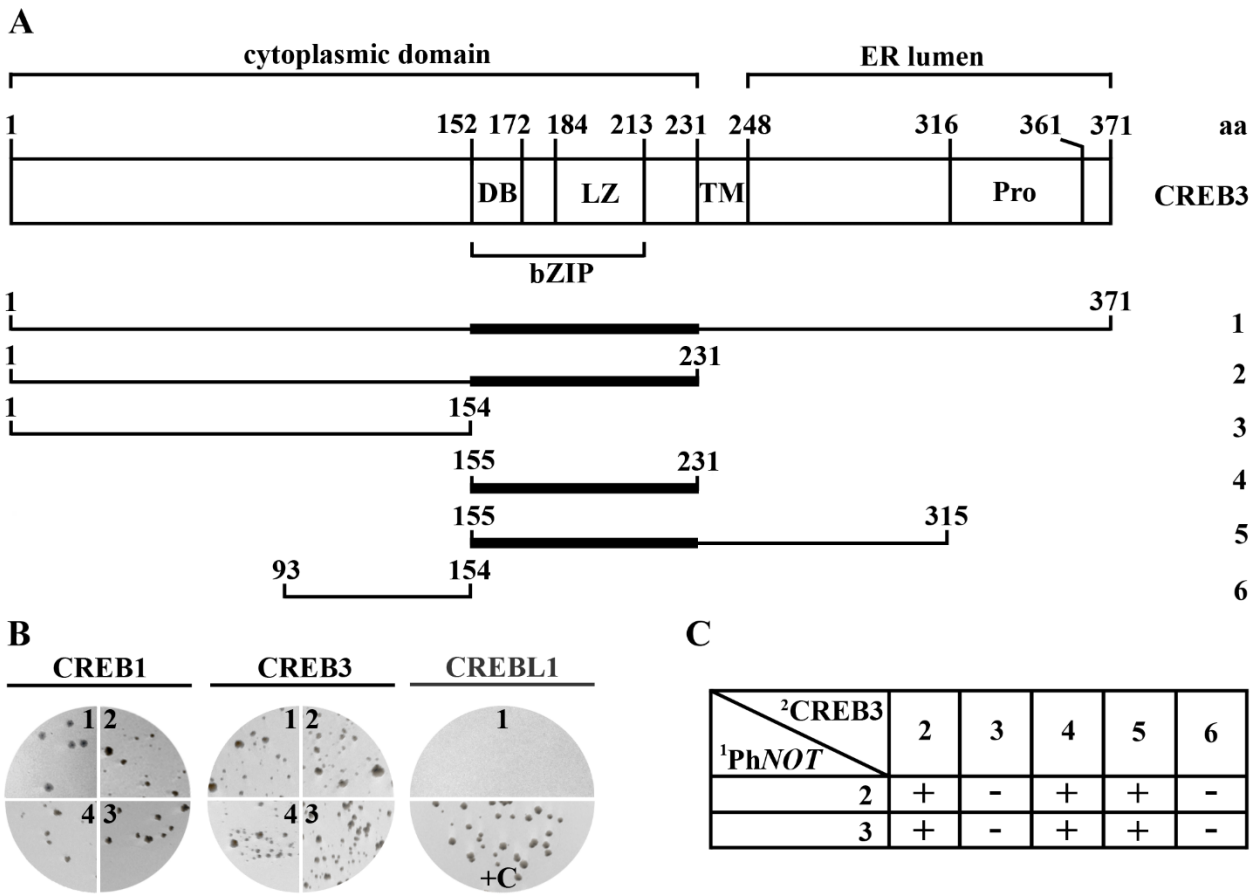

Fig. 28 Identification of CREB1, CREB3, and CREBL1 binding to the *NOT* promoter using the Y1H technique. (A) Schematic representation of CREB3 I2 (UniProtKB: O43889) and the deletion constructs generated to map its DNA-binding domain (thicker bars). DB: DNA-binding domain; LZ: Leucine zipper; TM: Transmembrane domain; Pro: Proline-rich domain. **(B)** Identification of CREB1, CREB3, and CREBL1 binding to the *NOT* promoter. Y187 cells were cotransformed with 500ng of the respective full-length expression construct (pACT2-CREB1, pACT2-CREB3, pACT2-CREBL1) and 500ng of either pHIS2.1-Ph*NOT*-1 (1150 to ATG; P1), pHIS2.1-Ph*NOT*-2 (704 to ATG; P2), pHIS2.1-Ph*NOT*-3 (525 to ATG; P3), and pHIS2.1-Ph*NOT*-4 (1115-686nt; P4) (Fig. 20). Cells were grown on SD/-His/-Trp/-Leu + 150mM 3-AT. Controls: +C: pGADT7-Rec2-p53 + p53pHIS2. **(C)** Determination of the CREB3 DNA-binding domain. Y187 cells were cotransformed with 500ng CREB3 constructs 2-6 (C) and 500ng P2-3. Cells were grown on SD/-His/-Trp/-Leu + 150mM 3-AT. 1: Promoter construct cloned into pHIS2.1; 2: CREB3 construct cloned into pACT2.

region within the 1.15kb *NOT* promoter, the Y1H assay was applied (Ch. 3.5.2). For this purpose, the *NOT* promoter constructs pHIS2.1-Ph*NOT*-1 (1150 to ATG; P1), pHIS2.1-Ph*NOT*-2 (704 to ATG; P2), pHIS2.1-Ph*NOT*-3 (525 to ATG; P3), and pHIS2.1-Ph*NOT*-4 (1115-686nt; P4) (Fig. 20, Ch. 4.3) were cotransformed with the full-length expression constructs pACT2-CREB1, pACT2-CREB3, and pACT2-CREBL1 (Fig. 28A and Ch. 3.3.14). The obtained results show that the promoter constructs P1-4 (Fig. 20) can be bound by CREB1 and CREB3 but not by CREBL1 (Fig. 28B).

4.5.2 Identification of the CREB3 DNA-binding domain using the Y1H technique

The DNA-binding domain of CREB3 was mapped using the Y1H technique (Ch. 3.5.2). For this purpose, diverse pACT2-CREB3 expression constructs (Fig. 28A; Ch. 3.3.14) were cotransformed with the *NOT* promoter constructs P2 (704 to ATG) and P3 (525 to ATG) (Fig. 20) into Y187 cells. The results show that CREB3 needs the bZIP-containing aa155-231 within the N-terminal cytoplasmic region to bind the *NOT* promoter (Fig. 28C).

4.5.3 Expression and nuclear activity of CREB1 and CREB3 in diverse cell lines

Since using Y1H yielded identification of CREB1 and CREB3 as putative *NOT* regulators, their binding to the *NOT* promotor was further validated by *in vitro* and *in vivo* protein DNA-binding assays such as EMSA, affinity chromatography, and ChIP (Ch. 4.5.4 - 4.5.8). To choose the appropriate cell system for these experiments, CREB1 and CREB3 expression was investigated in the HaCaT, HT-29, HeLa, HEK293, and T98G cells (Tab. 51) by western blot (Ch. 3.4.3). The obtained results show that CREB1 and CREB3 are expressed in all investigated cell lines (Fig. 29A). The transcriptional activity of CREB1, for which the two splice variants CREB1A (NCBI: NM_004379.3) and CREB1B (NM_134442.3) are described, depends on its phosphorylation, mostly at Ser133 (Mayr and Montminy 2001). Immunodetection using an antibody specific against this phosphorylated residue (Tab. 43; pCREB1) revealed two nuclear proteins, 43 and 38kDa (Fig. 29A). The 43kDa protein is also recognized by the anti-CREB1 antibody, which specifically detects CREB1A independent of its phosphorylation state. Thus, the 43kDa protein most likely represents phosphorylated CREB1A (Fig. 29A, ▷) and the 38kDa protein phosphorylated CREB1B (Fig. 29A, ○). The signal around 35kDa detected using the anti-CREB1 antibody (Fig. 29A, ►) fits with the predicted molecular weight of unmodified CREB1A. The bands between 55-70kDa are glycosylated forms of CREB1 (Rexach *et al*. 2012). For CREB3 three isoforms are known: CREB3 I1 (U88528), the longest isoform, was isolated from brain tissue (Hayashi and Tanaka 1997); CREB3 I2 (NM_006368.4) lacks aa 93-116 as compared to I1 and was originally isolated from pancreas carcinoma cells (Strausberg *et al.* 2002); CREB3 I3 (FJ263669) lacks aa 229-245 as compared to I2 and was isolated from monocytes as negative regulator of the glucocorticoid receptor (Kang *et al*. 2009). Because the variants I1 and I3 cannot be detected in the investigated cell lines (Hacker and Kurzik-Dumke, personnel communication) and almost all published data

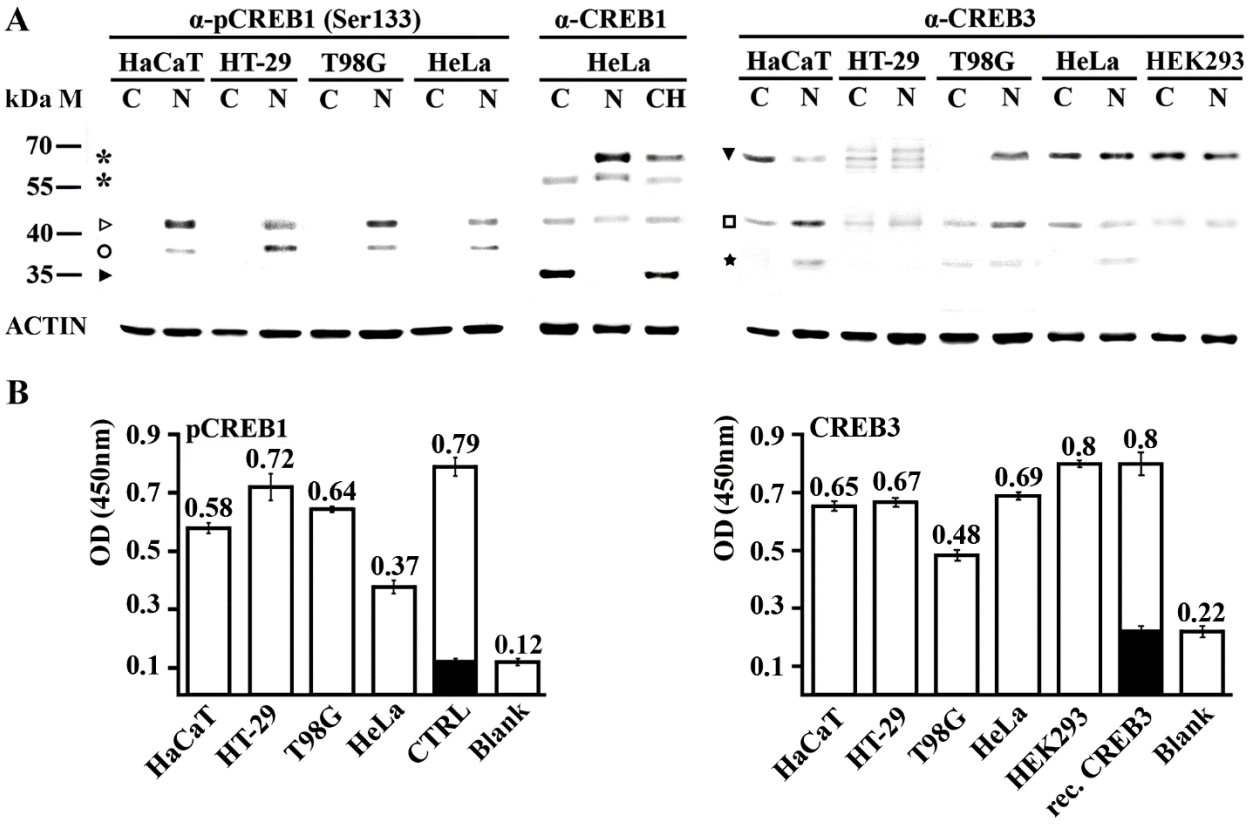

Fig. 29 Expression and nuclear activity of CREB1 and CREB3 in diverse cell lines. (A) Determination of CREB1 and CREB3 expression patterns by WB. For separation 15µg crude homogenates (CH), cytosolic (C), and nuclear (N) extracts were loaded on a 10% SDS-PAGE gel. Detection using the α-CREB1, α-pCREB1 (Ser133), and α-CREB3 antibodies. α-CREB1 detects phosphorylated CREB1A (▷), phosphorylated CREB1B (○), unmodified CREB1A (►) and glycosylated CREB1 forms (*). α-pCREB1 (Ser133) detects phosphorylated CREB1A (▷) and phosphorylated CREB1B (○). α-CREB3 detects full-length, ER-resident glycosylated CREB3 (▼) and its N-terminal cleavage products (□, ★). **(B)** Determination of nuclear activity of CREB1 and CREB3 using the CREB (Phospho-Ser^{133}) Transcription Factor Assay Kit. Pro well an aliquot of the nuclear extract corresponding to 7.5µg of total protein were loaded. Detection of CREB1 was performed using the TF CREB1 (phospho-Ser^{133}) primary antibody provided by the kit, detection of CREB3 with the antibody used in western blots. CREB1 readout: HaCaT: 0.58 (+/-0.02); HT-29: 0.72 (+/-0.05); T98G: 0.64 (+/-0.001); HeLa: 0.37 (+/-0.03); Kit Control (CTRL): PC-12 cells stimulated with 10µM Forskolin for 30min.: 0.79 (+/-0.03); Competition (black bar): 0.12 (+/-0.01); Blank: 0.12 (+/-0.01). CREB3 readout: HaCaT: 0.65 (+/-0.02); HT-29: 0.67 (+/-0.01); T98G: 0.48 (+/-0.02); HeLa: 0.69 (+/-0.01); Recombinant CREB3 (Abnova): 0.8 (+/-0.04); Competition (Black bar): 0.24 (+/-0.02); Blank: 0.22 (+/-0.01). M: Marker.

on CREB3 refers to I2, the I1 and I3 forms of CREB3 will not be considered further in this thesis. Instead, CREB3 will refer to CREB3 I2 in the following sections. Immunoblot analysis using an antibody directed against full-length CREB3 (Tab. 43) yields detection of three proteins consistent with the data published by Raggo *et al*. (2002) (Fig. 29A). The signal around 70kDa represents the

full-length, ER-resident glycosylated CREB3 protein (Fig. 29A, ▼). The bands around 40kDa (□) and 37kDa represent (★) the sequentially generated N-terminal cleavage products which mediate the transcriptional activity (Fig. 29A). The 37kDa fragment is considered to be mainly responsible for DNA-binding (Raggo *et al*. 2002). To assess the relative activity of the nuclear CREB proteins, the CREB (Phospho-Ser^{133}) Transcription Factor Assay Kit was used (Ch. 3.4.5). After incubation of nuclear extracts with CRE reference sites immobilized on microtiter plates, CREB binding detected using specific antibodies served as a measure for nuclear activity. This analysis revealed that CREB1 is active in all investigated cell lines with the highest nuclear activity in HT-29 cells (Fig. 29B). In the case of CREB3, the activity is identical in HaCaT, HT-29, and HeLa cells, whereas its activity in the glioblastoma cell line T98G is reduced. The highest activity is observed in HEK293 cells (Fig. 29B).

4.5.4 Identification of CREB1 and CREB3 binding sites in the *NOT* promoter using EMSA

The binding analysis performed using the Y1H technique indicates that CREB1 and CREB3 bind the 1.15kb *NOT* promoter (Fig. 28B). To determine which of the 16 predicted sites within this region (Tab. 36) can actually be bound by CREB1 and/or CREB3, EMSAs were performed (Ch. 3.5.3). Protein-DNA complexes were identified by incubating nuclear extracts from HT-29 cells with btn-labeled ds oligonucleotides representing the predicted binding sites. The specificity of the shift was demonstrated by competition with an excess of cold oligonucleotides. The results show shifted complexes for the *trans* sites 16 (710-724nt), 11 (509-522nt), 10 (480-501nt), 6 (162-175), and 1 (+2-10nt) and for the *cis* site 7 (217-206nt) (Fig. 30B). The detected shift is identical to the shift observed using the CRE reference site. However, this data does not allow to discern between bound CREB proteins, because the transcriptional active CREB1 and CREB3 proteins share similar molecular weights around 42kDa. To dissect the protein composition of the detected complexes, supershift assays were performed using specific antibodies against CREB1, pCREB1, and CREB3, respectively (Tab. 43). The results show that the complexes on site 16 and 7 are only supershifted with an antibody against CREB3, whereas the complex on site s1 is only supershifted with an antibody against CREB1 (Fig. 30C). The CRE reference site is supershifted with both, anti-CREB1 and anti-CREB3 antibodies. For the composite site 11/10 and s6 no supershift could be detected. This might be caused by the competitive binding of another CREB/ATF family member.

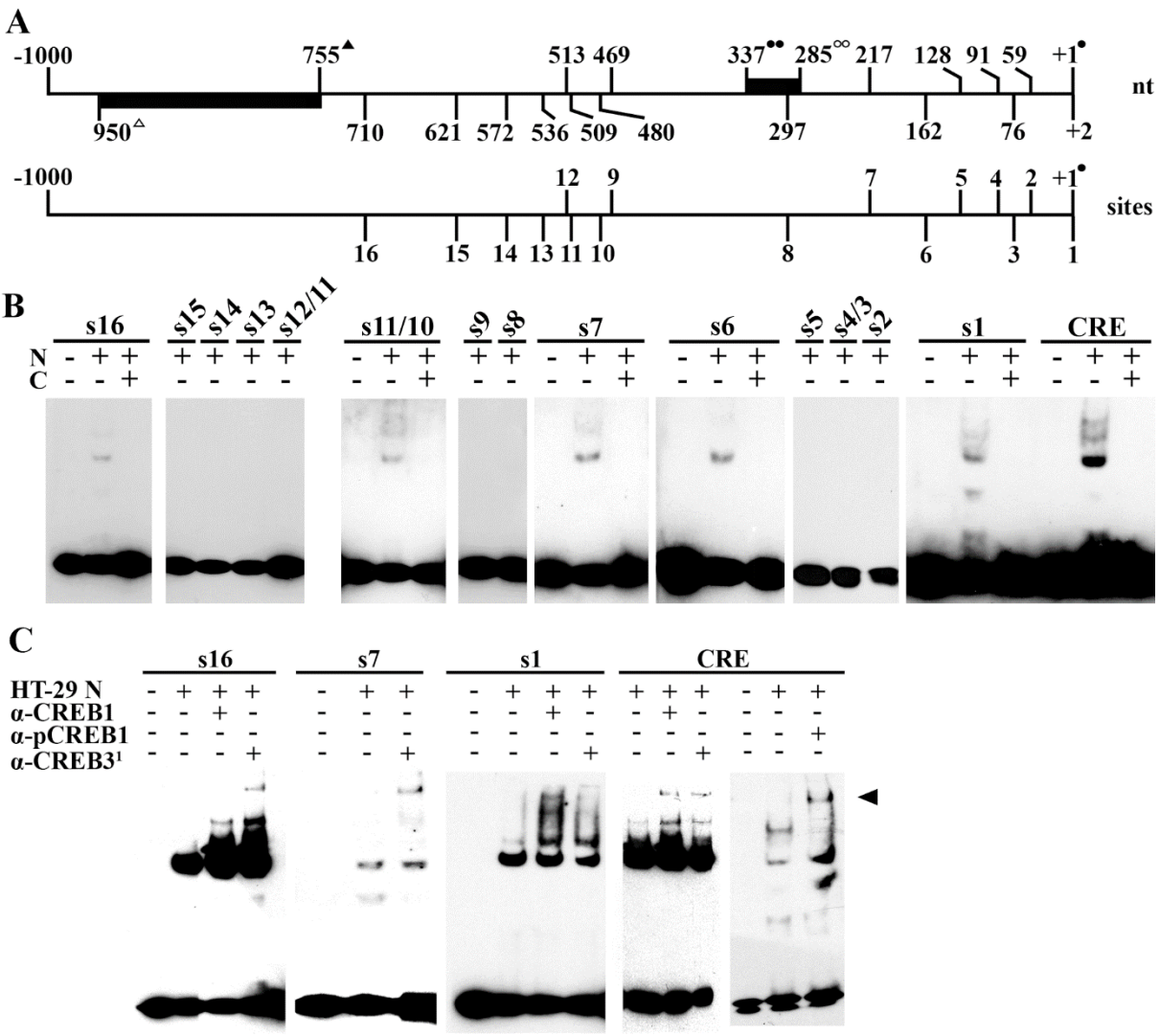

Fig. 30 Identification of CREB binding sites in the *NOT* promoter using EMSA. (A) Schematic representation of the *NOT* promoter region with potential CREB binding sites predicted using the P-MATCH™ algorithm (Chekmenev *et al*. 2005). Sites in *cis* are on the upper side, sites in *trans* below. The positions refer to the *NOT*-1 start codon (+1/●). The first exon of *NOT*-4 is located from 337nt (●●) to 285nt (○○). The first exon of *ECE2* is located from 755nt (▲) to 950nt (Δ). **(B)** Identification of CREB binding sites using EMSA. The protein-DNA complexes were detected by incubating 7µg nuclear extracts from HT-29 cells (N) with btn-labeled ds CREB binding sites. Protein-DNA complexes were separated on a 5% native PAGE gel and visualized using chemiluminescence. CREB specificity was determined by using published CRE reference oligos as comparison (Zhou and Chen 1999). C: Competition with 3000x excess of unlabeled ds oligos. **(C)** Supershift analysis to dissect the protein composition of shifted complexes. After binding (B), the formed of protein-DNA complexes were incubated with 500ng of the indicated antibodies. Separation and detection as in (B). Detected supershifts are indicated with an arrowhead.

4.5.5 Identification of CREB1 and CREB3 binding sites in the *NOT* promoter using affinity chromatography

For the positive sites 11/10 and 6 the EMSA experiments could not reveal which CREB protein is

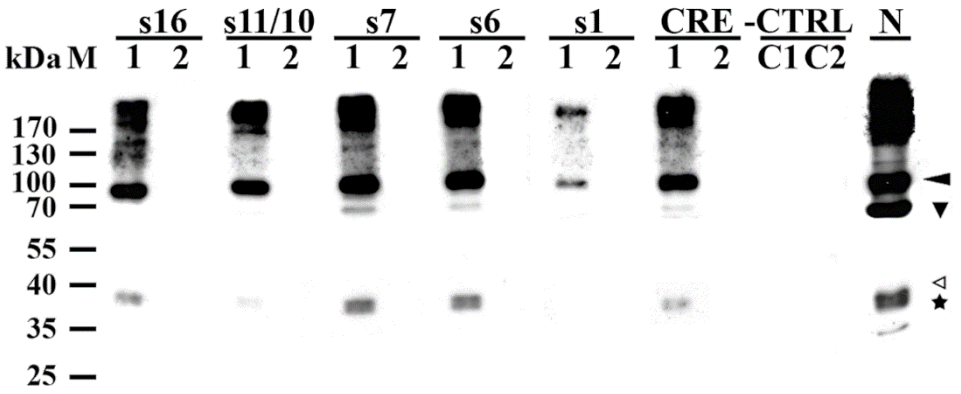

Fig. 31 Identification of CREB3 binding sites in the *NOT* promoter using affinity chromatography. Affinity chromatography was performed using biotinylated CREB binding sites and nuclear extracts (N) from pEGFP-CREB3 transfected HEK293 cells. Eluates were separated on a 10% SDS-PAGE gel and analyzed using an CREB3 antibody. 300µg beads alone (C1) or incubated with 20µg nuclear extracts (C2) served as negative control (-CTRL). 1: Binding; 2: Competition with 10x excess of cold oligo. ▼: Full-length, ER-resident glycosylated CREB3; ◄: CREB3-GFP; ◁, ★: Transcriptional active N-terminal CREB3 cleavage products. M: Marker.

actually bound (Fig. 30). To further analyze the binding capacity of these oligos and to confirm the results for the others, affinity chromatography was applied using Dynabeads M-280 (Ch. 3.5.5). Protein-DNA complexes were captured by incubating nuclear extracts with the btn-labeled binding sites (Tab. 36) immobilized on streptavidin-coated Dynabeads. After elution, the proteins of interest were detected using western blot. Neither CREB1 nor CREB3 could be pulled-down using nuclear extracts from HaCaT, HeLa, HT-29, and T98G cells (not shown). In the case of CREB3, this can be explained with the instability and high turnover of the transcriptional active CREB3 fragments (Raggo *et al*. 2002). To overcome this obstacle, nuclear extracts from HEK293 cells stably transfected with a pEGFP-CREB3 construct (Ch. 3.3.14) were used for binding. The results show that the 37kDa CREB3 product binds to sites 16, 7, 6, and the CRE reference but not to site 1 (Fig. 31, ★). The lack of a CREB3 signal for s1 can be interpreted as indirect confirmation of the exclusive CREB1-binding detected in the respective EMSA (Fig. 30C). In the case of the composite site 11/10, a weak CREB3 signal is observed (Fig. 31).

4.5.6 Identification of CREB1 and CREB3 binding sites in the *NOT* promoter by ChIP

To confirm the CREB binding results obtained using *in vitro* methods *in vivo*, ChIP was used (Ch. 3.5.7.) Because the transcriptional activity of Ser133-phosphorylated CREB1 (pCREB1) depends on recruitment of the acetyltransferases CBP and p300 (Yuan and Gambee 2001), they were also

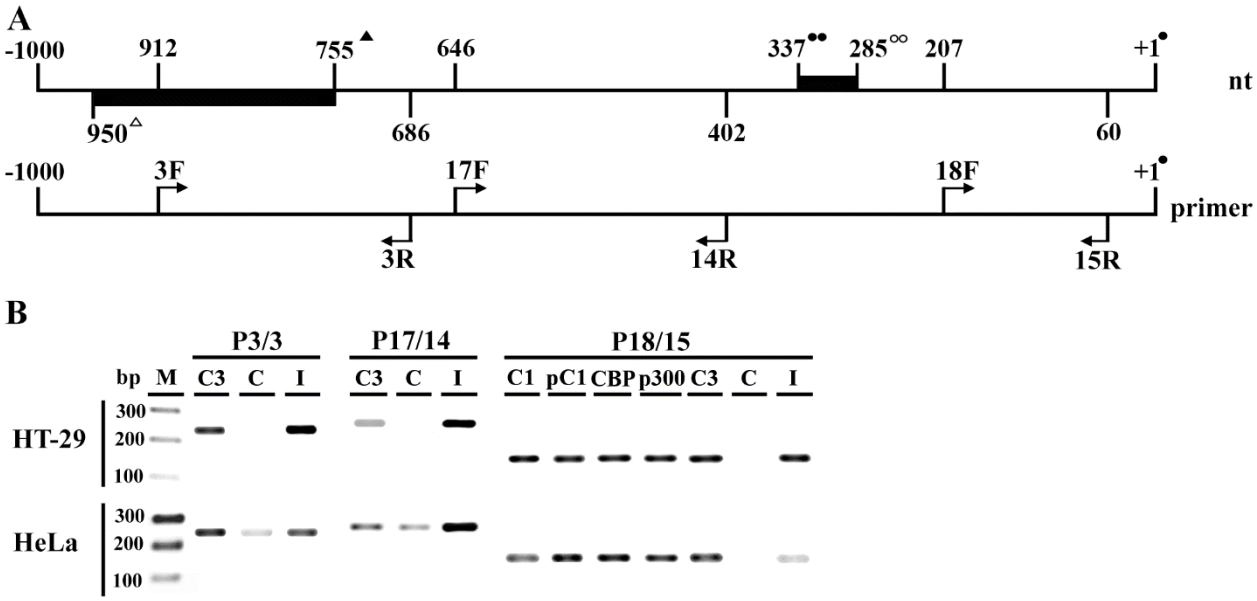

Fig. 32 Identification of CREB binding to the *NOT* promoter *in vivo* using the ChIP technique. (A) Schematic representation of the 1kb *NOT* promoter with primers used for ChIP amplification. Upper bar: Primer positions with indicated first exons of *ECE2* and *NOT*-4; lower bar: Primer names; F: Forward; R: Reverse. **(B)** Gel electrophoretic separation of DNA fragments amplified from ChIPs performed using antibodies directed against CREB1, Ser133-phosphorylated CREB1 (pCREB1), CREB3, CBP, p300, and p53. Electrophoretic separations were performed using a 2% agarose gel. ChIPs were performed using HT-29 and HeLa cells. C: p53 ChIP, negative control; I: Input DNA. M: Marker Gene Ruler 100bp ladder.

included in the analysis. CREB3 does not interact with these proteins (Kim *et al*. 2010). The CREB1, pCREB1, CREB1, CBP, and p300 antibodies used for ChIPs are listed in Tab. 43. Negative control ChIPs were performed with an antibody directed against the transcription factor p53 which cannot bind the *NOT* promoter (Ch. 4.4.1). Amplifications performed using ChIP DNA from HT-29 and HeLa cells and the primer combination P3/3 indicate binding of CREB3 to the 912-686nt fragment encompassing site 16 (Fig. 32B), whereas the corresponding results for CREB1 were negative (not shown). This is in accordance with the observations from EMSAs (Fig. 30; Ch. 4.5.4) and affinity chromatography (Fig. 31; Ch. 4.5.5). As shown in Fig. 32B, identical results were obtained for the P17/14-amplified 646-402nt fragment encompassing the composite site 11/10. The results for the P18/15-amplified 207-60nt fragment encompassing the sites 6-3 indicate binding of pCREB1 and CREB3 (Fig. 32B). CBP and p300 are also found in this area (Fig. 32B). However, these results do not allow to discern if CBP and/or p300 are actually attached to CREB1 and/or to the nearby-bound EGR-1 (Fig. 26). Similar results were obtained for HaCaT and T98G cells (not shown). As shown in Fig. 26C, the chromatin pool contains fragments spanning at least the site 10-1-containting region 492nt to ATG which can be used as template for amplification with P18/15. Hence, the ChIP results obtained for this region, together with the

results from EMSA (Ch. 4.5.4) and affinity chromatography (Ch. 4.5.5), argue for the *in vivo*-binding of CREB3 to s7 and/or s6 whereas s1 is bound by a complex consisting of Ser133-phosphorylated CREB1 and its coactivators CBP and p300 (Fig. 32B).

4.5.7 Influence of CREB3 overexpression on NOT expression

To determine the impact of CREB3 on *NOT* transcription, HEK293 cells overexpressing CREB3 (Ch. 4.5.5) were used to quantify *NOT* mRNA levels via qRT-PCR analysis (Ch. 3.3.17). For qRT-PCR analysis only *NOT*-1 and 4 were considered as they represent the protein coding *NOT* variants

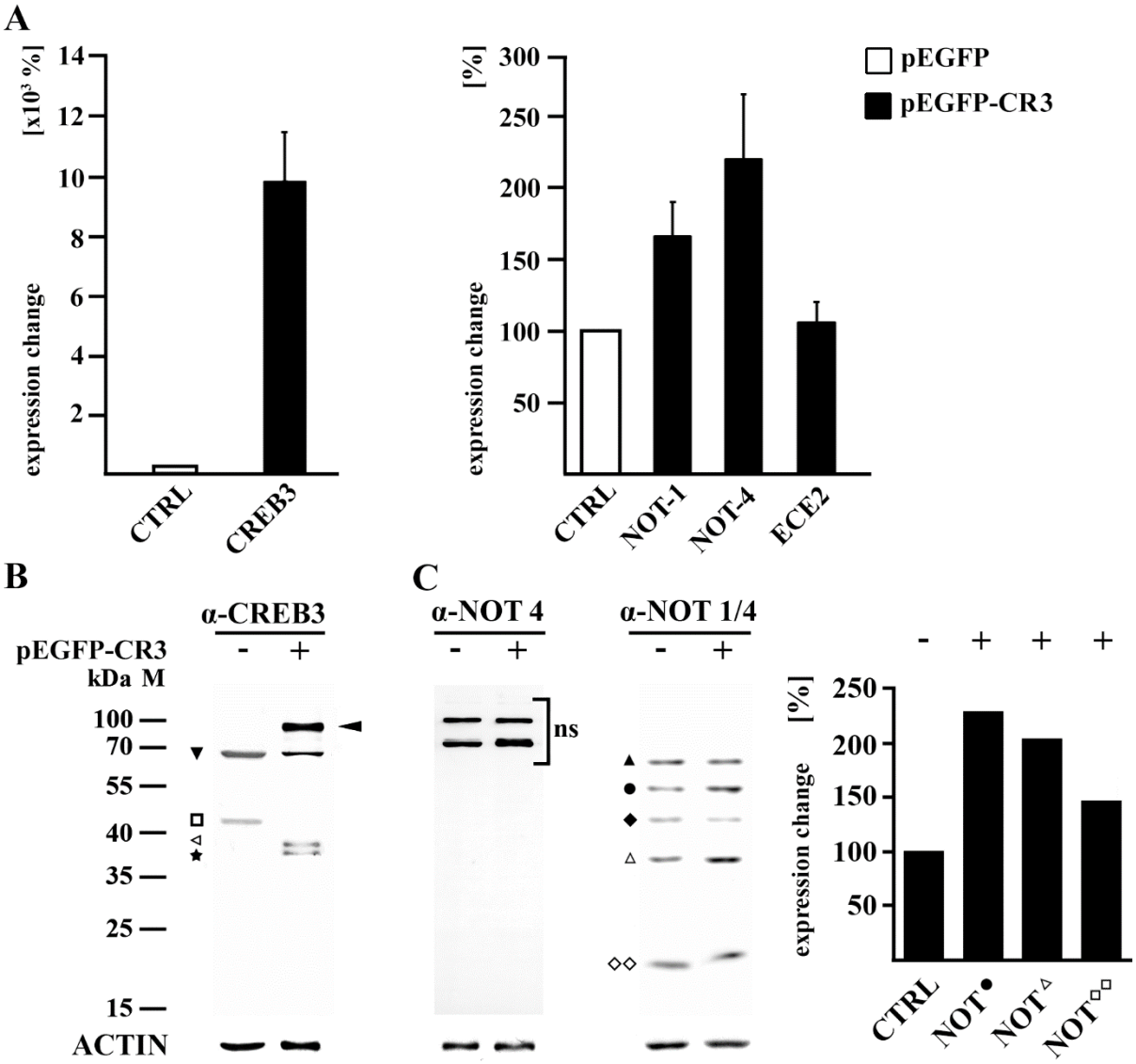

Fig. 33 Influence of CREB3 overexpression on *NOT* expression. (A) Quantification of mRNA levels via qRT-PCR. The evaluation of the amount of the targets investigated was performed using the comparative ΔΔCt method: $\Delta\Delta C_T = \Delta C_T$ (pEGFP) - ΔC_T (pEGFP-CREB3). The ΔC_T values are standardized to *HGPRT* used as endogenous control. The relative expression in % is calculated with respect to the pEGFP sample

(Ch. 4.1.4 - 4.1.5). As shown in Fig. 33A+B, transfection of HEK293 cells with the pEGFP-CREB3 construct increases the *CREB3* mRNA level by factor 10^4 and causes generation of recombinant CREB3 (Fig. 33B, ◄). The sustained generation of CREB3 allows the nuclear enrichment of its unstable N-terminal cleavage products (Fig. 33B). This is accompanied by an increase of the *NOT*-1(166%) and *NOT-4* (220%) transcripts (Fig. 33A). Concomitantly, the level of the full-length NOT-1 protein raises to 229% (Fig. 33C, ●). As a consequence, the NOT-1 cleavage products are also increased to 204% (37kDa product, Δ) and 146% (21kDa product, ◊◊) (Fig. 33C). The potential post-translational modified full-length NOT-1 remains unchanged (Fig. 33C, ▲). Despite the transcriptional activation of *NOT-4*, its protein level remains unchanged (Fig. 33C). CREB3 overexpression has no effect on *ECE2* (Fig. 33A).

4.5.8 Influence of Brefeldin A-mediated CREB3 activation on NOT expression

The macrocyclic lactone Brefeldin A (BFA) causes Golgi disassembly by inhibiting ER-Golgi protein trafficking (Nebenführ *et al*. 2002). BFA treatment also leads to the proteolytic activation of CREB3 in CREB3-transfected HeLa cells (Liang *et al*. 2006). To validate the BFA-mediated activation of CREB3 under native conditions and to assess its impact on NOT expression, HeLa, HT-29, and HEK293 cells were treated with 2µg/ml BFA for 10min., 30min., and 24h (Ch. 3.6.4.3) and analyzed using western blot (Ch. 3.4.3) and qRT-PCR (Ch. 3.3.17). As shown in Fig. 34B for HT-29 and in Fig. 35B for HeLa, BFA treatment causes the cleavage of CREB3 followed by the nuclear enrichment of its 37kDa N-terminal fragment after 24h. In both cases, activation goes along with an increase of CREB3 protein amount. As illustrated by the drastic rise of its mRNA levels in HT-29 (Fig. 34A) and Hela cells (Fig. 35A), BFA induces the transcription of *CREB3*. Furthermore, the BFA-mediated CREB3 activation is accompanied by an increase of the *NOT*-1 (155% in HT-29 and 144% in Hela) and *NOT*-4 (236% in HT-29 and 277% in HeLa) transcripts

---

as follows: $2^{-\Delta\Delta CT}$x 100%. **(B) + (C)** Immunoblot analysis of CREB3 and NOT protein levels in untransfected and pEGFP-CREB3 transfected HEK293 cells. For separation 15µg were loaded on a 10% SDS-PAGE gel. Detection was performed using the α-CREB3, α-NOT 1/4, and α-NOT 4 antibodies. α-CREB3 recognizes full-length, ER-resident glycosylated CREB3 (▼), CREB3-GFP (◄), the N-terminal fragments (□, ★), and an unspecified product (◃). α-NOT 1/4 recognizes the NOT-1 full-length precursor (●), the potential post-translational modified full-length NOT-1 (▲), the N-terminal NOT-1 cleavage product (Δ), and the C-Terminal NOT-1 cleavage product (◊◊). NOT-4 is not detectable. The expression change in transfected cells was determined relative to untransfected cells = 100%. The relative intensities (RI) measured with ImageJ (Schneider *et al*. 2012) were normalized with respect to Actin. M: Marker; ns: Non-specific.

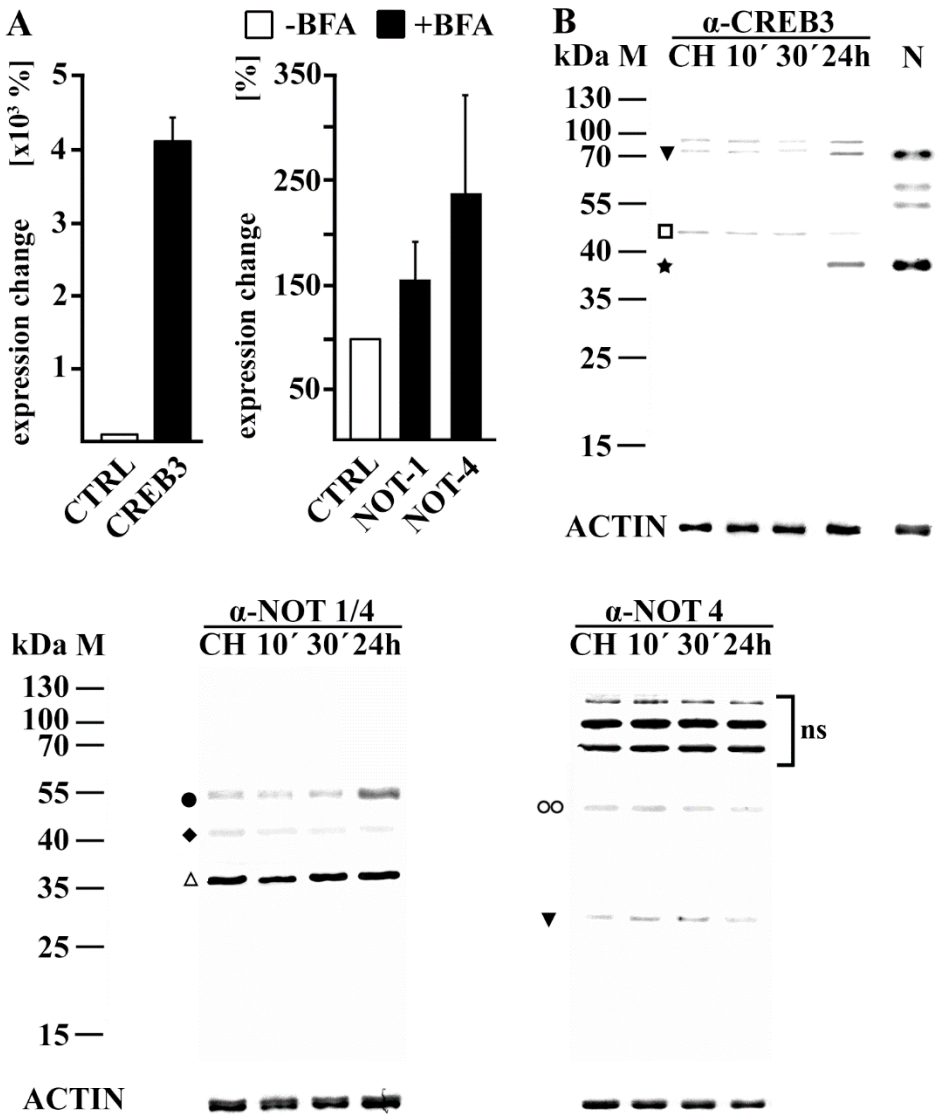

Fig. 34 Impact of Brefeldin A-mediated CREB3 activation on *NOT* expression in HT-29 cells. (A) Quantification of mRNA levels via qRT-PCR after 24h BFA treatment. The evaluation of the amount of the targets investigated was performed using the comparative ΔΔCt method: $\Delta\Delta C_T = \Delta C_T$ (BFA-treated) - ΔC_T (untreated). The ΔC_T values are standardized to *HGPRT* used as endogenous control. Relative expression is calculated with respect to the untreated sample as follows: $2^{-\Delta\Delta CT}$ x 100%. **(B)** Immunoblot analysis of CREB3 and NOT protein levels after treatment of HT-29 cells with 2µg/ml BFA for the indicated time points. For separation 15µg crude homogenates were loaded on a 10% SDS-PAGE gel. Detection was performed using the α-CREB3, α-NOT 1/4, and α-NOT 4 antibodies. α-CREB3 recognizes full-length, ER-resident glycosylated CREB3 (▼) and the N-terminal CREB3 cleavage products (□, ★). The α-NOT 1/4 antibody recognizes the NOT-1 full-length precursor (●), the 42kDa cleavage product (♦), and the N-terminal NOT-1 cleavage product (Δ). The α-NOT 4 antibody recognizes full-length NOT-4 (○○) and the N-terminal NOT-4 cleavage product (▼); ns: Non-specific.CH: Crude homogenate, untreated; M: Marker.

(Fig. 34A+35A). This transcriptional upregulation after 24h is accompanied by the fourfold increase of the full-length NOT-1 protein in HT-29 (Fig. 34B, ●) and HeLa cells (Fig. 35B, ●). An

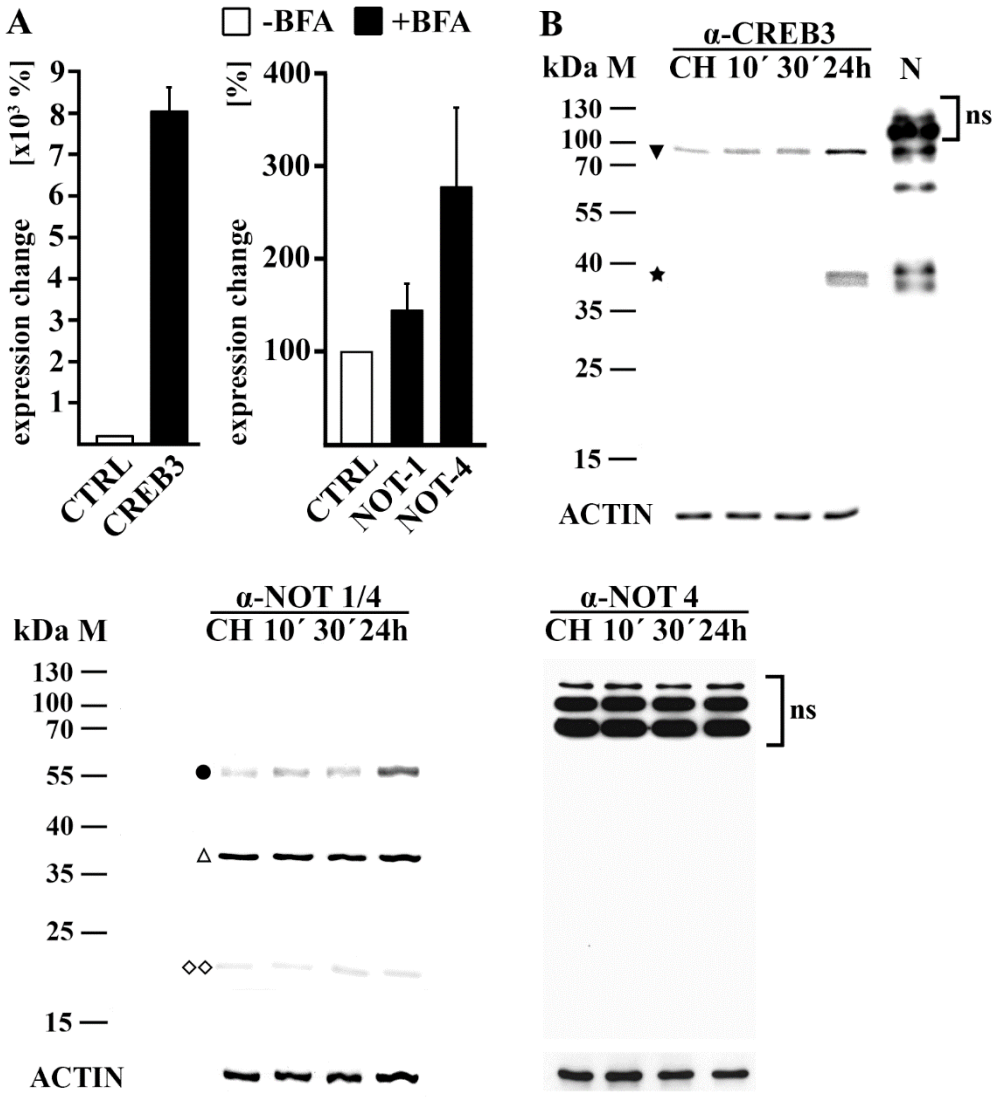

Fig. 35 Impact of Brefeldin A-mediated CREB3 activation on *NOT* expression in HeLa cells. (A) Quantification of mRNA levels via qRT-PCR after 24h BFA treatment. The evaluation of the amount of the targets investigated was performed using the comparative ΔΔCt method. The ΔC_T values are standardized to *HGPRT* used as endogenous control: $\Delta\Delta C_T = \Delta C_T$ (BFA-treated d) - ΔC_T (untreated). Relative expression is calculated with respect to the untreated sample as follows: $2^{-\Delta\Delta CT}$ x 100%. **(B)** Immunoblot analysis of CREB3 and NOT protein levels after treatment of HeLa cells with 2µg/ml BFA for the indicated time points. For separation 15µg crude homogenates were loaded on a 10% SDS-PAGE gel. Detection was performed using the α-CREB3, α-NOT 1/4, and α-NOT 4 antibodies. α-CREB3 recognizes full-length, ER-resident glycosylated CREB3 (▼) and the N-terminal CREB3 cleavage product (★). The α-NOT 1/4 antibody recognizes the NOT-1 full-length precursor (●), the N-terminal NOT-1 cleavage product (Δ), and the C-terminal NOT-1 cleavage product (◊◊). NOT 4 is not detectable. ns: Non-specific. CH: Crude homogenate, untreated; M: Marker.

increase of the NOT-4 protein or its cleavage products could not be detected in HT-29 or HeLa cells (Fig. 34B+35B). Short-time BFA treatment of HT-29 and HeLa cells for 10 or 30 min. has no

effect on CREB3 processing and NOT expression (Fig. 34B+35B). Interestingly, BFA has no effect at all on CREB3 activation and/or NOT expression in HEK293 cells (not shown).

4.6 Determination of NFκB binding to the *NOT* promoter

As determined using the P-MATCH^{TM} algorithm (Chekmenev *et al*. 2005; Ch. 3.5.1), the 1.15kb *NOT* promoter region contains 22 potential NFκB sites (ten in *cis*, twelve in *trans*) (Tab. 37+61; Fig. 40A). NFκB (nuclear factor of kappa light polypeptide gene enhancer in B-cells) constitutes a family of inducible transcription factors encompassing the members p50 (NFKB1), p52(NFKB2), p65 (RelA/NFKB3), c-Rel (Rel), and RelB (Hayden and Ghosh 2014). The five members share the highly conserved 300aa N-terminal Rel homology domain (RHD) that mediates DNA-binding and homo- and heterodimerization (Oeckinghaus and Ghosh 2009). NFκB proteins are held as inactive dimers in the cytoplasm, either as zymogen (p50 as p105 and p52 as p100) or via interaction with inhibitory IκB proteins (Oeckinghaus and Ghosh 2009). Depending on the stimulus different IκB kinase (IKK) complexes are activated which mark the precursors for processing or the IκB proteins for degradation via phosphorylation (Oeckinghaus *et al*. 2011). The NFκB dimers can then enter the nucleus and bind their target sequences. NFκB transcription factors are critical regulators of immunity, stress responses, apoptosis, proliferation, and differentiation (Oeckinghaus *et al*. 2011). To elucidate if NFκB binds the *NOT* promotor and acts as potential transcriptional regulator of the gene, Y1H (Ch. 4.6.1), EMSA (Ch. 4.6.5), affinity chromatography (Ch. 4.6.6), and ChIP (Ch. 4.6.7) experiments were performed. Here, the focus was on the NFκB subunits p50 (NCBI Gene ID: 4790) and p65 (NCBI Gene ID: 5970), because they build up the most prevalent NFκB dimer (Oeckinghaus and Ghosh 2009). The impact of the detected protein-DNA interactions on *NOT* expression was analyzed using qRT-PCR and western blot, either after pharmacological manipulation of the NFκB pathway using parthenolide and TNFα (Ch. 4.6.4) or after RNAi-mediated silencing of NFκB components (Ch. 4.6.8).

4.6.1 Identification of NFκB binding sites in the *NOT* promoter using the Y1H technique

To determine if the predicted sites can be bound by the NFκB subunits p50 and p65, the Y1H technique was used (Ch. 3.5.2). For that purpose the pACT2-p65 or the pACT2-p50 expression construct (Ch. 3.3.14) was cotransformed with either of the *NOT* promoter constructs pHIS2.1-

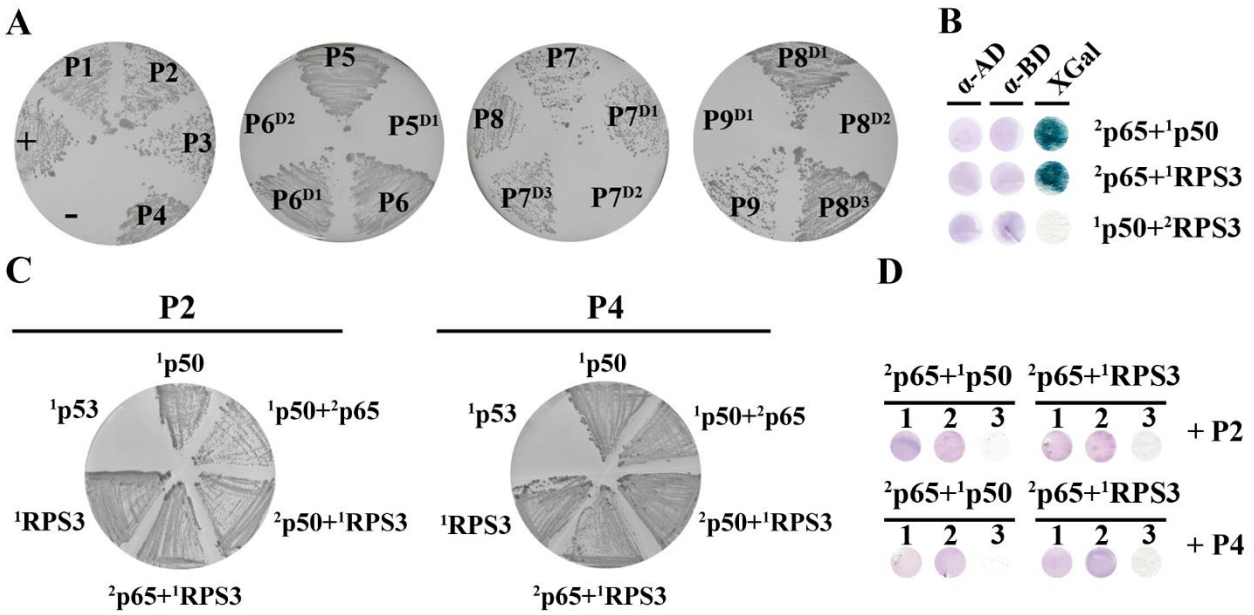

Fig. 36 Identification of NFκB binding to the *NOT* promoter using the Y1H technique. (A) Identification of NFκB binding sites in the *NOT* promoter. Y187 cells were cotransformed with 500ng pACT2-p65 and 500ng of the respective pHIS2.1-PhNOT promoter construct 1-9 (P1-9, Fig. 20) or their derivatives lacking single binding sites. Cells were grown on SD/-His/-Trp/-Leu + 150mM 3-AT. Controls: -: pACT2-p53; +: pGADT7-Rec2-p53 + p53pHIS2 (Fig. 6). **(B)** Identification of protein-protein interactions using Y2H. Indicated expression constructs were cotransformed into Y187 cells and grown on SD/-Trp/-Leu. Expression of the transformed proteins was determined using colony blot and antibodies directed against the AD or BD fusion domains. Interaction was monitored using the X-gal assay. **(C)** Identification of NFκB dimer binding to the *NOT* promoter. The clones from (B) were cotransformed with 500ng P2 and P4 and grown on SD/-His/-Trp/-Leu + 150mM 3-AT. In addition, pACT2-p50, pACT2-RPS3, and pACT2-p53 (negative control) were cotransformed with P2 and P4. After cotransformation the presence of the dimers was monitored using the β-Galactosidase/X-gal assay **(D)**. 1: Cloned into pACT2; 2: Cloned into pAS2-1.

Ph*NOT*-1 (1150 to ATG; P1), pHIS2.1-Ph*NOT*-2 (704 to ATG; P2), pHIS2.1-Ph*NOT*-3 (525 to ATG; P3), pHIS2.1-Ph*NOT*-4 (1115-686nt; P4), pHIS2.1-Ph*NOT*-5 (1115-932nt; P5) pHIS2.1-Ph*NOT*-6 (912-686nt; P6), pHIS2.1-Ph*NOT*-7 (704-504nt; P7), pHIS2.1-Ph*NOT*-9 (421-228nt; P8), and pHIS2.1-Ph*NOT*-9 (248-87nt; P9) (Fig. 20, Ch. 4.3) or one of their derivatives lacking single NFκB binding sites (Tab. 61) into Y187 cells. Because NFκB transcription factors always bind as dimers to their target sequences (Oeckinghaus and Ghosh 2009), the binding of the p50:p65 heterodimer to the *NOT* promoter was also assessed via Y1H. For this purpose, Y187 cells were first cotransformed with the pACT2-p50 and pAS2-1-p65 expression constructs according to the Y2H technique (Ch. 3.4.4) and dimer formation was monitored using the β-galactosidase assay (Ch. 3.4.4.3). The clones tested positive for dimer formation where then transformed with the P2 or P4 promoter constructs and plated on SD/-His/-Trp/-Leu medium supplemented with 150mM

Tab. 61 Identification of p50 and p65 binding to distinct sites in the *NOT* promoter using Y1H

Construct[1]	region[2]	NFκB sites[3]		deleted site[4]	Y1H results	
		cis	*Trans*		p50[5]	p65[5]
P5	1115 - 932	**22** (973-951)	**21** (953-962)		+	+
P5^{D1}	1115 - 932			22/21	-	-
P6	912 - 686	**19** (789-776); **17** (768-755)	**20** (880-893); **18** (777-811), **16** (756-765)		+	+
P6^{D1}	912 - 686	17	20, 16	19/18	-	+
P6^{D2}	912 - 686	19	20, 18	17/16	+	-
P7	704 - 504	**15** (679-670); **13** (638-624); **8** (544-535)	**14** (667-680); **12** (624-637); **11** (594-607); **10** (580-589); **9** (568-577)		+	+
P7^{D1}	704 - 504	13, 8	12, 11, 10, 9	15/14	+	+
P7^{D2}	704 - 504	15, 8	14, 11, 10, 9	13/12	-	-
P7^{D3}	704 - 504	15, 13	14, 12, 11, 10, 9	8	-	+
P8	421 - 228	**6** (375-362); **4** (339-330); **2** (265-252)	**7** (401-410); **5** (363-375); **3** (328-341)		+	+
P8^{D1}	421 - 228	4, 2	7, 3	6/5	+	+
P8^{D2}	421 - 228	6, 2	7, 5	4/3	+	-
P8^{D3}	421 - 228	6, 4	7, 5, 3	2	+	+
P9	248 - 87	**1** (223-214)			+	+
P9^{D1}	248 - 87			1	-	-

1: All promoter fragments were cloned into pHIS2.1. D: Deletion; 2: Nt promotor fragment upstream of *NOT*-1 ATG; 3: Positions of the potential NFκB binding sites predicted using the P-MATCH^{TM} algorithm (Chekmenev *et al*. 2005). 4: Sites refer to predicted sites in Fig. 41A; 5: Y1H results (+: Growth; -: No growth) for the expression constructs pACT2-p50 and pACT2-p65 cotransformed into Y187 cells with the indicated promoter constructs. The cells were plated on SD/-His/-Trp/-Leu + 150mM 3-AT.

3-AT. For control purposes, Y187 cells were cotransformed with the pACT2-p50 and pACT2-p53 expression constructs (Ch. 3.3.14) in combination with the P2 and P4 constructs. RPS3 was also included in this analysis because it is described as a pivotal cofactor for specific transactivation of the p50:p65 complex (Wan *et al*. 2007). The results show that both, p50 and p65, can bind the *NOT* promoter at multiple sites (Fig. 36; Tab. 61). The sites 22/21 (973-951nt), 13/12 (638-624nt), and 1 (223-214nt) are bound by p50 and p65 (Tab. 61). The sites 19/18 (789-776nt) and 8 (544-535nt) are only bound by p50, whereas sites 17/16 (768-755nt) and 4/3 (339-330nt) are only bound by p65 (Tab. 61). The sites 15/14 (680-667nt), 6/5 (375-362nt), and 2 (262-252nt) cannot be bound by either of the transformed subunits (Tab. 61). To assess the binding of NFκB dimers to the *NOT* promoter, Y187 cells exhibiting p65:p50 and p65:RPS3 complex formation could be established, whereas p50:RPS3 interactions were not detected (Fig. 36B). As shown in Fig. 36C, the yeast

clones forming p50:p65 and p65:RPS3 complexes can grow on triple-dropout medium after promoter transformation. However, the positive results do not necessarily depend on bound dimers, but may also derive from single NFκB and/or RPS3 molecules that do not exist in the dimeric state (Fig. 36A+C). Nevertheless, an indirect clue that actually the complexes are bound is given by the observation that the dimer-forming clones lose their β-galactosidase activity after promoter transformation (Fig. 36D). As the cells express both proteins (Fig. 36D) and grow on the triple-dropout medium containing 3-AT (Fig. 36C), this loss can only be explained with the competition between the X-gal reporter gene and the *NOT* promoter constructs for binding proteins. In this view, the available dimers preferentially bind to the multiple copies of the transformed promoter constructs which outnumber the single genomic copy of the X-gal reporter gene. Taken together, the Y1H results suggest that the NFκB heterodimers p50:p65 and p65:RPS3 can bind within the 704nt upstream ATG to the *NOT* promoter (Fig. 36C).

4.6.2 Identification of RPS3 binding to the *NOT* promoter using the Y1H technique

A Y1H screen to isolate transcriptional regulators of the human *tid* gene performed in the Kurzik-Dumke laboratory has yielded identification of RPS3 (NCBI Gene ID: 6188) as a DNA-binding protein (M. Szydlowski, PhD thesis: Identification of the regulatory elements and factors of the human tumor suppressor gene *tumorous imaginal discs*, 2011). The binding was confirmed and the single binding sites were mapped resulting in the identification of two consensus RPS3 binding elements (Schultheiss and Kurzik-Dumke, unpublished). The results obtained for the *NOT* promoter support RPS3 binding to DNA (Fig. 36C). To further confine the promoter region encompassing the binding sites, the full-length RPS3 construct (pACT2-RPS3-1, Fig. 37A) was cotransformed with the P5-P9 constructs (Fig. 20) into Y187 cells and plated on SD/-His/-Trp/-Leu supplemented with 150mM 3-AT. As shown in Fig. 37C RPS3 binds to at least one site in the fragments encompassing nts1115-932 (P5), nts 912-686 (P6), nts 704-504 (P7), and nts 421-228 (P8) but not to the fragment encompassing nts 248-87 (P9). To identify the necessary DNA-binding domain of RPS3, a N-terminal construct encompassing the KH domain (Fig. 37A; RPS3-2, aa21-92) and several C-terminal deletions (Fig. 37A; constructs 3-6) were generated (Ch. 3.3.14.5). The six RPS3 constructs were cotransformed with the P2 construct (Fig. 20) into Y187 cells and plated on SD/-His/-Trp/-Leu medium supplemented with 150mM 3-AT. The results show that RPS3 binds to the *NOT* promoter via aa101-194 (Fig. 37B). To gain further insight into potential regulatory

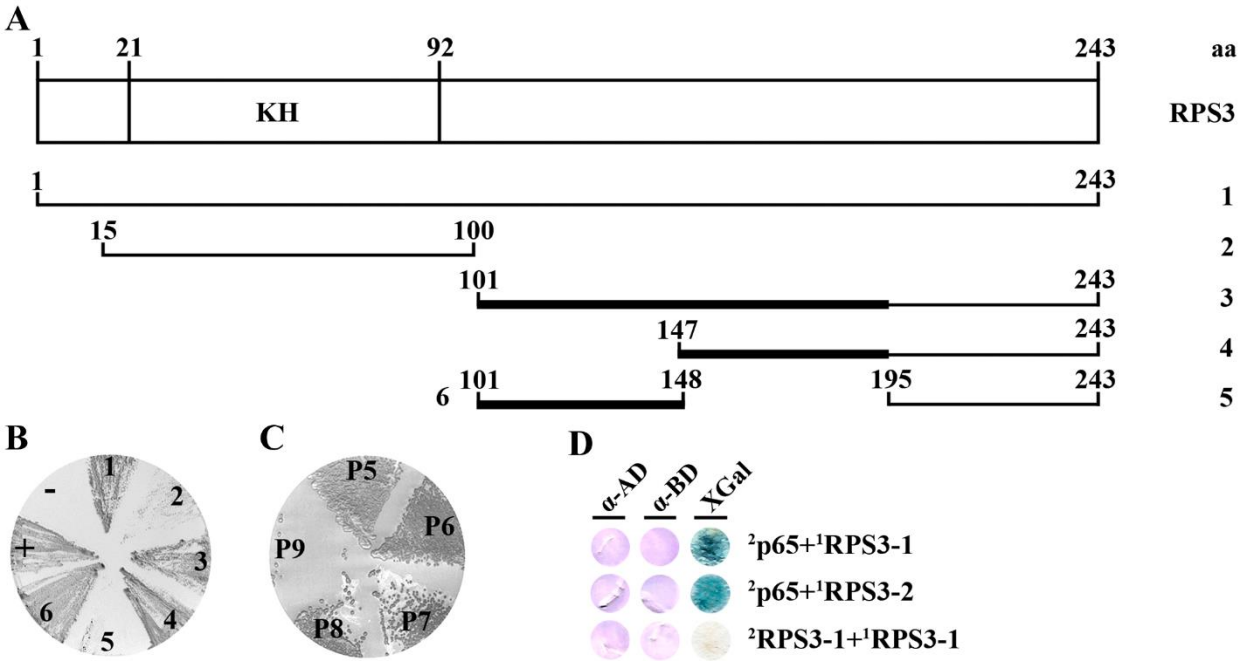

Fig. 37 Identification of RPS3 binding to the *NOT* promoter using the Y1H technique. (A) Schematic representation of RPS3 protein structure and the deletion constructs generated to map its DNA binding domain. The ribonucleoprotein S3 (RPS3) is composed of 243 aa (UniProt: P23396) and an integral part of the eukaryotic 40S ribosome subunit. The hnRNP K homology (KH) domain necessary for RNA recognition and interaction with the p65 subunit of NFκB (Wan *et al*. 2007) is located from aa 21-92. The generated deletion constructs are shown in bars, the mapped DNA-binding domain in thicker bars. **(B)** Determination of the RPS3 DNA binding domain. Y187 cells were cotransformed with 500ng P2 (Fig. 20) and 500ng of the indicated pACT2-RPS3 constructs 1-6. Cells were grown on SD/-His/-Trp/-Leu + 150mM 3-AT. Controls: -: pACT2-p53; +: pGADT7-Rec2-p53 + p53pHIS2. **(C)** Determination of RPS3 binding to the *NOT* promoter. Y187 cells were cotransformed with 500ng pACT2-RPS3 construct 1 and 500ng of the indicated promoter constructs (P5-P9, Fig. 20). Cells were grown on SD/-His/-Trp/-Leu + 150mM 3-AT. **(D)** Mapping of the RPS3-p65 interaction domain and test for RPS3 dimerization using Y2H. Y187 cells were cotransformed in the indicated combinations and plated on SD/-Trp/-Leu. Expression of transformed constructs was determined by colony blot using antibodies directed against the GAL4 activation domain (AD) and the GAL4 binding domain (BD). Interaction of the expressed fusion proteins was monitored using β-Galactosidase (X-gal) assay. 1: Cloned into pACT2; 2: Cloned into pAS2-1.

mechanisms of RPS3 DNA-binding activity, the Y2H technique was used to determine the homo-dimerization potential of RPS3. For that purpose, the pACT2-RPS3 construct was cotransformed with the pAS2-1-RPS3 construct into Y187 cells and plated on SD/-Trp/-Leu. Cotransformation of pAS2-1p65 either with full-length pACT2-RPS3 (Fig. 37A, RPS3-1) or the N-terminal construct containing the KH-domain (Fig. 37A, RPS3-2) served as positive controls. As shown in Fig. 37D, the β-galactosidase assay confirms the described KH-domain-mediated p65:RPS3 interaction (Wan *et al*. 2007) and indicates that RPS3 does not form homodimers.

4.6.3 Expression and nuclear activity of NFκB in diverse cell lines

The NFκB and RPS3 binding results obtained from Y1H (Ch. 4.6.1 - 4.6.2) were further validated by EMSA (Ch. 4.6.5), affinity chromatography (Ch. 4.6.6), and ChIP (Ch. 4.6.7). For this purpose, the HaCaT, HT-29, HeLa, and T98G cell lines (Tab. 51) were first checked for their applicability in these downstream experiments by determining the expression of canonical NFκB pathway components using western blot and by measuring the relative nuclear activity of the p50 and p65 subunits using the NF-κB (p65) Transcription Factor Assay Kit and the NF-κB (human p50) Transcription Factor Assay Kit (Ch. 3.4.5). To validate the quality of the applied extracts, p53 was included in the analysis. The results confirm the described expression and nuclear localization pattern of p53 in HaCaT (Lehman *et al*. 1993), HT-29 (Cooks *et al*. 2013), and T98G cells (Alonso *et al*. 2003) and its degradation in HeLa cells (Thomas *et al*. 1999) (Fig. 38A). In addition, Tid, a regulatory component of the inhibitory IκB complex, served as cytoplasmic control (Kurzik-Dumke and Czaja 2007) and TBP as nuclear control (Maston *et al*. 2006). The immunoblot analysis revealed constitutive expression of NFκB in all four cell lines investigated (Fig. 38A). However, there are considerable differences in the levels and the localization of the single components. In HT-29, T98G, and HeLa cells the p50 and p65 subunits are mainly found together with their inhibitors IκBα and IκBβ in the cytosol, whereas lower amounts of these proteins are also found in the nucleus (Fig. 38A). In resting cells the p50:p65:IκB complexes can shuttle between cytosol and nucleus, either as a whole (Huang *et al*. 2000) or after cytosolic dissociation and nuclear reassembling (Carlotti *et al*. 2000), thus contributing to the observed localization pattern of p50, p65, and the IκBs. Nevertheless, shuttling of NFκB complexes in unstimulated cells depends on diffusion (Shrum *et al*. 2009). It is for this reason why the nucleocytoplasmic detection of Importinα3 (KPNA4), which mediates the nuclear import and export of activated NFκB (Fagerlund *et al*. (2005), rather argues for the constitutive low-level activation of NFκB coupled to the described mechanism of IκBα-dependent p50:p65 complex removal from the target promoters (Sue *et al.*2011). The detection of p50 and p65 nuclear activity in HT-29, T98G, and HeLa cells, which can only be measured if p50:p65 complexes are not bound to IκB proteins, supports this notion (bars 2-5, Fig. 38B). The essential kinase for activation of the canonical pathway, IKKβ (Ley and Beyaert 2014), can also be detected in all cell lines, predominantly localized to the cytosol (Fig. 38A). The observation of smaller amounts of nuclear IKKβ is in line with recent findings (Tsuchiya *et al*. 2010). In contrast to HT-29, T98G, and HeLa cells, higher amounts of p50 and p65

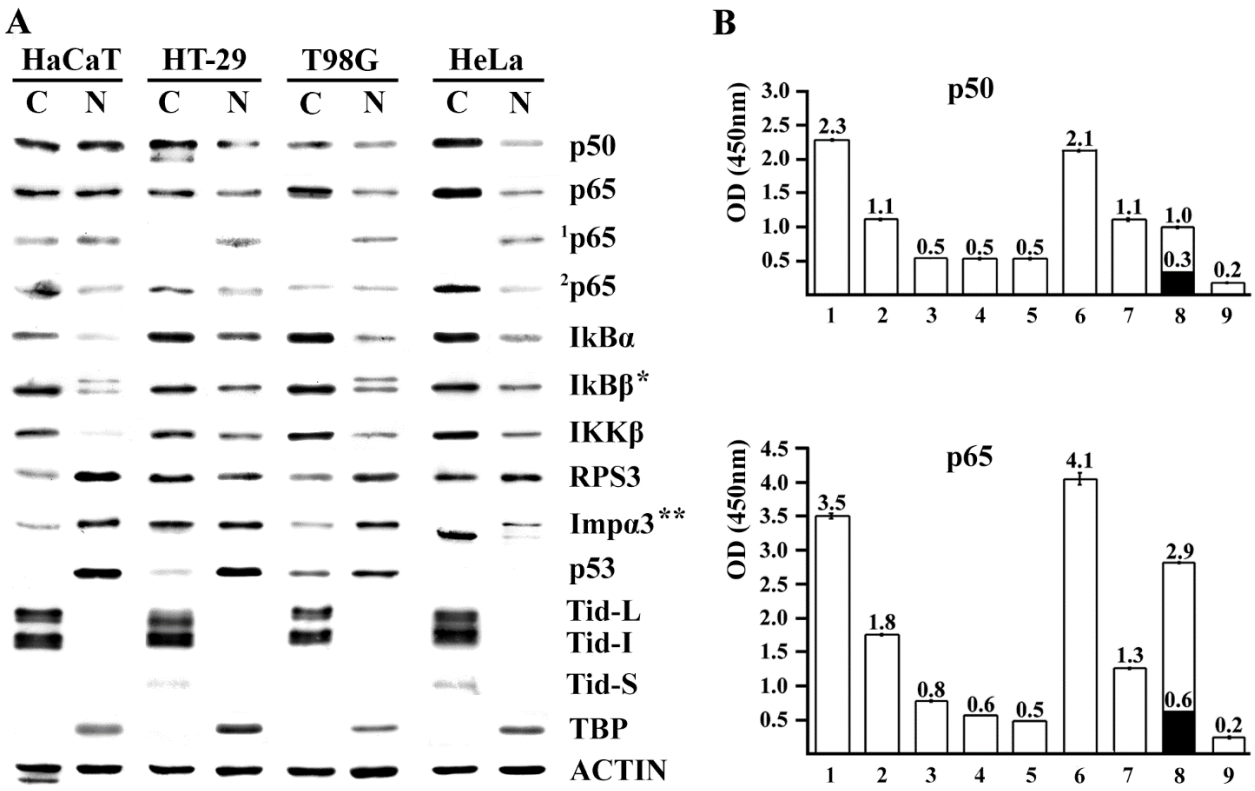

Fig. 38 Expression and nuclear activity of NFκB in diverse cell lines. (A) Expression analysis of components of the NFκB pathway using western blot. Cytosolic (C) and nuclear (N) extracts (15µg each) were separated on a 10% SDS-PAGE gel. TBP served as nuclear control; [1]p65: p65-Ser276P; [2]p65: p65-Ser536P; *: The upper IκBβ represents the phosphorylated form; **: Experiments performed in the Kurzik-Dumke laboratory suggest the existence of a yet undescribed Impα3 state/form with lower molecular weight (Schultheiss and Kurzik-Dumke, unpublished). **(B)** Determination of the nuclear activity of p50 and p65 using the NF-κB (p65) Transcription Factor Assay Kit and the NF-κB (human p50) Transcription Factor Assay Kit. Pro well an aliquot of the nuclear extract corresponding to 15µg of total protein were loaded. ELISA readout for p50: 1: HaCaT: 2.3 (+/-0.01); 2: HT-29: 1.1 (+/-0.007); 3: T98G: 0.5 (+/-0.005); 4: HeLa: 0.5 (+/-0.004); 5: HeLa nuclear extract (Active Motif): 0.5(+/-0.01); 6: HeLa + TNFα 20ng/ml, 30min. (Active Motif): 2.1 (+/-0.02); 7: HeLa + TPA 62ng/ml, 10min. (Active Motif): 1.1 (+/-0.007); 8: White bar: 1.25µl Cayman p50 positive control (recombinant p50): 1.0 (+/-0.009), black bar: Competition of 1.25µl recombinant p50 with 10µl dsDNA (NFκB consensus site): 0.3 (+/-0.003); 9: Blank: 0.2 (+/-0.01). Readout for p65: 1: HaCaT: 3.5 (+/0.04)-; 2: HT-29: 1.8 (+/-0.02); 3: T98G: 0.8 (+/-0.006); 4: HeLa: 0.6 (+/-0.002); 5: HeLa nuclear extract (Active Motif): 0.5(+/-0.005); 6: HeLa + TNFα 20ng/ml, 30min. (Active Motif): 4.1 (+/-0.09); 7: HeLa + TPA 62ng/ml, 10min. (Active Motif): 1.3 (+/-0.007); 8: White bar: 10µl Cayman p65 positive control (HeLa nuclear extract TNFα-stimulated: 20ng/ml, 30min.): 2.9 (+/-0.02), black bar: Competition of 10µl positive control with 10µl dsDNA (NFκB consensus site): 0.6 (+/-0.002); 9: Blank: 0.2 (+/-0.01).

are detected in HaCaT cells with an even nucleocytoplasmic distribution (Fig. 38A). Together with the lower levels of IκBα these results indicate that NFκB is highly active in HaCaT cells (Fig. 38A). Supporting evidence for this view comes from the detection of the by far highest levels of nuclear

NFκB activity in HaCaT cells (bar 1, Fig. 38B). Notably, the activity is almost identical to the activity observed in TNFα-stimulated HeLa cells (bars 1+6, Fig. 38B). This is in accordance with published data suggesting that immortalized HaCaT cells control their survival and growth via NFκB (Ren *et al*. 2006). To gain more insight into putative cell specific aspects of NFκB signaling, the expression and nucleocytoplasmic distribution of serine (Ser)-phosphorylated p65 (Ser276 and Ser536) were also assessed using western blot. In HT-29, T98G, and HeLa cells the Ser276-phosphorylated p65 is exclusively located in the nucleus, whereas HaCaT cells contain considerable amounts in both compartments (Fig. 38A). The Ser536-phosphorylated p65 is found in both fractions in all cell lines, whereas it is mainly localized to the cytosol in HaCaT, HT-29, and HeLa cells (Fig. 38A). Furthermore, the p65 cofactor RPS3 is detected in the cytosol and the nucleus of all cell lines with nuclear enrichment in HaCaT and T98G cells (Fig. 38A). Upon pharmacological induction, RPS3 colocalizes to the nucleus with similar kinetics as p50 and p65 (Fig. 39A, Ch. 4.6.4). In this context, the massive nuclear translocation of RPS3 in HaCaT cells might be coupled to the high activity of NFκB in these cells (Fig. 38A).

4.6.4 Pharmacological manipulation of NFκB signaling and its impact on *NOT* expression

The activity of the NFκB signaling pathway can be modulated by a plethora of pharmacological agents, among them the inhibiting sesquiterpene lactone Parthenolide (Hehner *et al*. 1999) and the activating cytokine tumor necrosis factor alpha (TNFα) (Hayden and Ghosh 2014). Both chemicals were used to measure the impact of NFκB on *NOT* expression via qRT-PCR (Ch. 3.3.17) and, in the case of parthenolide, to use its inhibitory properties to assess NFκB specificity in EMSA experiments (Ch. 4.6.5). To validate the activity of the two substances, serum-starved HT-29 cells were treated with 100μM Parthenolide (Ch. 3.6.4.2) or 50ng/ml TNFα (Ch. 3.6.4.3) for 10, 30, and 60min. and analyzed using immunoblotting (Ch. 3.4.3) and Southwestern blot (Ch. 3.5.6). As shown in Fig. 39A, the treatment of serum-starved HT-29 cells with 50ng/ml TNFα induces the expression and nuclear translocation of p50, p65, and RPS3 to similar extents during all investigated time points, whereas IκBα is degraded after 10 and 30min. (Fig. 39A). The expression and cytosolic localization of IκBα is reconstituted after 60min. (Fig. 39A). This kinetic is in accordance with the well-known time course of NFκB activation, which peaks at about 30min. before a NFκB-dependent negative feedback loop induces IκBα transcription to terminate the signaling (Hayden and Ghosh 2014). IKKβ cannot be detected after serum deprivation but is induced by TNFα

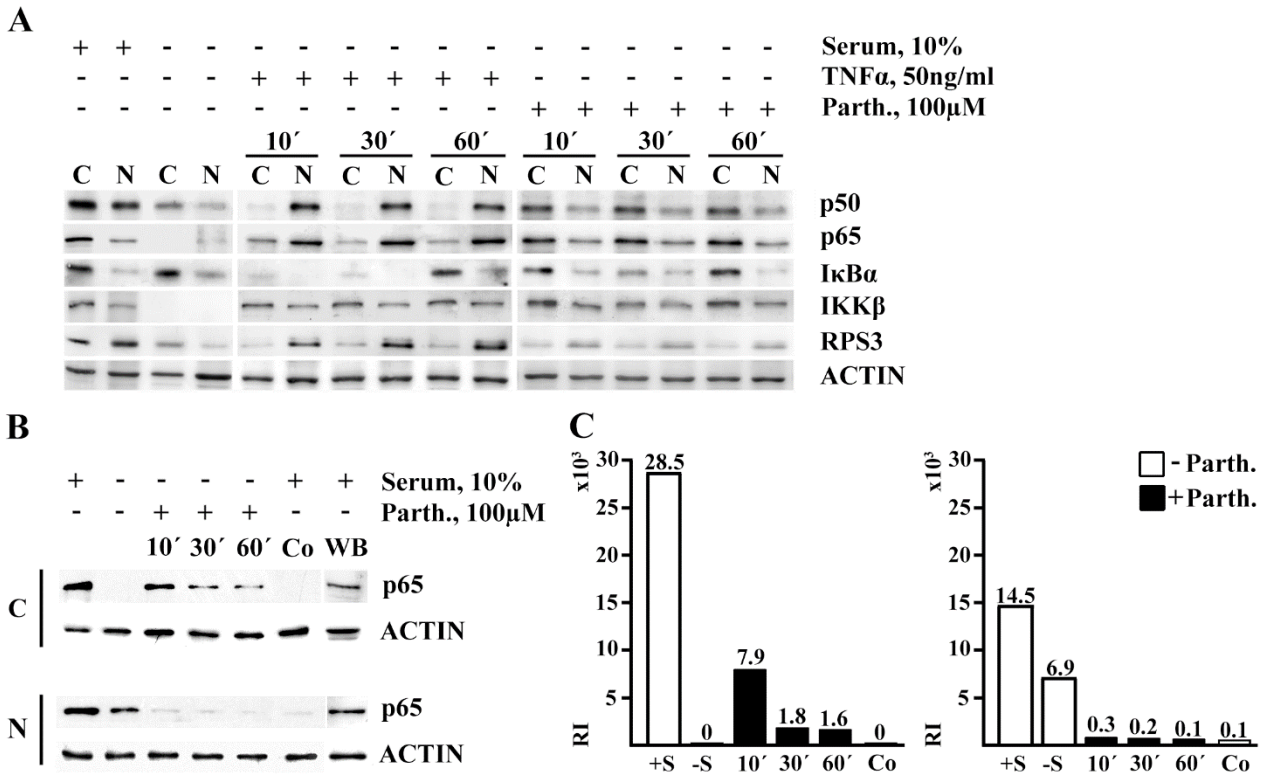

Fig. 39 Pharmacological manipulation of NFκB signaling using Parthenolide and TNFα. (A) HT-29 cells treated with Parthenolide (Parth.) or TNFα for the indicated concentrations and time points. After isolation of cytosolic (C) and nuclear (N) extracts 15µg of the respective fraction was separated on a 10% SDS-PAGE gel. Indicated proteins were detected using specific antibodies. **(B)** Determination of NFκB binding capacity in Parthenolide-treated HT-29 cells using Southwestern blot. Treatment and separation of 3µg extracts (C: Cytosolic; N: Nuclear) as in (A). The blots were hybridized with 20fmol of a btn-labeled NFκB reference site (Armstrong *et al*. 1993) and read out using chemiluminescence. After hybridization, equal loading was monitored by immunodetection of Actin. Signal specificity was determined by competition with 3000x excess of unlabeled probe (Co) and by immunodetection of p65 protein in a control lane loaded with 15µg extract (WB). **(C)** Signals from (B) were quantified using ImageJ software (Schneider *et al*. 2012). The determined relative intensities (RI) were normalized to Actin and are shown as bars. +S: Cultured under normal conditions; -S: Serum-free; Parth.: 100µM Parthenolide.

yielding the same nucleocytoplasmic localization pattern as observed in HT-29 cells cultured under normal conditions (Fig. 38A and 39A). Similar results were obtained for TNFα stimulated HeLa cells (not shown). In contrast, the treatment of HT-29 cells with Parthenolide results in an enrichment of p50 and p65 in the cytosol, whereas the predominantly cytosolic IκBα remains unchanged (Fig. 39A). The expression of RPS3 is not affected, but a slight enrichment in the nucleus as compared to the serum-free state can be observed (Fig. 39A). Interestingly, the obtained results indicate that Parthenolide can increase the expression of p50, p65, and IKKβ in serum-starved HT-29 cells (Fig. 39A). Similar results were obtained for Parthenolide-treated HeLa cells (not shown). Since IKKβ-mediated degradation of IκBα is the crucial step for NFκB activation, the

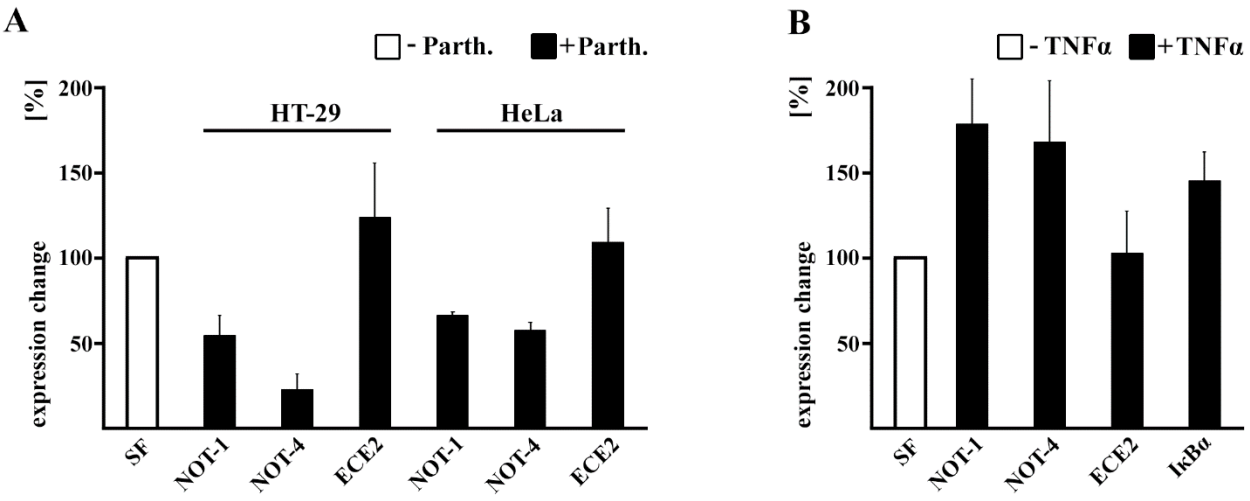

Fig. 40 Manipulation of the NFκB pathway influences *NOT* expression. (A) HT-29 and HeLa cells were treated with 100µM Parthenolide for 1h (Parth.). After incubation, RNA was isolated and mRNA levels were quantified using qRT-PCR. The evaluation of the amount of the targets investigated was performed using the comparative ΔΔCt method: $\Delta\Delta C_T = \Delta C_T$ (untreated) - ΔC_T (Parth. -treated). The ΔC_T values are standardized to *HGPRT* used as endogenous control. Relative expression is calculated with respect to the untreated sample as follows: $2^{-\Delta\Delta CT}$ x 100%. **(B)** HeLa cells were treated with 50ng/ml TNFα for 30min. The mRNA levels were quantified via qRT-PCR. Evaluation as in (A). SF: Serum-free.

detected nucleocytoplasmic distribution of p50, p65, and IκBα suggests that Parthenolide inhibits NFκB activation by targeting IKKβ activity as proposed by Kwok *et al*. (2001). However, there are also reports showing that Parthenolide prevents NFκB binding via alkylation of the p65 subunit (Garcia-Pineres *et al*. 2001). To test for this mechanism, the binding capacity of NFκB in the cytosolic and nuclear fractions of the Parthenolide-treated HT-29 cells was analyzed by Southwestern blot (SW) using a btn-labeled NFκB reference oligonucleotide (Armstrong *et al*. 1993) for hybridization as described in Ch. 3.5.6. The obtained results show, that NFκB binding is abrogated after incubation with Parthenolide in both compartments at all investigated time points, whereas the inhibitory effect becomes stronger with incubation time (Fig. 39B+C). Notably, the detected amounts of cytosolic and nuclear NFκB in Parthenolide-treated HT-29 cells are similar to the amounts observed in untreated cells grown under normal conditions (Fig. 38A+39A). This is of particular importance, because the signal detection in SWs solely depends on the available amount of proteins which were separated under denaturing conditions (Ch. 3.5.6). Thus, the decreased cytosolic binding capacity cannot be explained with the nucleocytoplasmic distribution or the presence of inhibitory IκB:NFκB complexes, but rather argues for the proposed alkylation mechanism (Garcia-Pineres *et al*. 2001). The binding of p50 could not be detected using SW (not shown). As the activity of NFκB peaks 30min. after TNFα stimulation (Hayden and Ghosh 2014)

and Parthenolide most effectively inhibits the binding of NFκB after 60min. (Fig. 39B+C), these two time points were selected for analysis of *NOT*-1 and -4 expression via qRT-PCR. As shown in Fig. 40A, Parthenolide-mediated NFκB inhibition in HT-29 cells decreases *NOT*-1 mRNA expression to 54% (66% in HeLa) and *NOT*-4 to 23% (57% in HeLa) of the level observed in serum-starved cells. In contrast, treatment with TNFα induced NFκB activation leads to an increase of *NOT*-1 to 179% and of *NOT*-4 to 168% of the level detected in serum-starved cells (Fig. 40B). In addition, the detected increase of IκBα expression to 145% is in accordance with the published activation of the negative feedback loop (Hayden and Ghosh 2014). NFκB manipulation via Parthenolide and TNFα has no effect on the expression of *ECE2* (Fig. 40A+B).

4.6.5 Identification of NFκB binding sites in the *NOT* promoter using EMSA

The binding analysis performed using the Y1H technique indicates that the NFκB subunits p50 and p65 bind to the *NOT* promoter via the *cis* sites at positions 973-951nt (site 22/21), 789-776nt (site 19/18), 768-755nt (site 17/16), 638-624nt (site 13/12), 544-535nt (site 8), 339-330nt (site 4/3), and 223-214nt (site 1) (Tab. 61). To confirm the binding capacity of these sites and to verify the negative results for the other potential NFκB sites, EMSAs were performed (Ch. 3.5.3). All predicted *trans* sites, which are not part of composite *cis*/*trans* sites, were also included in this analysis to get a complete insight of NFκB binding within the overlapping *NOT*-*ECE2* promoters. Protein-DNA complexes were identified by incubating the nuclear extracts from HT-29 and HeLa cells with btn-labeled ds oligonucleotides representing the predicted binding sites (Tab. 37). For HT-29 and HeLa extracts positive results have been obtained for sites 22/21, 19/18, 17/16, 13/12, 4/3, and 1 (Fig. 41A+B) confirming the Y1H data (Tab. 61). In addition, the oligo containing the closely arranged *trans* sites 10/9 (568-589nt) is positive in EMSA (Fig. 41A+B). The sites at positions 880-893nt (site 20), 777-811nt (site 18), 680-667nt (site 15/14), 594-607nt (site 11), 401-410nt (site 7), and 262-252nt (site 2) were negative (not shown). Controversial results have been obtained for site 8 (544-535nt), which is negative in EMSA but positive for p50 in Y1H (Tab. 61) and for site 6/5 (375-362nt), which is positive in EMSA but negative in Y1H (Fig. 41A+B; Tab. 61). The binding specificity was confirmed by competition with unlabeled oligonucleotides. The NFκB specificity of the shift was determined using Parthenolide-treated nuclear extracts as comparison. In addition, a control reaction was performed using an NFκB reference oligo (Ron *et al*. 1990) and all shifts were compared to the p65 and p50 signals obtained using native western blot.

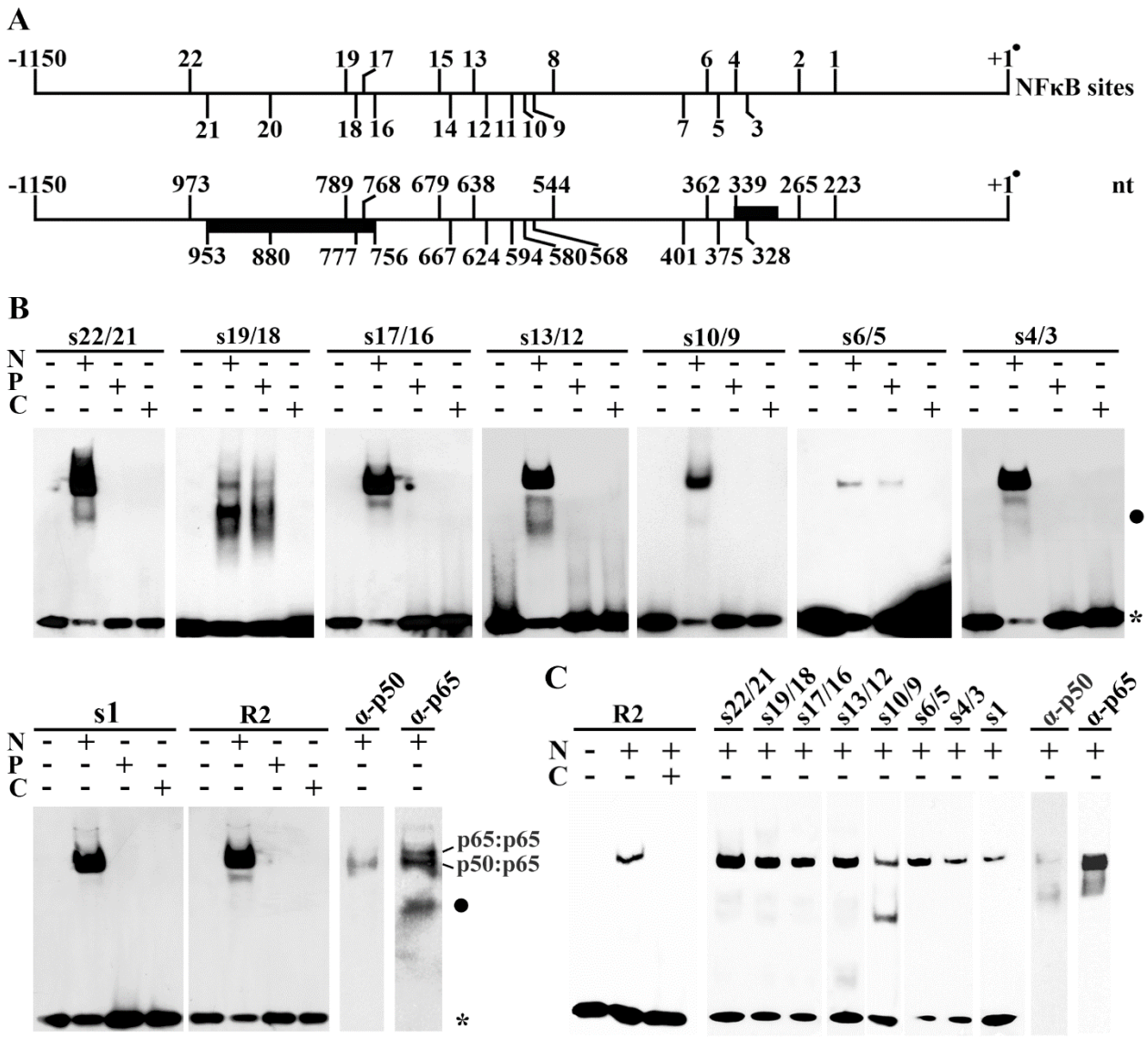

Fig. 41 Identification of NFκB binding sites in the *NOT* promoter using EMSA. (A) Schematic representation of the 1.15kb *NOT* promoter region with potential NFκB binding sites predicted using the P-MATCH™ algorithm (Chekmenev *et al*. 2005). Sites in *cis* on the upper side, sites in *trans* below. Positions are upstream the *NOT*-1 start codon (+1/●). The first exon of *NOT*-4 is located from 337-285nt. The first exon of *ECE2* is located from 755-950nt. **(B)+(C)** The protein-DNA complexes were detected by incubating 7µg nuclear extracts (N) from HT-29 **(B)** and HeLa **(C)** cells with btn-labeled ds NFκB binding sites. Complexes were separated on a 5% native PAGE gel and visualized using chemiluminescence. NFκB specificity was determined by using nuclear extracts from HT-29 cells treated with 100µM parthenolide for 1h (A) and a NFκB reference oligo as comparison: R2 (Ron *et al*. 1990). In addition, a lane on the EMSA blot was loaded with 40µg nuclear extract to detect p65 and p50 using western blot. P: 100µM Parthenolide; C: Competition with 3000x excess of unlabeled oligos; ●: Non-specific binding; *: Free oligo.

The control reactions indicate that the sites can be bound by the p50:p65 or the p65:p65 dimer (Fig. 41A+B). To assess, in the case of p50:p65, which of the subunits mediates the binding, the ELISA technique was applied (Ch. 3.5.4). For that purpose, the positive btn-labeled binding sites were

immobilized on streptavidin-coated microtiter plates and incubated with recombinant p50 or p65 (Tab. 45). The binding was detected with antibodies directed against p50 and p65 (Tab. 43). The specificity of the signals was assessed by using an NFκB reference oligo as comparison (Armstrong *et al*. 1993; R1, Tab. 37). The results show that the NFκB sites within the *NOT* promoter are only bound by p65, whereas binding of p50 was not detected for any site (not shown).

4.6.6 Identification of NFκB binding sites in the *NOT* promoter using affinity chromatography

The NFκB binding sites in the *NOT* promoter were also identified using Dynabeads M-280 (Ch. 3.5.5). Protein-DNA complexes were captured by incubating nuclear extracts from HeLa cells with the btn-labeled binding sites (Tab. 37) immobilized on streptavidin-coated Dynabeads. The eluted protein complexes have been investigated by western blot. The results show that all investigated sites are bound by a protein complex consisting of p50, p65, and RPS3, whereas the phosphorylation state of the p65 subunit varies (Fig. 42). Phosphorylation of p65 on Ser276 can be detected in the complexes bound to sites 22/21, 6/5, and the reference site R2 (Fig. 42). Phosphorylation of p65 on Ser536 can be detected in the complexes bound to sites 19/18 and 17/16. Phosphorylation on both residues is found in the complexes bound to sites 13/12, 19/9, 4/3, and 1 (Fig. 42).

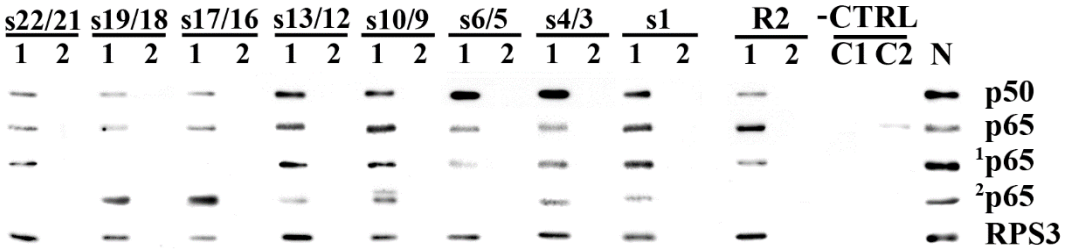

Fig. 42 Identification of NFκB binding sites in the *NOT* promoter using affinity chromatography. Affinity chromatography was performed using biotinylated NFκB binding sites and nuclear extracts from HeLa cells (N). Eluates were separated on a 10% SDS-PAGE gel and analyzed using the indicated antibodies. A NFκB reference oligo was used as positive control: R2 (Ron *et al*. 1990). Beads alone (C1) or incubated with 20µg nuclear extracts (C2) served as negative control (-CTRL). 1: Binding; 2: Competition with 10x excess of cold oligo. [1]p65: p65-Ser276P; [2]p65: p65-Ser536P.

4.6.7 Identification of NFκB binding sites in the *NOT* promoter using ChIP

To confirm the binding results for NFκB and RPS3 *in vivo*, the ChIP technique was used. CBP and p300 were included into the analysis because they are coactivators of NFκB (Zhong *et al*. 1998).

The p50, p65, phospho-p65, RPS3, CBP, and p300 antibodies used for ChIPs are listed in Tab. 43. Negative control ChIPs were performed with an antibody specific for p53 which cannot bind the *NOT* promoter (Ch. 4.4.1). The primers used for the amplifications are listed in Tab. 20. Amplifications performed using ChIP DNA from HT-29, HeLa, HaCaT, and T98G cells and the primer combination P1/1 indicate binding of p50, p65, and RPS3 to the 1115-932nt fragment encompassing site 22/21 (Fig. 43B-E). The p65 subunit is phosphorylated on serines 276 and 536 in HT-29, HaCaT, and T98G cells but only at Ser276 in HeLa cells (Fig. 43B-E). Identical results were obtained from affinity chromatography (Fig. 42, Ch. 4.6.6). CBP and p300 were detected on the same fragment in HaCaT and HeLa cells but not in HT-29 (Fig. 43B-D). Due to the strong p53 signal, the binding of CBP and p300 is considered negative on the P1/1 fragment in T98G cells (Fig. 43E). Amplifications performed using the primer combination P3/3 indicate binding of double-phosphorylated p65 and RPS3 but not p50 to the 912-686nt fragment encompassing sites 20-16 in HaCaT and T98G cells (Fig. 43D+E). In HeLa cells also p50 is bound, whereas in HT-29 no NFκB is present (Fig. 43B+C). RPS3 is positive within the P3/3 amplified region in all cell lines. To amplify the promoter region encompassing the sites 15-8, the primer combination P5/5 (704-505nt) was used in HT-29, HaCaT, and T98G cells, whereas for better evaluation the primer combination P6/6 (660-471nt) was used in HeLa. The obtained results for this region reveal occupancy of p50, p65, RPS3, and CBP in all cells, whereas p300 is only found in HT-29 and HaCaT cells (Fig. 43B-E). The phosphorylation of p65 on Ser276 and Ser536 is detected in all cell lines, whereas the intensity of the signals varies between cell lines. In HeLa and T98G cells there is strong phosphorylation of both serines (Fig. 43C+E), whereas in HT-29 the phosphorylation of p65 is significantly weaker (Fig. 43B). In HaCaT cells p65 is strongly phosphorylated on Ser536 but only weak at Ser276 (Fig. 43D). Amplifications performed using the primer combination P10/9 encompassing the composite site 4/3 indicate binding of p50, double-phosphorylated-p65 and RPS3 in HeLa and T98G cells, whereas in HaCaT cells only Ser276 is phosphorylated (Fig. 43C-E). In HT-29 only p65, phosphorylated on both serines, and RPS3 are bound (Fig. 43B). CBP and p300 were not found within the P10/9-amplified fragment (not shown). Notably, the P10/9-amplified fragment encompasses two nts of the composite site 6/5 (375-362nt), which was positive in EMSAs and affinity chromatography. However, amplification of the 421-268nt promoter region using the primer combination P9/9 yielded negative results in all four cell lines (not shown). Thus, site 6/5 is considered negative *in vivo*. Amplifications performed using the primer combination P11/10 encompassing site 1 yielded positive results for p50, double-phosphorylated p65, RPS3,

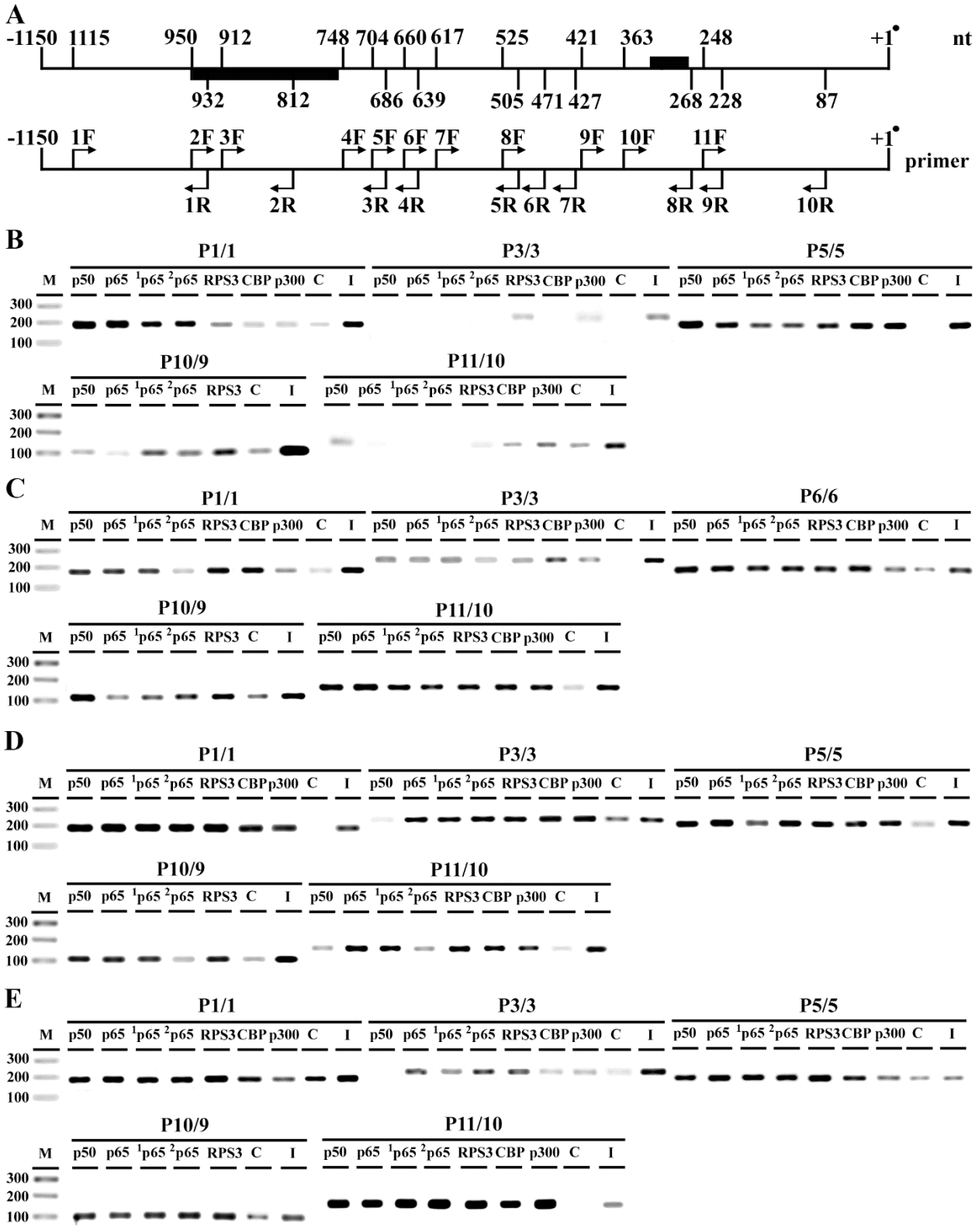

Fig. 43 Identification of NFκB, RPS3, CBP, and p300 binding to the *NOT* promoter *in vivo* using ChIP. (A) Schematic representation of the 1.15kb *NOT* promoter with primers used for ChIP amplification. Upper bar: Primer positions with indicated first exons of *ECE2* and *NOT*-4; lower bar: Primer names; F: Forward; R: Reverse. **(B)-(E)** Gel electrophoretic separation (2% agarose gel) of DNA fragments amplified from ChIPs performed using antibodies directed against p50, p65, Ser276, and Ser536-phosphorylated (P)

CBP and p300 in HeLa and T98G cells (Fig. 43C+E). In HaCaT cells p50 and Ser536-phosphorylated p65 cannot be detected in this region, whereas in HT-29 no binding of the investigated factors could be observed (Fig. 43B+D).

4.6.8 Influence of RNAi-mediated knockdown of NFκB on NOT expression

The DNA-binding analyses revealed the binding of RPS3 and the NFκB subunits p50 and p65 to the *NOT* promoter at different sites in diverse combinations. In addition, the pharmacological manipulation of the NFκB signaling pathway with Parthenolide or TNFα affects the transcription of *NOT*. To determine the impact of endogenous NFκB and RPS3 on the expression of *NOT* under physiological conditions, HeLa cells were transiently transfected with siRNAs targeting NFκB (*p50* and si *p65*) or RPS3 (si *RPS3*) (Ch. 3.6.5). HeLa cells transfected with 10nM scrambled siRNA (si *SCR*) served as control. The mRNA levels were quantified via qRT-PCR, the protein levels via immunoblotting. Transfection of HeLa cells with *p50* siRNA reduces the *p50* mRNA level to 19% and the protein amount to 22% of the level observed in the *SCR* control sample, but has no significant effects on *p65*, *RPS3*, *ECE2*, and *NOT* (not shown). Cells transfected with the *p65* and *RPS3* siRNAs displayed a reduction of the targeted transcripts to 9% (*p65*) and 3% (*RPS3*) (Fig. 44A), whereas the respective proteins cannot be detected (Fig. 44B). The knockdown of p65 decreases the level of *p50* mRNA to 61% (42% protein) and of *RPS3* to 67% (45% protein) (Fig. 44A+B). Silencing of *RPS3* has no effect on *p50* (109%) and *p65* (101%) mRNAs but reduces their protein amounts to 46% (p65) and 86% (p50) (Fig. 44A+B). This observation might depend on the translational functions RPS3 has as part of the ribosome. Notably, the loss of RPS3 leads to cell detachment from the surface after 48h. This effect is considerably enhanced if either *p50* or *p65* is silenced in parallel. Double transfection of the *p50* and *p65* siRNAs reduces *p50* mRNA to 2% (protein to 20%), but is less effective in reducing the *p65* mRNA amount (33%) as compared to the single *p65* siRNA transfection (9%; Fig. 44A+B). Nevertheless, no p65 protein can be detected in both cases (Fig. 44A+B). The double transfection has opposing, yet insignificant effects on RPS3 transcript and protein levels. It reduces the amount of protein to 78% whereas the transcript level increases to 122% (Fig. 44A+B). For control purposes, the expression levels of *IκBα*, which is

p65, CBP, p300, and p53. ChIPs were performed using chromatin from HT-29 (B), HeLa (C), HaCaT (D) and T98G (E) cells. $p65^{1}$: Ser276P; $p65^{2}$: Ser536P; C: p53 ChIP, negative control; I: Input DNA. M: Marker Gene Ruler 100bp ladder.

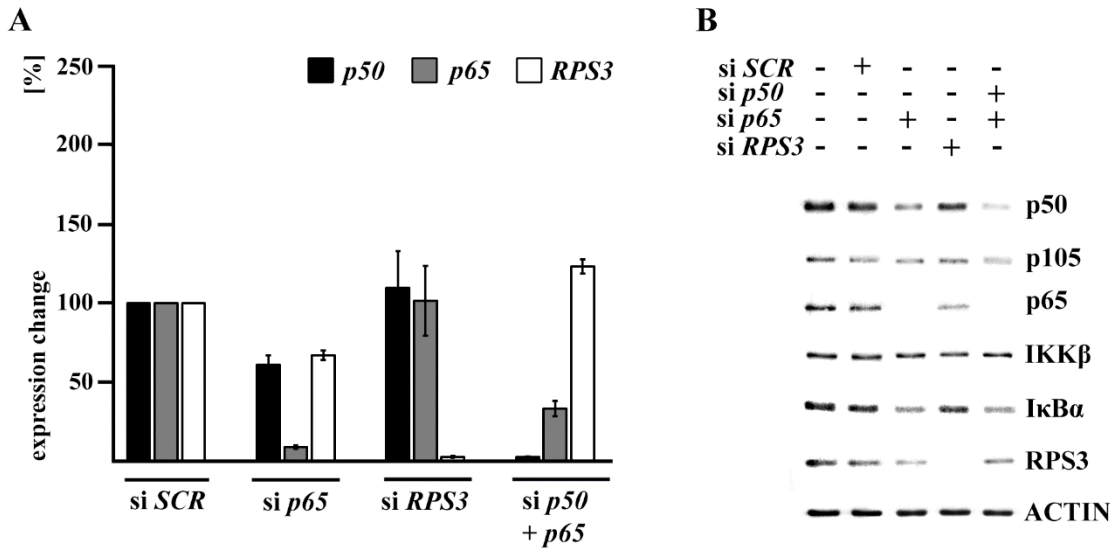

Fig. 44 RNAi-mediated knockdown of *p50*, *p65*, and *RPS3* in HeLa cells. HeLa cells were transiently transfected either with 25nM p65 siRNA (si *p65*), a 50nM RPS3 siRNA mix (si *RPS3*) or the indicated combination (25nM si *p65* + 50nM si *p50*) and analyzed using qRT-PCR and western blot. Transfection with 10nM scrambled siRNA (si *SCR*) served as control. **(A)** Quantification of mRNA levels via qRT-PCR. The evaluation of the amount of the targets investigated was performed using the comparative ΔΔCt method: $\Delta\Delta C_T = \Delta C_T$ (si-treated sample) - ΔC_T (si *SCR*). The ΔC_T values are standardized to *HGPRT* used as endogenous control. The relative expression in % is calculated with respect to the si *SCR* sample as follows: $2^{-\Delta\Delta CT}$ x 100%. **(B)** For western blot 15µg crude homogenates of untreated, si *SCR*-treated and si-treated cells were separated on a 10% SDS-PAGE gel. Detection of the indicated proteins was performed using specific antibodies.

regulated by p65 but not p50, were measured in the NFκB knockdown samples (not shown). Silencing of *p50* has no effect on IκBα, whereas the knockdown of *p65* causes a decrease of *IκBα* mRNA to 37% (60% protein). In accordance with the single transfections, the double transfection of the *p50* and *p65* siRNAs leads to a decrease of *IκBα* mRNA to 39% (60% protein), thus proofing the quality of the samples. In all samples IKKβ expression remains unaffected (Fig.44A+B).

The p65-depleted samples only display insignificant changes in the *NOT*-1 (84%), *NOT*-4 (112%) and *ECE2* (85%) transcript levels (Fig. 45A). The lack of RPS3 causes a decrease of *NOT*-1 mRNA to 70% and an increase of the *NOT*-4 and *ECE2* mRNA levels to 187% and 131%, respectively. The largest drop of *NOT* expression is achieved after double-knockdown of p50 and p65 (*NOT*-1 to 20% and *NOT*-4 to 49%). The double-knockdown as no effect on *ECE2* (97%; Fig. 45A). On the protein level, silencing of p65 causes a decrease of the full-length NOT-1 precursor to 32% (Fig. 45B, ●) and of its post-translational modified variant to 14% (▲). Because the changes in the amount of the NOT cleavage products are not caused by their specific transcriptional regulation, they were not quantified. Similar results are observed in the RPS3-depleted samples,

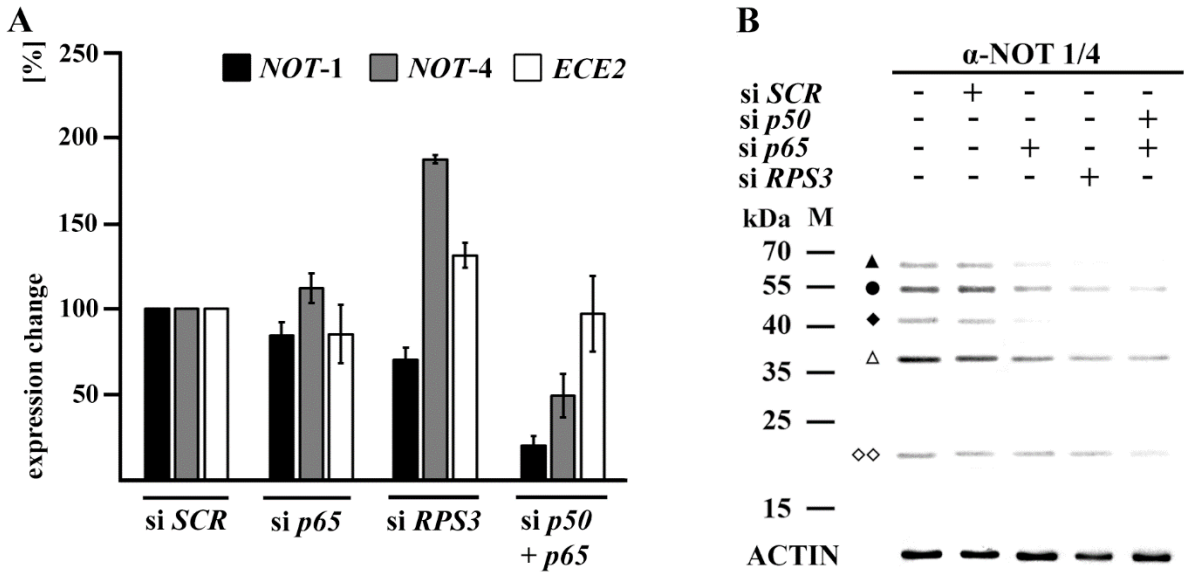

Fig. 45 Impact of RNAi-mediated knockdown of *NFκB* on the expression of *NOT* in HeLa cells. HeLa cells were transiently transfected either with 25nM p65 siRNA (si *p65*), a 50nM RPS3 siRNA mix (si *RPS3*) or the indicated combination (25nM si *p65* + 50nM si *p50*) and analyzed using qRT-PCR and western blot. Transfection with 10nM scrambled siRNA (si *SCR*) served as control. **(A)** Quantification of mRNA levels via qRT-PCR. The evaluation of the amount of the targets investigated was performed using the comparative ΔΔCt method: $\Delta\Delta C_T = \Delta C_T$ (*si*-treated sample) - ΔC_T (si *SCR*). The ΔC_T values are standardized to *HGPRT* used as endogenous control. The relative expression in % is calculated with respect to the si *SCR* sample as follows: $2^{-\Delta\Delta CT}$ x 100%. **(B)** For western blot 15µg crude homogenates of untreated, si *SCR*-treated and si-treated cells were separated on a 10% SDS-PAGE gel. Detection of NOT using the α-NOT 1/4 antibody which recognizes the full-length NOT-1 (●), the potential post-translational modified NOT-1 (▲), the 42kDa cleavage product (♦), the N-terminal NOT-1 cleavage product (Δ), and the C-terminal NOT-1 cleavage product (◊◊). M: Marker.

where the NOT-1 precursor decreases to 22% (Fig. 45B, ●). In accordance with the measured mRNA levels, the double-knockdown of p50 and p65 results in the highest decrease of NOT-1 protein (to 10%, ●, Fig. 45B). The modified NOT-1 cannot be detected after RPS3 depletion or p50/p65 double-knockdown (Fig. 45B, ▲).

4.6.9 Influence of Brefeldin A on activation of NFκB

BFA-induced activation of CREB3 leads to an upregulation of NOT after 24h in HT-29 and HeLa cells (Fig. 34+35). Recent experiments suggest that BFA treatment also causes apoptosis after 24h via upregulation of p53 mediated by the NFκB subunits p50 and p65 (Lin *et al*. 2011). To check, if the observed BFA-induced upregulation of NOT also depends on NFκB, the activation of NFκB in these samples was investigated using western blot (Ch. 3.4.3). In addition, p53 and caspase-3

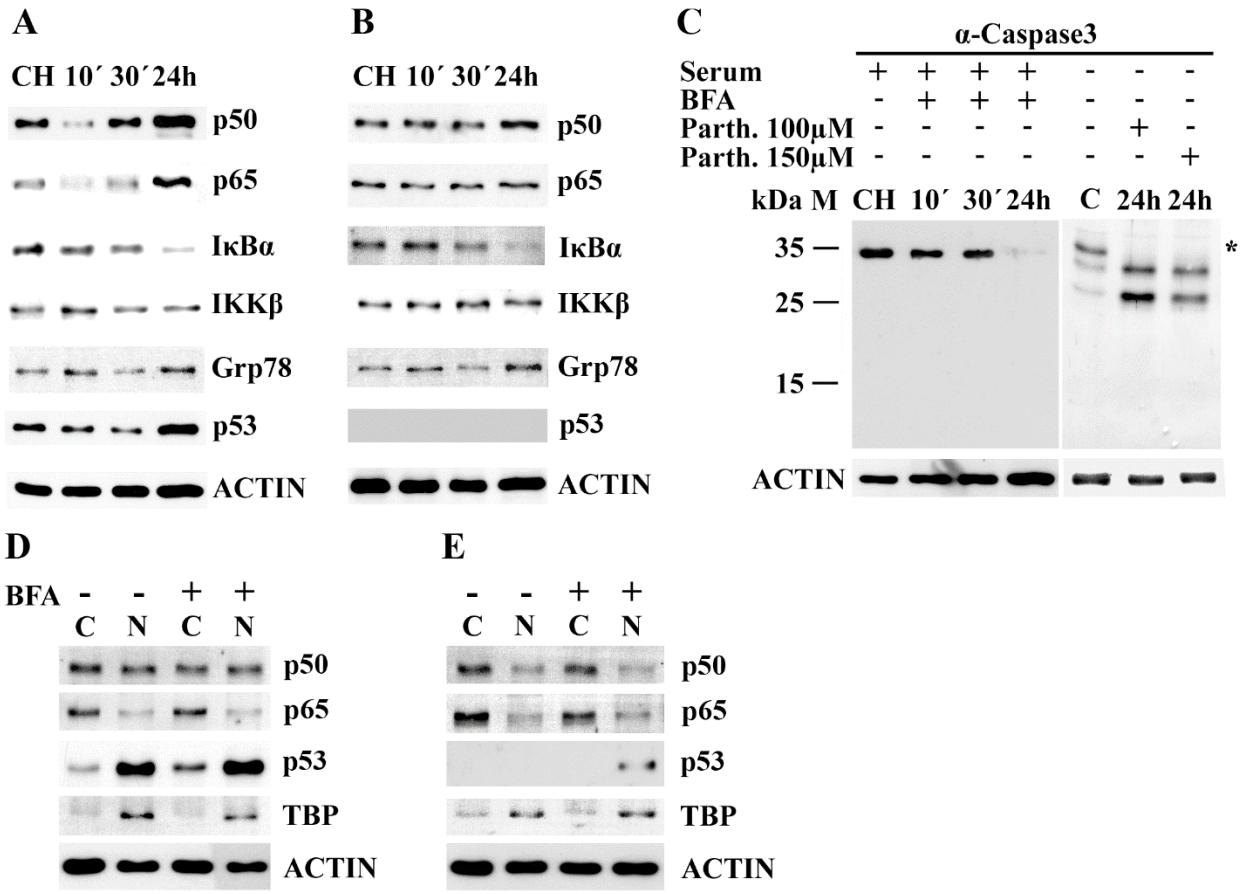

Fig. 46 Influence of Brefeldin A on NFκB, p53, and Caspase-3. Immunoblot analysis of HT-29 **(A+C)** and HeLa **(B)** cells treated with 2µg/ml Brefeldin A (BFA) for the indicated time points. As control for Caspase-3 cleavage during apoptosis serum-free HT-29 cells were treated with 100µM and 150µM Parthenolide for 24h. For separation 15µg were loaded on a 10% SDS-PAGE gel. Detection of the indicated proteins was performed using specific antibodies. *: Pro-Caspase-3 (full-length); CH: Crude homogenate; M: Marker. **(D+E)** Influence of BFA on nuclear localization of NFκB and p53 in HT-29 (D) and HeLa (E) cells. The cells were incubated with 2µg/ml BFA for 24h. Cytosolic (C) and nuclear (N) extracts (15µg each) were separated on a 10% SDS-PAGE gel. Indicated proteins were detected using specific antibodies. TBP was used as nuclear marker to assess fraction quality.

were included in this analysis to test the cells for potential apoptotic characteristics in order to gain further insight into the physiological state the *NOT* gene is upregulated in. The upregulation of the ER stress marker glucose regulated protein 78 (Grp78/BiP) after 24h was monitored as control for BFA induction (Liu *et al*. 1992; Fig. 46A, B). As shown in Fig. 46A, BFA treatment leads, after an initial decrease after 10min. incubation, to an increase of p50, p65, and p53 after 24h in HT-29 cells. This kinetic is consistent with published data for MCF-7 (Lin *et al*. 2011). NFκB only slightly increases after 24h in HeLa cells, whereas BFA has no effect after 10 and 30 min. (Fig. 46B). A slight upregulation of p53 is only visible in the enriched nuclear fractions (Fig. 46B). This can be

explained by the fact that in the HPV positive HeLa cell line the viral E6 protein interacts with p53 and mediates its rapid degradation via the ubiquitin-proteasome pathway (Thomas *et al*. 1999). In accordance with the common model of NFκB activation (Hayden and Ghosh 2014), the amount of the NFκB inhibitor IκBα constantly decreases, whereas IKKβ remains unaffected in both cells. Notably, CREB3 overexpression also reduces IκBα (not shown). However, p50 and p65 are not transported to the nucleus in BFA-treated cells, whereas p53 clearly is (Fig. 46D+E). This suggests that p53 is upregulated in a NFκB-independent manner in HT-29 and HeLa cells after BFA treatment. To assess if the observed BFA-induced expression changes of NFκB and p53 are accompanied by the induction of programmed cell death, physiological and phenotypic changes characteristic for apoptosis were measured. Caspase cleavage is a well-defined hallmark of the different extrinsic and intrinsic apoptotic signaling pathways which all together converge at activated caspase-3 making it a well suited means to measure apoptosis (McIlwain *et al*. 2013). In BFA-treated HT-29 cells the amount of procaspase-3 decreases after 24h but the cleaved, active products cannot be detected (Fig. 46C). Similar results were obtained for HeLa cells (not shown). Because active caspase-3 can be generally detected by the applied antibody as shown in Fig. 46C for serum-starved HT-29 cells treated for 24h with 100 or 150µM of the apoptosis inducing sesquiterpene parthenolide (Kim *et al*. 2012), caspase-3 is not activated but downregulated after BFA treatment in the investigated cells after 24h. Notably, the exposure of HT-29 and HeLa cells to BFA causes reduction of cell proliferation and considerable cell detachment from the surface (not shown). However, as determined using the trypan blue exclusion assay (Ch. 3.6.1), these cells have no compromised cell membranes like apoptotic or dead cells but are still viable (not shown).

4.7 Determination of MYCN binding to the *NOT* promoter

As determined using the P-MATCH^{TM} algorithm (Chekmenev *et al*. 2005), the 1.15kb *NOT* promoter region contains 10 potential MYCN sites (five in *cis*, five in *trans*) (Tab. 39; Fig. 48A). The myc myelocytomatosis viral related oncogene N (MYCN) belongs to the basic-helix-loop-helix-zipper (bHLHZ) domain containing family of Myc transcription factors that also comprises c-Myc, MYCB, and MYCL (Beltran 2014). MYCN regulates its target genes by binding to MYC sites (E-Box sequences) and is pivotal, especially in neuronal cells, for proliferation, stem cell homeostasis and differentiation (Westermark *et al*. 2011). To test the binding of MYCN to the *NOT* promoter, Y1H (4.7.1), EMSA, affinity chromatography, and ChIP assays (Ch. 4.7.3) were performed.

4.7.1 Identification of MYCN binding to the *NOT* promoter using the Y1H technique

To investigate the capacity of MYCN to bind the 1.15kb *NOT* promoter, the Y1H was performed. For this purpose, a pACT2-MYCN expression construct was generated (Ch. 3.3.14.4). This construct was cotransformed with either of the *NOT* promoter constructs pHIS2.1-Ph*NOT*-1 (1150 to ATG; P1), pHIS2.1-Ph*NOT*-2 (704 to ATG; P2), pHIS2.1-Ph*NOT*-3 (525 to ATG; P3), and pHIS2.1-Ph*NOT*-4 (1115-686nt; P4) (Fig. 20, Ch. 4.3) and plated on SD/-His/-Trp/-Leu + 150mM

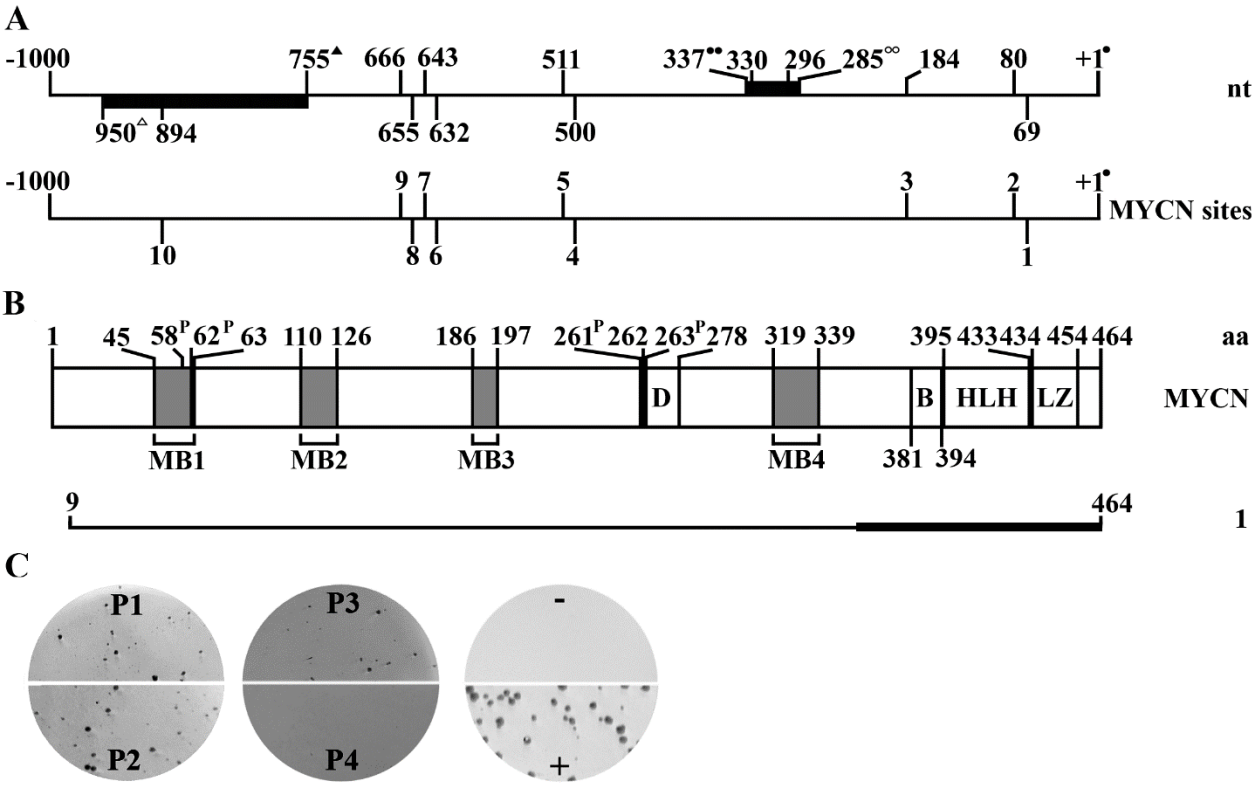

Fig. 47 Identification of MYCN binding to the *NOT* promoter using the Y1H technique. (A) Schematic representation of the *NOT* promoter region that encompasses potential MYCN binding sites (second bar; *cis* sites on top, *trans* sites below) predicted using the P-MATCH™ algorithm (Chekmenev *et al*. 2005). The 1.15kb region was analyzed but as there are no sites downstream site 10, only the 1kb region is depicted. Positions upstream the *NOT*-1 start codon (+1/●) are shown in the first bar. The first exon of *NOT*-4 is located from 337nt (●●) - 285nt (○○). The first exon of *ECE2* is located from 755nt (▲) - 950nt (Δ). **(B)** Schematic representation of the MYCN protein structure (UniProtKB: P04198) with the generated pACT2-MYCN expression construct below. The 464 aa MYCN protein contains at its C-terminus a basic motif (B; aa 381-394), a helix-loop-helix domain (HLH, aa 395-433), and a leucine zipper (LZ, aa 434-454) all involved in DNA-binding. An acidic region (D) located at aa 262-278. Residues Ser54, Thr58, Ser62, Ser261 and Ser263 are phosphorylated (P). The four Myc boxes (MB1-4) for protein-protein interactions are located at aa 45-63, 110-126, 186-197, and 319-339 (Otto 2015). **(C)** Determination of MYCN binding to the *NOT* promoter. Y187 cells were cotransformed with 500ng pACT2-MYCN and 500ng of either pHIS2.1-Ph*NOT*-1 (1150-ATG; P1), pHIS2.1-Ph*NOT*-2 (704-ATG; P2), pHIS2.1-Ph*NOT*-3 (525-ATG; P3) or pHIS2.1-Ph*NOT*-4 (1115-686nt; P4) (Fig. 20). Cells were grown on SD/-His/-Trp/-Leu + 150mM 3-AT. Control transformations: -: pACT2-p53; +: pGADT7-Rec2-p53 + p53pHIS2.

Tab. 62 Identification of MYCN binding sites in the *NOT* promoter using Y1H

Promoter construct[1]	Region (5´- 3´)[2]	MYCN binding sites (5´- 3´)[3] cis	MYCN binding sites (5´- 3´)[3] trans	Y1H result
P1	1150 -ATG	9 (666-655); 7 (643-632); 5 (511-500); 3 (184-173); 2 (80-69)	10 (894-905); 8 (655-666); 6 (632-643); 4 (500-511); 1 (69-80)	+
P2	704 - ATG	9, 7, 5, 3, 2	8, 6, 4, 1	+
P3	525 - ATG	5, 3, 2	4, 1	+
P4	1150 - 686		10	-

1: All promoter fragments were cloned into pHIS2.1; 2: Positions in nt upstream the *NOT*-1 ATG; 3: Potential MYCN binding sites predicted using the P-MATCH™ algorithm (Chekmenev *et al*. 2005); 4: Y1H results for the pACT2-MYCN construct cotransformed into Y187 cells with the indicated promoter constructs. The cells were plated on SD/-His/-Trp/-Leu + 150mM 3-AT. +: Growth; -: No growth.

3-AT. The results show that constructs P1, P2, and P3 (Fig. 20) can be bound by MYCN whereas P4 (Fig. 20) cannot (Fig. 47C and Tab. 62). This indicates that MYC site 10 is negative and that at least one of the sites 1-5 can be bound (Fig. 47C; Tab. 62). Notably, as compared to the Y1H results obtained for EGR-1 (Ch. 4.4.2), CREB3 (Ch. 4.5.1), and NFκB (Ch. 4.6.1), the colonies grown after MYCN transformation are considerably smaller indicating a weaker binding (Fig. 47C).

4.7.2 Expression of MYCN in diverse cell lines

Because the Y1H assay has identified MYCN as a putative *NOT* regulator, its binding to the *NOT* promotor was further validated by *in vitro* and *in vivo* protein DNA-binding assays (Ch. 4.7.3). To choose the appropriate cells for these experiments, MYCN expression was investigated in HaCaT, HT-29, HeLa, and T98G cells (Tab. 51) using immunoblotting (Ch. 3.4.3). The applied MYCN antibody detects four protein species: a cytosolic protein of about 60kDa (♦) only present in HT-29 and HeLa cells, a protein around 40kDa (●) predominantly located in the nucleus, a protein around 30kDa (▲) mainly found in the cytosol and a protein around 22kDa (■) found in both compartments (Fig. 48). According to the NCBI Reference Sequence (RefSeq) Database, the MYCN gene codes for three splice variants: v1 (NM_001293228.1/~50kDa), v2 (NM_001293233.1/ ~28kDa), and v3 (NM_001293231.1/~12kDa). The variants v2 and v3 differ from v1 at their N-termini, thus cannot be detected by the applied MYCN antibody recognizing the N-terminal 100aa of MYCN v1. As MYCN has a predicted molecular weight of 46kDa, the 40kDa (●) signal most likely represents the unmodified full-length MYCN protein (Fig. 48). Since MYCN is extensively

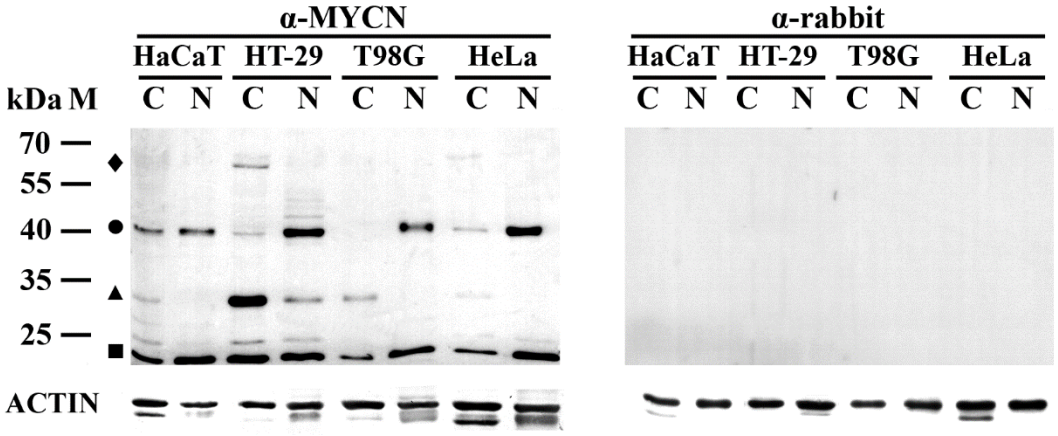

Fig. 48 Expression of MYCN in diverse cell lines. Cytosolic (C) and nuclear (N) extracts (15µg each) were separated on a 10% SDS-PAGE gel. Detection of MYCN and Actin with specific antibodies. As the secondary antibody (α-rabbit) recognizes no proteins, all signals are detected by the MYCN antibody. Potential MYCN products: 60kDa (♦), 40kDa (●), 30kDa (▲), and 22kDa (■).

phosphorylated (Otto 2015), the 60kDa form (Fig. 48, ♦) most likely represents the post-translational modified protein. The low level of this protein can be explained with its phosphorylation-mediated degradation (Sjostrom *et al.* 2005). In line with this mechanism, the lower band around 30kDa (▲) represents a N-terminal cleavage or degradation product (Fig 48). The nature of the 22kDa form (■) remains unclear. As shown in Fig. 49C, this protein can bind DNA. With respect to the N-terminal specificity of the applied antibody and the fact that MYCN binds its target sites via the C-terminus, this protein might represent a yet undescribed splice variant.

4.7.3 Identification of MYCN binding sites in the *NOT* promoter using EMSA, affinity chromatography, and ChIP

To confirm the negative Y1H result for site 10 and to determine which of the remaining 9 predicted sites (Fig. 47A, Tab. 62) can be bound by MYCN, EMSAs were performed. Protein-DNA complexes were identified by incubating nuclear extracts from HeLa cells with btn-labeled ds oligonucleotides representing the predicted binding sites (Tab. 39). The obtained results show shifted complexes for the composite *cis*/*trans* site 1/2 (80-69nt) and the *cis* site 3 (184-173nt). All other sites are negative (Fig. 49B). The detected shifts are identical to the shift observed using the MYC reference site (Fig. 49B). The specificity of the reference shift was confirmed by competition with unlabeled oligonucleotides (Fig. 49B). To determine if the detected EMSA shift pattern depends on the different MYCN species detected in the immunoblots, affinity chromatography

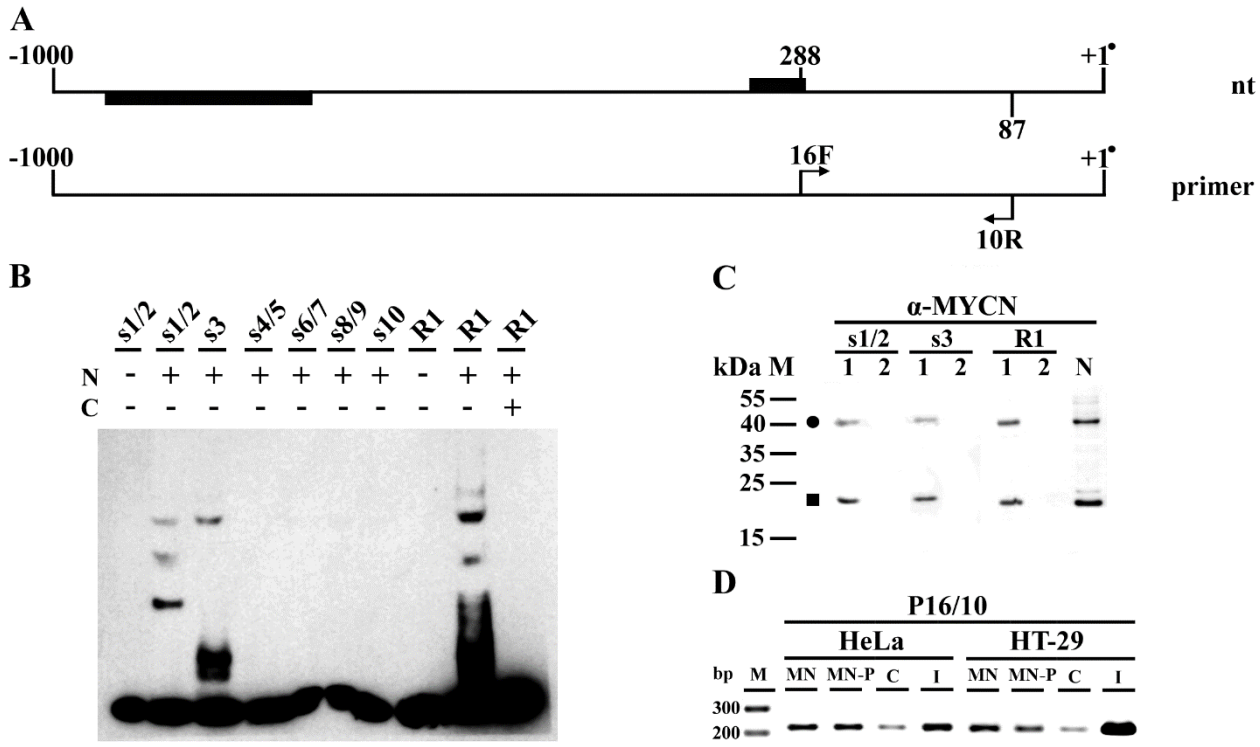

Fig. 49 Identification of MYCN binding in the *NOT* promoter. (A) Schematic representation of the 1kb *NOT* promoter with primers used for ChIP amplification. Upper bar: Primer positions with indicated first exons of *ECE2* and *NOT*-4; lower bar: Primer names; F: Forward; R: Reverse. **(B)** Identification of MYCN binding sites using EMSA. The protein-DNA complexes were detected by incubating 7µg nuclear extracts from HeLa cells (N) with btn-labeled ds MYCN sites. Protein-DNA complexes were separated on a 5% native PAGE gel and visualized using chemiluminescence. MYCN specificity was determined by using published reference oligos as comparison: R1 (Perini *et al*. 2005). C: Competition with 3000x excess of unlabeled ds oligos. **(C)** Identification of MYCN binding sites using affinity chromatography (AC). AC was performed using the btn-sites and extracts from (B). Eluates were separated on a 10% SDS-PAGE gel and analyzed using an MYCN antibody. 1: Binding; 2: Competition with 10x excess of cold oligo. M: Marker. **(D)** Identification of MYCN binding using ChIP. Gel electrophoretic separation (2% agarose gel) of DNA fragments amplified from ChIPs performed using HT-29 and HeLa cells and antibodies directed against MYCN (MN), serine 54-phosphorlyated MYCN (MN-P), and p53. C: p53 ChIP, negative control; I: Input DNA. M: Marker Gene Ruler 100bp ladder.

using Dynabeads M-280 was applied (Ch. 3.5.5). The results show that the sites 1/2 and 3 as well as the reference are bound by the putative unmodified full-length MYCN (Fig. 49C, ●) and the 22kDa protein (Fig. 49C, ■). Notably, immunodetection of eluted proteins showed that these sites are not bound by c-Myc (not shown). In addition, MYCN-binding was confirmed *in vivo* using ChIP (Ch. 3.5.7). Because phosphorylation of MYCN at Ser54 is linked to its transcriptional activity during oncogenesis (Kapeli and Hurlin 2011), this modified MYCN form was included in the experiments. The respective antibodies used for ChIPs are listed in Tab. 43. Negative control ChIPs were performed with an antibody directed against p53 which cannot bind the *NOT* promoter

(Ch. 4.4.1). Amplifications performed using ChIP DNA from HT-29 and HeLa cells and the primer combination P16/10 (Tab. 22) indicate binding of MYCN and phosphorylated MYCN to the 288-87nt fragment encompassing sites 1-3 (Fig. 49D). Similar results were obtained for HaCaT (not shown). However, MYCN *in vivo* binding could not be detected in T98G cells (not shown).

4.8 Identification and characterization of murine *NOT* splice variants

4.8.1 Isolation of different *NOT* transcripts from diverse murine cell lines

The murine homologue to the *NOT* gene, m*NOT*, is located on chromosome 16 (NCBI: NC_000082.6) and shares a similar chromosomal organization as its human counterpart (Fig. 1; Ch. 1.1.2). The m*NOT* promoter has been cloned and the minimal region necessary for its regulatory activity has been mapped (Kurzik-Dumke, personnel communication). In the mouse, only two transcripts, m*NOT*-1 (NCBI: NM_145939.2) and m*NOT*-2 (Kurzik-Dumke, personal communication), are currently known. To check if further murine homologues of the detected human transcripts exist, different primers for RT-PCR were designed (Tab. 34). As delineated in Ch. 4.1, the human *NOT* variants (v) can be grouped according to the composition of their first two exons into five classes. To investigate if these classes also exist in mouse, cDNA from 3T3 cells was amplified using a forward primer residing just upstream the ATG of m*NOT*-1 in combination with a reverse primer in exon 4 (Fig. 50, 1f/2r; Tab. 34). The obtained results show a three band pattern representing the murine homologues of *NOT*-1, -2, and -5. Variant 2 contains a shortened first exon (160-296nt are deleted) and lacks the second exon as compared to v1 leading to a

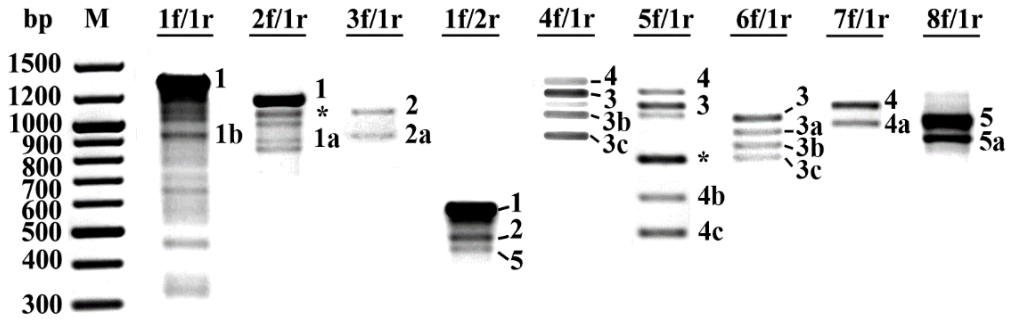

Fig. 50 Amplification and isolation of murine *NOT* splice variants. Gel electrophoretic separation of amplificates generated using the indicated primer combinations (f: Forward; r: Reverse) and cDNA from 3T3 cells on a 2% agarose gel. Bands were extracted from the gel and sequenced. The identified variants are indicated. *: Non-specific amplification; bp: Base pairs; M: Marker Gene Ruler 100bp ladder.

frameshift a premature stop codon in exon 2 at 208nt (Tab. 63). The murine *NOT*-5 variant lacks the second exon as compared to v1 resulting in a frameshift and a premature stop codon in exon 2 at 322nt (Tab. 63). Amplification using a forward primer residing just upstream the start codon of m*NOT*-1 in combination with a reverse primer in the 3´- UTR yielded detection of m*NOT*-1 and another yet undescribed variant termed m*NOT*-1b (Fig. 50, 1f/1r; Tab. 34). As compared to v1, v1b contains a deletion of the nts 203-296 in exon 2, lacks exons 3 and 4, and lacks the first four nts of exon 5 leading to a frameshift and a premature stop codon at 379nt. The strong signal of the 1f/1r amplification superimposes the v2 and v5 signals, but also suggests the existence of further variants. Using the m*NOT*-1 specific forward primer and the 3´-UTR reverse primer for amplification yielded detection of the new variant m*NOT*-1a (Fig. 50, 2f/1r; Tab. 34). This isoform lacks exon 4 as compared to v1 leading to a frameshift and a premature stop codon at 625nt (Tab. 63). Interestingly, the amino acid sequence deduced from the "frameshifted" region v1b is identical to the C-terminal sequence in the "frameshifted" v1a. Using a m*NOT*-2 specific forward primer and the 3´-UTR reverse primer for amplification yielded detection of a further form, termed m*NOT*-2a (Fig. 50, 3f/1r; Tab. 34). This variant lacks exon 3 as compared to v2. Amplification with a m*NOT*-5 specific forward primer in combination with the 3´-UTR reverse primer yielded detection of an additional variant termed m*NOT*-5a (Fig. 50, 8f/1r; Tab. 34). This variant lacks exon 3 as compared to v5. To establish the yet undescribed murine homologues of *NOT*-3 and -4, the first exon for this forms upstream the m*NOT*-1 start codon has to be identified. For that purpose, all upstream ATGs which are not in the coding region of *ECE2* were considered as potential start sites and forward primers containing the respective ATG as the first nts in their sequence were designed. Amplifications performed using these primers in combination with the 2r primer revealed that only the combination containing the ATG located 888nt upstream of the m*NOT*-1 ATG produces a signal consisting of two bands corresponding to the murine homologues of *NOT*-3 and -4. Notably, the first exon of these two variants contains a TAA stop codon at 34nt making all downstream splicing events irrelevant for translation (Tab. 63). To establish the full- length sequences and to identify alternative spliced derivatives, amplifications were performed using a forward primer either residing in the first exon of m*NOT*-3 and -4 (Tab. 34, 5f) or upstream ATG (Tab. 34, 4f) in combination with the 3´-UTR primer. In the case of 4f, the variants 3 and 4 could be confirmed and two additional forms, m*NOT*-3b and -3c, were detected (Fig. 50). Amplifications performed using the 5f primer yields detection of v3 and v4 and two further variants, m*NOT*-4a and -4b (Fig. 50). As compared to m*NOT*-3 v3b lacks exon 3 and v3c lacks exons 6 and 7. V4a lacks exon 4

Tab. 63 Characterization of m*NOT* splice variants

Variant	CDS/Stop[1]	Length[2]	Molecular weight[3]	Reference[4]
m*NOT*-1	TGA/1315	438	50.2	KP189259
m*NOT*-2	TGA/208	69	7.95	KP189262
m*NOT*-3	TAA/34	11	1.23	KP189264
m*NOT*-4	TAA/34	11	1.23	KP189268
m*NOT*-5	TGA/322	107	12.12	KP189272
m*NOT*-1a	TGA/625*	209	23.04	KP189260
m*NOT*-1b	TGA/379*	126	13.75	KP189261
m*NOT*-2a	TGA/208	69	7.95	KP189263
m*NOT*-3a	TAA/34	11	1.23	KP189265
m*NOT*-3b	TAA/34	11	1.23	KP189266
m*NOT*-3c	TAA/34	11	1.23	KP189267
m*NOT*-4a	TAA/34	11	1.23	KP189269
m*NOT*-4b	TAA/34	11	1.23	KP189270
m*NOT*-4c	TAA/34	11	1.23	KP189271
m*NOT*-5a	TGA/322	107	12.12	KP189273

1: Size of the coding sequence (CDS) in nt. The position indicates the T in the TGA/TAA stop codon with respect to ATG = 1. m*NOT*-1a and -1b share the same TGA (*); 2: Length of the translated proteins in aa; 3: Molecular weight in kDa calculated using the deducted aa sequences and the Protein Identification and Analysis Tools on the ExPASy Server (Artimo *et al*. 2012): http://web.expasy.org/compute_pi/; 4: GenBank accession numbers; All variants were sequenced from 3T3 cDNA.

whereas v4b lacks exons4-7 as compared to v4. Using the m*NOT*-3 specific forward primer and the 3´-UTR reverse primer for amplification v3, v3b, and v3c could be confirmed and an additional variant, m*NOT*-3a, was identified (Fig. 50, 6f/1r; Tab. 34). As compared to v3, the nts 205-292 are deleted in v3a. Amplifications performed using the m*NOT*-4 specific forward primer and the 3´-UTR reverse primer confirmed v4 and v4a (Fig. 50, 7f/1r; Tab. 34). All amplifications were also performed using cDNA from MOCHA, BC3H1, and C127I cells yielding similar signal patterns (not shown). In those cells only v1-5 were sequenced. Taken together, 13 yet unidentified murine *NOT* variants were isolated from diverse cell lines. The identified transcripts, which show similar splicing patterns as observed for their human counterparts (Ch. 4.1), can also be grouped according to the composition of their first two exons into transcripts derived from m*NOT*-1, -2, -3, -4, or -5. In contrast to man, m*NOT*-1 is the only variant that contains a full-length open reading frame. All obtained nucleotide sequences were deposited in the GenBank Sequence Database.

4.8.2 Identification of splicing motifs for the m*NOT* transcripts

Sequence analysis of the diverse murine *NOT* variants suggests that they are generated by alternative splicing (Ch. 4.8.1). To identify the core splicing motifs, different bioinformatics tools were applied. The Alternative splice site predictor (ASSP) (Wang and Marin 2006) was used to identify the 5´and 3´splice sites and The Human splicing finder (Desmet *et al*. 2009) to determine the branch points (BPs). The pyrimidine-rich sequence which is located nearest to the 3´ end of the respective intron is considered as polypyrimidine tract (PPT) (Tab. 64). The results show that the calculated splice sites fit with the exon boundaries of all isolated variants with exception of m*NOT*-2, -2a, -1b, -3a, and -4c. Because these five isoforms contain shortened exons, it is most likely that they are spliced via cryptic splice sites. However, the applied ASSP tool could not identify such sites. That is why in these cases the cryptic 5´ and 3´ splice sites were deduced from the respective sequence (Tab. 64). Notably, the sequence-deduced splice sites share high similarity with the canonical motifs.

Tab. 64 Splicing motifs for the different m*NOT* variants

In.	5´splice site	Branch point	Polypyr. tract	3´ splice site
1	(51) 5´-GAGgtaaga	(782) 5´-ggctcAg	(843) 5´-ttggttttccc	(2536) 5´-tccagAC
1[c]	(48) 5´-ACCgaggta	---	---	(4823) 5´-ccaccTT
2	(1082) 5´-CATgtgagt	(2504) 5´-gactcAg	(2527) 5´-ttatcttcttcc	(2536) 5´-tccagAC
2[c]	(1045) 5´-GAGgtgggc	(2712) 5´-ggctcAt	(2720) 5´-tttcctttcatcttcc	(2733) 5´-tccagCT
3[c]	(2544) 5´-CAGagattg	(3582) 5´-ctctcAg	(3717) 5´-cttttcctgtcctttgtccat	(3742) 5´-gcctgGC
3	(2638) 5´-TGTgtgagt	(2712) 5´-ggctcAt	(2720) 5´-tttcctttcatcttcc	(2733) 5´-tccagCT
4	(2883) 5´-AAGgtgagt	(2940) 5´-ggctcAg	(2967) 5´-tgcccaccctt	(2976) 5´-tttagGT
4[c]	(2883) 5´-AAGgtgagt	---	---	(3065) 5´-gtagcTA
5	(3139) 5´-CAGgtcaga	(3582) 5´-ctctcAg	(3717) 5´-cttttcctgtcctttgtccat	(3738) 5´-ttcagCC
6	(3861) 5´-CAGgtaact	(4582) 5´-ctctcAc	(4646) 5´-cttcacccattccc	(4657) 5´-cccagGT
7	(4865) 5´-CAGgtaaga	(4917) 5´-agctcAg	(5014) 5´-cttctcttc	(5020) 5´-ttcagAA
8	(5099) 5´-ACCatatcc	(5563) 5´-cccccAc	(5603) 5´-ccttaaccatcacatc	(5616) 5´-atcacAG
9	(5763) 5´-CAGgtacta	(5812) 5´-tcctcAc	(5892) 5´-cccgtttctcattccc	(5905) 5´-cccagGT

All positions relate to ATG of m*NOT*-4 = +1. In.: Intron 1 between exons 1 and 2 of the m*NOT* variants 3 and 4. Sequence derived from the BAC clone Mus musculus strain C57BL/6J rp23-101h1 (NCBI: AC087898). Splice sites (SS) were calculated using the Alternative splice site predictor (ASSP) at http://wangcomputing.com/assp/index.html. Exon sequences are in capital letters. The branch points were calculated using the Human splicing finder at http://www.umd.be/HSF3.Variants 2, 2a, 1b, 3a, and 4c use cryptic splice sites which were not recognized by the ASSP program. The indicated sites are deducted from the sequence analysis. The cryptic sites are marked c. 1[c]: SS for v4c; 2[c]: SS for v2 and v2a; 3[c]: SS for v1b; 4[c]: SS for v3a.

4.8.3 Determination of m*NOT* and m*ECE2* transcription start sites

The transcription start sites (TSSs) of the murine *NOT* variants were determined with the RACE-technique using cDNA from 3T3 and MOCHA cells as described in Ch. 3.3.18. All primers used for the amplifications are listed in Tab. 28 and 34. Amplification of RACE cDNA using a reverse primer residing in the 3´-UTR (1r, Tab. 34) in combination with the RACE-tag-specific forward primer (USP primer) yields detection of one strong signal (Fig. 51A). Gel extraction (Ch. 3.3.5) and sequencing (Ch. 3.3.6) revealed that the isolated band corresponds to m*NOT*-1 with the TSS located 10nt upstream ATG. In addition, smaller and significantly weaker signals were detected potentially corresponding to other m*NOT* variants. Because of their slight intensities, they could not be sequenced. As shown above, the human and murine *NOT* transcripts can be classified depending on the compositions of their first two exons. To determine if class-specific TSSs exist in mice, RACE cDNA from MOCHA and 3T3 was amplified using group-specific reverse primers in combination with the USP primer. The obtained results confirm the TSS for m*NOT*-1 and show that this TSS is also shared by m*NOT*-2 and -5 (Fig. 51A). The TSS of m*NOT*-4 is located 109nt upstream ATG (Fig. 51A). Amplification performed using a m*NOT*-3-specific reverse primer yielded no results, presumably due to low expression of this variant (Fig. 51A). Nevertheless, it is likely that it shares the same TSS with v4 as it is observed in man. Because m*NOT* and m*ECE2*

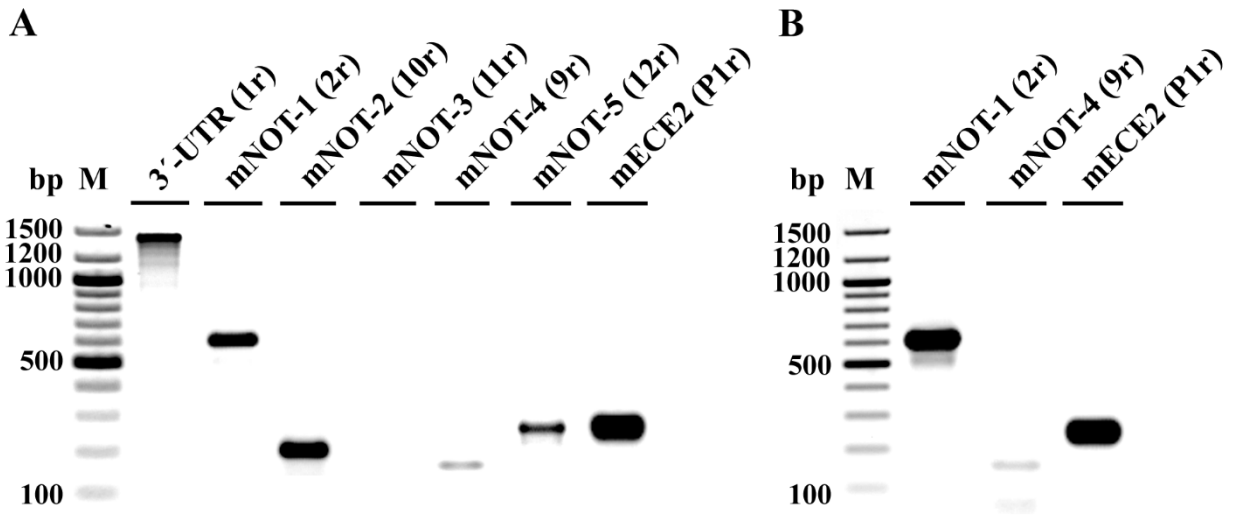

Fig. 51 Determination of m*NOT* and m*ECE2* transcription start sites using RACE. Gel electrophoretic separation of DNA fragments amplified using RACE cDNA from MOCHA **(A)** and 3T3 **(B)** cells. Applied reverse primers (r) are shown in brackets. The complete PCR samples were separated on a 1.5% agarose gel. For TSS identification all detected amplification products were extracted from the gel and sequenced using the respective reverse primer. bp: Base pairs; M: Marker Gene Ruler 100bp ladder.

contain overlapping promoter regions, the TSS of m*ECE2* was also determined. For that purpose, RACE cDNA from was amplified using a reverse primer specific for *ECE2* variants 1 and 3 (because only these two variants contain the first exon 887nt upstream the m*NOT*-1 ATG) in combination with the USP primer. The detected TSS of m*ECE2* is located 30nt upstream its start codon (Fig. 51B). In conclusion, there are two different TSSs for the murine *NOT* variants. The variants which share the same first exon also share the same TSS.

4.8.4 Identification of RNA motifs within the m*NOT* UTRs

To check for the presence of RNA motifs within the UTRs of the m*NOT* variants, their sequence was analyzed using the RegRNA2.0 web tool (Chang *et al*. 2013). The analysis showed that there exist no known motifs within the 5´ and 3´-UTRs of any m*NOT* transcript. In addition, the murine mRNAs were also tested for the presence of the Kozak sequence (Kozak 2005). As shown in Fig. 52, m*NOT*-1 shares the two important positions for effective translation with the Kozak reference. The sequence from -3 to +4 is identical to the human counterpart (Fig. 17, Ch. 4.1.4). The m*NOT*-4 mRNA shares only the -3 position with the Kozak sequence.

Fig. 52 Kozak sequences within the m*NOT* transcripts. Alignment of the sequences around the ATGs (bold and underlined) of the m*NOT*-1 and 4 mRNAs with the Kozak sequence (Kozak 2005). Kozak key positions in bold. Other sequence matches are underlined. R: Purine (A/G).

4.8.5 Quantification of the expression of the m*NOT* transcripts in diverse cell lines

The m*NOT* gene encodes 15 splice forms generated by alternative splicing (Ch. 4.8.1 + 4.8.2). To determine the splice variant specific expression of the distinct m*NOT* transcripts in diverse cell lines, qRT-PCR analysis was performed (Ch. 3.3.17). Splice variant specific primers were designed (Tab. 35) and their efficiencies were determined (Table S5-S8). The evaluation of the amount of the targets investigated was performed using the comparative C_T (ΔC_T) method as described in Ch. 3.3.17. As shown in Tab. 65, the *NOT* splice forms are expressed at distinct levels in different cells. The $2^{-\Delta CT}$ values indicate that m*NOT*-1 and m*NOT*-4c are the highest expressed variants in all four cell lines. The m*NOT*-1 mRNA levels are almost identical in 3T3 and C127I (0.07 and 0.08) and

Tab. 65 Quantification of the relative amounts ($2^{-\Delta Ct}$) of the m*NOT* transcripts in diverse cell lines

Target \ $2^{-\Delta CT}$	3T3	MOCHA	C127I	BC3H1
m*NOT*-1	0.07	0.14	0.08	0.14
m*NOT*-2	0.12 x10^{-2}	0.18 x10^{-2}	0.07 x10^{-2}	3.26 x10^{-2}
m*NOT*-3	0.38 x10^{-3}	4.34 x10^{-3}	0.32 x10^{-3}	0.77 x10^{-3}
m*NOT*-4	0.16 x10^{-3}	0.14 x10^{-3}	0.16 x10^{-3}	0.17 x10^{-3}
m*NOT*-5	1.09 x10^{-2}	01.31 x10^{-2}	0.47 x10^{-2}	2.80 x10^{-2}
m*NOT*-1a	0.35 x10^{-2}	0.54 x10^{-2}	0.18 x10^{-2}	0.78 x10^{-2}
m*NOT*-1b	0.73 x10^{-3}	0.48 x10^{-3}	0.29 x10^{-3}	1.41 x10^{-3}
m*NOT*-2a	0.37 x10^{-3}	0.46 x10^{-2}	0.21 x10^{-2}	1.32 x10^{-2}
m*NOT*-3a	0.23 x10^{-4}	0.12 x10^{-4}	0.21 x10^{-4}	0.35 x10^{-4}
m*NOT*-3b	0.28 x10^{-3}	0.25 x10^{-3}	0.16 x10^{-3}	0.28 x10^{-3}
m*NOT*-3c	0.13 x10^{-3}	0.14 x10^{-3}	0.11 x10^{-3}	0.15 x10^{-3}
m*NOT*-4a	0.81 x10^{-4}	0.70 x10^{-4}	0.19 x10^{-4}	0.59 x10^{-4}
m*NOT*-4b	0.41 x10^{-5}	0.24 x10^{-5}	---	---
m*NOT*-4c	0.09	0.13	0.1	0.19
m*NOT*-5a	0.39 x10^{-2}	0.49 x10^{-2}	0.19 x10^{-2}	1.35 x10^{-2}

The ΔCt value is determined by subtracting the m*HGPRT* (endogenous reference) C_T-value from the C_T value of the target investigated: $\Delta C_T = C_T$ (m*NOT* target) - C_T (m*HGPRT*); The relative concentration of the target (amount of target), $2^{-\Delta CT}$, is calculated for the average ΔC_T values.

identical in MOCHA and BC3H1 (0.14) (Tab. 65). All other *NOT* variants are expressed at significant lower levels. Regarding the five classes of *NOT* transcripts (Ch. 4.1.1), the expression data shows that in all cells investigated the basic variants 1, 2, and 5 are expressed at a higher level than the derivatives of these forms (Tab. 65). A constant ratio of the amount of the basic variants to the amount of their derivatives could not be detected.

4.9 Identification of m*NOT* and m*ECE2* core promoter elements

To check if the murine *NOT* promoter contains a similar composition of core promoter elements as its human counterpart, the Elements Navigation Tool (ElemeNT; Sloutskin *et al.* 2015) and the Jaspar database (Mathelier *et al*. 2014) were used to predict these elements (Ch. 3.5.1). As the core promoter is always defined relative to the TSS, the region 100nt up- and downstream of the determined m*NOT*-1, m*NOT*-4, and m*ECE2* TSSs (Ch. 4.1.3) were analyzed. The obtained results show that the TSSs for *NOT*-1 and *NOT*-4 are both located at an Initiator (Inr) element (Tab. 66). Other elements were not found (Tab. 66). For m*ECE2* no core promoter elements were detected.

Tab. 66 Potential core promoter elements within the m*NOT* promoter

CPE[1] \ Sequence	*NOT*-1[2]	*NOT*-4[2]	Consensus[3]
Initiator	(-11)5´- GCACTGT	(-110)5´- CCAGAGT	YYANWYY
TATA	---	---	TATAWAAR
BRE^{u}	---	---	SSRCGCC
BRE^{d}	---	---	RTDKKKK
DPE	---	---	DSWYVY
DCE	---	---	N_{5-7}CTTCN$_{7-8}$CTGTN$_{7-11}$AGCN$_{1-2}$

1: Core promoter elements; The BRE element can be located upstream (u) or downstream (d) of the transcription start site (TSS) (Sloutskin *et al*. 2015); 2: Sequence relative to ATG, the identified TSS is underlined; 3: Consensus motifs from Sloutskin *et al*. (2015); N_x: Any base in the next x positions; Y: C or T; W: A or T; R: A or G; S: G or C; D: A or G or T; K: G or T; V: A or C or G. The putative core promoter elements were predicted using the ElemeNT tool (Sloutskin *et al*. 2015). The lack of TATA boxes was confirmed using the Jaspar Database (Mathelier *et al*. 2014).

To validate the lack of TBP-binding core promoter elements and to exclude the binding of TBP independent of these sites *in vivo*, ChIPs were performed using chromatin from 3T3 cells (Ch. 3.5.7). The results show that TBP does not bind the m*NOT* promoter (not shown).

4.10 Identification of transcription factor binding sites in the murine *NOT* promoter

Diverse binding studies revealed that the transcription factors EGR-1 (Ch. 4.4), CREB1 and 3 (Ch. 4.5), NFκB (Ch. 4.6), and MYCN (Ch. 4.7) can bind to the human *NOT* (h*NOT*) promoter and regulate the expression of h*NOT* (Ch. 4.4.6; 4.5.7; 4.5.8; 4.6.4; 4.6.9). To check if this regulation is conserved in mice, the P-MATCH^{TM} algorithm (Chekmenev *et al*. 2005) was used to determine potential binding sites for these factors within 1.15kb promoter region. This analysis yielded identification of 10 putative CREB sites (Tab. 41; Fig. 54A) and 22 putative NFκB sites (Fig. 57A). The binding capacities of the predicted sites were determined using the EMSA, affinity chromatography, and ChIP techniques (Ch. 4.9.1 - 4.9.3). Potential binding sites were also predicted for EGR-1 (3 sites) and MYCN (14 sites), but yielded negative results in ChIPs (not shown). As a consequence, no further binding studies were performed.

4.10.1 Regulation of m*NOT* by CREB1 and CREB3

4.10.1.1 Expression and nuclear activity of CREB1 and CREB3 in murine cell lines

To check the applicability of the 3T3, MOCHA, BC3H1, and C127I cell lines (Tab. 50) for EMSAs

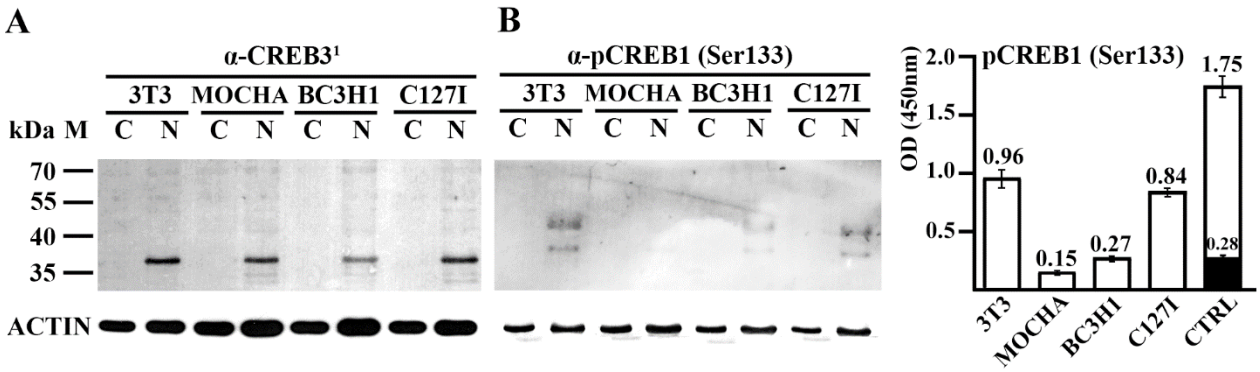

Fig. 53 Expression and nuclear activity of murine CREB1 and CREB3. Cytosolic (C) and nuclear (N) extracts (15µg each) were separated on a 10% SDS-PAGE gel. Detection of CREB3 in **(A)**, CREB1 in **(B)**. Determination of nuclear activity of CREB1 using the CREB (Phospho-Ser[133]) Transcription Factor Assay Kit. Pro well an aliquot of the nuclear extract corresponding to 7.5µg of total protein were loaded. Detection of CREB1 was performed using the TF CREB1 (phospho-Ser[133]) primary antibody provided by the kit. ELISA readout: 3T3: 0.96 (+/- 0.07); MOCHA: 0.15 (+/- 0.009); BC3H1: 0.27 (+/- 0.013); C127I: 0.84 (+/- 0.03); CTRL: 5µl Cayman CREB1 positive control (PC-12 + 10µM Forskolin, 30min., whole cell lysate): 1.75 (+/- 0.08); Competition of 5µl CREB1 positive kit control and 10µl dsDNA shown as black bar: 0.28 (+/- 0.008); blank: 0.12 (+/- 0.02). M: Marker.

and ChIPs (Ch. 4.9.1.2), their CREB1 and CREB3 expression was determined using western blot. The obtained results show a 37kDa CREB3 protein in the nucleus of all four cell lines investigated (Fig. 53A).There are currently no publications regarding murine CREB3, but the high identity of the human and murine CREB3 sequences suggests a similar proteolytic-dependent regulation of CREB3 activity. Thus, the detected 37kDa protein potentially represents the N-terminal cleavage product that mediates DNA-binding. The full-length CREB3 protein is not detectable (Fig. 53A). In the case of CREB1, the murine gene encodes, homologous to man, two isoforms, mCREB1A (NM_133828.2) and mCREB1B (NM_009952.2). As a consequence, immunoblotting performed using the pCREB1 (Ser133) antibody shows a band pattern in the 3T3, BC3H1, and C127I extracts (Fig. 53B) identical to the pattern found in the human cell lines (Fig. 29A). To assess the relative activity of the nuclear CREB proteins, the CREB (Phospho-Ser[133]) Transcription Factor Assay Kit was used (Ch. 3.4.5). The nuclear extracts were incubated with the CRE reference sites immobilized on the plates and CREB binding detected using specific antibodies served as a measure for nuclear activity. The results show that CREB1 has its highest activity in 3T3 and C127I cells and its lowest activity in BC3H1 cells. The measured activity confirms the band intensities observed in the immunoblots (Fig. 53B). CREB1 is not active in MOCHA cells (Fig. 53B). with respect to these observations, the 3T3 and C127I cell lines were chosen for the DNA-binding assays.

4.10.1.2 Identification of CREB1 and CREB3 binding sites in the m*NOT* promoter

To determine which of the 10 predicted CRE sites (three in *cis*, seven in *trans*) (Fig. 54A) can be bound by CREB1 and/or CREB3, EMSAs were performed (Ch. 3.5.3). Protein-DNA complexes were identified by incubating nuclear extracts from 3T3 and C127I cells with biotin btn-labeled ds

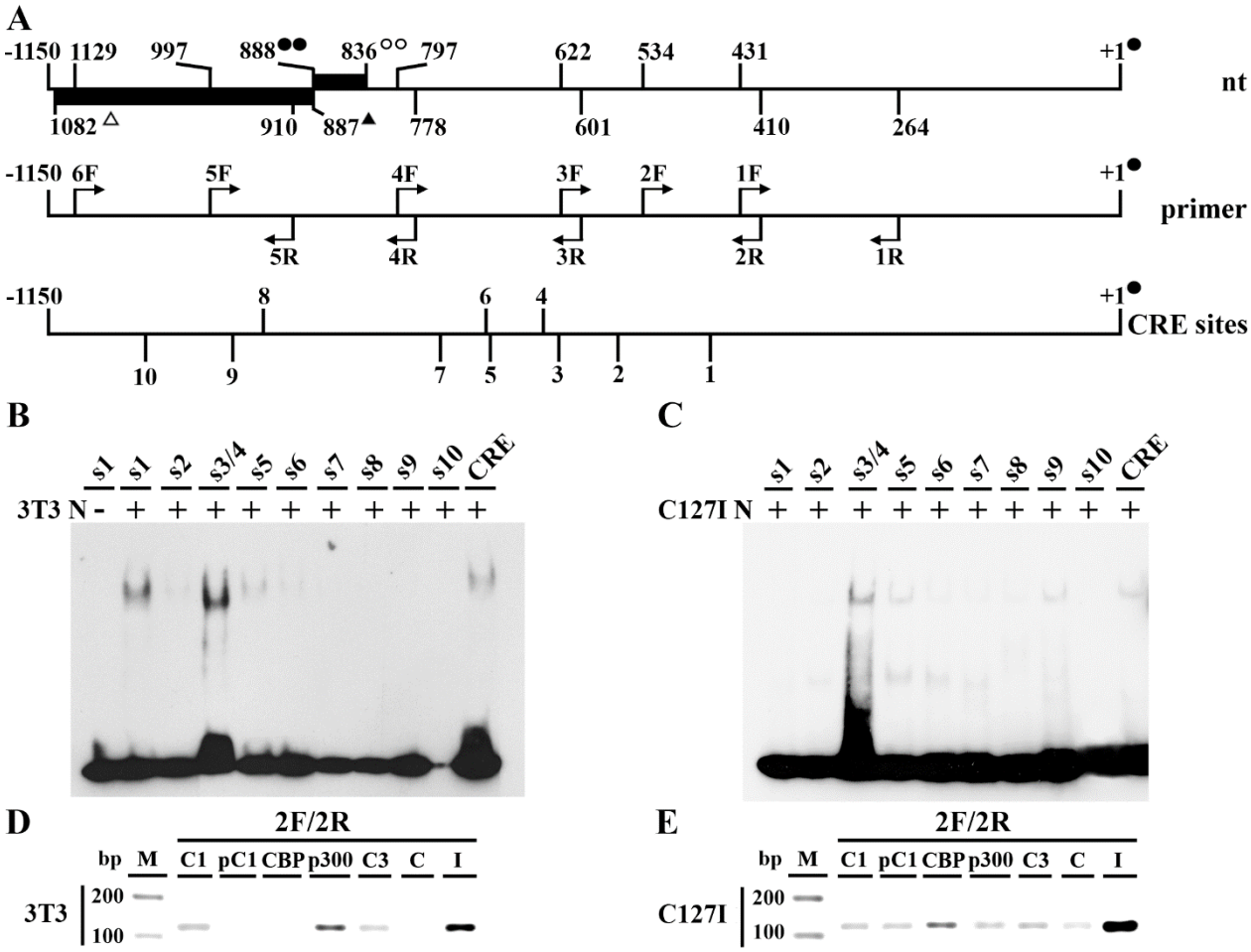

Fig. 54 Identification of CREB binding sites in the m*NOT* promoter. (A) Schematic representa-tion of the 1.15kb m*NOT* promoter region with primers used for ChIP amplification. Positions are upstream the *NOT*-1 start codon (+1/●). The first exon of *NOT*-4 is located from 888nt (●●) to 836nt (○○). The first exon of *ECE2* v1 and v3 is located from 877nt (▲) to 1082nt (Δ). Primer names; F: Forward; R: Reverse. Third bar shows the potential CREB binding sites predicted using the P-MATCH^{TM} algorithm (Chekmenev *et al.* 2005). Sites in *cis* on the upper side, sites in *trans* below. **(B) + (C)** Identification of CREB binding sites using EMSA. The protein-DNA complexes were detected by incubating 7µg nuclear extracts (N) from 3T3 (B) and C127I cells (C) with btn-labeled ds CREB binding sites. Protein-DNA complexes were separated on a 5% native PAGE gel and visualized using chemiluminescence. CREB specificity was determined by using a published CRE reference oligos as comparison (Zhou and Chen 1999). C: Competition with 3000x excess of unlabeled ds oligos. **(D) + (E)** Gel electrophoretic separation (2% agarose gel) of DNA fragments amplified from ChIPs performed using antibodies directed against CREB1, Ser133-phosphorylated CREB1 (pC1), CREB3, CBP, p300, and p53. ChIPs were performed using 3T3 (D) and C127I (E) cells. C: p53 ChIP, negative control; I: Input DNA. M: Marker Gene Ruler 100bp ladder.

oligonucleotides representing the predicted binding sites (Tab. 41). The 3T3 results show shifted complexes for the composite site 3/4 (624-650nt) and the *trans* sites 5 (698-711nt) and 1 (464-479nt) (Fig. 54B). In the case of C127I, the sites 3/4, 5, and the *trans* site 9 (975-988nt) are positive (Fig. 54C). Notably, signals for s5 and s9 are very weak. The detected shifts are identical to the shift observed using the CRE reference site (Fig. 54B+C). The specificity of the reference shift was demonstrated by competition with excess of cold oligonucleotides (Fig. 54B+C). To confirm the EMSA results *in vivo*, ChIPs were performed using the CREB1, pCREB1, CREB3, CBP, and p300 antibodies listed in Tab. 43. Negative control ChIPs were performed with an antibody directed against p53 which cannot bind the *NOT* promoter (Ch. 4.4.1). The comparative analysis of the obtained results revealed that the investigated factors only bind in the region encompassing nts 622-410. Thus, the P2/2-amplified fragment is representative to detect the occupancy of the sites 1 and 3/4. As shown in Fig. 54D, CREB1, CREB3, and p300 bind to this region in 3T3 cells, whereas in C127I cells all investigated factors are present (Fig. 54E). The binding patterns in MOCHA and BC3H1 cells are identical to the results obtained from C127I (not shown).

4.10.1.3 Influence of Brefeldin A on mNOT expression

The data obtained from EMSAs and ChIPs experiments show that CREB3 binds the m*NOT* promoter (Fig. 54). BFA triggers the proteolytic activation of CREB3 in HT-29 and HeLa cells resulting in an upregulation of h*NOT* (Fig. 34+35). To test if this mechanism is also active in mice, 3T3 cells were treated with 2µg/ml BFA for 10min., 30min., and 24h followed by western blot and qRT-PCR analysis. The immunoblots show that mCREB3 is constantly activated at high levels in untreated 3T3 cells (Fig. 53A+55A). As a result, an enrichment of the unstable N-terminal mCREB3 cleavage product after BFA treatment cannot be observed at any time point investigated (Fig. 55A). However, the amount of full-length mCREB3 protein increases after 24h (Fig. 55A). The induction of mCREB3 expression is also illustrated by the drastic rise of m*CREB3* mRNA levels (Fig. 55B). BFA also causes an increase of the full-length mNOT-1 protein (●), its putative post-translational derivate (▲), and the 20kDa cleavage product (◊◊) (Fig. 55A). The putative mNOT cleavage product around 42kDa (♦) remains unaffected (Fig. 55A). In the murine cells the α-NOT 1/4 antibody detects an additional high-molecular, yet unspecified, protein which is also upregulated after 24h BFA treatment (▽, Fig. 55A). On the transcriptional level, BFA-mediated induction in 3T3 cells leads to an increase of m*NOT*-1 expression to 153% of the level observed in

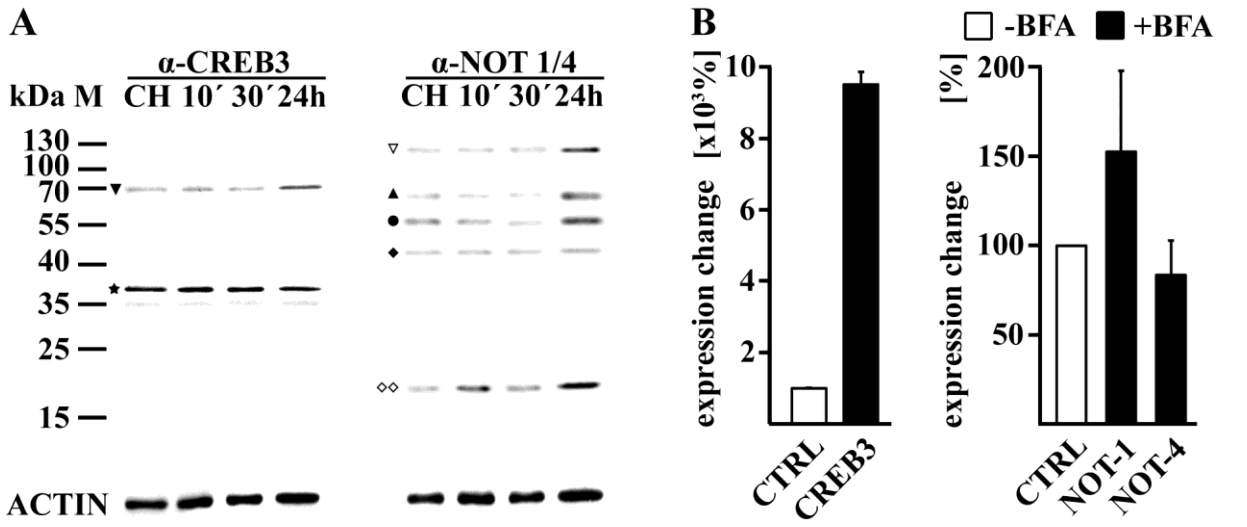

Fig. 55 Brefeldin A treatment of 3T3 cells upregulates mCREB3 and mNOT expression. (A) Immunoblot analysis of mCREB3 and mNOT protein levels after treatment of 3T3 cells with 2µg/ml Brefeldin A (BFA) for the indicated time points. For separation 15µg crude homogenates were loaded on a 10% SDS-PAGE gel. Detection was performed using the α-CREB3 and a-NOT 1/4 antibodies. α-CREB3 detects the full-length, ER-resident glycosylated CREB3 (▼) and an N-terminal cleavage product (★). α-NOT 1/4 detects the full-length mNOT-1 (●), the potential post-translational modified mNOT-1 (▲), the 42kDa cleavage product (♦), the C-terminal cleavage product (◊◊), and a not specified signal (▽). M: Marker. **(B)** Quantification of mRNA levels via qRT-PCR after 24h BFA treatment. The evaluation of the amount of the targets investigated was performed using the comparative ΔΔCt method: $\Delta\Delta C_T = \Delta C_T$ (untreated) - ΔC_T (BFA-treated). The ΔC_T values are standardized to m*HGPRT* used as endogenous control. Relative expression is calculated with respect to the untreated sample as follows: $2^{-\Delta\Delta CT}$ x 100%.

untreated cells (Fig. 55B). The slightly drop of the m*NOT*-4 mRNA level to 84% is not significant.

4.10.2 Regulation of m*NOT* by NFκB

4.10.2.1 Expression and nuclear activity of NFκB in murine cell lines

To choose the appropriate cell line for EMSAs and ChIPs (Ch. 4.9.1.2), the expression of canonical NFκB pathway components was determined in the 3T3, MOCHA, BC3H1, and C127I cell lines (Tab. 50) using western blot (Ch. 3.4.3). In addition, the relative nuclear activity of the p65 subunit was measured in all four murine cell lines using the NF-kB (p65) Transcription Factor Assay Kit (Ch. 3.4.5). The immunoblot analysis revealed the constitutive expression of NFκB (Fig. 56). However, some differences in the levels of the single proteins exist. In 3T3 and MOCHA the p50 protein is present in both, the cytosolic and nuclear fraction, whereas in BC3H1 p50 is only found in the cytosol (Fig. 56A). In C127I cells, p50 is predominantly located in the nucleus (Fig. 56A).

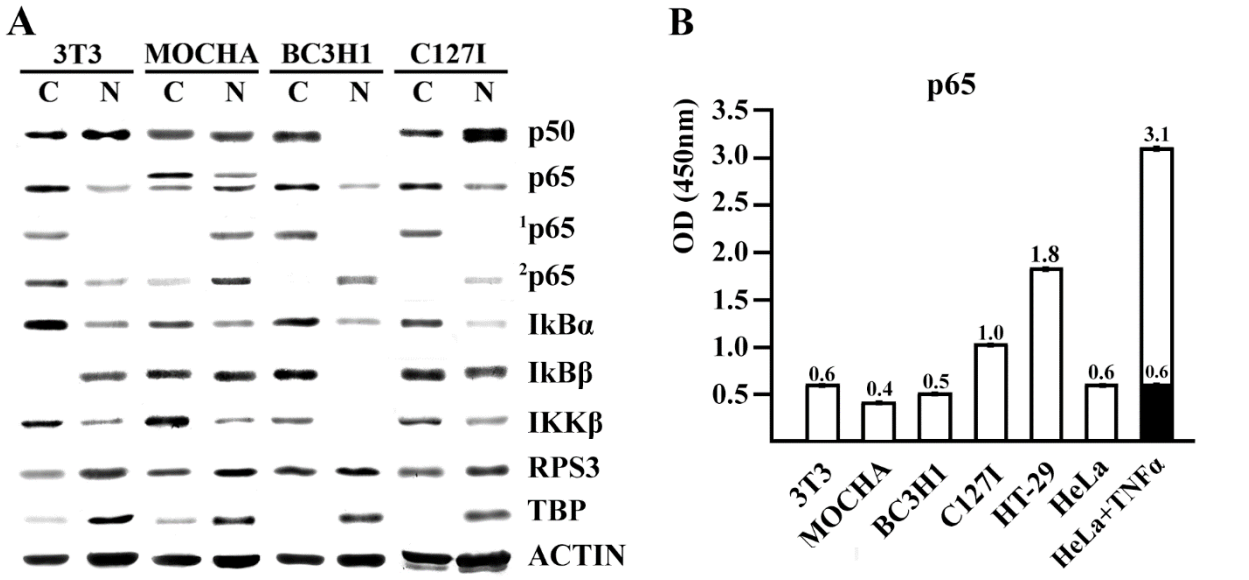

Fig. 56 Expression and nuclear activity of NFκB in different murine and human cell lines. (A) Expression analysis of components of the NFκB pathway using western blot. Cytosolic (C) and nuclear (N) extracts (15µg each) were separated on a 10% SDS-PAGE gel. Indicated proteins were detected using specific antibodies. TBP served as nuclear control. [1]p65: p65-Ser276P; [2]p65: p65-Ser536P. **(B)** Determination of p65 nuclear activity using NF-kB (p65) Transcription Factor Assay Kit. Plates were loaded with 15µg nuclear extract/well. Readout: 3T3: 0.6 (+/-0.01); MOCHA: 0.4 (+/-0.003); BC3H1: 0.5 (+/-0.003); C127I: 1.0 (+/-0.01); HT-29: 1.8 (+/-0.02); HeLa: 0.6 (+/-0.002); HeLa + TNFα, 20ng/ml, 30min. (Cayman p65 positive control, 10µl): 3.1 (+/-0.02); Black bar: Competition of 10µl positive control with 10µl dsDNA (NFκB consensus site): 0.6 (+/-0.001); Blank: 0.24 (+/-0.001)

In contrast to p50, the p65 subunit is expressed at lower levels and, with the exception of MOCHA cells, predominantly resides in the nucleus (Fig. 56A). The second p65 band detected in MOCHA cells presumably represents a post-translational modified form (Fig. 56A). The Ser276-phosphorylated p65 is either found exclusively in the cytosol (3T3, BC3H1, and C127I) or nucleus (MOCHA) (Fig. 56A). The Ser536-phosphorylated p65 is mainly found in the nucleus (MOCHA, BC3H1 and C127I), whereas 3T3 cells contain most of this modified p65 in the cytosol (Fig. 56A). The NFκB cofactor RPS3 is detected in the cytosol and the nucleus of all cell lines with a clear nuclear preference in 3T3, MOCHA, and C127I cells (Fig. 56A). IκBα protein displays a uniform expression pattern with a predominant cytosolic localization in all cell lines, whereas IκBβ shows considerable cell-specific differences (Fig. 56A). In contrast to BC3H1 cells where IκBβ is only detectable in the cytosol, the complete amount of IκBβ is shifted to the nucleus (Fig. 56A). An even nucleocytoplasmic distribution of highly expressed IκBβ can be found in MOCHA and C127I cells (Fig. 56A). The IKKβ kinase is found in all cytosolic fractions and in addition in the nuclei of 3T3, MOCHA, and C127I cells (Fig. 56A). TBP was used as nuclear control (Fig. 56A).

Measurement of the nuclear activity shows that 3T3, MOCHA, and BC3H1 cells exhibit a similar nuclear activity of p65 (Fig. 56B). Because p65 has the highest activity in C127I cells, they were chosen for the binding studies (Ch. 4.9.2.2).

4.10.2.2 Identification of NFκB binding sites in the m*NOT* promoter

Using the P-MATCH^{TM} algorithm (Chekmenev *et al*. 2005) 22 potential NFκB binding sites (11 in *cis*, 11 in *trans*) were predicted in the 1.15kb m*NOT* promoter (Fig. 57A). For the binding

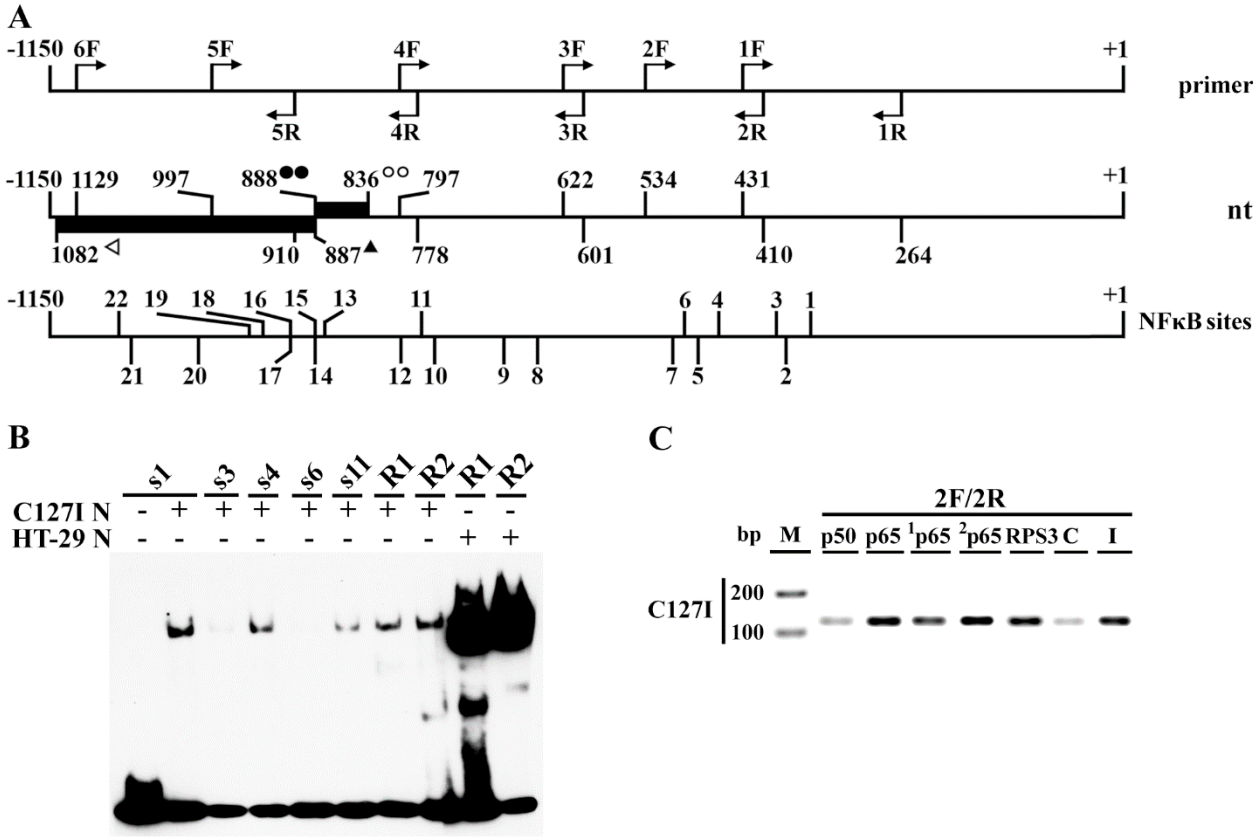

Fig. 57 Identification of NFκB binding sites in the m*NOT* promoter. (A) Schematic representation of the 1.15kb m*NOT* promoter region with primers used for ChIP amplification. Positions are upstream the *NOT*-1 start codon (+1/●). The first exon of *NOT*-4 is located from 888nt (●●) to 836nt (○○). The first exon of *ECE2* v1 and v3 is located from 877nt (▲) to 1082nt (Δ). Primer names; F: Forward; R: Reverse. Third bar shows the potential NFκB binding sites predicted using the P-MATCH^{TM} algorithm (Chekmenev *et al.* 2005). Sites in *cis* on the upper side, sites in *trans* below. **(B)** Identification of NFκB binding sites using EMSA. The protein-DNA complexes were detected by incubating 7µg nuclear extracts from C127I cells (N) with btn-labeled ds NFκB binding sites. Protein-DNA complexes were separated on a 5% native PAGE gel and visualized using chemiluminescence. NFκB specificity was determined by using a published CRE reference oligos as comparison (Zhou and Chen 1999). C: Competition with 3000x excess of unlabeled ds oligos. **(C)** Gel electrophoretic separation (2% agarose gel) of DNA fragments amplified from ChIPs performed using antibodies directed against p50, p65, Ser276 and Ser536-phosphorylated (P) p65, CBP, p300, and p53. ChIPs were performed using chromatin from C127I cells. p65^{1}: Ser276P; p65^{2}: Ser536P; C: p53 ChIP, negative control; I: Input DNA. M: Marker Gene Ruler 100bp ladder.

analysis using EMSA (Ch.3.5.3) the five *cis* sites that are located between the ATGs of m*NOT*-1 and m*ECE2* (s1, s3, s4, s6, and s11; Tab. 40) were analyzed. Protein-DNA complexes were identified by incubating nuclear extracts from C127I cells with biotin btn-labeled ds oligonucleotides representing the predicted binding sites. Positive results have been obtained for sites 1 (357-344nt), 4 (456-447nt), and 11 (774-760nt) (Fig. 57B). Because of their localization downstream the first exon of m*NOT*-4, these sites most likely regulate the transcription of m*NOT*-1. The NFκB specificity of the shift was determined in a control reaction performed using NFκB reference oligos (Ron *et al*. 1990; Armstrong *et al.* 1993) and nuclear extracts from HT-29 as comparison. The intensities of the detected shifts indicate that the murine NFκB has a lower binding affinity as compared to its human counterpart (Fig. 57B). To confirm the *in vitro* binding results for NFκB *in vivo,* ChIPs were performed (Ch. 3.5.7). The p50, p65, phospho-p65, and RPS3 antibodies used for ChIPs are listed in Tab. 43. Negative control ChIPs were performed with an antibody directed against p53 transcription factor which cannot bind the *NOT* promoter. The primers used for the amplifications are listed in Tab. 23 and Fig. 57A. The only positive signal was obtained in C127I for the P2/2-amplified 534-431nt fragment encompassing sites 1 and 4 (Fig. 57C). This region can be bound by all investigated factors. Similar results were found for NFκB in 3T3, MOCHA, and BC3H1 cells where no RPS3 could be detected (not shown).

5 Discussion

Recent research in the Kurzik-Dumke laboratory towards the human *NOT* gene (Kurzik-Dumke and Kaymer 1996; B. Hacker, PhD thesis: Beitrag zur Aufklärung der zellulären Rolle des humanen *neighbour of tid* (*not*) Gens, 2016), the homologue of the *Drosophila* gene *l(2)not* (Kurzik-Dumke *et al*. 1997), substantiates its relevant role in diverse cellular processes. To gain further insight into the function(s) of *NOT*, this thesis focuses on the elucidation of the yet unknown regulatory mechanisms controlling the expression of the human and murine *NOT* genes. For this purpose, bioinformatics tools and the Y1H technique were used to identify *NOT* promotor DNA binding factors. This analysis identified the transcription factors EGR-1, CREB3, NFκB, and MYCN to bind within the putative 1.15kb *NOT* promoter region. The binding was confirmed in both species and the binding sites for each factor have been identified using diverse *in vitro* and *in vivo* techniques. The impact of the detected protein-DNA interactions for *NOT* expression was assessed using RNAi (for EGR-1 and NFκB), pharmacological activation or inhibition of the respective transcription factor (TNFα and Parthenolide for NFκB, BFA for CREB3), or overexpression (CREB3).

5.1 Multiple *NOT* transcripts are degraded by the NMD pathway

In the frame of this thesis thirteen novel human *NOT* transcript variants were identified. Sequence analysis revealed that these transcripts are made up from the combinatorial use of 10 different exons, whereas exon 1 and 2 are mutually exclusive. All *NOT* transcripts can be seen as derivatives of either *NOT*-1 or *NOT*-4. Notably, the only variants containing a full-length ORF are *NOT*-1, -1a, -1b, -4, -4a, and -4b. All other transcripts harbor a premature stop/termination codon (PTC), a phenomenon shared by about 30% of all human transcripts (Lewis *et al*. 2003; Green *et al*. 2003). The qRT-PCR analysis proved that all *NOT* isoforms are expressed in all investigated cell lines at different levels. The bioinformatical analysis using the RegRNA2.0 web tool (Chang *et al*. 2013; http://regrna2.mbc.nctu.edu.tw/) revealed the presence of two upstream ORFs (uORFs; Wethmar 2014) and one Musashi binding element (MBE; MacNicol *et al*. 2011) in the 5´-UTRs of *NOT*-4. Both elements are described as translational inhibitors or to restrict translation to distinct time points during early differentiation and cell fate specification as well as to self-renewing mammalian stem cells (Wethmar 2014; MacNicol *et al*. 2011). In addition, the identified Kozak sequences (Kozak 2005) indicate that *NOT*-1 is more efficiently translated as *NOT*-4. However, the functional

relevance of these elements has to be determined in further experiments.

Because PTC-containing transcripts can have dominant-negative or deleterious gain-of-function effects if they are translated into truncated proteins, they are removed by an evolutionary conserved quality control mechanism called the nonsense-mediated mRNA decay (NMD) (Chang *et al*. 2007). The pharmacological inhibition of the NMD pathway by caffeine results in the enrichment of all PTC-containing *NOT* transcripts. This indicates that these *NOT* variants are constantly degraded under normal conditions by the NMD pathway and thus have no physiological function in HaCaT, HT-29, T98G, and HeLa cells. They rather represent the outcome of randomly occurring erroneous background splicing events. Interestingly, *NOT*-1a and -1b, which contain a terminal stop codon, are also enriched after caffeine treatment. Similar observations were made for other genes, however the mechanism is not fully understood yet (Maquat 2004). In addition to the original concept of NMD as an exclusive means to clear aberrant transcripts from the cell, growing evidence indicates the importance of this pathway for gene regulation (Maquat 2004; Lareau *et al.* 2007). Pan *et al*. (2006) discovered that many PTC-containing transcripts are conserved between man and mouse and suggested as a consequence that these transcripts have a functional role, because otherwise evolutionary pressure would have selected against them. In this view, the simultaneous generation of unproductive PTC-containing isoforms reduces productive translation to fine-tune gene expression (Lareau *et al.* 2007). The relevance of this mechanism for *NOT* regulation is corroborated by the identification and isolation of diverse similar yet undiscovered PTC-containing *NOT* variants in mice. Nevertheless, it requires further investigation to determine which of the transcripts originates from transcriptional and/or splicing noise and which transcript is to what extent integrated in the process of gene regulation.

5.2 The *ECE2*-overlapping *NOT* promoter region shares pivotal features of alternative promoters

The RACE experiments revealed that the transcription of the human *NOT* gene is initiated from two different TSSs. The TSS for *NOT*-1 is located 23nt upstream its ATG (termed T^{N1}), the TSS for *NOT*-4 285nt upstream its ATG (termed T^{N4}). The presence of two TSSs argues for the generation of two distinct *NOT* pre-mRNAs with non-overlapping alternative first exons from which all other isoforms are generated via alternative splicing. In all cell lines investigated the mRNA levels of *NOT*-1 are significantly higher than the levels of *NOT*-4. Notably, upstream T^{N1}

and downstream T^{N4} three NFκB, one EGR-1, one CREB3, and two MYCN *cis* binding sites are used *in vivo*, whereas in the region upstream of T^{N4} three occupied NFκB sites were found. If one takes into account that TSSs define the downstream boundaries of functional promoters (Sandelin *et al*. 2007) and that Pol II-transcribed genes normally do not contain transcription factor binding sites downstream their TSSs (Maston *et al*. 2006), these findings suggest the existence of two different (or alternative) *NOT* promoters that regulate the transcription of two *NOT* pre-mRNAs with a different strength. In this view, the three NFκB sites downstream T^{N4} (site 13/12, 4/3, and 1) as well as all detected binding sites for EGR-1, CREB, and MYCN are constituent parts of the *NOT*-1 promoter, whereas the *NOT*-4 promoter contains three NFκB binding sites located within the coding region of *ECE2* (sites 22/21, 19/18, and 17/16). However, the available data is not sufficient to define the complete region for the two *NOT* promoters. Both, *NOT*-1 and *NOT*-4, are simultaneously upregulated by the sustained activation of CREB3 or downregulated after the RNAi-mediated silencing of EGR-1. Thus, there have to exist further yet unidentified CREB3 and EGR-1 binding sites upstream the analyzed 1.15kb promoter region which are involved in the regulation of *NOT*-4. In addition, more experiments are needed to clarify if the *NOT*-1 promoter only encompasses the genomic region between the two TSSs or if *NOT*-1 is also regulated by factors which bind to sites upstream T^{N4}.

The complexity of the *NOT* promoter region is further increased by its close proximity to the *ECE2* gene, which has its TSS 33nt upstream ATG (termed T^{E}) or, with respect to the position of *NOT*, 100nt upstream of T^{N4} on the complementary strand. The localization and orientation of the two genes in combination with the position of their TSSs indicates that the *ECE2* and *NOT* promoter regions overlap. The three promoter model is also corroborated by the pattern of promoter-specific histone modifications deduced from available ChIP-seq data generated in the context of the ENCODE project (ENCODE project consortium 2012; www.genome.gov/10005107/encode-project/). Notably, none of the investigated factors affects the expression of *ECE2* indicating their irrelevance for the regulation of this gene. This observation also argues against the bidirectional operating mode of the nested *ECE2-NOT* promoters, which would entail a co-regulation of both genes (Yang and Elnitski 2014). As a consequence, the available data does not allow to define the *ECE2* promoter region. The overall three promoter architecture is also found in mice, nevertheless there are some differences. First, the distance between the first exons of m*NOT*-1 and m*ECE2* is 133nt longer and, second, the ATGs of m*NOT*-4 and m*ECE2* are partially overlapping. Thus, the second *NOT* promoter is completely located within the coding region of

m*ECE2*. In addition, all so-far identified binding sites for NFκB, EGR-1, CREB3, and MYCN are located within the m*NOT*-1 promoter. Whether the m*NOT*-4 promoter also encompasses binding elements for these factors has to be investigated.

The existence of alternative promoters is a conserved feature for nearly half of all mammalian genes (Baek *et al*. 2007). In the simplest form alternative promoters can be interpreted as a means to produce isoforms with distinct N-termini to modulate protein function and/or sub-cellular localization (Landry *et al*. 2003). A striking feature of alternative promoters is their direct influence on the splicing process (Pal *et al*. 2012). There is growing evidence that genes with alternative promoters exhibit increased alternative splicing with a bias to select distinct splice sites over others depending on the promoter the pre-mRNA was described from (Xin *et al*. 2008; Pal *et al*. 2011). The detection of the diverse *NOT* variants supports this observation, but the details of their generation remain unclear. In addition, the usage of alternative promoters allows a more versatile control of gene expression in a tissue and cell-specific or development time/stage-specific manner (Pal *et al*. 2012). Although the context-dependent promoter selection is still not fully understood, it has been suggested that structural variations of the core promoter have a relevant impact (Pal *et al*. 2012). Distinct combinations of core promoter elements may favor the assembly of different PIC components which enhance or limit the regulatory input of distal promoters (Lenhard *et al*. 2012). In the case of *NOT*, both promoters contain an Inr element but lack TATA boxes or BRE sequences. Inr elements are often found in the core promoters of ubiquitously expressed or housekeeping genes in contrast to the cooperating TATA and BRE elements which are linked to tissue-specific genes (Roy and Singer 2015). This model is in accordance with the widespread expression of *NOT* (Asmann *et al*. 2012; Djebali *et al*. 2012). In addition, the *NOT*-1 promoter contains a DPE element and the *NOT*-4 promoter a MTE element. DPE and MTE elements are dependent of and act in cooperation with Inr elements to fine-tune transcription levels (Juven-Gershon and Kadonaga 2010). The detection of TBP on chromatin fragments encompassing these sites in ChIP experiments indicates that they are used *in vivo*. However, if these two elements actually recruit different components of the PIC and if this accounts for the observed differences in promoter strength needs further investigation. In the mouse, the two *NOT* promoters contain Inr sequences but lack any other core promoter element. The finding that a plethora of vertebrate genes, including housekeeping genes, do not contain any core promoter elements lead to the hypothesis that epigenetic marks may replace the classical sequence-dependent promoter selection (Roy and Singer 2015). Whether or not this also applies for murine *NOT* promoters has to be examined.

5.3 *NOT* is regulated by EGR-1, NFκB, CREB3, and MYCN in a cell-specific manner

The performed DNA-binding analysis demonstrated the binding of the transcription factors NFκB, CREB, EGR-1, and MYCN to diverse *cis* and *trans* sites within the overlapping *NOT-ECE2* promoter region *in vitro*. The ChIP experiments performed using the cell lines HaCaT, HT-29, HeLa, and T98G demonstrated that varying combinations of the EGR-1, CREB3, NFκB, and MYCN transcription factors and their cofactors CBP, p300, and RPS3 bind to distinct sites depending on the cell. Because the qRT-PCR analysis showed that the modulation or silencing of the NFκB, CREB3, and EGR-1 transcription factors only affects the expression of *NOT* but not *ECE2*, all *in vitro*-detected *trans* binding sites (or the *trans* parts of the complementary sites) are irrelevant *in vivo*. As a consequence, the detected *in vivo*-binding patterns of NFκB, CREB3, and EGR-1 solely reflect the varying occupancy of *NOT*-regulating *cis* elements. Notably, the ChIPs indicate binding of CREB3 to the *trans* CRE site 16 (710-724nt) and of CREB1, CBP, and p300 to the *trans* CRE site 1 (+2-10nt) in all four cell lines. As mentioned above, all analyses towards *ECE2* were conducted with respect to its isoforms 1 and 3, because they encompass the *NOT* neighboring exon. It cannot be excluded that the occupancy of these two *trans* sites is part of the regulation of the other *ECE2* variants.

In all cell lines investigated CREB3 binds its target site at nts 217-206 (site 7). In contrast, the binding of EGR-1 at nts 330-312 (site 4) and of Ser54-pohsphorylated MYCN to a fragment containing the sites at nts 184-173 (site 3) and 80-69 (site 1/2) is only observed in HaCaT, HT-29 and HeLa cells. Notably, the ChIP results for MYCN do not allow to discern if both or only one of the detected site is bound. The most complex binding pattern is observed for NFκB. In general, NFκB can use the binding elements at nts 973-951 (site 22/21), 789-776 (site 19/18), 768-755 (site 17/16), 638-624 (site 13/12), 339-330 (site 4/3), and 223-214 (site1), but the occupancy of these sites as well as the composition and phosphorylation status of the bound NFκB dimers varies significantly between cells. In the case of the closely located sites 19/18 and 17/16 the obtained ChIP signals do not allow to discern if NFκB binds both or only one site. For simplicity, both sites together will be referred to as site 19-16 in the following. NFκB binds the sites 22/21, 13/12, and 4/3 in all tested cell lines. The sites 19-16 and 1 are only bound in HaCaT, HeLa, and T98G cells. Regarding the composition of NFκB, sites 22/21 and 13/12 are always bound by p50:p65 heterodimers, whereas sites 19-16, 4/3, and 1 can be bound by p50:p65 heterodimers or p65 homodimers. Notably, in all cells except HeLa at least one of the sites is bound by a p65

homodimer. The only element which is always occupied by exactly the same proteins is site 13/12 which is bound by a p50:p65 heterodimer with double-phosphorylated p65 (at Ser276 and Ser536). An almost identical pattern is also observed for site 22/21 which only differs in HeLa cells where p65 is mono-phosphorylated at Ser276. The site 19-16 is bound by p65 homodimers in HaCaT and T98G cells, but by a p50:p65 homodimer in HeLa cells. In all cases p65 is phosphorylated at both serines. Site 4/3 is bound by a p50:p65 heterodimer in HeLa, HaCaT, and T98G cells. At this site the p65 subunit is phosphorylated at Ser276 in HaCaT cells, at Ser536 in HeLa cells and at both residues in T98G cells. In contrast, site 4/3 occupied by a double-phosphorylated p65 homodimer in HT-29 cells. Site 1 is occupied by a p50:p65 heterodimer with double-phosphorylated p65 in HeLa and T98G cells but with a p65 homodimer mono-phosphorylated at Ser276 in HaCaT cells.

All NFκB signals are accompanied by signals of its cofactor RPS3. Because RPS3 mediates the preferential recruitment of p50:p65 and p65:p65 dimers to the promoters of selected target genes and enhances the DNA-binding and transactivation of p65 (Wan *et al*. 2007), this data suggests that *NOT* belongs to the group of RPS3-dependent NFκB target genes. However, RPS3 can also act as DNA-binding protein (M. Szydlowski, PhD thesis: Identification of the regulatory elements and factors of the human tumor suppressor gene *tumorous imaginal discs*, 2011). The data presented here indicates that RPS3 might function in both ways within the alternative *NOT* promoters. Although the ChIP results are negative for NFκB at site 19-16 in HT-29 cells, the amplified 912-686nt fragment still contains bound RPS3. This finding suggests that RPS3 acts as NFκB-independent transcription factor within the *NOT*-4 promoter. Support for this view comes from the RNAi experiments. Depletion of RPS3 leads to an almost doubled *NOT*-4 transcript level, whereas knockdown of p65 has no effect. In contrast, *NOT*-1 is slightly reduced to a comparable level in RPS3 and p65 depleted cells. Thus, RPS3 most likely represents a NFκB-independent negative regulator of *NOT*-4, but, as part of NFκB, a positive regulator of *NOT*-1. If this functional diversification of RPS3 is really that splice form-specific, needs further investigation. It cannot be ruled out that the observed impact NFκB has on the expression of *NOT*-4 also depends on RPS3. Moreover, the Y1H results indicate that RPS3 not only binds within the *NOT*-4 promoter but also within the *NOT*-1 promoter. If this is the case *in vivo*, needs further investigation. In addition, the exact binding site(s) of RPS3 have to be determined.

The acetyltransferases CBP and p300 are bound in all cell lines investigated. Because both proteins are described as binding partners of, among others, CREB1 (Yuan and Gambee 2001), NFκB (Zhong *et al*. 1998), and EGR-1 (Silverman *et al*. 1998), the ChIP results do not allow to

clearly discern which of the factor(s) is associated with either or both of the coactivators. However, the cell-specific binding patterns provide a bias for the actual bound transcription factor. CBP and p300 signals are detected in the region encompassing the NFκB site 1 and the closely located *trans* CRE site 1. Because CREB1, CBP, and p300 are bound in all cells, whereas NFκB is not in HT-29 cells, CBP and p300 are most likely associated with CREB1. Similar observations are made for the NFκB site 4/3 which partially overlaps with the EGR-1 binding site 4. EGR-1, CBP, and p300 are detected at this position in HaCaT, HT-29, and HeLa cells but not in T98G cells, whereas NFκB is bound in all four cells. Thus, the two cofactors are most likely associated with EGR-1. All other CBP and p300 signal can be linked to bound NFκB complexes. CBP and p300 modulate the NFκB activity at site 13/12 in all cell lines and at sites 22/21 and 19-16 in HaCaT and HeLa cells. The NFκB dimers bound to site 22/21 in HT-29 and T98G and to site 19-16 in T98G act independent of CBP and p300. In general, CBP and p300 can contribute to *NOT* transcription by acetylating the identified *NOT* regulators, by modifying chromatin or by acting as scaffold for more efficient recruitment of further yet unidentified regulators and/or the polymerase complex. Which of these mechanisms applies to what extent for the regulation of *NOT* needs further investigation.

The described transcription factor binding patterns indicate that CREB3 and NFκB together with RPS3, CBP, and p300 are general, cell-independent regulators of *NOT*. In contrast, the regulation of *NOT* by EGR-1 and MYCN is cell-specific. Although it is tempting to link these patterns to the expression of the *NOT* transcripts, the current data is not sufficient to explain the differences in the measured mRNA levels. To pick one example, *NOT*-1 is evenly expressed in HT-29 and HeLa cells which share the same binding pattern for CREB3, EGR-1, and MYCN but significantly differ in NFκB binding. Thus, there have to exist additional yet unidentified regulatory mechanisms which influence *NOT* transcription.

The binding of NFκB, RPS3, CREB3, CREB1, CBP, and p300 was also detected within the m*NOT* promoter. However, the murine promoter contains less binding sites as its human counterpart. EGR-1 and MYCN were not detected. In the case of the CREB proteins two CRE elements were positive in the *in vitro* DNA-binding assays: the *cis* site 4/3 (624-650nt) and the *trans* site 1 (464-479nt). ChIPs performed using MOCHA, BC3H1, and C127I cells revealed binding of CREB3, CREB1, CBP, and p300 to a fragment encompassing both sites in all cell lines. 3T3 share the same pattern with the exception of CBP. Because the relative position of the murine *trans* site resembles the one of the CREB1-bound *trans* site in the human promoter (downstream the CREB3-binding *cis* site and upstream the *NOT*-1 ATG), it is assumed that this site is also bound

by CREB1 in mice. As a consequence, site 4/3 is considered to be bound by CREB3. In the immediate vicinity, NFκB binds two sites *in vitro*: site 1 (357-344nt) and site 4 (456-447nt). The ChIPs revealed binding of p50 and double-phosphorylated p65 to a fragment encompassing both sites in all cells. RPS3 was only detected in C127I cells on the same fragment. The ChIPs do not allow to state which of the NFκB sites is bound by what dimer. Furthermore, the close arrangement of the CRE and NFκB sites does not allow to clearly ascribe the CBP and p300 signals to either of the factors. Notably, all positive sites reside within the m*NOT*-1 promoter. As BFA treatment only affects m*NOT*-1, the analysis towards CREB3 binding sites is complete. However, further experiments are required to determine relevant binding elements for the regulation of m*NOT*-4.

5.4 CREB3 regulates *NOT* under physiological and Golgi stress conditions

Recent experiments in the Kurzik-Dumke laboratory demonstrated that the ATF6-related transcription factor CREB3 interacts with NOT (B. Hacker, PhD thesis: Beitrag zur Aufklärung der zellulären Rolle des humanen *neighbour of tid* (*not*) Gens, 2016). The evolutionary conserved CREB3 (cAMP responsive element binding protein 3, Luman, lZIP) belongs to the CREB/ATF family of basic leucine zipper (bZIP) domain containing transcription factors (Ortega-Martinez 2015). Within this family, CREB3 and four other structurally related proteins (CREB3L1/OASIS, CREB3L2/BBF2H7, CREB3L3/CREB-H, and CREB3L4/CREB4/AIbZIP/JAL/hJAL/ATCE1) constitute the CREB3 subfamily of membrane bound bZIP transcription factors with critical roles in regulating development, metabolism, secretion, survival, and tumorigenesis (Chan *et al*. 2011). The results presented here show that CREB3 also binds the *NOT* promoter and positively regulates the expression of *NOT* under normal and specific Golgi stress conditions.

The *in vitro* and *in vivo* DNA-binding studies revealed that CREB3 binds to the 5´- TGAG GAGT CREB response element (CRE) located at nts 217-210 (site 7). As compared to the canonical CRE element (5´- TGACGTCA), which consists of two half-sites (TGACG/CGTCA), site 7 contains only one half-site (TGAGG). CREB proteins activate transcription from different CRE elements at the same level, irrespective of whether they comprise two half-sites or a single half-site (Muchardt *et al*. 1990). However, the composition influences the level of gene expression in the absence of CREB proteins, because other factors like c-Fos and c-Jun, which share a similar binding site (5´-TGACT), can occupy CRE sites and drive transcription (Muchardt *et al*. 1990). Whether this applies for site 7 needs further investigation. Notably, CREB3 has been reported to

bind unfolded protein response (UPR) elements (DenBoer *et al*. 2005) or ER stress response elements (ERSE) upon distinct ER stress signals (Liang *et al*. 2006). Such binding sequences are found within the promoters of ER stress associated genes and govern the activation of a specific recovery program to overcome ER stress symptoms (Dufey *et al*. 2014). However, none of these elements is found within the 1.15kb *NOT* promoter region. Because CREB3 binds via a CRE site to the *NOT* promoter, *NOT* most likely does not represent an ER stress-related gene. This is also illustrated by the finding that the prototypic UPR transducer ATF6 (CREBL1) cannot bind the *NOT* promoter.

The activation of CREB3 requires its proteolytic processing via a mechanism termed regulated intramembrane proteolysis (RIP) (Raggo *et al*. 2002). This mechanism includes the transport of CREB3 to the Golgi apparatus in COP-II-coated vesicles followed by the sequential activity of the site 1 and site 2 proteases (S1P and S2P) which generate an unstable and rapidly degraded 231aa N-terminal CREB3 fragment with DNA-binding activity (Raggo *et al*. 2002; Nadanaka *et al*. 2007; Chan *et al*. 2011). Using diverse CREB3 deletion constructs and the Y1H technique the DNA-binding properties of this fragment were confirmed and refined by showing that the DNA-binding properties of CREB3 only depend on aa155-231 and not the N-terminus as a whole. The binding of the N-terminus was also confirmed by affinity chromatography. Notably, all published data regarding CREB3 activation is based on experiments performed using diverse cell lines overexpressing this protein under induced ER stress conditions. The herein reported detection of the N-terminal CREB3 fragments in the nuclei of untransfected HaCaT, HT-29, T98G, HeLa, and HEK293 cells shows that CREB3 is also activated under physiological conditions. The *in vivo*-binding of CREB3 at nts 217-210 in HaCaT, HT-29, T98G, and HeLa cells corroborates this finding and demonstrates the relevance of CREB3 for the regulation of *NOT* in unstressed cells. Furthermore, the constant activity of the RIP mechanism in unstressed cells helps to explain why HEK293 cells overexpressing CREB3 enrich the processed protein in their nuclei resulting in the upregulation of *NOT*-1 and -4.

To date, the only reported CREB3 activators are the Golgi compromising agents GCA, Exo1, monensin, Thapsigargin, and BFA, with the latter being the most studied (Liang *et al*. 2006; Reiling *et al.* 2013). The fungal macrocyclic lactone BFA disrupts the function of the ADP-ribosylation factor (ARF) family of guanosine triphosphatases (GTPases) via interaction with their exchange factors (GEFs) (Reiling *et al.* 2013). Since ARFs fulfil essential roles in ER-Golgi cargo transport and endocytosis (Reiling *et al.* 2013), their functional inactivation results in the reversible

disassembly/collapse of the Golgi leading to the redistribution of Golgi proteins (including S1P and S2P) within the ER (Oslowski and Urano 2011). The relocated S1P and S2P proteins can then cleave CREB3 directly in the ER. This mechanism is also functional in untransfected HT-29 and HeLa cells. BFA exposure causes the time-dependent cleavage of endogenous CREB3 and the nuclear enrichment of its N-terminal fragment after 24h. In addition, BFA also leads to an upregulation of CREB3 on the transcriptional and translational level. The only so-far identified transcriptional regulator of CREB3, NFκB (Jang *et al*. 2007), is not activated by BFA in HT-29 and HeLa cells. Thus, there have to exist other yet unidentified BFA-induced CREB3 regulators. The BFA-mediated CREB3 activation is accompanied by an upregulation of the *NOT*-1 and -4 mRNAs, but on the protein level only NOT-1 increases. The NOT-4 protein and its cleavage products cannot be detected. This observation might depend on the stability or turnover of NOT-4. However, it remains possible that *NOT*-4 is also regulated on the translational level. Interestingly, BFA is not able to activate CREB3 or upregulate *NOT* in HEK293 cells suggesting a cell-specific sensitivity towards BFA. This sensitivity might be given by the fact that the HEK293 cell line was immortalized via transfection of type-5 adenoviruses (Graham *et al.* 1977). Gallimore and Turnell (2001) speculated that adenoviruses of this type can dynamically regulate Golgi (dis-) assembly processes. In this view the cellular activity of the adenovirus would counteract the BFA-mediated Golgi collapse to some extent.

BFA has been reported to induce apoptosis in MCF-7 breast cancer cells by increasing the expression of p53 via activated NFκB (Lin *et al*. 2011). This observation could not be confirmed in HT-29 and HeLa cells. Despite the BFA-mediated decrease of IκBα in both cell lines and the simultaneous increase of p50 (in HT-29 and HeLa) and p65 (in HT-29), the NFκB subunits are not shifted into the nucleus. It remains elusive whether the nuclear translocation is prevented by other IκB proteins compensating IκBα function or by the BFA-mediated blocking of the nuclear shuttling mechanism. Interestingly, IκBα is also lost in cells overexpressing CREB3 indicating its possible downregulation not degradation in BFA-treated cells. Nevertheless, BFA triggers the upregulation of p53 which is accompanied by a reduction of proliferation in HT-29 and HeLa cells. This suggests that p53 is not activated to elicit apoptosis but orchestrates growth arrest (reviewed in Zilfou and Lowe 2009), which would provide a distinct time window for Golgi recovery. Since no compromised cells have been detected, their detachment from the surface solely results from the loss of adhesion molecules whose availability depends on the secretory pathway. This is in line with the reported anti-apoptotic effects of overexpressed CREB3 (Liang *et al*. 2006). Whether the

BFA-induced upregulation of NOT has a functional relevance for antiapoptotic processes, the enhancement of stress tolerance and/or the reconstitution of the secretory pathway and Golgi homeostasis needs further experimental verification.

The *in vitro* and *in vivo* DNA-binding studies also revealed that CREB3 binds the 5´-TGACCAGG CRE site at 633-626nt (site 4) in the m*NOT* promoter. Like the CREB3 binding site in the human promoter, this element contains only one half site. Although the only available publications concerning murine CREB3 do not address its activation (Burbelo *et al*. 1994; Lan *et al*. 2013), the structural homology indicates that CREB3 is also processed via the RIP mechanism in mice. The exclusive detection of the cleaved N-terminal CREB3 fragments in the nuclei of 3T3, MOCHA, C127I, and BC3H1 cells supports this notion and also indicates, as compared to men, a higher activation in unstressed cells. The binding of CREB3 to the site at 633-626nt *in vivo* shows the relevance of this interaction for the regulation of m*NOT* under physiological conditions. In accordance with the findings from human cell lines, the treatment of 3T3 cells with BFA leads to an upregulation of m*NOT* after 24h. However, only m*NOT*-1 increases, whereas m*NOT*-4 remains unaffected. Notably, this finding cannot reliably attributed to the activity of CREB3. BFA induces *CREB3* transcription in 3T3 cells, but the processing of the protein was not observed. It requires further investigation to clarify whether BFA actually can elicit CREB3 activation in 3T3 cells at all or whether the basal, high-level CREB3 activity prevents the visible enrichment of the N-terminus. It remains possible that other BFA-induced factors drive the transcription of m*NOT*.

5.5 *NOT* is regulated by the products of the mitogen-dependent immediate early genes *EGR-1* and *MYCN*

Immediate early genes (IEGs) or primary response genes are a specific class of genes that are rapidly and transiently activated as response to extracellular proliferation signals like mitogens, growth factors and hormones without requiring prior protein synthesis (Herschman 1991). Prototypic IEGs are members of the *Fos*/*Jun*, *MYC*, and *EGR* gene families which code for transcription factors that govern distinct gene expression programs for proliferation, differentiation, metabolism, and the immune response (Herschman 1991; Healy *et al*. 2013). The data presented here shows that the products of two IEGs, EGR-1, and MYCN, regulate the expression of *NOT in vivo* via direct interaction with the genes promoter. Furthermore, EGR-1 exhibits a mitogen-dependent *NOT* promoter binding pattern that correlates with the up- or downregulation of *NOT*.

EGR-1 (zif268, NGFI-A, Krox-24, TIS8, ZENK; NCBI: NM_001964) is the most prominent member of the early growth response (EGR) family of C2H2-type zinc finger transcription factors which also comprises EGR-2, -3, and -4 (O'Donovan *et al*. 1999). EGR-1 was identified as potential *NOT* regulator in a Y1H screen (C. Schultheiss, diploma thesis: Identification and isolation of regulatory proteins of the novel human tumor-related gene h*NOT*, 2009). The *in vitro* DNA-binding studies presented here confirm this finding and also show that EGR-1 binds at nts 330-313 (5´-CAGCGCAGGCGAAGGAGA; site 4) within the putative 1.15kb *NOT* promoter. EGR-1 always binds as a monomer via its three zinc fingers to the major grove of its 9nt target element 5´-GCG(G/T)GGGCG with each finger binding a triplet of this sequence (Chapman and Perkins 2000; Mikles *et al.* 2013). Thus, the 9nts 5´-GCAGGCGAAGG of site 4 exhibiting the highest identity with the consensus motif most likely represent the actual binding site (EGR-1 core site). This assumption is consistent with the finding that deletion of the first four nts of site 4 ($s4^5$), which represent the 3´ end of the NFκB site 4/3 (5´-CAGC), did not prevent the binding of EGR-1 in EMSAs. The EGR-1 core site contains four nts which do not match with the consensus sequence. This is of importance, because there are many examples for EGR-1 target elements which (partially) overlap with the SP1/SP3 binding site 5´-GGGGCGGGG (Cao *et al*. 1993; Trejo *et al* 1997; Raychowdhury *et al*. 2002; Zhang *et al*. 2007; Hu *et al*. 2010; Qiao and May 2011). The evenly high GC content of both elements allows EGR-1, SP1, and SP3 to compete for the binding site, resulting in a characteristic three band pattern in gel retardation assays (Cao *et al*. 1993; Hu *et al*. 2009). This pattern is not observed for site 4, presumably because the lower GC content renders the site inappropriate for SP1/SP3 but specific for EGR-1. Thus, the SP1/SP3-EGR-1 competition is not relevant for the regulation of *NOT*. The *in vivo*-binding of EGR-1 to site 4 in HaCaT, HT-29, and HeLa cells was demonstrated by ChIP and the impact of this interaction for *NOT* transcription by the downregulation of *NOT*-1 and *NOT*-4 mRNA levels after the RNAi-mediated knockdown of *EGR-1*. However, on the protein level only NOT-1 decreases whereas the amount of NOT-4 remains unaffected arguing for its stability in HT-29 cells. The EMSAs performed using nuclear extracts from HT-29 cells suggest the ability of EGR-1 to bind at nts 685-673 (site 5), 296-285 (site 3), and 41-30 (site 2) *in vitro*. Since the ChIPs documented the irrelevance of these sites in all investigated cell lines, they were not considered further.

The mitogen-induced activation of IEG gene expression is the first response of postmitotic or of mitotic cells resting in the G0 state in order to re-enter the cell cycle (Lemaire *et al*. 1990; Schratt *et al*. 2001). It is mainly orchestrated by the MAPK-regulated serum response factor (SRF),

which activates target genes like *c-fos* and *EGR-1* by binding to their promoters (Schratt *et al*. 2001). The activated genes then stimulate a specific program to trigger G1 transition and cell cycle progression (Poser *et al*. 2000). This process can be mimicked in permanent cell systems by supplying serum-starved cells with serum. Consistent with that, EGR-1 is not expressed in HeLa and HT-29 cells and only scarcely in HaCaT cells without serum, but re-expressed at high levels in response to serum. As a consequence, EGR-1 binds the *NOT* promoter only in the presence of serum. The mitogen-dependent binding of EGR-1 is also reflected in NOT-1 protein expression. Interestingly, the expression of NOT-4 is not affected by serum in HT-29 cells.

MYCN is a short lived protein that belongs to the myelocytomatosis viral related oncogene (MYC) family of proto-oncogenes including c-Myc, MYCB, and MYCL which act as transcriptional regulators by forming heterodimeric complexes with Max/Mad family members (Bonvini *et al*. 1997; Baudino and Cleveland 2001; Cowling and Cole 2006). MYCN expression is normally restricted to developing cells (mainly of neuronal origin) and thus barely detectable in most adult tissues (Malynn *et al*. 2000; Westermark *et al*. 2011). The tissue-specific MYCN expression correlates with the tumor types MYCN is amplified or upregulated in, including neuroblastoma, retinoblastoma, rhabdomyosarcoma, medulloblastoma, glioblastoma, small cell lung cancer, and Wilm´s Tumor (Westermark *et al*. 2011). Notably, MYCN is amplified in about 30% of neuroblastoma and serves as a marker for poor outcome (Westermark *et al*. 2011).

MYC proteins regulate transcription by binding with their C-terminal basic-helix-loop-helix-zipper (bHLHZ) domains to the so-called E-Box sequences 5´- CACGTG in the promoters of their target genes (Claassen and Hann 1999; Beltran 2014). The *in vitro* DNA-binding assays revealed the binding of MYCN to two E-Boxes within the *NOT* promoter: one in *cis* orientation at nts 184-173 (5´- TGGAGCGTGAG; site 3) and a composite *cis*/*trans* element at nts 80-69 (5´- GG CACGGGAAG; site 2/1). It has been reported that MYCN and c-MYC, in contrast to MYCL, share similar DNA-binding affinities. However, the results from affinity chromatography indicate a specificity of the detected sites for MYCN. Prochownik and VanAntwerp (1993) reported that E-Boxes with two preceding purines have a higher affinity for MYCN, whereas c-Myc preferentially binds E-Boxes with a preceding C. In line with this observation, site 3 as well as the *cis* part of site 2/1 contain two Gs before the E-Box, whereas the *trans* part has a preceding T. This suggests that the *cis* part of site 2/1 mediates the binding of MYCN. Notably, the data presented here indicates that, besides the unmodified full-length protein, a 22kDa MYCN form binds the target sequences. The results imply that this protein encompasses the N- and C-terminus of MYCN. Given the

specificity of the applied antibody, the 22kDa MYCN form might represent a novel splice variant of MYCN. The ChIP experiments demonstrated the *in vivo*-binding of MYCN and Ser54-phosphorypated MYCN to a fragment encompassing both sites in HaCaT, HT-29, and HeLa. There is experimental evidence that during mitosis the phosphorylation of MYCN at Ser54 promotes its proteasome-mediated degradation resulting in an increased transcriptional activity, especially in the presence of oncogenic Ras (Sjostrom *et al*. 2005; Kapeli and Hurin 2011). However, the relevance of this mechanism and its impact on *NOT* expression has to be assessed in further experiments. The murine counterparts of EGR-1 and MYCN could not be detected to bind the m*NOT* promoter. If *NOT* regulation by these two IEGs is actually restricted to human cells has to be confirmed in other murine cell systems.

5.6 The NFκB dimers p50:p65 and p65:p65 regulate *NOT* in a cell-specific manner

The nuclear factor of kappa light polypeptide gene enhancer in B-cells (NFκB) family represents a group of inducible transcription factors comprising p50 (NFKB1), p52 (NFKB2), p65 (RelA/ NFKB3), c-Rel (Rel), and RelB (Hayden and Ghosh 2014). NFκB proteins are characterized by their N-terminal Rel homology domain (RHD) which mediates DNA-binding and dimerization between family members (Hayden and Ghosh 2012). In contrast to p50 and p52, the proteins p65, c-Rel and RelB encompass transactivation domains which can recruit coactivator molecules to stimulate or repress transcription (Hayden and Ghosh 2014). NFκB dimers are sequestered in the cytosol, either as zymogen (p50 as p105 and p52 as p100) or via interaction with inhibitory IκB proteins (Oeckinghaus and Ghosh 2009). Upon stimulation different IκB kinase (IKK) complexes either trigger the degradation of the IκBs or the non-degradative processing of the precursors, both of which are mediated by the proteasome (Hayden and Ghosh 2014). The NFκB dimers can now translocate to the nucleus and bind their cognate 10nt κB site 5′-GGGRNWYYCC (Hayden and Ghosh 2014). There are also reports of shorter κB elements comprising only 9 or 8nts (Siggers *et al*. 2011). The high degeneration of the κB element in combination with the ability of the five NFκB subunits to form homo- or heterodimers in all possible variations allows a versatile regulation of gene expression (Smale 2012). NFκB is a key regulator of inflammation, innate and adaptive immune responses, cell survival, differentiation, proliferation, development, stress responses, and apoptosis (Karin 2006; Hayden and Ghosh 2008; Oeckinghaus *et al*. 2011; Hayden and Ghosh 2014). The function of NFκB is in many cases context-dependent, e. g. NFκB can either

act as tumor suppressor or promoter or elicit pro- or anti-apoptotic programs (Karin 2006; Oeckinghaus *et al*. 2011).

The herein presented *in vitro* DNA-binding analyses identified six *cis*-acting κB elements within the *NOT* promoter that can be bound by NFκB: (the putative 10nt κB element within the predicted sites is underlined): the composite *cis*/*trans* sites 22/21 (5´-GGGGCCGCGCCGGGATTACCCAC; 973-951nt), 19/18 (5´-TCCGGAGGCGCCCT; 789-776nt), 17/16 (5´- CCTGGAGAGGCCAT; 768-755nt), 13/12 (5´-CGTGGAACTTCCGTC; 638-624nt), 4/3 (5´-CAGATGTTCCC; 339-330nt), and the *cis* site 1 (5´-GGGTATAAAC; 223-214nt). The native immunoblots and EMSAs showed that these sites are bound by either p50:p65 or p65:p65 dimers. As demonstrated by the ELISAs, the binding of the dimers is always mediated by the p65 subunit. There are several reports suggesting that, apart from the affinity and cell-specific availability of different NFκB dimers, the recognition of κB elements depends to some extent on the target sequence (Zabel *et al.* 1991; Kunsch *et al*. 1992; Wong *et al*. 2011; Siggers *et al*. 2011). Crystal structure and numerous DNA-binding studies revealed that sequences which contain the typical 5´-GGR half-site are preferentially bound by p65 (Wong *et al*. 2011; Siggers *et al*. 2011). The fact that sites 22/21, 19/18, 17/16, 13/12, and 1 contain this 5´ half-sites might explain their p65-binding preference. Since site 4/3 does not contain this half-site but features the same binding properties as the other sites, it is considered an atypical κB site. However, the sequence is not sufficient to explain why some sites are either bound by p50:p65 or p65:p65 in a cell-specific manner *in vivo*. As both dimers are generally found in these cells, there have to be other mechanisms that determine binding site selection. One possibility is phosphorylation, which provides a selective and inducible mechanism to modulate the DNA-binding properties of NFκB either directly via induction of conformational changes or indirectly via recruitment of cofactors (Viatour *et al*. 2005; Sen and Smale 2010). The impact of phosphorylation-dependent target site selection is illustrated by the results from affinity chromatography, where site 22/21 is preferentially bound by a p50:p65 heterodimer encompassing a Ser276-phosphorylated p65. All other sites are bound by p50:p65 dimers phosphorylated at Ser276 and Ser536. The ChIPs confirmed this preference in HeLa cells, but also showed that, depending on the cell line, sites 19/18, 4/3, and 1 are either bound by p50:p65 or p65:p65 dimers. Zhong *et al*. (1998) reported that phosphorylation of p65 at Ser276 also enhances the ability to recruit CBP and p300. Similar observations were also made for phosphorylation at Ser536 and p300 (Hu *et al*. 2004). As scaffolding proteins, CBP and p300 can bridge a plethora of transcriptional regulators (Wang *et al*. 2013), thus assisting correct positioning

of transcription factors. Furthermore, CBP and p300 are acetyltransferases which acetylate histones and transcription factors (Wang *et al*. 2013). In this role, CBP and p300 can render the chromatin landscape accessible for DNA-binding proteins or they might be involved in the widespread acetylation of p65 which modulates NFκB binding properties (Oeckinghaus and Ghosh 2009; Sen and Smale 2010). Further experiments are needed to unveil the actual influence of the detected post-translational p65 modifications on cell-specific target site selection by different NFκB dimers.

An important non-Rel factor for NFκB binding site selection is RPS3. Wan *et al*. (2007) reported that, as integral part of the p65 homodimer and the p50:p65 heterodimer, RPS3 stabilizes the association of the NFκB subunits and enhances their DNA-binding. Notably, RPS3-containing NFκB complexes chose distinct binding sites over others (Wan *et al*. 2007). The relevance of RPS3 for the binding of NFκB is corroborated by affinity chromatography and ChIPs which show the presence of RPS3 at all NFκB sites. However, since RPS3 can also bind to DNA independent of NFκB, it remains possible that NFκB binds the *NOT* promoter without RPS3 which in turn independently occupies neighboring regions. As mentioned above, the data presented here indicate that RPS3 functions in both ways within the *NOT* promoter, but further experiments are needed to link the transcriptional impact of RPS3 on *NOT* expression to the respective function as transcription factor or coregulator.

The relevance of the detected NFκB binding is substantiated by the downregulation of *NOT*-1 and -4 after the RNAi-mediated knockdown of NFκB in HeLa cells. Notably, an effective downregulation is only achieved if the p50 and p65 subunits are simultaneously depleted. The lack of p50 has no effect, whereas knockdown of p65 only slightly decreases *NOT*-1 and *NOT*-4. This indicates that the loss of one NFκB subunit can be compensated. Whether this is achieved by the formation of other NFκB dimers or additional transcriptional regulators remains elusive.

Furthermore, manipulation of the NFκB signaling pathway using TNFα and parthenolide alters the expression of *NOT*. TNFα belongs to the TNF cytokine family which is linked to inflammation, cancer, and apoptosis (Hayden and Ghosh 2014). The receptor TNFR1 oligomerizes upon binding of TNFα thus causing the assembly of different signaling molecules on the intracellular receptor domain resulting in the activation of the IKKs (Hayden and Ghosh 2014). IKKβ-mediated phosphorylation of IκB proteins triggers their degradation and allows NFκB to enter the nucleus. Activation of NFκB by TNFα peaks after 30min. before it is abrogated via an autoregulatory loop. Active p65 can drive the expression of its inhibitor IκBα which then enters the nucleus and removes bound NFκB complexes from their promoters to terminate the signaling (Hayden and Ghosh 2014).

This kinetic is also observed in serum-starved HeLa and HT-29 cells after treatment with TNFα. Moreover, it is accompanied by an increase of *NOT*-1 and *NOT*-4 expression after 30min. NFκB activation is a key step for many cells (including HeLa) to trigger anti-apoptotic programs that counteract the TNFα-induced activation of cell death pathways (Hayden and Ghosh 2014). In contrast, the apoptosis inducing sesquiterpene lactone (SL) parthenolide leads to a downregulation of *NOT*-1 and -4 after 1h. The SL parthenolide specifically inhibits activation of NFκB rendering cells susceptible for apoptosis (Kwok *et al*. 2001; Garcia-Pineres *et al*. 2001). Two models of parthenolide-mediated NFκB inhibition are proposed. One depends on the inhibition of the IKKβ complex via direct interaction with parthenolide (Kwok *et al*. 2001), the other suggests the abrogation of NFκB DNA-binding activity via alkylation of its p65 subunit (Garcia-Pineres *et al*. 2001). The data presented here indicate that both mechanisms contribute to the inhibition of NFκB. Parthenolide-treated cells enrich NFκB in the cytosolic fractions which hints for the inhibition of the IKK complex. However, the Southwestern assays showed, that the NFκB reference binding site cannot hybridize with nuclear and cytosolic p65 in Parthenolide-treated cells. Regarding the amounts of p65 that are still detected in the nuclei of these cells, the alkylation mechanism seems to represent the predominant inhibitory mechanism of Parthenolide.

The *in vitro* DNA-binding studies also revealed that NFκB binds the sites 1 (5´-TCTGAAAGGGACATACACCGAGAA; 357-344nt), 4 (5´-ACTCTGGGCATAGGCAGAGT, 456-447nt), and 11 (5´-AAACACGTGGAACTTCCGTCACCTT; 774-760nt) in the m*NOT* promoter. The EMSAs indicate that these sites are bound by the p50:p65 heterodimer. Sites 1 and 11, but not site 4, contain the 5´-GGRR half-site suggesting the preferential binding of p65. The ChIPs revealed that *in vivo* only sites 1 and 4 are occupied in the C127I, 3T3, MOCHA, and BC3H1 cell lines. In all cases the p65 subunit is phosphorylated at Ser276 and Ser536, whereas RPS3 is only detected in C127I. As mentioned above, RPS3 is not an optional component of the NFκB dimer but a particular specifier that mediates the selection of distinct target sites over others (Wan *et al*. 2007). The observation that RPS3 is only found in one out of four cell lines to be located in the same region as NFκB argues that the murine NFκB binding sites are actually selected independent of RPS3. As a consequence, the detected signal in C127I would represents the autonomous binding of RPS3. However, the actual mechanisms of target site selection as well as the impact of the detected interactions on the expression of m*NOT* has to be determined in further experiments.

6 Summary

The human *NOT* gene (Kaymer and Kurzik-Dumke 1997) is the homologue of the *l(2)not* gene from *Drosophila* (Kurzik-Dumke *et al*. 1997) and suggested to be relevant for diverse cellular processes including tumorous growth and N-glycosylation (Kurzik-Dumke, personnel communication; Aebi 2013). This PhD thesis provides the first insight into the cell-specific mechanisms controlling the expression of the *NOT* gene. The first part focuses on the identification and characterization of *NOT* splice variants. This analysis revealed the existence of 17 *NOT* transcripts which, depending on the alternative first exon, can be separated into two groups. The transcripts *NOT*-1 and *NOT*-4 are translated. Most of the other *NOT* isoforms harbor premature stop codons and are degraded by the nonsense-mediated mRNA decay (NMD) pathway. The discovery of two different transcription start sites suggests the existence of two different *NOT* promoters that regulate the transcription of two pre-mRNAs from which all other isoforms are generated via alternative splicing.

The second part describes the identification of transcription factor binding sites within a putative 1.15kb *NOT* promoter region. Bioinformatics tools predicted 7 potential binding sites for the transcription factor EGR-1, 22 for NFκB, 16 for CREB, and 10 for MYCN. From these putative sites one EGR-1-binding site (nts 330-312), two MYCN-binding sites (nts 184-173 and 80-69), one CREB3-binding site (nts 217-206), and six NFκB binding sites (nts 973-951, 789-776, 768-755, 638-624, 339-330, and 223-214) were confirmed *in vitro* using the yeast one-hybrid, EMSA, ELISA, and affinity chromatography techniques. *In vivo*-binding analysis using chromatin immunoprecipitation (ChIP) showed cell-specific occupancy of the EGR-1 and MYCN binding elements, whereas CREB3 and NFκB bind in all investigated cell lines. In the case of NFκB, the number of occupied sites as well as the composition and phosphorylation of the bound NFκB dimers varies between cells. The ChIP results also showed that all NFκB signals are accompanied by signals of its cofactor RPS3. In accordance with previous results obtained in our laboratory, the data presented here substantiates the DNA binding of RPS3. Furthermore, the paralogue histone acetyltransferases CBP and p300, which are described as transcriptional coactivators of NFκB and EGR-1, are bound in all investigated cell lines. The impact of the detected protein-DNA interactions on *NOT* expression was assessed using RNAi (for EGR-1 and NFκB), pharmacological activation or inhibition of the respective transcription factor (TNFα and Parthenolide for NFκB, BFA for CREB3), or overexpression (CREB3). Comparative studies in murine cell lines identified

homologues of the human splice variants and showed that the promoter architecture is identical. Moreover, the murine *NOT* gene is also regulated by NFκB, CREB3, CBP, p300, and RPS3.

7 Zusammenfassung

NOT, das humane Homologe des *Drosophila* Gens *l(2)not* (Kurzik-Dumke *et al*. 1997; Kaymer und Kurzik-Dumke 1997), wird mit diversen zellulären Prozessen wie Tumorwachstum und der N-Glykosylierung in Verbindung gebracht (Kurzik-Dumke, persönliche Mitteilung; Aebi 2013). Die vorliegende Dissertation liefert die ersten Einblicke in die zellspezifischen Mechanismen, welche die Expression des *NOT* Gens kontrollieren. Der erste Teil der Arbeit beschreibt die Identifizierung und Charakterisierung von *NOT* Spleißvarianten. Diese Analyse erbrachte den Nachweis von 17 *NOT* Transkripten, die entsprechend ihres alternativen ersten Exons in zwei Gruppen eingeteilt werden können. Die Transkripte *NOT*-1 und *NOT*-4 werden translatiert. Die meisten anderen *NOT* Isoformen beinhalten ein vorzeitiges Stoppcodon und werden vom Nonsense-mediated mRNA Decay (NMD) Signalweg abgebaut. Der Nachweis von zwei verschiedenen Transkriptionsstarts deutet auf die Existenz von zwei verschiedenen *NOT* Promotoren hin, die die Transkription zweier pre-mRNAs regulieren, aus denen alle anderen Isoformen durch alternatives Spleißen generiert werden.

Der zweite Teil der Arbeit beschreibt die Identifizierung von Transkriptions-faktorbindestellen innerhalb der mutmaßlichen 1,15kb großen *NOT* Promoter Region. Mithilfe bioinformatischer Tools wurden 7 potenzielle Bindestellen für den Transkriptionsfaktor EGR-1, 22 für NFκB, 16 für CREB und 10 für MYCN berechnet. Von diesen wurde durch Yeast one-hybrid, EMSA, ELISA und Affinitätschromatographie eine EGR-1 Bindestelle (nts 330-312), zwei MYCN Bindestellen (nts 184-173 and 80-69), eine CREB3 Bindestelle (nts 217-206) und sechs NFκB Bindestellen (nts 973-951, 789-776, 768-755, 638-624, 339-330 und 223-214) *in vitro* bestätigt. Die *in vivo*-Bindungsstudien mittels Chromatin-Immunopräzipitation (ChIP) belegen eine zellspezifische Bindung von EGR-1 und MYCN, wohingegen CREB3 und NFκB in allen untersuchten Zelllinien gebunden waren. Im Fall von NFκB zeigten sich sowohl bei der Anzahl der besetzten Stellen als auch bei der Zusammensetzung und Phosphorylierung der jeweils gebundenen NFκB Dimere zellspezifische Unterschiede. Die Resultate der ChIP-Analyse zeigen zudem, dass alle NFκB Signale einhergehen mit Signalen des NFκB Kofaktors RPS3. Darüber hinaus bekräftigen die hier präsentierten Daten die in unserer Arbeitsgruppe bereits nachgewiesene RPS3 Bindung an DNA. Ebenfalls belegt wurde die *in vivo*-Bindung der paralogen Histon-Acetyltransferasen CBP und p300, die als transkriptionelle Koaktivatoren von NFκB und EGR-1 beschrieben sind. Die Auswirkungen der detektierten Protein-DNA Interaktionen auf die *NOT*

Expression wurden unter Anwendung von RNAi (für EGR-1 und NFκB), pharmakologischer Aktivierung oder Inaktivierung des entsprechenden Transkriptionsfaktros (TNFα und Parthenolid für NFκB, BFA für CREB3) oder Überexpression (CREB3) ermittelt. Vergleichende Studien in murinen Zelllinien führten zur Identifizierung von homologen Spleißvarianten und veranschaulichten, dass die Promotorstruktur identisch ist. Darüber hinaus wird das murine *NOT* Gen ebenfalls von NFκB, CREB3, CBP, p300 und RPS3 reguliert.

8 References

Aebi, M., Gassenhuber, J., Domdey, H. and te Heesen, S. (1996). Cloning and characterization of the ALG3 gene of Saccharomyces cerevisiae. Glycobiology. **6**(4):439-44.

Aebi, M. (2013). N-linked protein glycosylation in the ER. Biochim. Biophys. Acta. **1833**(11):2430-7.

Alifano, P., Fani, R., Liò, P., Lazcano, A., Bazzicalupo, M., Carlomagno, M. S. and Bruni, C. B. (1996). Histidine biosynthetic pathway and genes: structure, regulation, and evolution. Microbiol. Rev. **60**(1): 44-69.

Alonso, M., Tamasdan, C., Miller, D. C. and Newcomb, E. W. (2003). Flavopiridol induces apoptosis in glioma cell lines independent of retinoblastoma and p53 tumor suppressor pathway alterations by a caspase-independent pathway. Mol. Cancer Ther. **2**(2):139-50.

Armstrong, A. P., Franklin, A. A., Uittenbogaard, M. N., Giebler, H. A. and Nyborg, J. K. (1993). Pleiotropic effect of the human T-cell leukemia virus Tax protein on the DNA binding activity of eukaryotic transcription factors. Proc. Natl. Acad. Sci. USA. **90**(15): 7303-7.

Artimo, P., Jonnalagedda, M., Arnold, K., Baratin, D., Csardi, G., de Castro, E., Duvaud, S., Flegel, V., Fortier, A., Gasteiger, E., Grosdidier, A., Hernandez, C., Ioannidis, V., Kuznetsov, D., Liechti, R., Moretti, S., Mostaguir, K., Redaschi, N., Rossier, G., Xenarios, I. and Stockinger, H. (2012). ExPASy: SIB bioinformatics resource portal, Nucleic Acids Res. **40**(W1):W597-W603.

Asmann, Y. W., Necela, B. M., Kalari, K. R., Hossain, A., Baker, T. R., Carr, J. M., Davis, C., Getz, J. E., Hostetter, G., Li, X., McLaughlin, S. A., Radisky, D. C., Schroth, G. P., Cunliffe, H. E., Perez, E. A. and Thompson, E. A. (2012). Detection of redundant fusion transcripts as biomarkers or disease-specific therapeutic targets in breast cancer. Cancer Res. **72**(8):1921-8.

Baek, D., Davis, C., Ewing, B., Gordon, D. and Green, P. (2007). Characterization and predictive discovery of evolutionarily conserved mammalian alternative promoters. Genome Res. **17**(2):145-55.

Bailey, U. M. and Schulz, B. L. (2013). Deglycosylation systematically improves N-glycoprotein identification in liquid chromatography-tandem mass spectrometry proteomics for analysis of cell wall stress responses in Saccharomyces cerevisiae lacking Alg3p. J. Chromatogr. B. Analyt. Technol. Biomed. Life Sci. **924**:16-21.

Baron, V., Adamson, E. D., Calogero, A., Ragona, G. and Mercola, D. (2006). The transcription factor Egr1 is a direct regulator of multiple tumor suppressors including TGFbeta1, PTEN, p53, and fibronectin. Cancer Gene Ther. **13**(2): 115-24.

Baudino, T. A. and Cleveland, J. L. (2001). The Max network gone mad. Mol. Cell Biol. **21**(3):691-702.

Beltran, H. (2014). The N-myc Oncogene: Maximizing its Targets, Regulation, and Therapeutic Potential. Mol. Cancer Res. **12**(6):815-22.

Bernstein, B. E., Humphrey, E. L., Erlich, R. L., Schneider, R., Bouman, P., Liu, J. S., Kouzarides, T. and Schreiber, S. L. (2002). Methylation of histone H3 Lys 4 in coding regions of active genes. Proc. Natl. Acad. Sci. USA. **99**(13):8695-700.

Birnboim, H. C. and Doly, J. (1979). A rapid alkaline extraction procedure for screening recombinant plasmid DNA. Nucleic Acids Res. **9**(16): 1513-23.

Bonvini, P., Nguyen, P., Trepel, J. and Neckers, L. M. (1998). In vivo degradation of N-myc in neuroblastoma cells is mediated by the 26S proteasome. Oncogene. **16**(9):1131-9.

Boukamp, P., Petrussevska, R. T., Breitkreutz, D., Hornung, J., Markham, A. and Fusenig, N. E. (1988). Normal keratinization in a spontaneously immortalized aneuploid human keratinocyte cell line. J. Cell Biol. **106**(3): 761-71.

Bradford, M. M. (1976). A rapid and sensitive method for the quantitation of microgram quantities of protein utilizing the principle of protein-dye binding. Anal. Biochem. **7**(72):248-54.

Burbelo, P. D., Gabriel, G. C., Kibbey, M. C., Yamada, Y., Kleinman, H. K. and Weeks, B. S. (1994). LZIP-1 and LZIP-2: two novel members of the bZIP family. Gene. **139**(2):241-5.

Burnette, W. N. (1981). "Western blotting": electrophoretic transfer of proteins from sodium dodecyl sulfate--polyacrylamide gels to unmodified nitrocellulose and radiographic detection with antibody and radioiodinated protein A. Anal. Biochem. **112**(2): 195-203.

Bywater, M. J., Pearson, R. B., McArthur, G. A. and Hannan, R. D. (2013). Dysregulation of the basal RNA polymerase transcription apparatus in cancer. Nat. Rev. Cancer. **13**(5):299-314.

Cao, X., Mahendran, R., Guy, G. R. and Tan, Y. H. (1993). Detection and characterization of cellular EGR-1 binding to its recognition site. J. Biol. Chem. **268**(23):16949-57.

Carlotti, F., Dower, S. K. and Qwarnstrom, E. E. (2000). Dynamic shuttling of nuclear factor kappa B between the nucleus and cytoplasm as a consequence of inhibitor dissociation. J. Biol. Chem. **275**(52):41028-34.

Chan, C. P., Kok, K. H. and Jin, D. Y. (2011). CREB3 subfamily transcription factors are not created equal: Recent insights from global analyses and animal models. Cell Biosci. **1**(1):6. doi: 10.1186/2045-3701-1-6.

Chang, Y. F., Imam, J. S. and Wilkinson, M. F. (2007). The nonsense-mediated decay RNA surveillance pathway. Annu. Rev. Biochem. **76**:51-74.

Chang, T. H., Huang, H. Y., Hsu, J. B., Weng, S. L., Horng, J. T. and Huang, H. D. (2013). An enhanced computational platform for investigating the roles of regulatory RNA and for identifying functional RNA motifs. BMC Bioinformatics. 14 Suppl 2:S4. doi: 10.1186/1471-2105-14-S2-S4.

Chapman, N. R. and Perkins, N. D. (2000). Inhibition of the RelA(p65) NF-kappaB subunit by Egr-1. J. Biol. Chem. **275**(7):4719-25.

Chekmenev, D. S., Haid, C. and Kel, A. E. (2005). P-Match: transcription factor binding site search by combining patterns and weight matrices. Nucleic Acids Res. **33**(web server issue): W432-7.

Chen, X. L., Shi, T., Yang, J., Shi, W., Gao, X., Chen, D., Xu, X., Xu, J. R., Talbot, N. J. and Peng, Y. L. (2014). N-glycosylation of effector proteins by an α-1,3-mannosyltransferase is required for the rice blast fungus to evade host innate immunity. Plant Cell. **26**(3):1360-76.

Chomczynski, P. and Sacchi, N. (1987). Single-step method of RNA isolation by acid guanidinium thiocyanate-phenol-chloroform extraction. Anal. Biochem. **162**(1):156-9.

Claassen, G. F. and Hann, S. R. (1999). Myc-mediated transformation: the repression connection. Oncogene. **18**(19):2925-33.

Cohen, S. N., Chang, A. C. and Hsu, L. (1972). Nonchromosomal antibiotic resistance in bacteria: genetic transformation of Escherichia coli by R-factor DNA. Proc. Natl. Acad. Sci. USA. **69**(8):2110-4.

Conaway, R. C. and Conaway, J. W. (2011). Origins and activity of the Mediator complex. Semin. Cell Dev. Biol. **22**(7):729-34.

Cooks, T., Pateras, I. S., Tarcic, O., Solomon, H., Schetter, A. J., Wilder, S., Lozano, G., Pikarsky, E., Forshew, T., Rosenfeld, N., Harpaz, N., Itzkowitz, S., Harris, C. C., Rotter, V., Gorgoulis, V. G. and Oren, M. (2013). Mutant p53 prolongs NF-κB activation and promotes chronic inflammation and inflammation-associated colorectal cancer. Cancer Cell. **23**(5):634-46.

Cowling, V. H. and Cole, M. D. (2006). Mechanism of transcriptional activation by the Myc oncoproteins. Semin. Cancer Biol. **16**(4):242-52.

Dai, Z., Aryal, U. K., Shukla, A., Qian, W. J., Smith, R. D., Magnuson, J. K., Adney, W. S., Beckham, G. T., Brunecky, R., Himmel, M. E., Decker, S. R., Ju, X., Zhang, X. and Baker, S. E. (2013). Impact of alg3 gene deletion on growth, development, pigment production, protein secretion, and functions of recombinant Trichoderma reesei cellobiohydrolases in Aspergillus niger. Fungal Genet. Biol. **61**:120-32.

Dassesse, D., Vanderwinden, J. M., Goldberg, I., Vanderhaeghen, J. J. and Schiffmann, S. N. (1999). Caffeine-mediated induction of c-fos, zif-268 and arc expression through A1 receptors in the striatum: different interactions with the dopaminergic system. Eur. J. Neurosci. **11**(9):3101-14.

Davidson, R. C., Nett, J. H., Renfer, E., Li, H., Stadheim, T. A., Miller, B. J., Miele, R. G., Hamilton, S. R., Choi, B. K., Mitchell, T. I. and Wildt, S. (2004). Functional analysis of the ALG3 gene encoding the Dol-P-Man: Man5GlcNAc2-PP-Dol mannosyltransferase enzyme of P. pastoris. Glycobiology. **14**(5):399-407.

De Backer, O., Elinck, E., Priem, E., Leybaert, L. and Lefebvre, R. A. Peroxisome proliferator-activated receptor gamma activation alleviates postoperative ileus in mice by inhibition of Egr-1 expression and its downstream target genes. J. Pharmacol. Exp. Ther. **331**(2):496-503.

DenBoer, L. M., Hardy-Smith, P. W., Hogan, M. R., Cockram, G. P., Audas, T. E. and Lu, R. (2005). Luman is capable of binding and activating transcription from the unfolded protein response element. Biochem. Biophys. Res. Commun. **331**(1):113-9.

Denecke, J., Kranz, C., Kemming, D., Koch, H. G. and Marquardt, T. (2004). An activated 5' cryptic splice site in the human ALG3 gene generates a premature termination codon insensitive to nonsense-mediated mRNA decay in a new case of congenital disorder of glycosylation type Id (CDG-Id). Hum. Mutat. **23**(5):477-86.

Desmet, F. O., Hamroun, D., Lalande, M., Collod-Béroud, G., Claustres, M. and Béroud, C. (2009). Human Splicing Finder: an online bioinformatics tool to predict splicing signals. Nucleic Acids Res. **37**(9):e67. doi: 10.1093/nar/gkp215.

Djebali, S., Davis, C. A., Merkel, A., Dobin, A., Lassmann, T., Mortazavi, A., Tanzer, A., Lagarde, J., Lin, W., Schlesinger, F., Xue, C., Marinov, G. K., Khatun, J., Williams, B. A., Zaleski, C., Rozowsky, J., Röder, M., Kokocinski, F., Abdelhamid. R. F., Alioto, T., Antoshechkin, I., Baer, M. T., Bar, N. S., Batut, P., Bell, K., Bell, I., Chakrabortty, S., Chen, X., Chrast, J., Curado, J., Derrien, T., Drenkow, J., Dumais, E., Dumais, J., Duttagupta, R., Falconnet, E., Fastuca, M., Fejes-Toth, K., Ferreira, P., Foissac, S., Fullwood, M. J., Gao, H., Gonzalez, D., Gordon, A., Gunawardena, H., Howald, C., Jha, S., Johnson, R., Kapranov, P., King, B., Kingswood, C., Luo, O. J., Park, E., Persaud, K., Preall, J. B., Ribeca, P., Risk, B., Robyr, D., Sammeth, M., Schaffer, L., See, L. H., Shahab, A., Skancke, J., Suzuki, A. M., Takahashi, H., Tilgner, H., Trout, D., Walters, N., Wang, H., Wrobel, J., Yu, Y., Ruan, X., Hayashizaki, Y., Harrow, J., Gerstein, M., Hubbard, T., Reymond, A., Antonarakis, S. E., Hannon, G., Giddings, M. C., Ruan, Y., Wold, B., Carninci, P., Guigó, R. and Gingeras, T. R. (2012). Landscape of transcription in human cells. Nature. **489**(7414):101-8.

Dufey, E., Sepúlveda, D., Rojas-Rivera, D. and Hetz, C. (2014). Cellular mechanisms of endoplasmic reticulum stress signaling in health and disease. 1. An overview. Am. J. Physiol. Cell Physiol. **307**(7):C582-94.

Durfee, T., Becherer, K., Chen, P.L., Yeh, S.H., Yang, Y., Kilbburn, A. E., Lee, W. H. and Elledge,S. J. (1993). The retinoblastoma protein associates with the protein phophatase type 1 cytalytic subunit. Genes Devel. **7**: 555-569.

Fields, S. and Song, O. (1989). A novel genetic system to detect protein-protein interactions. Nature. **340**(6230):245-6.

ENCODE Project Consortium. (2012). An integrated encyclopedia of DNA elements in the human genome. Nature. **489**(7414):57-74.

Fagerlund, R., Kinnunen, L., Köhler, M., Julkunen, I. and Melén, K. (2005). NF-{kappa}B is transported into the nucleus by importin {alpha}3 and importin {alpha}4. J. Biol. Chem. **280**(16):15942-51.

Fields, S. (1993). The two-hybrid system to detect protein-protein interactions. METHODS: A companion to Meth. Enzymol. 5, 116-124.

Fogh, T., Fogh, J. M., and Orfeo, T. (1975). One hundred and twenty-seven cultured human cell lines producing tumors in nude mice. J. Nati. Cancer Inst. **59**:221-226.

Forbes, S. A., Beare, D., Gunasekaran, P., Leung, K., Bindal, N., Boutselakis, H., Ding, M., Bamford, S., Cole, C., Ward, S., Kok, C. Y., Jia, M., De, T., Teague, J. W., Stratton, M. R., McDermott, U, and Campbell, P. J. (2015). COSMIC: exploring the world's knowledge of somatic mutations in human cancer. Nucleic Acids Res. doi: 10.1093/nar/gku1075.

Fried, M. and Crothers, D. M. (1981). Equilibria and kinetics of lac repressor-operator interactions by polyacrylamide gel electrophoresis. Nucleic Acids Res. **9**(23):6505-25.

Fuda, N. J., Ardehali, M. B. and Lis, J. T. (2009). Defining mechanisms that regulate RNA polymerase II transcription in vivo. Nature. **461**(7261):186-92.

Gallimore, P. H. and Turnell, A. S. (2001). Adenovirus E1A: remodelling the host cell, a life or death experience. Oncogene. **20**(54):7824-35.

García-Piñeres, A. J., Castro, V., Mora, G., Schmidt, T. J., Strunck, E., Pahl, H. L. and Merfort, I. (2001). Cysteine 38 in p65/NF-kappaB plays a crucial role in DNA binding inhibition by sesquiterpene lactones. J. Biol. Chem. **276**(43):39713-20.

Gey, G.O., Coffman, W.D., and Kubicek, M.T. (1952). Tissue culture studies of the proliferative capacity of cervical carcinoma and normal epithelium, Cancer Res. **12**: 264-265.

Gietz, R. D. and Woods, R. A. (2002). Transformation of yeast by lithium acetate/single-stranded carrier DNA/polyethylene glycol method. Methods Enzymol. **350**:87-96.

Graham, F. L., Smiley, J., Russell, W. C. and Nairn, R. (1977). Characteristics of a human cell line transformed by DNA from human adenovirus type 5. J. Gen. Virol. **36**(1):59-74.

Green, R. E., Lewis, B. P., Hillman, R. T., Blanchette, M., Lareau, L. F., Garnett, A. T., Rio, D. C. and Brenner, S. E. (2003). Widespread predicted nonsense-mediated mRNA decay of alternatively-spliced transcripts of human normal and disease genes. Bioinformatics. 19 Suppl 1:i118-21.

Guo, Z. Y., Hao, X. H., Tan, F. F., Pei, X., Shang, L. M., Jiang, X. L. and Yang, F. (2011). The elements of human cyclin D1 promoter and regulation involved. Clin. Epigenetics. **2**(2):63-76.

Hacker, B. (2016). Beitrag zur Aufklärung der zellulären Rolle des humanen *neighbour of tid* (*not*) Gens. PhD thesis, submitted at the Johannes Gutenberg-University Mainz, Germany.

Haeuptle, M. A. and Hennet, T. (2009). Congenital disorders of glycosylation: an update on defects affecting the biosynthesis of dolichol-linked oligosaccharides. Hum. Mutat. **30**(12):1628-41.

Hanahan, D. (1983). Studies on transformation of Escherichia coli with plasmids. J. Mol. Biol. **166**(4): 557-80.

Hayashi, M. and Tanaka, T. (1997). Novel activation and inhibitory domains of LZIP isoforms, retinoic acid-inducible genes in P19 embryonal carcinoma cell, differentially activate transcription in mouse development. NCBI Data Base, accession number: U88528.

Hayden, M. S. and Ghosh. S. (2008). Shared principles in NF-kappaB signaling. Cell. **132**(3):344-62.

Hayden, M. S. and Ghosh, S. (2012). NF-κB, the first quarter-century: remarkable progress and outstanding questions. Genes Dev. **26**(3):203-34.

Hayden, M. S. and Ghosh, S. (2014). Regulation of NF-κB by TNF family cytokines. Semin. Immunol. **26**(3):253-66.

Healy, S., Khan, P. and Davie, J. R. (2013). Immediate early response genes and cell transformation. Pharmacol. Ther. **137**(1):64-77.

Hehner, S. P., Hofmann, T. G., Dröge, W. and Schmitz, M. L. (1999). The antiinflammatory sesquiterpene lactone parthenolide inhibits NF-kappa B by targeting the I kappa B kinase complex. J. Immunol. **163**(10):5617-23.

Henquet, M., Lehle, L., Schreuder, M., Rouwendal, G., Molthoff, J., Helsper, J., van der Krol, S. and Bosch, D. (2008). Identification of the gene encoding the alpha1,3-mannosyltransferase (ALG3) in Arabidopsis and characterization of downstream n-glycan processing. Plant Cell. **20**(6):1652-64.

Hernandez-Garcia, C. M. and Finer, J. J. (2013). Identification and validation of promoters and cis-acting regulatory elements. Plant Sci. **218**:109-19.

Herschman, H. R. (1991). Primary response genes induced by growth factors and tumor promoters. Annu. Rev. Biochem. **60**:281-319.

Hochheimer, A. and Tjian, R. (2003). Diversified transcription initiation complexes expand promoter selectivity and tissue-specific gene expression. Genes Dev. **17**(11):1309-20.

Hoffman, B. G., Zavaglia, B., Witzsche, J., Ruiz de Algara, T., Beach, M., Hoodless, P. A., Jones, S. J., Marra, M. A. and Helgason, C. D. (2008). Identification of transcripts with enriched expression in the developing and adult pancreas. Genome Biol. **9**(6):R99. doi: 10.1186/gb-2008-9-6-r99.

Hsin, J. P. and Manley, J. L. (2012). The RNA polymerase II CTD coordinates transcription and RNA processing. Genes Dev. **26**(19):2119-37.

Hu, J., Nakano, H., Sakurai, H. and Colburn, N. H. (2004). Insufficient p65 phosphorylation at S536 specifically contributes to the lack of NF-kappaB activation and transformation in resistant JB6 cells. Carcinogenesis. **25**(10):1991-2003.

Hu, C. T., Chang, T. Y., Cheng, C. C., Liu, C. S., Wu, J. R., Li, M. C. and Wu, W. S. (2010). Snail associates with EGR-1 and SP-1 to upregulate transcriptional activation of p15INK4b. FEBS J. 2010 **277**(5):1202-18.

Huang, T. T., Kudo, N., Yoshida, M. and Miyamoto, S. (2000). A nuclear export signal in the N-terminal regulatory domain of IkappaBalpha controls cytoplasmic localization of inactive NF-kappaB/IkappaBalpha complexes. Proc. Natl. Acad. Sci. USA. **97**(3):1014-9.

Isogai, T. and Yamamoto, J. (2007). Homo sapiens cDNA FLJ50188 complete cds, highly similar to Dolichyl-P-Man:Man(5)GlcNAc(2)-PP-dolichylmannosyltransferase (EC 2.4.1.-). NCBI Data Base, accession number: AK299575.1

Jaeken, J., Hennet, T., Freeze, H. H. and Matthijs, G. (2008). On the nomenclature of congenital disorders of glycosylation (CDG). J. Inherit. Metab. Dis. **31**(6):669-72.

Jainchill, J. L., Aaronson, S. A. and Todaro, G. J. (1969). Murine sarcoma and leukemia viruses: assay using clonal lines of contact-inhibited mouse cells. J. Virol. **4**(5):549-53.

Jang, S. W., Kim, Y. S., Kim, Y. R., Sung, H. J. and Ko, J. (2007). Regulation of human LZIP expression by NF-kappaB and its involvement in monocyte cell migration induced by Lkn-1. J. Biol. Chem. **282**(15):11092-100.

Johnson, J. K., Waddell, N., kConFab Investigators and Chenevix-Trench, G. (2012). The application of nonsense-mediated mRNA decay inhibition to the identification of breast cancer susceptibility genes. BMC Cancer. **12**:246. doi: 10.1186/1471-2407-12-246.

Juven-Gershon, T. and Kadonaga, J. T. (2010). Regulation of gene expression via the core promoter and the basal transcriptional machinery. Dev. Biol. **339**(2):225-9.

Kajiura, H., Seki, T. and Fujiyama, K. (2010). Arabidopsis thaliana ALG3 mutant synthesizes immature oligosaccharides in the ER and accumulates unique N-glycans. Glycobiology. **20**(6):736-51.

Kang, H., Kim, Y. S. and Ko, J. (2009). A novel isoform of human LZIP negatively regulates the transactivation of the glucocorticoid receptor. Mol. Endocrinol. **23**(11):1746-57.

Kapeli, K. and Hurlin, P. J. (2011). Differential regulation of N-Myc and c-Myc synthesis, degradation, and transcriptional activity by the Ras/mitogen-activated protein kinase pathway. J. Biol. Chem. **286**(44):38498-508.

Karin, M. (2006). Nuclear factor-kappaB in cancer development and progression. Nature. 441(7092):431-6.

Kawai, S., Hashimoto, W. and Murata, K. (2010). Transformation of Saccharomyces cerevisiae and other fungi: methods and possible underlying mechanism. Bioeng. Bugs. **1**(6):395-403.

Kaymer, M., Debes, A., Kress, H., Kurzik-Dumke, U. 1997. Sequence, molecular organization und products of the *Drosophila virilis* homologs of the *Drosophila* melanogaster nested genes *lethal(2)tumorous imaginal discs* (*l(2)tid*) und *lethal(2)neighbour of tid* (*l(2)not*). Gene **204**:91-103.

Kent, W. J., Sugnet, C. W., Furey, T. S., Roskin, K. M., Pringle, T. H., Zahler, A. M. and Haussler, D. (2002). The human genome browser at UCSC. Genome Res.**12**(6):996-1006.

Kim, H. C., Choi, K. C., Choi, H. K., Kang, H. B., Kim, M. J., Lee, Y. H., Lee, O. H., Lee, J., Kim, Y. J., Jun, W., Jeong, J. W. and Yoon, H. G. (2010). HDAC3 selectively represses CREB3-mediated transcription and migration of metastatic breast cancer cells. Cell Mol. Life Sci. **67**(20):3499-510.

Kim, S. L., Trang, K. T., Kim, S. H., Kim, I. H., Lee, S. O., Lee, S. T., Kim, D. G. and Kim, S. W. (2012). Parthenolide suppresses tumor growth in a xenograft model of colorectal cancer cells by inducing mitochondrial dysfunction and apoptosis. Int. J. Oncol. **41**(4):1547-53.

Kornberg, R. D. (2007). The molecular basis of eucaryotic transcription. Cell Death Differ. **14**(12):1989-97.

Körner, C., Knauer, R., Stephani, U., Marquardt, T., Lehle, L. and von Figura, K. (1999). Carbohydrate deficient glycoprotein syndrome type IV: deficiency of dolichyl-P-Man:Man(5)GlcNAc(2)-PP-dolichyl mannosyltransferase. EMBO J. **18**(23): 6861-22.

Kozak, M. (2005). A second look at cellular mRNA sequences said to function as internal ribosome entry sites. Nucleic Acids Res. **33**(20):6593-602.

Kranz, C., Sun, L., Eklund, E. A., Krasnewich, D., Casey, J. R. and Freeze, H. H. (2007). CDG-Id in two siblings with partially different phenotypes. Am. J. Med. Genet. A. **143A**(13):1414-20.

Krones-Herzig, A., Adamson, E. and Mercola, D. (2003). Early growth response 1 protein, an upstream gatekeeper of the p53 tumor suppressor, controls replicative senescence. Proc. Natl. Acad. Sci. USA. **100**(6): 3233-8.

Kunsch, C., Ruben, S. M. and Rosen, C. A. (1992). Selection of optimal kappa B/Rel DNA-binding motifs: interaction of both subunits of NF-kappa B with DNA is required for transcriptional activation. Mol. Cell Biol. **12**(10):4412-21.

Kurzik-Dumke, U., Gundacker, D., Rentrop, M. and Gateff, E. (1995). Tumor suppression in *Drosophila* is causally related to the function of the *lethal(2)tumorous imaginal discs gene*, a *dnaJ* homolog. Dev. Genetics **16**: 64-76.

Kurzik-Dumke, U. (1996). Nested Gene Arrangement of the *Drosophila melanogaster* Tumor Suppressor Locus *lethal(2)tumorous imaginal discs* (*l(2)tid*) consisting of at least three Genes. In: Control Mechanisms of Carcinogenesis. Eds. Hengstler, J. und Oesch, F. Thieme Verlag, Stuttgart, pp. 224-244.

Kurzik-Dumke, U. and Kaymer, M. **(**1996). Sequence of the human homolog of the *Drosophila melanogaster* gene *lethal(2)neighbour of tid* (*l(2)not*). NCBI Data Base, access number: Y09022.

Kurzik-Dumke, U., Kaymer, M., Gundacker, D., Debes, A., Labitzke, K. (1997). Gene within gene configuration und expression of the *Drosophila melanogaster* genes *lethal(2) neighbour of tid* [*l(2)rot*] und *lethal(2) relative of tid* [*l(2)rot*]. Gene **200**:45-58.

Kurzik-Dumke, U. and Czaja, J. (2007). Htid-1, the human homolog of the Drosophila melanogaster *l(2)tid* tumor suppressor, defines a novel physiological role of APC. Cell Signal. **19**(9):1973-85.

Kwok, B. H., Koh, B., Ndubuisi, M. I., Elofsson, M. and Crews, C. M. (2001). The anti-inflammatory natural product parthenolide from the medicinal herb Feverfew directly binds to and inhibits IkappaB kinase. Chem. Biol. **8**(8):759-66.

Kyhse-Andersen, J. (1984). Electroblotting of multiple gels: a simple apparatus without buffer tank for rapid transfer of proteins from polyacrylamide to nitrocellulose. J. Biochem. Biophys. Methods **10**(3-4): 203-9.

Lan, X., Jin, Y., Yang, Y., Lin, P., Hu, L., Cui, C., Li, Q., Li, X. and Wang, A. (2013). Expression and localization of Luman RNA and protein during mouse implantation and decidualization. Theriogenology. **80**(2):138-44.

Landry, J. R., Mager, D. L. and Wilhelm, B. T. (2003). Complex controls: the role of alternative promoters in mammalian genomes. Trends Genet. **19**(11):640-8.

Lareau, L. F., Brooks, A. N., Soergel, D. A., Meng, Q. and Brenner, S.E. (2007). The coupling of alternative splicing and nonsense-mediated mRNA decay. Adv. Exp. Med. Biol. **623**:190-211.

Lee, L.G., Connell, C.R., Woo, S.L., Cheng, R.D., McArdle, B.F., Fuller, C.W., Halloran, N.D. and Wilson, R.K. (1992). DNA sequencing with dye-labeled terminators and T7 DNA polymerase: effect of dyes and dNTPs on incorporation of dye-terminators and probability analysis of termination fragments. Nucl. Acids Res. **20**: 2471-83.

Lehman, T. A., Modali, R., Boukamp, P., Stanek, J., Bennett, W. P., Welsh, J. A., Metcalf, R. A., Stampfer, M. R., Fusenig, N. and Rogan, E. M. (1993). p53 mutations in human immortalized epithelial cell lines. Carcinogenesis. **14**(5):833-9.

Lenhard, B., Sandelin, A. and Carninci, P. (2012). Metazoan promoters: emerging characteristics and insights into transcriptional regulation. Nat. Rev. Genet. **13**(4):233-45.

Lemaire, P., Vesque, C., Schmitt, J., Stunnenberg, H., Frank, R. and Charnay, P. (1990). The serum-inducible mouse gene Krox-24 encodes a sequence-specific transcriptional activator. Mol. Cell Biol. **10**(7):3456-67.

Lepais, L., Cheillan, D., Frachon, S. C., Hays, S., Matthijs, G., Panagiotakaki, E., Abel, C., Edery, P. and Rossi M. (2015). ALG3-CDG: Report of two siblings with antenatal features carrying homozygous p.Gly96Arg mutation. Am. J. Med. Genet. A. **167A**(11):2748-54.

Lewis, B. P., Green, R. E. and Brenner, S. E. (2003). Evidence for the widespread coupling of alternative splicing and nonsense-mediated mRNA decay in humans. Proc. Natl. Acad. Sci. USA. **100**(1):189-92.

Ley, S. C. and Beyaert, R. (2014). Priming IKKβ kinase for action. Biochem. J. **463**(1):e1-2. doi: 10.1042/BJ20140989

Li, W.B., Gruber, C., Jessee, J. and Polayes, D. (2001). Full-length cDNA libraries and normalization. NCBI Data Base, accession number: BX339649.2

Li, G. M. (2013). Decoding the histone code: Role of H3K36me3 in mismatch repair and implications for cancer susceptibility and therapy. Cancer Res. **73**(21):6379-83.

Liang, G., Audas, T. E., Li, Y., Cockram, G. P., Dean, J. D., Martyn, A. C., Kokame, K. and Lu, R. (2006). Luman/CREB3 induces transcription of the endoplasmic reticulum (ER) stress response protein Herp through an ER stress response element. Mol. Cell Biol. **26**(21):7999-8010.

Lin, W. C., Chuang, Y. C., Chang, Y. S., Lai, M. D., Teng, Y. N., Su, I. J., Wang, C. C., Lee, K. H. and Hung, J. H. (2012). Endoplasmic reticulum stress stimulates p53 expression through NF-κB activation. PLoS One. **7**(7):e39120. doi: 10.1371/journal.pone.0039120.

Liu, E. S., Ou, J. H. and Lee, A. S. (1992). Brefeldin A as a regulator of grp78 gene expression in mammalian cells. J. Biol. Chem. **267**(10):7128-33.

Liu, C., Yao, J., Mercola, D. and Adamson, E. (2000). The transcription factor EGR-1 directly transactivates the fibronectin gene and enhances attachment of human glioblastoma cell line U251. J. Biol. Chem. **275**(27): 20315-23.

Livak, K. J. and Schmittgen, T. D. (2001). Analysis of relative gene expression data using real-time quantitative PCR and the 2(-Delta Delta C(T)) Method. Methods. **25**(4):402-8.

Lorenzo, M. N., Khan, R. Y., Wang, Y., Tai, S. C., Chan, G. C., Cheung, A. H. and Marsden, P. A. (2001). Human endothelin converting enzyme-2 (ECE2): characterization of mRNA species and chromosomal localization. Biochim. Biophys. Acta. **1522**(1):46-52.

Lowy, D. R., Rands, E. and Scolnick, E. M. (1978). Helper-independent transformation by unintegrated Harvey sarcoma virus DNA. J. Virol. **26**(2):291-8.

Luse, D. (2014). The RNA polymerase II preinitiation complex. Through what pathway is the complex assembled? Transcription. **5**(1):e27050. doi: 10.4161/trns.27050.

MacNicol, M. C., Cragle, C. E. and MacNicol, A. M. (2011). Context-dependent regulation of Musashi-mediated mRNA translation and cell cycle regulation. Cell Cycle. **10**(1):39-44.

Manthri, S., Güther, M. L., Izquierdo, L., Acosta-Serrano, A. and Ferguson, M. A. (2008). Deletion of the TbALG3 gene demonstrates site-specific N-glycosylation and N-glycan processing in Trypanosoma brucei. Glycobiology. **18**(5):367-83.

Malynn, B. A., de Alboran, I. M., O'Hagan, R. C., Bronson, R., Davidson, L., DePinho, R. A. and Alt, F. W. (2000). N-myc can functionally replace c-myc in murine development, cellular growth, and differentiation. Genes Dev. **14**(11):1390-9.

Maquat, L. E. (2004). Nonsense-mediated mRNA decay: splicing, translation and mRNP dynamics. Nat. Rev. Mol. Cell Biol. **5**(2):89-99.

Maston, G. A., Evans, S. K. and Green, M. R. (2006). Transcriptional regulatory elements in the human genome. Annu. Rev. Genomics Hum. Genet. **7**:29-59.

Mathelier, A., Zhao, X., Zhang, A. W., Parcy, F., Worsley-Hunt, R., Arenillas, D. J., Buchman, S., Chen, C. Y., Chou, A., Ienasescu, H., Lim, J., Shyr, C., Tan, G., Zhou, M., Lenhard, B., Sandelin, A. and Wasserman, W. W. (2014). JASPAR 2014: an extensively expanded and updated open-access database of transcription factor binding profiles. Nucleic Acids Res. 42(Database issue):D142-7. doi: 10.1093/nar/gkt997.

Matys, V., Fricke, E., Geffers, R., Gössling, E., Haubrock, M., Hehl, R., Hornischer, K., Karas, D., Kel, A. E., Kel-Margoulis, O. V., Kloos, D. U., Land, S., Lewicki-Potapov, B., Michael, H., Münch, R., Reuter, I., Rotert, S., Saxel, H., Scheer, M., Thiele, S. and Wingender. E. (2003). TRANSFAC: transcriptional regulation, from patterns to profiles. Nucleic Acids Res. **31**(1):374-8.

McIlwain, D. R., Berger, T. and Mak, T. W. (2013). Caspase functions in cell death and disease. Cold Spring Harb. Perspect. Biol. **5**(4):a008656. doi: 10.1101/cshperspect.a008656.

Miao, F. and Natarajan, R. (2005). Mapping global histone methylation patterns in the coding regions of human genes. Mol. Cell Biol. **25**(11):4650-61.

Mikles, D. C., Bhat, V., Schuchardt, B. J., Deegan, B. J., Seldeen, K. L., McDonald, C. B. and Farooq, A. (2013). pH modulates the binding of early growth response protein 1 transcription factor to DNA. FEBS J. **280**(15):3669-84.

Muchardt, C., Li, C., Kornuc, M. and Gaynor, R. (1990). CREB regulation of cellular cyclic AMP-responsive and adenovirus early promoters. J. Virol. **64**(9):4296-305.

Nadanaka, S., Okada, T., Yoshida, H. and Mori, K. (2007). Role of disulfide bridges formed in the luminal domain of ATF6 in sensing endoplasmic reticulum stress. Mol. Cell Biol. **27**(3):1027-43.

Narlikar, L. and Ovcharenko, I. (2009). Identifying regulatory elements in eukaryotic genomes. Brief Funct. Genomic Proteomic. **8**(4):215-30.

Nebenführ, A., Ritzenthaler, C. and Robinson, D. G. (2002). Brefeldin A: deciphering an enigmatic inhibitor of secretion. Plant Physiol. 130(3):1102-8.

Oeckinghaus, A. and Ghosh, S. (2009). The NF-kappaB family of transcription factors and its regulation. Cold Spring Harb. Perspect. Biol. **1**(4):a000034. doi: 10.1101/cshperspect.a000034.

Oeckinghaus, A., Hayden, M. S. and Ghosh, S. (2011). Crosstalk in NF-κB signaling pathways. Nat. Immunol. **12**(8):695-708.

O'Donovan, K. J., Tourtellotte, W. G., Millbrandt, J. and Baraban, J. M. (1999). The EGR family of transcription-regulatory factors: progress at the interface of molecular and systems neuroscience. Trends Neurosci. **22**(4):167-73.

Ohtsubo, K. and Marth, J. D. (2006). Glycosylation in cellular mechanisms of health and disease. Cell. **126**(5):855-67.

Okada, T., Haze, K., Nadanaka, S., Yoshida, H., Seidah, N. G., Hirano, Y., Sato, R., Negishi, M. and Mori, K. (2003). A serine protease inhibitor prevents endoplasmic reticulum stress-induced cleavage but not transport of the membrane-bound transcription factor ATF6. Biol. Chem. **278**(33):31024-32.

Ortega-Martínez, S. (2015). A new perspective on the role of the CREB family of transcription factors in memory consolidation via adult hippocampal neurogenesis. Front. Mol. Neurosci. **8**:46. doi: 10.3389/fnmol.2015.00046.

Oslowski, C. M. and Urano, F. (2011). Measuring ER stress and the unfolded protein response using mammalian tissue culture system. Methods Enzymol. **490**:71-92.

Otto, T. (2015). MYCN and Its Posttranslational Regulation in Neuroblastoma. In: Progressive Neuroblastoma: Innovation and Novel Therapeutic Strategies. Eds. Christiansen H. and Christiansen. Karger Verlag, Basel, pp. 47-58.

Pal, S., Gupta, R. and Davuluri, R. V. (2012). Alternative transcription and alternative splicing in cancer. Pharmacol. Ther. **136**(3):283-94.

Pan, Q., Saltzman, A. L., Kim, Y. K., Misquitta, C., Shai, O., Maquat, L. E., Frey, B. J. and Blencowe, B. J. (2006). Quantitative microarray profiling provides evidence against widespread coupling of alternative splicing with nonsense-mediated mRNA decay to control gene expression. Genes Dev. **20**(2):153-8.

Parra, E., Ferreira, J. and Ortega, A. (2011). Overexpression of EGR-1 modulates the activity of NF-κB and AP-1 in prostate carcinoma PC-3 and LNCaP cell lines. Int. J. Oncol. **39**(2):345-52.

Peden, A. A., Rudge, R. E., Lui, W. W. and Robinson, M. S. (2002). Assembly and function of AP-3 complexes in cells expressing mutant subunits. J. Cell Biol. **156**(2):327-36.

Perini, G., Diolaiti, D., Porro, A. and Della Valle, G. (2005). In vivo transcriptional regulation of N-Myc target genes is controlled by E-box methylation. Proc. Natl. Acad. Sci. USA. **102**(34):12117-22.

Pfaffl, M. W. (2001). A new mathematical model for relative quantification in real-time RT-PCR. Nucleic Acids Res. **29**(9):e45.

Pfaffl, M. W. (2006). Relative Quantification. In: Real-time PCR. Ed. Tevfik Dorak, M. Taylor & Francis Group, New York, pp. 63-82.

Phatnani, H. P. and Greenleaf, A. L. (2006). Phosphorylation and functions of the RNA polymerase II CTD. Genes Dev. **20**(21):2922-36.

Pheiffer, B. H. and Zimmerman, S. B. (1983). Polymer-stimulated ligation: enhanced blunt- or cohesive-end ligation of DNA or deoxyribooligonucleotides by T4 DNA ligase in polymer solutions. Nucleic Acids Res. **11**(22): 7853-71.

Porrua, O. and Libri, D. (2015). Transcription termination and the control of the transcriptome: why, where and how to stop. Nat. Rev. Mol. Cell Biol. **16**(3):190-202.

Poser, S., Impey, S., Trinh, K., Xia, Z. and Storm, D. R. (2000). SRF-dependent gene expression is required for PI3-kinase-regulated cell proliferation. EMBO J. **19**(18):4955-66.

Poss, Z. C., Ebmeier, C. C. and Taatjes, D. J. (2013). The Mediator complex and transcription regulation. Crit. Rev. Biochem. Mol. Biol. **48**(6):575-608.

Prochownik, E. V. and VanAntwerp, M. E. (1993). Differential patterns of DNA binding by myc and max proteins. Proc. Natl. Acad. Sci. USA. **90**(3):960-4.

Qiao, H. and May, J. M. (2011). Regulation of the human ascorbate transporter SVCT2 exon 1b gene by zinc-finger transcription factors. Free Radic. Biol. Med. **50**(9):1196-209.

Raggo, C., Rapin, N., Stirling, J., Gobeil, P., Smith-Windsor, E., O'Hare, P. and Misra, V. (2002). Luman, the cellular counterpart of herpes simplex virus VP16, is processed by regulated intramembrane proteolysis. Mol. Cell Biol. **22**(16):5639-49.

Ramakers, C., Ruijter, J. M., Deprez, R. H. and Moorman, A. F. (2003). Assumption-free analysis of quantitative real-time polymerase chain reaction (PCR) data. Neurosci. Lett. **339**(1):62-6.

Raychowdhury, R., Schäfer, G., Fleming, J., Rosewicz, S., Wiedenmann, B., Wang, T. C. and Höcker, M. (2002). Interaction of early growth response protein 1 (Egr-1), specificity protein 1 (Sp1), and cyclic adenosine 3'5'-monophosphate response element binding protein (CREB) at a proximal response element is critical for gastrin-dependent activation of the chromogranin A promoter. Mol. Endocrinol. **16**(12):2802-18.

Rearick, J. I., Chapman, A. and Kornfeld, S. (1981). Glucose starvation alters lipid-linked oligosaccharide biosynthesis in Chinese hamster ovary cells. J. Biol. Chem. **256**(12):6255-61.

Reiling, J. H., Olive, A. J., Sanyal, S., Carette, J. E., Brummelkamp, T. R., Ploegh, H. L., Starnbach, M. N. and Sabatini, D. M. (2013). A CREB3-ARF4 signalling pathway mediates the response to Golgi stress and susceptibility to pathogens. Nat. Cell Biol. **15**(12):1473-85.

Ren, Q., Kari, C., Quadros, M. R., Burd, R,. McCue, P., Dicker, A. P. and Rodeck, U. (2006). Malignant transformation of immortalized HaCaT keratinocytes through deregulated nuclear factor kappaB signaling. Cancer Res. **66**(10):5209-15.

Rexach, J. E., Clark, P. M., Mason, D. E., Neve, R. L., Peters, E. C. and Hsieh-Wilson, L. C. (2012). Dynamic O-GlcNAc modification regulates CREB-mediated gene expression and memory formation. Nat. Chem. Biol. **8**(3):253-61.

Riess, S., Reddihough, D. S., Howell, K. B., Dagia, C., Jaeken, J., Matthijs, G. and Yaplito-Lee, J. (2013). ALG3-CDG (CDG-Id): clinical, biochemical and molecular findings in two siblings. Mol. Genet. Metab. **110**(1-2):170-5.

Rimella-Le-Huu, A., Henry, H., Kern, I., Hanquinet, S., Roulet-Perez, E., Newman, C. J., Superti-Furga, A., Bonafé, L. and Ballhausen, D. (2008). Congenital disorder of glycosylation type Id (CDG Id): phenotypic, biochemical and molecular characterization of a new patient. J. Inherit. Metab. Dis. Suppl 2:S381-6.

Ron, D., Brasier, A. R., Wright, K. A., Tate, J. E. and Habener, J. F. (1990). An inducible 50-kilodalton NF kappa B-like protein and a constitutive protein both bind the acute-phase response element of the angiotensinogen gene. Mol. Cell Biol. **10**(3):1023-32.

Rosenbloom, K. R., Sloan, C. A., Malladi, V. S., Dreszer, T. R., Learned, K., Kirkup, V. M., Wong, M. C., Maddren, M., Fang, R., Heitner, S. G., Lee, B. T., Barber, G. P., Harte, R. A., Diekhans, M., Long, J. C., Wilder, S. P., Zweig, A. S., Karolchik, D., Kuhn, R. M., Haussler, D. and Kent, W. J. (2013). ENCODE data in the UCSC Genome Browser: year 5 update. Nucleic Acids Res. 2013 Jan;41(Database issue):D56-63. doi: 10.1093/nar/gks1172.

Rosenbloom, K. R., Armstrong, J., Barber, G. P., Casper, J., Clawson, H., Diekhans, M., Dreszer, T. R., Fujita, P. A., Guruvadoo, L., Haeussler, M., Harte, R. A., Heitner, S., Hickey, G., Hinrichs, A. S., Hubley, R., Karolchik, D., Learned, K., Lee, B. T., Li, C. H., Miga, K. H., Nguyen, N., Paten, B., Raney, B. J., Smit, A. F., Speir, M. L., Zweig, A. S., Haussler, D., Kuhn, R. M. and Kent, W. J. (2015). The UCSC Genome Browser database: 2015 update. Nucleic Acids Res. 2015 Jan;43(Database issue):D670-81. doi: 10.1093/nar/gku1177.

Rossi, A., Elia, G. and Santoro, M. G. (1997). Inhibition of nuclear factor kappa B by prostaglandin A1: an effect associated with heat shock transcription factor activation. Proc. Natl. Acad. Sci. USA. **94**(2):746-50.

Roy, A. L. and Singer, D. S. (2015). Core promoters in transcription: old problem, new insights. Trends Biochem. Sci. **40**(3):165-71.

Ruijter, J. M., Ramakers, C., Hoogaars, W. M., Karlen, Y., Bakker, O., van den Hoff, M. J. and Moorman, A. F. (2009). Amplification efficiency: linking baseline and bias in the analysis of quantitative PCR data. Nucleic Acids Res. **37**(6):e45. doi: 10.1093/nar/gkp045.

Saiki, R. K., Scharf, S., Faloona, F., Mullis, K. B., Horn, G. T., Erlich, H. A. and Arnheim, N. (1985). Enzymatic amplification of beta-globin genomic sequences and restriction site analysis for diagnosis of sickle cell anemia. Science. **230**(4732):1350-4.

Sandelin, A., Carninci, P., Lenhard, B., Ponjavic, J., Hayashizaki, Y. and Hume, D. A. (2007). Mammalian RNA polymerase II core promoters: insights from genome-wide studies. Nat. Rev. Genet. **8**(6):424-36.

Sanger, F., Nicklen, S. and Coulson, A. R. (1977). DNA sequencing with chain-terminating inhibitors. Proc. Natl. Acad. Sci. USA. **74**(12): 5463-7.

Schmittgen, T. D. and Livak, K. J. (2008). Analyzing real-time PCR data by the comparative C(T) method. Nat. Protoc. **3**(6):1101-8.

Schneider, C.A., Rasband, W.S. and Eliceiri, K.W. (2012). NIH Image to ImageJ: 25 years of image analysis. Nature Methods **9**: 671-675.

Schollen, E., Grünewald, S., Keldermans, L., Albrecht, B., Körner, C. and Matthijs, G. (2005). CDG-Id caused by homozygosity for an ALG3 mutation due to segmental maternal isodisomy UPD3(q21.3-qter). Eur. J. Med. Genet. **48**(2):153-8.

Schratt, G., Weinhold, B., Lundberg, A. S., Schuck, S., Berger, J., Schwarz, H., Weinberg, R. A., Rüther, U. and Nordheim, A. (2001). Serum response factor is required for immediate-early gene activation yet is dispensable for proliferation of embryonic stem cells. Mol. Cell Biol. **21**(8):2933-43.

Schubert, D., Harris, A. J., Devine, C. E. and Heinemann, S. (1974). Characterization of a unique muscle cell line. J. Cell Biol. **61**(2):398-413.

Schultheiss, C. (2009). Identification and isolation of regulatory proteins of the novel human tumor-related gene h*NOT*. Diploma thesis, submitted at the Johannes Gutenberg-University Mainz, Germany.

Sen, R. and Smale, S. T. (2010). Selectivity of the NF-κB Response. Cold Spring Harb. Perspect. Biol. **2**(4): a000257. doi: 10.1101/cshperspect.a000257

Shahbazian, M. D. and Grunstein, M. (2007). Functions of site-specific histone acetylation and deacetylation. Annu. Rev. Biochem. **76**:75-100.

Sharma, C. B., Knauer, R. and Lehle, L. (2001). Biosynthesis of lipid-linked oligosaccharides in yeast: the ALG3 gene encodes the Dol-P-Man:Man5GlcNAc2-PP-Dol mannosyltransferase. Biol. Chem. **382**(2):321-8.

Shi, Z. Z., Jiang, Y. Y., Hao, J. J., Zhang, Y., Zhang, T. T., Shang, L., Liu, S. G., Shi, F. and Wang, M. R. (2014). Identification of putative target genes for amplification within 11q13.2 and 3q27.1 in esophageal squamous cell carcinoma. Clin. Transl. Oncol. **16**(7):606-15.

Siggers, T., Chang, A. B., Teixeira, A., Wong, D., Williams, K. J., Ahmed, B., Ragoussis, J., Udalova, I. A., Smale, S. T. and Bulyk, M. L. (2011). Principles of dimer-specific gene regulation revealed by a comprehensive characterization of NF-κB family DNA binding. Nat. Immunol. **13**(1):95-102.

Sikorski, R. S. and Hieter, P. (1989). A system of shuttle vectors and yeast host strains designed for efficient manipulation of DNA in Saccharomyces cerevisiae. Genetics. **122**(1):19-27.

Shrum, C. K., Defrancisco, D. and Meffert, M. K. (2009). Stimulated nuclear translocation of NF-kappaB and shuttling differentially depend on dynein and the dynactin complex. Proc. Natl. Acad. Sci. USA. **106**(8):2647-52.

Silverman, E. S., Du, J., Williams, A. J., Wadgaonkar, R., Drazen, J. M. and Collins, T. (1998). cAMP-response-element-binding-protein-binding protein (CBP) and p300 are transcriptional co-activators of early growth response factor-1 (Egr-1). Biochem. J. **336**(Pt 1): 183-9.

Sims 3rd, R. J., Nishioka, K. and Reinberg, D. (2003). Histone lysine methylation: a signature for chromatin function. Trends Genet. **19**(11):629-39.

Siu, F. K., Lee, L. T. and Chow, B. K. (2008). Southwestern blotting in investigating transcriptional regulation. Nat. Protoc. **3**(1):51-8.

Sjostrom, S. K., Finn, G., Hahn, W. C., Rowitch, D. H. and Kenney, A. M. (2005). The Cdk1 complex plays a prime role in regulating N-myc phosphorylation and turnover in neural precursors. Dev. Cell. **9**(3):327-38.

Sloutskin, A., Danino, Y. M., Orenstein, Y., Zehavi, Y., Doniger, T., Shamir, R. and Juven-Gershon, T. (2015). ElemeNT: a computational tool for detecting core promoter elements. Transcription. **6**(3):41-50.

Smale, S. T. (2012). Dimer-specific regulatory mechanisms within the NF-κB family of transcription factors. Immunol. Rev. **246**(1):193-204.

Snider, M. D. and Rogers, O. C. (1984). Transmembrane movement of oligosaccharide-lipids during glycoprotein synthesis. Cell. **36**(3):753-61.

Stein, G. H. (1979). T98G: an anchorage-independent human tumor cell line that exhibits stationary phase G1 arrest in vitro. J. Cell Phyiol. **99**(1): 43-54.

Stibler, H., Stephani, U. and Kutsch, U. (1995). Carbohydrate-deficient glycoprotein syndrome--a fourth subtype. Neuropediatrics. **26**(5):235-7.

Stormo, G. D. (2000). DNA binding sites: representation and discovery. Bioinformatics. **16**(1):16-23.

Strausberg, R. (1999). NIH-MGC EST Sequencing Project. National Institutes of Health, Mammalian Gene Collection (MGC). NCBI Data Bas, acession number: BM920198.1.

Strausberg, R. L., Feingold, E. A., Grouse, L. H., Derge, J. G., Klausner, R. D., Collins, F. S., Wagner, L., Shenmen, C. M., Schuler, G. D., Altschul, S. F., Zeeberg, B., Buetow, K. H., Schaefer, C. F., Bhat, N. K., Hopkins, R. F., Jordan, H., Moore, T., Max, S. I., Wang, J., Hsieh, F., Diatchenko, L., Marusina, K., Farmer, A. A., Rubin, G. M., Hong, L., Stapleton, M., Soares, M. B., Bonaldo, M. F., Casavant, T. L., Scheetz, T. E., Brownstein, M. J., Usdin, T. B., Toshiyuki, S., Carninci, P., Prange, C., Raha, S. S., Loquellano, N. A., Peters, G. J., Abramson, R. D., Mullahy, S. J., Bosak, S. A., McEwan, P. J., McKernan, K. J., Malek, J. A., Gunaratne, P. H., Richards, S., Worley, K. C., Hale, S., Garcia, A. M., Gay, L. J., Hulyk, S. W., Villalon, D. K., Muzny, D. M., Sodergren, E. J., Lu, X., Gibbs, R. A., Fahey, J., Helton, E., Ketteman, M., Madan, A., Rodrigues, S., Sanchez, A., Whiting, M., Madan, A., Young, A. C., Shevchenko, Y., Bouffard, G. G., Blakesley, R. W., Touchman, J. W., Green, E. D., Dickson, M. C., Rodriguez, A. C., Grimwood, J., Schmutz, J., Myers, R. M., Butterfield, Y. S., Krzywinski, M. I., Skalska, U., Smailus, D. E., Schnerch, A., Schein, J. E., Jones, S. J., Marra, M. A. and Mammalian Gene Collection Program Team. (2002). Generation and initial analysis of more than 15,000 full-length human and mouse cDNA sequences. Proc. Natl. Acad. Sci. USA. **99**(26):16899-903.

Sue, S. C., Alverdi, V., Komives, E. A. and Dyson, H. J. (2011). Detection of a ternary complex of NF-kappaB and IkappaBalpha with DNA provides insights into how IkappaBalpha removes NF-kappaB from transcription sites. Proc. Natl. Acad. Sci. USA. **108**(4):1367-72.

Sun, L., Eklund, E. A., Chung, W. K., Wang, C., Cohen, J. and Freeze, H. H. (2005). Congenital disorder of glycosylation id presenting with hyperinsulinemic hypoglycemia and islet cell hyperplasia. J. Clin. Endocrinol. Metab. **90**(7):4371-5.

Swulius, M. T. and Waxham, M. N. (2008). Ca(2+)/calmodulin-dependent protein kinases. Cell Mol. Life Sci. **65**(17):2637-57.

Szydlowski, M. (2011). Identification of the regulatory elements and factors of the human tumor suppressor gene *tumorous imaginal discs*. PhD thesis, submitted at the Johannes Gutenberg-University Mainz, Germany.

Tempel, W., Wu, H., Dombrovsky, L., Zeng, H., Loppnau, P., Zhu, H., Plotnikov, A. N. and Bochkarev, A. (2009). An intact SAM-dependent methyltransferase fold is encoded by the human endothelin-converting enzyme-2 gene. Proteins. **74**(3):789-93.

Trejo, S. R., Fahl, W. E. and Ratner, L. (1997). The tax protein of human T-cell leukemia virus type 1 mediates the transactivation of the c-sis/platelet-derived growth factor-B promoter through interactions with the zinc finger transcription factors Sp1 and NGFI-A/Egr-1. J. Biol. Chem. **272**(43):27411-21.

Tansey, W. P. (2014). Mammalian MYC Proteins and Cancer. New Journal of Science, vol. 2014, Article ID 757534, 27 pages, 2014. doi:10.1155/2014/757534

Thomas, M., Pim, D. and Banks, L. (1999). The role of the E6-p53 interaction in the molecular pathogenesis of HPV. Oncogene. **18**(53):7690-700.

Thukral, S. K., Blain, G. C., Chang, K. K. and Fields, S. (1994). Distinct residues of human p53 implicated in binding to DNA, simian virus 40 large T antigen, 53BP1, and 53BP2. Mol. Cell. Biol. **14**(12): 8315-21.

Traven, A., Jelicic, B. and Sopta, M. (2006). Yeast Gal4: a transcriptional paradigm revisited. EMBO Rep. **7**(5): 496-9.

Tsuchiya, Y., Asano, T., Nakayama, K., Kato, T. Jr., Karin, M. and Kamata, H. (2010). Nuclear IKKbeta is an adaptor protein for IkappaBalpha ubiquitination and degradation in UV-induced NF-kappaB activation. Mol. Cell. **39**(4):570-82.

Varelas, X., Bouchie, M. P. and Kukuruzinska, M. A. (2014). Protein N-glycosylation in oral cancer: dysregulated cellular networks among DPAGT1, E-cadherin adhesion and canonical Wnt signaling. Glycobiology. **24(**7):579-91.

Viatour, P., Merville, M. P., Bours, V. and Chariot, A. (2005). Phosphorylation of NF-kappaB and IkappaB proteins: implications in cancer and inflammation. Trends Biochem. Sci. **30**(1):43-52.

Wan, F., Anderson, D. E., Barnitz, R. A., Snow, A., Bidere, N., Zheng, L., Hegde, V., Lam, L. T., Staudt, L. M., Levens, D., Deutsch, W. A. and Lenardo, M. J. (2007). Ribosomal protein S3: a KH domain subunit in NF-kappaB complexes that mediates selective gene regulation. Cell. **131**(5):927-39.

Wang, Z. and Burge, C. B. (2008). Splicing regulation: from a parts list of regulatory elements to an integrated splicing code. RNA. **14**(5):802-13.

Wang, M. and Marin, A. (2006). Characterization and prediction of alternative splice sites. Gene. **366**(2):219-27.

Wang, F., Marshall, C. B. and Ikura, M. (2013). Transcriptional/epigenetic regulator CBP/p300 in tumorigenesis: structural and functional versatility in target recognition. Cell. Mol. Life Sci. **70**(21):3989-4008.

Weerapana, E. and Imperiali, B. (2006). Asparagine-linked protein glycosylation: from eukaryotic to prokaryotic systems. Glycobiology. **16**(6):91R-101R.

Weeraratna, A.T., Kalehua, A., Deleon, I., Bertak, D., Maher, G., Wade, M. S., Lustig, A., Becker, K. G., Wood, W. 3rd, Walker, D. G., Beach, T. G. and Taub, D. D. (2007). Alterations in immunological and neurological gene expression patterns in Alzheimer's disease tissues. Exp. Cell Res. **313**(3):450-61.

Westermark, U. K., Wilhelm, M., Frenzel, A. and Henriksson, M. A. (2011). The MYCN oncogene and differentiation in neuroblastoma. Semin. Cancer Biol. **21**(4):256-66.

Wethmar, K. (2014). The regulatory potential of upstream open reading frames in eukaryotic gene expression. Wiley Interdiscip. Rev. RNA. **5**(6):765-78.

Wilhelm, J. and Pingoud, A. (2003). Real-time polymerase chain reaction. Chembiochem. **4**(11):1120-8.

Wittwer, C. T., Herrmann, M. G., Moss, A. A. and Rasmussen, R. P. (1997). Continuous fluorescence monitoring of rapid cycle DNA amplification. Biotechniques. **22**(1):134-8.

Wong, D., Teixeira, A., Oikonomopoulos, S., Humburg, P., Lone, I. N., Saliba, D., Siggers, T., Bulyk, M., Angelov, D., Dimitrov, S., Udalova, I. A. and Ragoussis, J. (2011). Extensive characterization of NF-κB binding uncovers non-canonical motifs and advances the interpretation of genetic functional traits. Genome Biol. **12**(7):R70. doi: 10.1186/gb-2011-12-7-r70.

Xiao, D., Chinnappan, D., Pestell, R., Albanese, C. and Weber, H. C. (2005). Bombesin regulates cyclin D1 expression through the early growth response protein Egr-1 in prostate cancer cells. Cancer Res. **65**(21):9934-42.

Xin, D., Hu, L. and Kong, X. (2008). Alternative promoters influence alternative splicing at the genomic level. PLoS One. **3**(6):e2377. doi: 10.1371/journal.pone.0002377.

Yang, M. and Elnitski, L. (2014). Orthology-driven mapping of bidirectional promoters in human and mouse genomes. BMC Bioinformatics. 15 Suppl 17:S1. doi: 10.1186/1471-2105-15-S17-S1.

Yuan, L. W and Gambee, J. E. (2001). Histone acetylation by p300 is involved in CREB-mediated transcription on chromatin. Biochim. Biophys. Acta. **1541**(3):161-9.

Zabel, U., Schreck, R. and Baeuerle, P. A. (1991). DNA binding of purified transcription factor NF-kappa B. Affinity, specificity, Zn2+ dependence, and differential half-site recognition. J. Biol. Chem. **266**(1):252-60.

Zhang, P., Tchou-Wong, K. M. and Costa, M. (2007). Egr-1 mediates hypoxia-inducible transcription of the NDRG1 gene through an overlapping Egr-1/Sp1 binding site in the promoter. Cancer Res. **67**(19):9125-33.

Zhong, H., Voll, R. E. and Ghosh, S. (1998). Phosphorylation of NF-kappa B p65 by PKA stimulates transcriptional activity by promoting a novel bivalent interaction with the coactivator CBP/p300. Mol. Cell. **1**(5):661-71.

Zhou, D. and Chen, S. (1999). Identification and characterization of a cAMP-responsive element in the region upstream from promoter 1.3 of the human aromatase gene. Arch. Biochem. Biophys. **371**(2):179-90.

Zhu, T., Qin, G. and Royer-Pokora, B. (2001). A novel post-transcriptional splicing form of the acute T cell leukemia proto-oncogene Lmo2. Sci. China C. Life Sci. **44**(6):561-9.

Zilfou, J. T. and Lowe, S. W. (2009). Tumor suppressive functions of p53. Cold. Spring Harb. Perspect. Biol. **1**(5):a001883. doi: 10.1101/cshperspect.a001883.

9 Appendix

Table S1 Determination of qRT-PCR efficiencies of *NOT*, *ECE2*, *ACTIN* and *HGPRT* using HaCaT cDNA

	Efficiency (E)						Correlation coefficient (R^2)					
Target	**n1**	**n2**	**n3**	**n4**	**Ø E**	**+/-**	**n1**	**n2**	**n3**	**n4**	**Ø R^2**	**+/-**
***NOT*-1**	1.935	1.726	1.86	1.804	**1.831**	0.07	0.9987	0.9994	0.9931	0.9891	**0.9951**	0.004
***NOT*-2**	1.724	1.771	1.711	1.662	**1.717**	0.03	0.9959	0.9983	0.9936	0.9997	**0.9969**	0.002
***NOT*-3**	1.796	1.806	1.837	1.713	**1.788**	0.04	0.9938	0.9965	0.9928	0.9949	**0.9945**	0.001
***NOT*-4**	1.806	1.824	1.828	1.667	**1.781**	0.06	0.9890	0.9907	0.9980	0.9996	**0.9943**	0.004
***NOT*-5**	1.838	1.802	1.863	1.868	**1.843**	0.02	0.9929	0.9923	0.9996	0.9956	**0.9951**	0.002
***NOT*-1a**	1.797	1.854	1.893	1.918	**1.866**	0.04	0.9999	0.9970	0.9942	0.9999	**0.9978**	0.002
***NOT*-1b**	1.822	1.833	1.641	1.775	**1.768**	0.06	0.9997	0.9999	0.9995	0.9966	**0.9989**	0.001
***NOT*-2a**	1.904	1.92	1.937	1.912	**1.918**	0.01	0.9993	0.9988	0.9945	0.9960	**0.9972**	0.002
***NOT*-2b**	1.87	1.876	1.91	1.766	**1.856**	0.04	0.9986	0.9958	0.9987	0.9997	**0.9982**	0.001
***NOT*-3a**	1.792	1.84	1.842	1.814	**1.822**	0.02	0.9994	0.9994	0.9983	0.9994	**0.9991**	0.0004
***NOT*-3b**	1.885	1.731	1.853	1.938	**1.852**	0.06	0.9994	0.9994	0.9988	0.9990	**0.9992**	0.0003
***NOT*-3c**	1.883	1.887	1.868	1.943	**1.895**	0.02	0.9977	0.9989	0.9993	0.9970	**0.9982**	0.001
***NOT*-4a**	1.928	1.894	1.93	1.766	**1.880**	0.06	0.9977	0.9986	0.9965	0.9992	**0.9980**	0.001
***NOT*-4b**	1.869	1.922	1.784	1.913	**1.872**	0.05	0.9957	0.9998	0.9992	0.9979	**0.9981**	0.001
***NOT*-5a**	1.875	1.877	1.857	1.876	**1.870**	0.01	0.9994	0.9957	0.9998	0.9973	**0.9976**	0.001
***NOT*-5b**	1.741	1.551	1.476	1.744	**1.590**	0.10	0.9994	0.9954	0.9757	0.9993	**0.9901**	0.010
***NOT*-5c**	1.604	1.786	1.88	1.896	**1.792**	0.10	0.9910	0.9906	0.9952	0.9952	**0.9930**	0.002
ECE2	1.707	1.847	1.817	1.862	**1.808**	0.05	0.9994	0.9981	0.9990	0.9928	**0.9973**	0.002
ACTIN	1.963	1.982	---	----	**1.97**	0.01	0.9959	0.9986	---	---	**0.9762**	0.001
***HGPRT*[1]**	1.718	1.83	1.887	1.961	**1.849**	0.08	0.9996	0.9931	0.9980	0.9978	**0.9971**	0.002
***HGPRT*[2]**	1.661	1.851	1.742	1.799	**1.763**	0.06	0.9939	0.9986	0.9998	0.9974	**0.9974**	0.002

Performed as described in Ch. 3.3.17. Primers used for amplification are listed in Tab. 31+33. n: measured samples; 1: *HGPRT* from the *NOT* isoform plate; 2: *HGPRT* from the *ACTIN*, *ECE2* plate.

Table S2 Determination of qRT-PCR efficiencies of *NOT*, *ECE2*, *ACTIN* and *HGPRT* using HT-29 cDNA

	Efficiency (E)						Correlation coefficient (R^2)					
Target	**n1**	**n2**	**n3**	**n4**	**Ø E**	**+/-**	**n1**	**n2**	**n3**	**n4**	**Ø R^2**	**+/-**
***NOT*-1**	1.745	1.829	1.862	1.907	**1.836**	0.05	0.9968	0.9999	0.9694	0.9992	**0.9913**	0.01
***NOT*-2**	1.809	1.833	1.831	1.837	**1.828**	0.01	0.9992	0.9982	0.9939	0.9926	**0.9959**	0.003
***NOT*-3**	1.889	1.792	1.721	1.642	**1.761**	0.08	0.9905	0.9966	0.9795	0.9998	**0.9916**	0.007
***NOT*-4**	1.863	1.862	1.887	1.801	**1.853**	0.03	0.9948	0.9998	0.9999	0.9901	**0.9962**	0.004
***NOT*-5**	1.742	1.915	1.802	1.761	**1.805**	0.06	0.9997	0.9972	0.9998	0.9994	**0.9990**	0.001
***NOT*-1a**	1.774	1.905	1.854	1.929	**1.866**	0.05	0.9931	0.9911	0.9982	0.9991	**0.9954**	0.003
***NOT*-1b**	1.912	1.852	1.873	1.921	**1.890**	0.03	0.9909	0.9855	0.9923	0.9970	**0.9914**	0.003
***NOT*-2a**	1.801	1.803	1.787	1.827	**1.805**	0.01	0.9999	0.9945	0.9993	0.9990	**0.9982**	0.002
***NOT*-2b**	1.753	1.88	1.747	1.862	**1.811**	0.06	0.9998	0.9985	0.9991	0.9991	**0.9991**	0.0003
***NOT*-3a**	1.864	1.706	1.741	1.949	**1.815**	0.09	0.9982	0.9999	0.9999	0.9990	**0.9992**	0.001
***NOT*-3b**	1.865	1.969	1.818	1.719	**1.843**	0.07	0.9996	0.9901	0.9990	0.9999	**0.9972**	0.004
***NOT*-3c**	1.85	1.516	1.746	1.957	**1.767**	0.14	0.9999	0.9967	0.9999	0.9997	**0.9990**	0.001
***NOT*-4a**	1.631	1.803	1.926	1.716	**1.769**	0.10	0.9991	0.9996	0.9963	0.9992	**0.9985**	0.001
***NOT*-4b**	1.918	1.881	1.883	1.812	**1.874**	0.03	0.9987	0.9977	0.9991	0.9975	**0.9983**	0.001
***NOT*-5a**	1.957	1.724	1.783	1.867	**1.791**	0.05	0.9980	0.9993	0.9993	0.9991	**0.9993**	0.0001
***NOT*-5b**	1.904	1.608	1.608	1.846	**1.687**	0.11	0.9983	0.9996	0.9985	0.9993	**0.9991**	0.0004
***NOT*-5c**	1.983	1.948	1.734	1.929	**1.899**	0.08	0.9972	0.9980	0.9992	0.9912	**0.9964**	0.003
ECE2	1.839	1.916	1.855	1.867	**1.869**	0.02	0.9991	0.9972	0.9996	0.9999	**0.9989**	0.001
ACTIN	1.861	1.883	---	---	**1.872**	0.01	0.9998	0.9874	---	---	**0.9936**	0.006
***HGPRT*[1]**	1.978	1.772	1.926	1.83	**1.877**	0.08	0.9988	0.9994	0.9997	0.9998	**0.9994**	0.0003
***HGPRT*[2]**	1.877	1.952	1.962	1.953	**1.936**	0.03	0.9991	0.9978	0.9957	0.9985	**0.9978**	0.001

Performed as described in Ch. 3.3.17. Primers used for amplification are listed in Tab. 31+33. n: measured samples; 1: *HGPRT* from the *NOT* isoform plate; 2: *HGPRT* from the *ACTIN*, *ECE2* plate.

Table S3 Determination of qRT-PCR efficiencies of *NOT*, *ECE2*, *ACTIN* and *HGPRT* using T98G cDNA

	Efficiency (E)						Correlation coefficient (R^2)					
Target	**n1**	**n2**	**n3**	**n4**	**Ø E**	**+/-**	**n1**	**n2**	**n3**	**n4**	**Ø R^2**	**+/-**
***NOT*-1**	1.871	1.776	1.896	1.776	**1.830**	0.05	0.9958	0.9988	0.9970	0.9996	**0.9978**	0.001
***NOT*-2**	1.774	1.808	1.698	1.781	**1.765**	0.03	0.9980	0.9998	0.9990	0.9997	**0.9991**	0.001
***NOT*-3**	1.738	1.829	1.7	1.745	**1.753**	0.04	0.9991	0.9969	0.9992	0.9900	**0.9963**	0.003
***NOT*-4**	1.978	1.871	1.749	1.903	**1.875**	0.07	0.9970	0.9968	0.9990	0.9919	**0.9961**	0.002
***NOT*-5**	1.871	1.791	1.916	1.938	**1.879**	0.05	0.9947	0.9897	0.9994	0.9977	**0.9954**	0.003
***NOT*-1a**	1.983	1.9	1.718	1.971	**1.893**	0.09	0.9960	0.9958	0.9992	0.9981	**0.9973**	0.001
***NOT*-1b**	1.735	1.869	1.802	1.858	**1.816**	0.05	0.9933	0.9996	0.9957	0.9976	**0.9965**	0.002
***NOT*-2a**	1.771	1.889	1.97	1.86	**1.873**	0.06	0.9991	0.9998	0.9908	0.9993	**0.9972**	0.003
***NOT*-2b**	1.893	1.963	1.923	1.799	**1.895**	0.05	0.9982	0.9995	0.9929	0.9953	**0.9965**	0.002
***NOT*-3a**	1.862	1.816	1.841	1.717	**1.809**	0.05	0.9991	0.9927	0.9998	0.9999	**0.9979**	0.003
***NOT*-3b**	1.865	1.948	---	1.954	**1.922**	0.04	0.9983	0.9995	---	0.9934	**0.9971**	0.002
***NOT*-3c**	1.942	1.979	1.816	1.874	**1.903**	0.06	0.9990	0.9991	0.9999	0.9996	**0.9994**	0.0004
***NOT*-4a**	1.917	1.898	1.87	1.938	**1.906**	0.02	0.9982	0.9998	0.9832	0.9967	**0.9945**	0.006
***NOT*-4b**	1.996	1.925	1.819	1.986	**1.932**	0.06	0.9957	0.9951	0.9946	0.9934	**0.9947**	0.001
***NOT*-5a**	1.882	1.843	1.841	1.66	**1.781**	0.08	0.9951	0.9996	0.9999	0.9997	**0.9998**	0.0001
***NOT*-5b**	1.789	1.749	1.889	1.836	**1.825**	0.05	0.9973	0.9987	0.9975	0.9997	**0.9986**	0.001
***NOT*-5c**	1.817	1.764	1.898	1.842	**1.830**	0.04	0.9961	0.9997	0.9987	0.9913	**0.9965**	0.003
ECE2	1.707	1.689	1.868	1.849	**1.778**	0.08	0.9997	0.9990	0.9992	0.9927	**0.9977**	0.00
ACTIN	1.862	1.853	---	---	**1.858**	0.01	0.9999	0.9988	---	---	**0.9993**	0.001
***HGPRT*[1]**	1.98	1.928	1.963	1.741	**1.903**	0.08	0.9990	0.9891	0.9909	0.9922	**0.9928**	0.003
***HGPRT*[2]**	1.861	1.947	1.931	1.957	**1.924**	0.03	0.9958	0.9989	0.9991	0.9999	**0.9984**	0.001

Performed as described in Ch. 3.3.17. Primers used for amplification are listed in Tab. 31+33. n: measured samples; 1: *HGPRT* from the *NOT* isoform plate; 2: *HGPRT* from the *ACTIN*, *ECE2* plate.

Table S4 Determination of qRT-PCR efficiencies of *NOT*, *ECE2*, *ACTIN* and *HGPRT* using HeLa cDNA

	Efficiency (E)						Correlation coefficient (R^2)					
Target	**n1**	**n2**	**n3**	**n4**	**Ø E**	**+/-**	**n1**	**n2**	**n3**	**n4**	**Ø R^2**	**+/-**
***NOT*-1**	1.958	1.936	1.74	1.7	**1.834**	0.11	0.9975	0.9999	0.9995	0.9996	**0.9991**	0.001
***NOT*-2**	1.814	1.946	1.898	1.722	**1.845**	0.01	0.9997	0.9999	0.9965	0.9997	**0.999**	0.001
***NOT*-3**	1.775	1.746	1.948	1.872	**1.835**	0.08	0.9995	0.9987	0.9714	0.9997	**0.9923**	0.01
***NOT*-4**	1.955	1.88	1.934	1.722	**1.873**	0.08	0.9968	0.9925	0.9501	0.9997	**0.9848**	0.02
***NOT*-5**	2.009	1.915	1.95	1.936	**1.953**	0.03	0.9963	0.9961	0.9867	0.9842	**0.9908**	0.01
***NOT*-1a**	1.922	1.9	1.932	1.994	**1.937**	0.03	0.9988	0.9996	0.9830	0.9907	**0.993**	0.01
***NOT*-1b**	1.934	1.828	1.828	1.912	**1.876**	0.05	0.9863	0.9977	0.9999	0.9993	**0.9958**	0.01
***NOT*-2a**	1.708	1.759	1.76	1.96	**1.797**	0.08	0.9990	0.9971	0.9962	0.9982	**0.9976**	0.001
***NOT*-2b**	1.919	1.868	1.915	1.744	**1.862**	0.06	0.9987	0.9986	0.9967	0.9978	**0.998**	0.001
***NOT*-3a**	1.718	1.836	1.864	1.803	**1.805**	0.04	0.9973	0.9999	0.9990	0.9985	**0.9987**	0.001
***NOT*-3b**	1.984	1.738	1.826	1.853	**1.850**	0.07	0.9961	0.9956	0.9977	0.9991	**0.9971**	0.001
***NOT*-3c**	1.834	1.511	1.775	1.764	**1.721**	0.11	0.9946	0.9958	0.9990	0.9991	**0.9971**	0.002
***NOT*-4a**	1.928	1.889	1.89	1.99	**1.924**	0.03	0.9958	0.9978	0.9893	0.9867	**0.9924**	0.004
***NOT*-4b**	1.981	1.926	1.852	1.917	**1.919**	0.03	0.9999	0.9999	0.9983	0.9967	**0.9987**	0.001
***NOT*-5a**	1.839	1.8	1.825	1.903	**1.843**	0.04	0.9984	0.9963	0.9991	0.9946	**0.9967**	0.002
***NOT*-5b**	1.42	---	1.574	1.675	**1.556**	0.09	0.9662	---	0.9999	0.9954	**0.9872**	0.01
***NOT*-5c**	1.846	1.926	1.957	2.087	**1.954**	0.07	0.9985	0.9998	0.9981	0.9964	**0.9982**	0.001
ECE2	1.919	1.886	1.888	1.898	**1.898**	0.01	0.9941	0.9989	0.9997	0.9984	**0.9978**	0.002
ACTIN	1.951	1.835	---	---	**1.893**	0.06	0.9999	0.9991	---	---	**0.9995**	0.0004
***HGPRT*[1]**	1.595	1.611	1.632	1.663	**1.625**	0.02	0.9997	0.9999	0.9998	0.9999	**0.9998**	0.0001
***HGPRT*[2]**	1.973	1.99	1.884	1.829	**1.919**	0.06	0.9999	0.9997	0.9973	0.9974	**0.9986**	0.001

Performed as described in Ch. 3.3.17. Primers used for amplification are listed in Tab. 31+33. n: measured samples; 1: *HGPRT* from the *NOT* isoform plate; 2: *HGPRT* from the *ACTIN*, *ECE2* plate.

Table S5 Determination of qRT-PCR efficiencies of m*NOT*, m*CREB3* and m*HGPRT* using 3T3 cDNA

	Efficiency (E)						Correlation coefficient (R^2)					
Target	**n1**	**n2**	**n3**	**n4**	**Ø E**	**+/-**	**n1**	**n2**	**n3**	**n4**	**Ø R^2**	**+/-**
m*NOT*-1	1.669	1.88	1.758	1.91	**1.804**	0.09	0.9996	0.9946	0.9987	0.9960	**0.9972**	0.002
m*NOT*-2	1.73	1.861	1.836	1.865	**1.823**	0.05	0.9925	0.9964	0.9938	0.9983	**0.9953**	0.002
m*NOT*-3	1.698	1.636	1.677	1.685	**1.674**	0.02	0.9985	0.9999	0.9962	0.9930	**0.9969**	0.002
m*NOT*-4	1.706	1.807	1.751	1.748	**1.753**	0.03	0.9998	0.9996	0.9979	0.9999	**0.9993**	0.001
m*NOT*-5	1.987	1.961	1.911	1.926	**1.946**	0.03	0.9956	0.9986	0.9978	0.9998	**0.9979**	0.001
m*NOT*-1a	1.92	1.948	1.881	1.907	**1.914**	0.02	0.9992	0.9886	0.9938	0.9941	**0.9939**	0.003
m*NOT*-1b	1.827	1.883	1.65	1.964	**1.831**	0.09	0.9829	0.9994	0.9995	0.9985	**0.995**	0.006
m*NOT*-2a	1.893	1.966	1.754	1.877	**1.873**	0.06	0.9993	0.9934	0.9997	0.9970	**0.9974**	0.002
m*NOT*-3a	1.648	1.789	1.618	1.571	**1.657**	0.07	0.9963	0.9976	0.9994	0.9981	**0.9979**	0.001
m*NOT*-3b	1.781	1.721	1.938	1.801	**1.810**	0.06	0.9991	0.9970	0.9971	0.9987	**0.998**	0.001
m*NOT*-3c	1.511	1.872	1.897	1.809	**1.772**	0.13	0.9975	0.9939	0.9975	0.9955	**0.9961**	0.001
m*NOT*-4a	1.852	1.893	1.851	1.601	**1.799**	0.10	0.9982	0.9999	0.9976	0.9995	**0.9988**	0.001
m*NOT*-4b	---	---	---	---	**---**	---	---	---	---	---	**---**	---
m*NOT*-4c	1.973	1.932	1.977		**1.961**	0.02	0.9951	0.9967	0.9973		**0.9964**	0.001
m*NOT*-5a	1.91	1.813	1.919	1.931	**1.888**	0.05	0.9983	0.9982	0.9999	0.9984	**0.9988**	0.001
m*CREB3*	1.595	1.619	1.473	1.662	**1.587**	0.06	0.9986	0.9999	0.9997	0.9999	**0.9995**	0.001
m*HGPRT*	1.779	1.879	1.814	1.625	**1.7743**	0.07	0.9995	0.9946	0.9981	0.9993	**0.9978**	0.002

Performed as described in Ch. 3.3.17. Primers used for amplification are listed in Tab. 31+35. n: measured samples.

Table S6 Determination of qRT-PCR efficiencies of m*NOT* and m*HGPRT* using MOCHA cDNA

	Efficiency (E)						Correlation coefficient (R^2)					
Target	**n1**	**n2**	**n3**	**n4**	**Ø E**	**+/-**	**n1**	**n2**	**n3**	**n4**	**Ø R^2**	**+/-**
m*NOT*-1	1.917	1.981	1.912	1.924	**1.934**	0.02	0.9991	0.9967	0.9919	0.9975	**0.9963**	0.002
m*NOT*-2	1.797	1.663	1.877	1.863	**1.8**	0.07	0.9997	0.9983	0.9976	0.9944	**0.9975**	0.002
m*NOT*-3	1.584	1.835	1.747	1.767	**1.733**	0.07	0.9999	0.9957	0.9984	0.9991	**0.9983**	0.001
m*NOT*-4	1.853	1.843	1.891	1.729	**1.829**	0.05	0.9921	0.9979	0.9916	0.9993	**0.9952**	0.003
m*NOT*-5	1.94	1.936	1.821	1.923	**1.905**	0.04	0.9970	0.9924	0.9898	0.9952	**0.9936**	0.002
m*NOT*-1a	1.884	1.663	1.836	1.78	**1.791**	0.07	0.9926	0.9987	0.9979	0.9995	**0.9972**	0.002
m*NOT*-1b	1.623	1.798	1.817	1.91	**1.787**	0.08	0.9917	0.9981	0.9990	0.9842	**0.9933**	0.005
m*NOT*-2a	1.941	1.767	1.961	1.936	**1.901**	0.07	0.9985	0.9999	0.9999	0.9991	**0.9994**	0.001
m*NOT*-3a	1.634	1.652	1.721	1.706	**1.678**	0.04	0.9993	0.9989	0.9928	0.9975	**0.9971**	0.002
m*NOT*-3b	1.817	1.582	1.845	1.761	**1.751**	0.08	0.9953	0.9949	0.9990	0.9969	**0.9965**	0.001
m*NOT*-3c	1.722	1.628	1.533	1.789	**1.668**	0.09	0.9982	0.9996	0.9998	0.9984	**0.999**	0.001
m*NOT*-4a	1.769	1.783	1.771	1.823	**1.787**	0.02	0.9972	0.9922	0.9979	0.9985	**0.9965**	0.002
m*NOT*-4b	1.5	1.866	1.365	---	**1.577**	0.19	0.9958	0.9985	0.9891	---	**0.9945**	0.004
m*NOT*-4c	1.764	1.874	1.931	1.908	**1.869**	0.05	0.9998	0.9906	0.9819	0.9983	**0.9926**	0.006
m*NOT*-5a	1.626	1.706	1.902	1.878	**1.829**	0.08	0.9993	0.9928	0.9975	0.9994	**0.9966**	0.002
m*HGPRT*	1.927	1.859	---	1.834	**1.847**	0.01	0.9992	0.9972	---	0.9999	**0.9986**	0.001

Performed as described in Ch. 3.3.17. Primers used for amplification are listed in Tab. 31+35. n: measured samples.

Table S7 Determination of qRT-PCR efficiencies of m*NOT* and m*HGPRT* using C127I cDNA

	Efficiency (E)						Correlation coefficient (R^2)					
Target	**n1**	**n2**	**n3**	**n4**	**Ø E**	**+/-**	**n1**	**n2**	**n3**	**n4**	**Ø R^2**	**+/-**
m*NOT*-1	1.955	1.876	1.615	1.741	**1.797**	0.12	0.9990	0.9992	0.9999	0.9997	**0.9994**	0.0003
m*NOT*-2	1.818	1.827	1.825	1.899	**1.842**	0.03	0.9992	0.9999	0.9927	0.9988	**0.9976**	0.002
m*NOT*-3	1.811	1.864	1.634	1.778	**1.772**	0.07	0.9975	0.9914	0.9986	0.9992	**0.9967**	0.003
m*NOT*-4	1.735	1.831	1.849	1.727	**1.786**	0.05	0.9991	0.9969	0.9907	0.9990	**0.9964**	0.003
m*NOT*-5	1.974	1.956	1.734	1.908	**1.893**	0.08	0.9964	0.9965	0.9979	0.9973	**0.997**	0.001
m*NOT*-1a	1.904	1.883	1.921	1.777	**1.871**	0.0	0.9997	0.9928	0.998	0.9992	**0.9975**	0.002
m*NOT*-1b	1.894	1.825	1.858	1.729	**1.827**	0.05	0.9970	0.9999	0.99892	0.9997	**0.9989**	0.001
m*NOT*-2a	1.912	1.8	1.785	1.894	**1.848**	0.06	0.9913	0.9943	0.9978	0.9950	**0.9946**	0.002
m*NOT*-3a	1.855	1.922	1.825	1.548	**1.788**	0.12	0.9971	0.9951	0.9999	0.9998	**0.998**	0.002
m*NOT*-3b	1.693	1.688	1.73	1.715	**1.707**	0.02	0.9995	0.9997	0.9999	0.9984	**0.9994**	0.001
m*NOT*-3c	1.55	1.557	1.649	1.645	**1.600**	0.05	0.9998	0.9982	0.9989	0.9999	**0.9992**	0.001
m*NOT*-4a	1.802	1.545	1.75	1.81	**1.727**	0.09	0.9941	0.9963	0.9987	0.9973	**0.9966**	0.001
m*NOT*-4b	---	---	---	---	**---**	---	---	---	---	---	**---**	---
m*NOT*-4c	1.753	1.896	1.831	1.813	**1.823**	0.04	0.9993	0.9991	0.9955	0.9995	**0.9984**	0.001
m*NOT*-5a	1.74	1.855	1.751	1.886	**1.831**	0.05	0.9993	0.9984	0.9993	0.9984	**0.9987**	0.0004
HGPRT	1.925	1.94	1.688	1.915	**1.848**	0.11	0.9966	0.9980	0.9999	0.9974	**0.9984**	0.001

Performed as described in Ch. 3.3.17. Primers used for amplification are listed in Tab. 31+35. n: measured samples.

Table S8 Determination of qRT-PCR efficiencies of m*NOT* and m*HGPRT* using BC3H1 cDNA

	Efficiency (E)						Correlation coefficient (R^2)					
Target	**n1**	**n2**	**n3**	**n4**	**Ø E**	**+/-**	**n1**	**n2**	**n3**	**n4**	**Ø R^2**	**+/-**
m*NOT*-1	1.75	1.928	1.869	1.928	**1.869**	0.06	0.9998	0.9990	0.9919	0.9980	**0.9972**	0.003
m*NOT*-2	1.841	1.901	1.816	1.685	**1.811**	0.06	0.9988	0.9955	0.9993	0.9999	**0.9984**	0.001
m*NOT*-3	1.728	1.723	1.603	1.612	**1.667**	0.06	0.9958	0.9938	0.9996	0.9992	**0.9971**	0.002
m*NOT*-4	1.896	1.758	1.831	1.85	**1.834**	0.04	0.9971	0.9999	0.9969	0.9946	**0.9971**	0.001
m*NOT*-5	1.826	1.808	1.943	1.829	**1.852**	0.05	0.9986	0.9956	0.9995	0.9978	**0.9979**	0.001
m*NOT*-1a	1.927	1.923	1.818	1.947	**1.904**	0.04	0.9971	0.9970	0.9938	0.9960	**0.996**	0.001
m*NOT*-1b	---	1.828	1.974	1.88	**1.894**	0.05	---	0.9998	0.9833	0.9994	**0.9942**	0.01
m*NOT*-2a	1.857	1.643	1.858	1.924	**1.821**	0.09	0.9991	0.9989	0.9952	0.9974	**0.9976**	0.001
m*NOT*-3a	1.707	1.648	1.684	1.701	**1.685**	0.02	0.9999	0.9991	0.9972	0.9917	**0.997**	0.003
m*NOT*-3b	1.705	1.618	1.635	1.793	**1.688**	0.06	0.9924	0.9931	0.9977	0.9975	**0.9952**	0.002
m*NOT*-3c	1.746	1.812	1.683	1.554	**1.699**	0.08	0.9999	0.9995	0.9966	0.9999	**0.999**	0.001
m*NOT*-4a	1.868	1.658	1.839	1.674	**1.760**	0.09	0.9943	0.9996	0.9960	0.9957	**0.9964**	0.002
m*NOT*-4b	---	---	---	---	**---**	---	---	---	---	---	**---**	---
m*NOT*-4c	1.878	1.951	1.889	1.722	**1.86**	0.07	0.9980	0.9952	0.9965	0.9994	**0.9973**	0.001
m*NOT*-5a	1.973	1.768	1.922	1.93	**1.8733**	0.07	0.9967	0.9987	0.9917	0.9936	**0.9947**	0.003
m*HGPRT*	1.896	1.841	1.987	1.851	**1.893**	0.06	0.9999	0.9979	0.9981	0.9977	**0.9979**	0.0002

Performed as described in Ch. 3.3.17. Primers used for amplification are listed in Tab. 31+35. n: measured samples.

Table S9 Determination of qRT-PCR efficiencies using HeLa cDNA

	Efficiency (E)						Correlation coefficient (R^2)					
Target	**n1**	**n2**	**n3**	**n4**	**Ø E**	**+/-**	**n1**	**n2**	**n3**	**n4**	**Ø R^2**	**+/-**
p50	1.719	1.729	1.764	1.76	**1.743**	0.02	0.9992	0.9993	0.9934	0.9999	**0.9979**	0.002
p65	1.881	1.856	1.831	1.86	**1.857**	0.01	0.9971	0.9895	0.9998	0.9984	**0.9962**	0.003
RPS3	1.917	1.892	1.902	1.914	**1.906**	0.01	0.9911	0.9875	0.9974	0.9931	**0.9923**	0.003
IκBα	1.929	1.851	1.922	1.924	**1.907**	0.03	0.9955	0.9997	0.9977	0.9959	**0.9972**	0.001
EGR-1	1.826	1.902	1.916	1.967	**1.903**	0.04	0.9999	0.9991	0.9997	0.9963	**0.9987**	0.001
CREB1	1.784	1.794	1.785	1.792	**1.789**	0.004	0.9930	0.9969	0.9984	0.9999	**0.9971**	0.002
CREB3	1.669	1.624	1.621	1.664	**1.645**	0.02	0.9971	0.9953	0.9999	0.9998	**0.9980**	0.002
ECE2	1.903	1.804	1.839	1.898	**1.861**	0.04	0.9999	0.9953	0.9994	0.9984	**0.9983**	0.001

Performed as described in Ch. 3.3.17. Primers used for amplification are listed in Tab. 31. n: measured samples.

Eidesstattliche Erklärung

Ich erkläre hiermit an Eides Statt, dass ich die vorliegende Arbeit selbstständig und ohne Benutzung anderer als der angegebenen Hilfsmittel angefertigt habe; die aus fremden Quellen direkt oder indirekt übernommenen Gedanken sind als solche kenntlich gemacht. Die Arbeit wurde bisher in gleicher oder ähnlicher Form keiner anderen Prüfungskommission vorgelegt und auch nicht veröffentlicht.

_____ _____

Ort, Datum Unterschrift (Vor- und Nachname)

Acknowledgments

Curriculum vitae

Personal data

Name:	Christoph Schultheiß
Address:	Adam-Karrillon-Str. 1-3, 55118 Mainz, Germany
Born:	18.08.1983 in Coburg, Germany
Email:	chschult83@gmail.com

Studies and education

04/2009 – 07/2016	Institute for Medical Microbiology and Hygiene, Mainz **Scientific assistant / PhD student**
04/2004 – 03/2009	Johannes Gutenberg-University, Mainz **Diploma in biology**

Advanced training and internships

09/2009	Center for Advanced Safety Training of the Johannes Gutenberg-University, Mainz **Advanced training „Safety in genetic engineering according to § 15 Abs. 2 Satz 1 Nr. 3 of the Genetic Engineering Act (GenTG)"**
10/2007 – 11/2007	German Cancer Research Center (DKFZ), Heidelberg **Internship Cellular Senescence** Supervisor: Dr. Hofmann

Scholarships

04/2010 – 06/2012	**PhD scholarship from Stipendienstiftung Rhineland-palatine**
05/2009 – 04/2010	**Scholarship from Johannes Gutenberg-University Mainz in the context of the scientific-clinical profile and focus formation**